

MULTI-FUNCTIONAL APPLICATIONS OF GRAPHENE RELATED MATERIALS IN CEMENTITIOUS COMPOSITES



Ioanna Papanikolaou

Department of Engineering
University of Cambridge

This dissertation is submitted for the degree of

Doctor of Philosophy

King's College

September 2020

Multi-functional applications of graphene related materials in cementitious composites

Author: Ioanna Papanikolaou

Supervisor: Professor Abir Al-Tabbaa

Advisor: Professor Gopal Madabhushi

DECLARATION

I hereby declare that this dissertation is the result of my own work and includes nothing, which is the outcome of work done in collaboration except where specifically indicated in the text. The contents of this dissertation are original and have not been previously submitted, or, are being concurrently submitted, in part or whole, for consideration for a degree or diploma or other qualification at the University of Cambridge or any other University or similar institution except as declared in the Preface and specified in the text.

In accordance with the Department of Engineering guidelines, this thesis does not exceed 65,000 words, inclusive of appendices, footnotes, tables and equations and it does not contain more than 150 figures.

Ioanna Papanikolaou

Cambridge, September 2020

ABSTRACT

Author: Ioanna Papanikolaou

Cementitious composites are the most widely used construction materials with 4.1 billion tonnes of cement being produced globally in 2017. However, cement production is associated with ~7% of the total global anthropogenic CO₂ emissions. Moreover, concrete structures suffer from poor durability, with a fifth of the total civil engineering output in the UK being spent on repair and maintenance. The poor durability of concrete structures necessitates frequent inspections and an enhanced structural monitoring regime. Despite the advancements in material science over the years, cementitious composites remain passive structural materials and do not possess any functionalities.

The motivation for this research was to take advantage of emerging graphene-related materials (GRMs) to solve the challenges associated with concrete infrastructure and to instigate additional functionalities that would make the material smarter. Initially, the homogenous dispersion of GRMs was experimentally investigated in detail, as this was recognised as a key challenge in the literature. The results showed that a combination of sonication and the use of a polycarboxylate superplasticiser, were effective in homogeneously dispersing the main GRM material, graphene nanoplatelets (GNPs), in cementitious systems. Subsequently, the effect of the GRMs on the early age, mechanical and permeability performance of cement pastes and mortars was investigated. It was found that GNPs reduced the fluidity, delayed the hydration, and had a poor microstructural interaction with the cement hydration products. This consequently led to a reduction in the flexural and compressive strengths. An early age beneficial effect with GNPs was found for water, gas, and chloride permeability. The use of GRMs to improve the electrical conductivity performance was also investigated, with the aim to create electrically conductive networks in the composite that could then be used to monitor changes in loading or damage, by triggering a self-sensing response. Natural graphite and GNPs were found to be effective, however, their use in bulk applications would be challenging and instead, their use in coatings was proposed. Finally, an industry survey was carried out to understand the industry perceptions of this novel material and a Lifecycle Assessment (LCA) study was also undertaken to establish the sustainability performance of a novel GNP-cement composite. The results demonstrated the potential of GRMs to improve the permeability performance of cementitious composites and to instigate a functional behaviour.

ACKNOWLEDGEMENTS

This thesis would not have been possible without the help and support of many. I will be forever grateful to the guidance that I received from my supervisor, Professor Abir Al-Tabbaa, who always supported me to improve and grow. Secondly, I must express my gratitude to Tim Embley, who has provided endless support for my development.

I would like to acknowledge the Engineering and Physical Sciences Research Council (EPSRC) (Grant No. EP/L016095/1-EPSRC Centre for Doctoral Training in Future Infrastructure and Built Environment and Grant No. EP/P02081X/1 - Resilient Materials for Life (RM4L)) and Costain Group PLC for funding my research.

I would like to thank Bill Hewlett, Angus Mackenzie, and Andy Firth from Costain – without your continuous support, my PhD would not have been possible. My gratitude also goes to Chris Knight, for all the help in the laboratory and Dr Noemi Arena, my co-author and friend, who expanded my horizons around sustainability. A huge thanks to Dr Fei Jin, who helped me immensely with the experimental work, Dr Simon Smith for taking the time to read and comment on my thesis, and Ian Ellis from BASF, who provided great technical support and advice. I also need to thank two fantastic research groups that have supported me in the past four years – FIBE and the GRO Group. Especially, Chrysoula, Benyi, Zijing, Livia and Heba. Thank you for always being there and providing a great environment to work. I hugely appreciate all the support that I received from HeidelbergCement Group for my secondment, and from Marco Goisis, Marcello Molfetta, Flavio Rampinelli, Aronne Carminati, Stefano Allevi, Pietro Tavasci and Sergio Tortelli. Grazie mille!

On a personal note, I need to thank all my friends that have not only mentally supported me through this journey but also spent countless of hours discussing my research– Mark Hobbs, Socrates Angelides, Paul Siberry, Dr Oliver Teall and Dr Efi Tzoura. Thank you!

Θέλω να ευχαριστήσω τις φίλες μου, Αναστασία και Ζωή, που ήταν πάντα διαθέσιμες να συζητήσουν τα προβλήματα και τις ανησυχίες μου. Επίσης, θέλω να ευχαριστήσω τον Χαράλαμπο Κωνσταντίνου, που μέσα σε τέσσερα χρόνια γνωριμίας μου στάθηκε απίστευτα πολύ και ήταν πάντα διαθέσιμος να βοηθήσει την ερευνα μου. Ένα τεράστιο ευχαριστώ στα ξαδέρφια μου, Χριστίνα, Ανδρονίκη, Αναστάσης, Γιάννης. Τέλος, το πιο μεγάλο ευχαριστώ το απευθύνω στους γονείς μου, Βασίλη και Χαρά, για όλες τις ευκαιρίες που μου έδωσαν καθώς και στον σύζυγο μου, Θανάση, για όλες τις θυσίες και τις υπέροχες στιγμές των τελευταίων 5 χρόνων.

LIST OF PUBLICATIONS

The author is named as the first author and co-author on the following journal papers:

- **Papanikolaou, I.**, Arena, N. and Al-Tabbaa, A. (2019) ‘Graphene nanoplatelet reinforced concrete for self-sensing structures - A lifecycle assessment perspective’, *Journal of Cleaner Production*. Elsevier Ltd, 240, p. 118202.
<https://doi.org/10.1016/j.jclepro.2019.118202>
- Litina C., Cao B., Chen J., Li Z., **Papanikolaou I.**, Al-Tabbaa A. (2019) ‘First UK commercial deployment of microcapsule-based self-healing reinforced concrete’, *Journal of Materials in Civil Engineering – under review*

The author is named as the first author and co-author on the following conference papers and proceedings:

- **Papanikolaou I.**, Al-Tabbaa A., Goisis M. “An industry survey on the use of graphene-reinforced concrete for self-sensing applications” in International Conference on Smart Infrastructure and Construction (ICSIC), Cambridge, UK, 2019
<https://doi.org/10.1680/icsic.64669.613>
- **Papanikolaou I.**, Litina C., and Al-Tabbaa A., “Biomimetic self-sensing infrastructure using graphene nanoplatelets in cement composites” in 7th International Conference on Self-Healing Materials (ICSHM 2019), Yokohama, Japan, 2019
- Litina C., Cao B., Chen J., Li Z., **Papanikolaou I.**, Al-Tabbaa A., “Microcapsule-based self-healing concrete: From development to commercial deployment” in 7th International Conference on Self-Healing Materials (ICSHM 2019), Yokohama, Japan, 2019
- **Papanikolaou I.**, Litina C., and Al-Tabbaa A., “A preliminary study into the effect of superplasticisers on the dispersion of graphene materials in cement” in 12th fib international PhD Symposium in Civil Engineering, Prague, Czech Republic, 2018 – Recipient of the **Best Paper Award** and the **BASF Award for the Best Research paper in Materials**
- **Papanikolaou I.**, Davies A., Jin F., Litina C., and Al-Tabbaa A., “Graphene oxide/cement composites for sprayed concrete tunnel linings,” in ITA - AITES WORLD TUNNEL CONGRESS 2018, Dubai, United Arab Emirates, 2018, pp. 103–108

TABLE OF CONTENTS

Chapter 1. INTRODUCTION	1
1.1. Background.....	1
1.2. Research motivation.....	2
1.3. Aim and objectives.....	3
1.4. Thesis outline.....	4
Chapter 2. LITERATURE REVIEW	5
2.1. Concrete infrastructure and associated challenges.....	5
2.1.1. Environmental impact of concrete.....	5
2.1.2. Durability challenge.....	6
2.1.3. Monitoring challenge.....	8
2.2. Biomimetic and nano-engineered cementitious materials	10
2.2.1. Self-sensing structures	10
2.2.2. Nano-engineered concrete.....	14
2.3. Graphene-related materials (GRMs)	15
2.3.1. GRM structures	15
2.3.2. GRM production methods and applications	18
2.4. Graphene nanoplatelets (GNPs) in cement composites.....	20
2.4.1. Dispersion studies	20
2.4.2. Early age performance and microstructure.....	32
2.4.3. Mechanical properties.....	42
2.4.4. Permeability and durability	45
2.4.5. Electrical conductivity.....	47
2.5. Environmental performance of GRMs.....	54
2.6. Summary	58
Chapter 3. MATERIALS AND EXPERIMENTAL PROCEDURES	59

3.1.	Materials.....	59
3.1.1.	Cementitious materials	59
3.1.2.	Aggregates	60
3.1.3.	Graphene-related materials (GRMs)	61
3.1.4.	Chemical admixtures for dispersion.....	62
3.2.	Sample preparation.....	63
3.2.1.	GNP suspension preparation.....	63
3.2.2.	Cementitious composites	64
3.3.	Experimental procedures	67
3.3.1.	Microstructure, dispersion and thermal characterisation	67
3.3.2.	Mechanical characterisation	74
3.3.3.	Permeability assessment.....	76
3.3.4.	Electrical conductivity	80
Chapter 4.	GRAPHENE-RELATED MATERIALS (GRMs) DISPERSION STUDIES.....	83
4.1.	GRM characterisation	83
4.1.1.	Overview of the GRMs used.....	83
4.1.2.	Characterisation of the different GRMs used	84
4.2.	GNPs dispersion in water	89
4.3.	Effect of chemical admixtures on the dispersion of GNPs.....	90
4.3.1.	Dispersion using zeta-potential testing.....	91
4.3.2.	Dispersion using UV-Visible spectroscopy (UV-Vis)	94
4.3.3.	GNPs dispersion in cement.....	99
4.3.4.	Other dispersion studies.....	105
4.4.	Dispersion of natural graphite.....	106
4.5.	Dispersion studies at the HeidelbergCement <i>i-lab</i>	111
4.5.1.	High-speed shear mixing.....	111
4.5.2.	Hydrophobic mixing of carbon nanotubes (CNTs)	112

4.5.3.	Effect of GRMs on the properties of CEMI mortars	115
4.5.4.	Alternative and CEMI blended cementitious binders	122
4.6.	Summary	128
Chapter 5.	GRM-CEMENT COMPOSITES PERFORMANCE.....	131
5.1.	GNPs in cement paste	132
5.1.1.	Cement characterisation.....	132
5.1.2.	Effect on hydration	133
5.1.3.	Effect on microstructure.....	140
5.1.4.	Effect on mechanical properties	143
5.2.	GNPs in CEMI mortars.....	148
5.2.1.	Fluidity of mortars with GNPs	148
5.2.2.	Effect on hydration	149
5.2.3.	Effect on microstructure.....	154
5.2.4.	Effect on mechanical properties	160
5.2.5.	Effect on permeability	164
5.3.	Effect of natural graphite on CEMI paste.....	172
5.3.1.	Rheological performance with graphite.....	172
5.3.2.	Effect on hydration	174
5.3.3.	Effect on microstructure.....	177
5.3.4.	Effect on mechanical properties	179
5.4.	Summary.....	181
Chapter 6.	ELECTRICAL CONDUCTIVITY OF CEMENT COMPOSITES WITH GRMs	183
6.1.	Effect of intrinsic material properties on the electrical conductivity	183
6.1.1.	Effect of w/c and curing regime	184
6.1.2.	Relationship between embedded electrodes and surface conductivity	187
6.2.	Effect of GRMs on the electrical conductivity of cement paste	189

6.2.1.	Effect of natural graphite using 4 probe and direct current tests.....	189
6.2.2.	Effect of natural graphite using electrical impedance spectroscopy.....	193
6.2.3.	Effect of GNPs on the electrical conductivity	201
6.3.	GNP-cement pastes as electrically conductive coatings	204
6.3.1.	Water-based GNP coating layer	204
6.3.2.	Cement-based GNP coating layer	207
6.4.	Summary	210
Chapter 7. INDUSTRY SURVEY AND LIFECYCLE ASSESSMENT ON THE USE OF GRMs IN CEMENT COMPOSITES.....		212
7.1.	Industry survey	212
7.1.1.	Industry survey design	212
7.1.2.	Industry survey results	214
7.2.	Lifecycle Assessment (LCA)	221
7.2.1.	LCA goal and scope definition.....	221
7.2.2.	LCA inventory.....	223
7.2.3.	GNPs production.....	226
7.2.4.	GNPs incorporation in concrete	230
7.2.5.	Sensitivity analysis.....	234
7.3.	Summary	237
Chapter 8. CONCLUSIONS AND FUTURE OUTLOOK.....		238
8.1.	Conclusions.....	238
8.1.1.	Overview	238
8.1.2.	Literature review.....	238
8.1.3.	Materials and experimental procedures	241
8.1.4.	GRM dispersion studies	241
8.1.5.	Effect of GRMs on the performance of cement composites	242
8.1.6.	Electrical conductivity studies of GRM-cement composites.....	243

8.1.7. Industry survey and LCA	244
8.2. Future outlook.....	245
Bibliography.....	247

SYMBOLS AND ABBREVIATIONS

AC	Alternating current
bwoc	By weight of cement
CEMI	Ordinary Portland cement
CEMII/A-LL	Limestone blend cement
CNTs	Carbon nanotubes
CO ₂	Carbon dioxide
DC	Direct current
DTA	Differential thermal analysis
DTG	Differential thermogravimetry
EIS	Electrical impedance spectroscopy
GNP	Graphite/graphene nanoplatelets
GO	Graphene oxide
GRMs	Graphene related materials
LCA	Lifecycle assessment
LPE	Liquid phase exfoliation
MIP	Mercury intrusion porosimetry
PC	Portland cement
RCPT	Rapid chloride penetration testing
rGO	Reduced graphene oxide
SSA	Specific surface area
SEM	Scanning electron microscopy
SHM	Structural health monitoring
SF	Silica fume
UV-Vis	Ultraviolet – visible spectroscopy
w/c	water/cement ratio
wt.%	% dosage by weight of cement
XRD	X-ray diffraction

Chapter I. INTRODUCTION

I.1. Background

Cementitious composites, such as pastes, mortars and concrete, are the most widely used construction materials for infrastructure projects. Global cement production reached 4.1 billion tonnes in 2017 (Cembureau, 2017) and in the UK alone, the infrastructure pipeline from 2016-2021 accounts for more than £400 billion (IPA, 2016), therefore demand for cement remains substantially high. However, cementitious composites are associated with several challenges including a high environmental impact, poor durability and an ongoing need for inspection and monitoring of structures. Portland cement accounts for ~7% of the total global anthropogenic CO₂ emissions (Fischedick *et al.*, 2014) and it is estimated that each tonne of concrete has approximately 100-300 kg of embodied CO₂ (NRMCA, 2012). Consequently, there is an impending need to reduce the carbon intensity of cementitious composites and improve their sustainability performance.

The poor durability of structures is a further challenge that leads to frequent repair and maintenance (R&M) activities, which are expensive, and lead to a great environmental impact and disruption. From 2011 to 2015, approximately a fifth of the civil engineering output in the UK was due to R&M (HM Treasury, 2010). In the US, ~\$3.6 trillion had to be invested in infrastructure by 2020 to restore it to a “B” grade from “C, with Americans undertaking over 200 million trips a day across deficient bridges (Whiteley *et al.*, 2015). The inadequate durability has also led to structural inspections being undertaken across the network (Gardner *et al.*, 2018). Such inspections are usually carried out visually, however, due to the inherent uncertainties and risks with visual surveys, the use of sensors has started to flourish. For example, over two thousand sensors have been installed on the Queensferry Crossing in Scotland, to monitor the global behaviour of the bridge and its environment (Arup, 2020). However, the use of external sensors has often resulted in high costs, low sensitivity, need for frequent calibration and incompatibility with structural materials (Ou and Han, 2009; Spencer, 2009; Webb *et al.*, 2015). Overall, the materials currently employed in infrastructure are passive and inert, far from being carbon neutral, maintained reactively and serve no additional functionality. However, recent scientific advances in biomimetic materials – referring to materials that mimic natural systems - could enable the

infrastructure industry to turn the cementitious structures into fully digitised, cognitive assets that can provide additional functionalities to their owners and maintainers.

1.2. Research motivation

Due to the numerous challenges with sustainability, durability and monitoring of concrete infrastructure, there is a pressing need to improve the performance of such structures and to instigate additional functionalities. Over the last decades, research has focused on the potential for a wide range of nanomaterials to enhance the performance of structural materials. Nanomaterials are defined as those that are <100 nanometers in one of their dimensions (Royal Society of Chemistry, 2013). One such nanomaterial is graphene, which was isolated in 2004 through graphite exfoliation, and its properties include high strength and electrical conductivity, high flexibility and toughness, low weight and thickness as well as barrier properties to aggressive atoms (Geim and Novoselov, 2007). However, graphene comes in many different forms and graphene-related materials (GRMs) include graphene oxide (GO), reduced graphene oxide (rGO), graphite nanoplatelets (GNPs) as well as natural graphite which is the starting material for graphene fabrication. Since graphene's discovery, there has been an increasing research interest in the use of GRMs in composite applications with authors investigating the potential use of a GRM-cement composite.

Despite the increasing research efforts in GRM-cement composites, the literature is not always in agreement and there are often contradictory results around the effect of GRMs on the hydration, mechanical and durability properties of cement composites. Furthermore, most studies to date are primarily focused on enhancing the strength and mechanical performance, rather than improving the durability or adding functionalities. A key challenge with GRMs is their homogenous dispersion in the cement matrix due to their nano-size and attractive forces. Many different dispersion protocols have been used by the authors, who consequently report different effects of GRMs on the cement composites performance. Furthermore, GRMs are a new family of materials, with most GRMs being experimental products with varying fundamental properties. Therefore, this research aimed to identify a suitable GRM for use in cementitious applications and then to develop an appropriate dispersion protocol to ensure homogenous dispersion. The motivation for using GRMs is two-fold; firstly, to enhance the durability and maintainability of cement composites and

secondly, to instigate an additional functionality, such as a self-sensing mechanism which would solve the monitoring challenge.

However, sustainability of concrete infrastructure is also a key challenge and the motivation was to develop a composite material with reduced environmental impact. The literature on the environmental effects of GRM production and their use in cement composites is scarce as GRM production is still at its infancy. To ensure that a novel GRM-cement composite is also sustainable, this research also carried out a detailed Lifecycle Assessment (LCA) study to assess the environmental impact of producing one of the GRMs, graphite nanoplatelets (GNPs), and their consequent impact when they are added in a standard concrete mix design. This would allow for a spherical assessment of the use of GRMs in cement composites and whether they could help in solving the sustainability, durability and infrastructure monitoring challenges faced by the civil engineering industry.

1.3. Aim and objectives

The aim of this research was to understand the role of graphene-related materials (GRMs) in cementitious composites and to develop a novel, sustainable cementitious composite with improved durability and additional functionalities, in particular, an enhanced electrical conductivity for self-sensing applications. The specific objectives were to:

- Develop a suitable dispersion protocol for introducing the GRMs in the cement composites which would ensure their homogenous dispersion;
- Evaluate the GRM-cement composite performance in terms of early age, mechanical and permeability aspects;
- Investigate the role of GRMs in enhancing the electrical conductivity of cement composites;
- Understand the industry views and the environmental impact of introducing GRMs in concrete to promote sustainable development.

1.4. Thesis outline

This thesis is divided into eight chapters. This introduction forms *Chapter 1* and presents the background to the problem, the motivation for carrying out this research and the objectives as well as the thesis outline. *Chapter 2* starts by providing a comprehensive literature review of the concrete infrastructure challenges and the emergence of biomimetic and nano-engineered cementitious materials. The chapter further discusses the different GRMs and their resultant use in cement composites by focusing on their dispersion; the early age performance; the mechanical and permeability properties and finally the electrical conductivity of cement composites with GRMs. A literature review on the environmental performance of GRMs is also presented. This is followed by *Chapter 3*, which provides a detailed description of the materials used, and the experimental procedures followed. *Chapter 4* then focuses on the experimental work carried out to characterise the GRMs and develop a practical GRM dispersion protocol in cement composites. A detailed analysis of the effect of GRMs on cement pastes and mortars in terms of early age performance, mechanical and durability properties is then presented in *Chapter 5*. *Chapter 6* focuses on the effects of GRMs on the electrical conductivity of cement pastes and explores the potential use of a functional cement-based electrically conductive coating for infrastructure. *Chapter 7* presents the findings from an industry survey that was conducted to understand the industry views on the use of GRM-cement composites as well as the results from a cradle-to-gate Lifecycle Assessment (LCA) study of GNPs fabrication and their subsequent incorporation in concrete. Finally, *Chapter 8* summarises the key findings from this research and provides recommendations for future work.

Chapter 2. LITERATURE REVIEW

This chapter presents a critical literature review on aspects that are relevant to the research carried out in this thesis. Initially, the concrete infrastructure challenges are discussed, including the sustainability, durability and monitoring challenges faced across the infrastructure sector. This is followed by a discussion on the emergence of biomimetic materials. Focus is then given to the use of graphene-related materials (GRMs) in cementitious composites to solve some of the pressing concrete infrastructure challenges.

2.1. Concrete infrastructure and associated challenges

Cementitious materials, such as mortars and concrete, have been used for hundreds of years for infrastructure and housing and are the most commonly used man-made materials (Neville, 2011). One of the most notable infrastructure projects, the Three Gorges Dam in China, used over 28 million m³ of concrete during its construction (Minghua, 2001). Portland cement (PC), one of the key constituents of cementitious composites, is a finely ground inorganic material that is produced by sintering a mixture of limestone, clay and other minerals at approximately 1450°C in a kiln (Lea, 1970). When cement is mixed with water, it forms a paste that can be used as a binder for fine aggregates to produce mortars, or with fine and coarse aggregates to produce concrete (Neville, 2011). This binding paste gains strength over time due to an ongoing process termed as cement hydration, where chemical bonds are formed continuously. The final composite material comprises of a hydrated binding cement paste, aggregates and pores, and possesses a certain strength and stability.

2.1.1. Environmental impact of concrete

Concrete production is associated with several environmental impacts, including carbon emissions, waste, water use and natural resources depletion (The Concrete Centre, 2016a). Carbon dioxide (CO₂) is a greenhouse gas that contributes to anthropogenic climate change and is primarily emitted during fossil fuel combustion and industrial processes (IPCC, 2013). One of the key constituents of concrete is cement, and the global cement production accounts for ~7% of the total anthropogenic CO₂ emissions (Worrell *et al.*, 2009; Fishedick *et al.*, 2014). It is estimated that each tonne of concrete has ~100-300 kg of embodied CO₂

(NRMCA, 2012) depending on its composition. A standardised mix (based on the 2008 composition and CO₂ emissions) results in 73.8 kgCO₂ per tonne of concrete (The Concrete Centre 2016a). Demand for concrete has been found to grow in developing economies to ~\$10-15,000 per person until demand for new infrastructure has been saturated (Allwood and Cullen, 2012). Global cement production reached 4.1 billion tonnes in 2017, with over half taking place in China, as illustrated in Figure 2-1 by the European Cement Association (Cembureau, 2017). The market is projected to reach ~6.2 billion tonnes by 2024, exhibiting a 3.5% compound annual growth rate (CAGR) during 2019 to 2024, which is underpinned by the rising population and urbanisation as well as the construction of new mega-projects, such as China's One Belt (IMARC, Group 2019). In the UK, the infrastructure pipeline from 2016 to 2021 accounts for more than £400 billion (IPA, 2016), whilst in 2023, the global civil engineering sector is forecast to be worth over £3,306 billion which a 4.8% CAGR (MarketLine, 2020). Therefore, in the next few years, demand for cementitious materials is expected to remain very high.

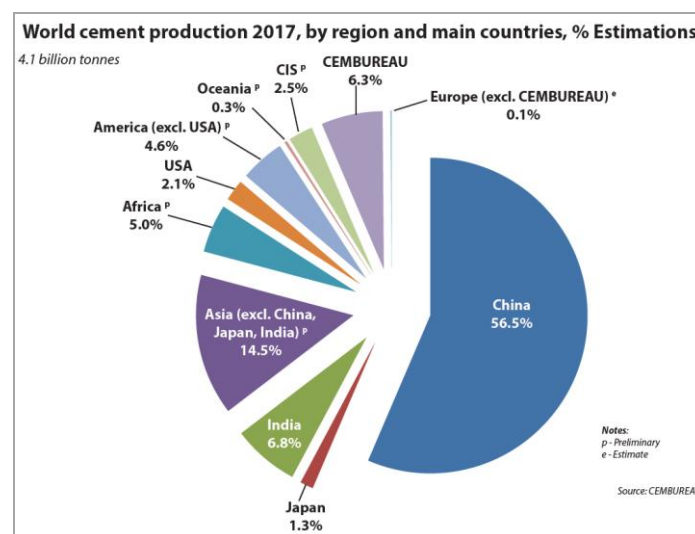


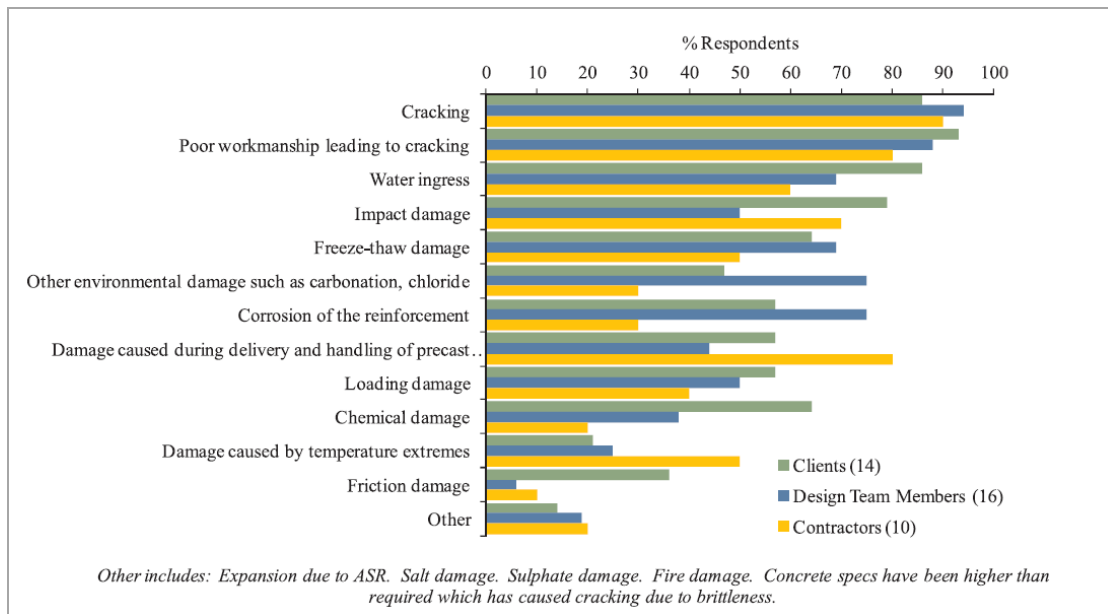
Figure 2-1: World cement production by region or key countries in 2017 (Cembureau, 2017)

2.1.2. Durability challenge

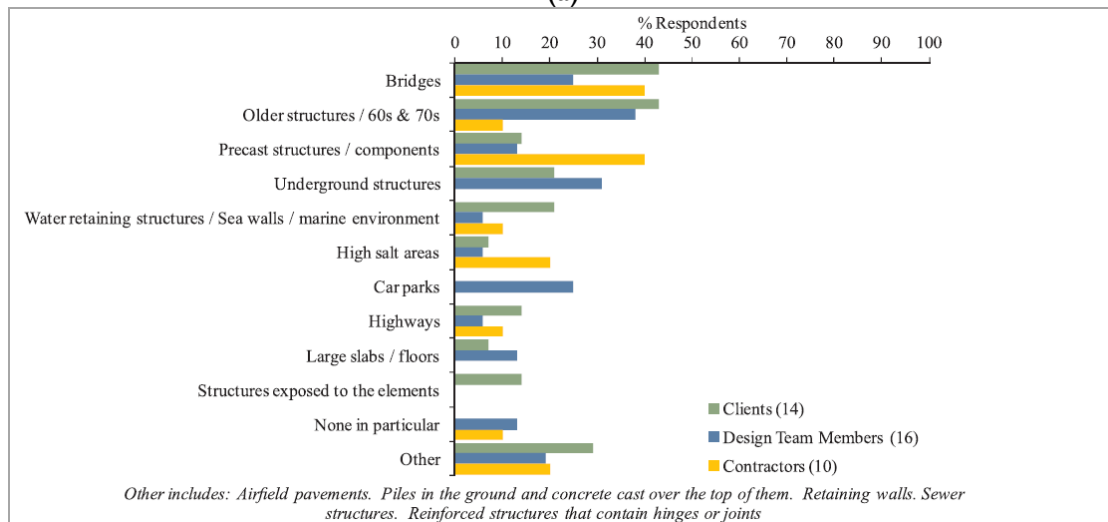
A durable structure is one that can maintain its mechanical and serviceability performance over its design life under the prescribed environmental and working conditions. Concrete is very strong in compression but weak in tension, which leads to consequent cracking and physical damage (Neville, 2011). Other common causes of concrete deterioration include, reinforcement corrosion; chemical attack (due to acids, salts and sulphates); freeze-thaw

deterioration and cracking due to volumetric changes as a result of shrinkage or thermal stresses (PCA, 2002). Durability of concrete structures and an enhanced service life have the potential to reduce the demand for new materials and the CO₂ emissions from concrete production. Despite technical developments in civil and materials engineering, durability of concrete structures is still a challenge and many structures are subject to frequent repair and maintenance (R&M), which is expensive and leads to a great environmental cost and disruption for the public (Al-Tabbaa *et al.*, 2018; Gardner *et al.*, 2018). In the UK, ~£10 bn was spent on R&M from 2011 to 2015, which accounted for 35-45% of the total infrastructure budget (HM Treasury, 2010). In the US, it was estimated that \$3.6 trillion in 2010 dollars had to be invested in infrastructure by 2020 to restore it to a “B” grade from “C” (Whiteley *et al.*, 2015). Market analysts predict that the global concrete repair mortars market will grow at a 8% CAGR by 2021 (Businesswire, 2017). Furthermore, climate change, is likely to affect concrete deterioration further and a study for Australia showed that carbonation-induced damage can increase by 400% until 2100 (Stewart *et al.*, 2011). Other than the environmental and financial impacts, the social implications of deteriorated infrastructure are also very important. The Genoa (Morandi) bridge collapse in Italy in August 2018 resulted in 43 fatalities (Horgan, 2019). The road conditions cost the U.S. motorists an estimated \$101 billion a year in wasted time and fuel (Whiteley *et al.*, 2015).

Despite the evidence that concrete structures suffer from poor durability and require an investment in R&M, there is a lack of quantitative data that identify the underlying factors that result in such performance. Even when concrete structures are repaired, a study showed that 20% of the repairs fail within 5 years and 55% fail after 10 years (Tilly and Jacobs, 2007). A more recent industry survey was commissioned in the UK (Gardner *et al.*, 2018) to identify the causes of damage in concrete structures and the consequences. As illustrated in Figure 2-2(a), an average of 90% of the respondents identified cracking as a key issue, followed by water ingress and impact damage, whilst bridges, older structures and underground structures (e.g. tunnels) were found to be particularly vulnerable (Figure 2-2(b)). Bridge deterioration is also a challenge for the US, as Americans undertake over 200 million trips a day across deficient bridges and it is estimated that \$20.5 billion a year until 2028 is required to eliminate the nation’s deficient bridge backlog (Whiteley *et al.*, 2015).



(a)



(b)

Figure 2-2: The main causes of damage in concrete structures (a) and concrete structures vulnerable to damage (b) according to survey participants (Gardner et al. 2018)

2.1.3. Monitoring challenge

The main consequences of concrete deterioration according to Gardner’s survey, were repairs from the contractor and an enhanced structural health monitoring (SHM) regime (Gardner et al., 2018). In the UK, asset owners, such as Highways England and Network Rail, traditionally use visual inspections as the primary source of data for their asset condition (Bennetts et al., 2016). This not only leads to network disruption whilst carrying out the inspections, but it also increases the health and safety risk and cost. The accuracy of visual surveys is also relatively poor, and it was found that asset condition ratings in routine

inspections were assigned with significant variability (Graybeal *et al.*, 2002). To reduce the uncertainty and risks associated with visual inspections, SHM has been used over the recent years to assess structural condition and damage. SHM involves the integration of sensors, data transmission and processing that allow an informed decision-making process about the condition of structures (Xu, 2012). SHM can be classified in 5 levels, as proposed by Taheri (2019), depending on the degree of complexity and level of performance (Figure 2-3). A similar 5-category system was proposed by Webb *et al.* (2015) that comprises of: (1) anomaly detection, (2) sensor deployment studies, (3) model validation, (4) threshold check, and (5) damage detection.

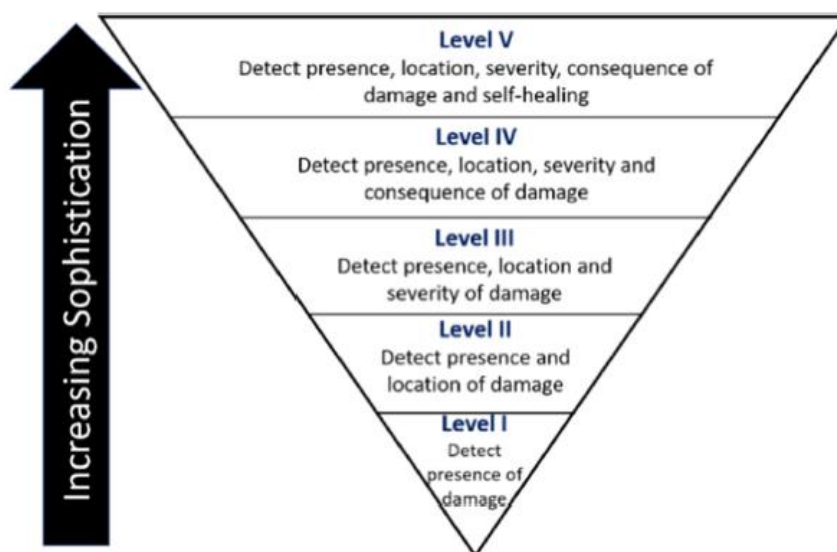


Figure 2-3: Classification of SHM based on the degree of complexity and sophistication (Taheri, 2019)

The sensors used for SHM can monitor several parameters, such as humidity, temperature, reinforcement corrosion and structural stress and strain. Some of the sensor technologies include fibre optics, piezoelectric and electrochemical sensors (Taheri, 2019). For example, ~2000 sensors have been installed on the Queensferry Crossing in Scotland, to monitor the global behaviour of the bridge and its environment in real time (Arup, 2020). However, the use of external sensors has often resulted in high costs, low sensitivity, incompatibility with structural materials and poor durability (Ou and Han, 2009; Spencer, 2009; Horszczaruk *et al.*, 2016). Long-term drift of sensors has been observed in some cases, therefore, calibration of sensing equipment is vital for the infrastructure owners to have confidence in

the sensor data (Webb *et al.*, 2015). The limitations of visual inspections and SHM systems, necessitate a re-evaluation of how structural monitoring is carried out.

In summary, concrete is a versatile construction material that is widely used for engineering structures. However, its production and use are associated with sustainability and durability challenges. Poor durability performance often results in a consequent need to monitor the condition and behaviour of concrete structures, however, monitoring presents some of its own challenges. Therefore, there is an impending need to improve the durability of concrete structures to reduce the inspections and repairs needed.

2.2. Biomimetic and nano-engineered cementitious materials

To mitigate some of the concrete infrastructure challenges, one approach would be to adopt biomimicry principles by developing materials that mimic natural systems (Schlangen and Joseph, 2008; de Rooij *et al.*, 2013). This approach will help in extending the service life of the structures and in turn, reducing the demand for inspections and repairs (de Rooij *et al.*, 2013; Van Tittelboom and De Belie, 2013; Al-Tabbaa *et al.*, 2018). Indeed, over the last years there has been an increasing research interest for smart and biomimetic construction materials. Smart materials can perform several functions such as self-diagnose their condition and environment, self-heal if they are damaged, trigger a response (e.g. shrink or swell) or even self-clean. Some biomimetic materials have already been trialled in construction projects and commercialised. Self-healing concrete was successfully trialled on construction sites in the UK (Davies *et al.*, 2018; Al-Tabbaa *et al.*, 2019). Other examples of biomimetic materials include photocatalytic cements that help in improving air quality by removing volatile organic compounds from the atmosphere (Italcementi, 2010), or pavements that glow in the dark (Tarmac, 2015).

2.2.1. Self-sensing structures

One emerging area of biomimetic materials focuses on self-sensing structures. Self-sensing concrete refers to a material that can sense its condition and identify any damage, whilst maintaining or improving the structural performance (Han *et al.*, 2015). Research in self-sensing concrete is emerging with no known commercial applications to date. Such material would reduce the number of inspections of the infrastructure network and would help in mitigating the monitoring challenge. This could either be achieved with external sensing

mechanisms on the structure's surface or with an intrinsically self-sensing material. The latter approach is preferred since, as discussed earlier, external sensing can lead to several limitations. Therefore, self-sensing concrete in this thesis refers to a two-phase material consisting of a cementitious matrix and functional, conductive fillers as illustrated in Figure 2-4 by Han *et al.* (2014). Conductive fillers are essential, as dried concrete is insulating to electricity and does not allow the passage of current (Neville, 2011). Here, the term *filler* refers to electrically conductive materials that can be added in the cementitious matrix and some of these fillers could also be added to improve the structural performance (such as macroscale fibers).

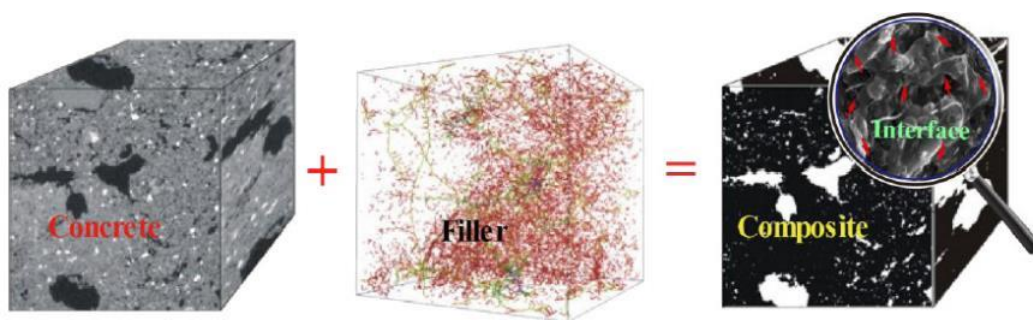


Figure 2-4: Composition of self-sensing concrete, a 2-phase material comprising of the cementitious matrix and functional fillers (Han *et al.*, 2014)

The principle of self-sensing concrete is that when the functional fillers are homogeneously dispersed in a cementitious binder and allow the passage of current; as the material is deformed or stressed, the conductive network will change and consequently affect the electrical resistivity (Han *et al.*, 2014). There are different types of sensing that have been investigated in the literature. One is piezoresistivity, which refers to the change in electrical resistivity with strain (Chung, 2002). The sensing of irreversible strain is what allows damage sensing, whilst the sensing of reversible strain allows dynamic load monitoring (Chen and Chung, 1996). Damage sensing is mainly based on the hypothesis that damage would cause breakage of the conductive network, thereby resulting in an irreversible increase in the electrical resistance. Temperature sensing of cement-based materials has also been developed (Chung, 2012) with carbon and steel fibres.

In terms of functional fillers, at least 10 different types, along with hybrid combinations, have been investigated in different studies and can be classified based on their shape and scale (Figure 2-5). The choice of the functional filler is important as it will dictate the resulting

mechanical, durability, and electrical properties of the composite. The minimum filler dosage that is needed to form continuous electrical paths inside the composite is known as the percolation threshold (Horszczaruk *et al.*, 2016). The percolation threshold depends on many parameters such as filler composition (size and shape); concentration and degree of aggregation (Han *et al.*, 2015). For example, fibrous fillers with a high aspect ratio, reach a percolation threshold at a lower dosage compared to particle fillers. The effective concentration is ~1.5% for fibrous fillers and rises to >5% for particle fillers (Han *et al.*, 2014).

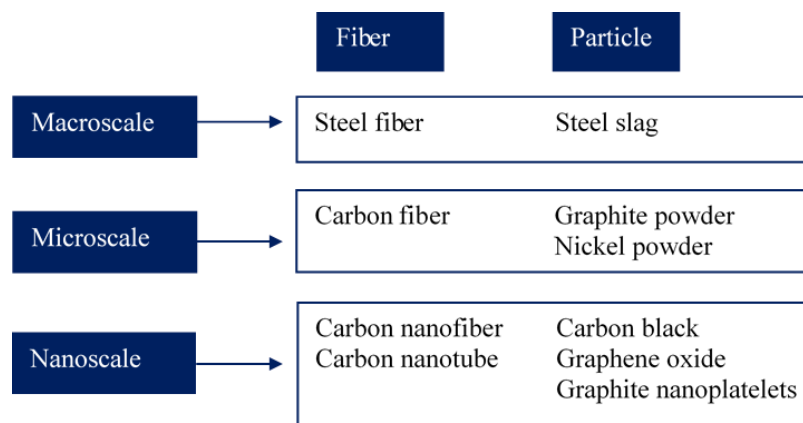


Figure 2-5: Functional fillers that can be used for self-sensing applications based on their size and shape (adjusted from Horszczaruk *et al.*, 2016)

Looking at the macroscale fillers, steel fibres comprise of different types and shapes and can be used as alternatives to large scale reinforcement for applications such as sprayed concrete (Seabrook *et al.*, 2001). The main challenge with steel fibres, is that they could corrode over time if electric current is passed through them (Tang, 2019). Steel slag is an industrial by-product from the steel manufacturing industry, with an annual production of 21 million tonnes in Europe, that can be used as cement replacement or as aggregate replacement in concrete (Jiang *et al.*, 2018). However, there are certain challenges to overcome with using steel slags in concrete, such as the volumetric instability during hydration and the fact that they have low cementitious ability and require activation (Jiang *et al.*, 2018).

Moving to the microscale level, the effect of carbon fibres on the electrical conductivity of cement composites has been extensively researched, and fibre volume fraction, length,

hydration time and mortar composition have all been found to affect the measurements (Fu and Chung, 1997; Wen and Chung, 2006a; Azhari and Banthia, 2012; Loamrat *et al.* 2014). The electrical conductivity has been found to increase as the volume fraction of the carbon fibres increased and with increasing fibre length. This is due to the percolation phenomenon between points 2-3 in Figure 2-6(a), where the carbon fibres start coming into contact (Chiarello and Zinno, 2005) and the longer fibres will form this percolation threshold at a lower dosage. An excess dosage of fibres past the percolation threshold, will not help with an increase in electrical conductivity.

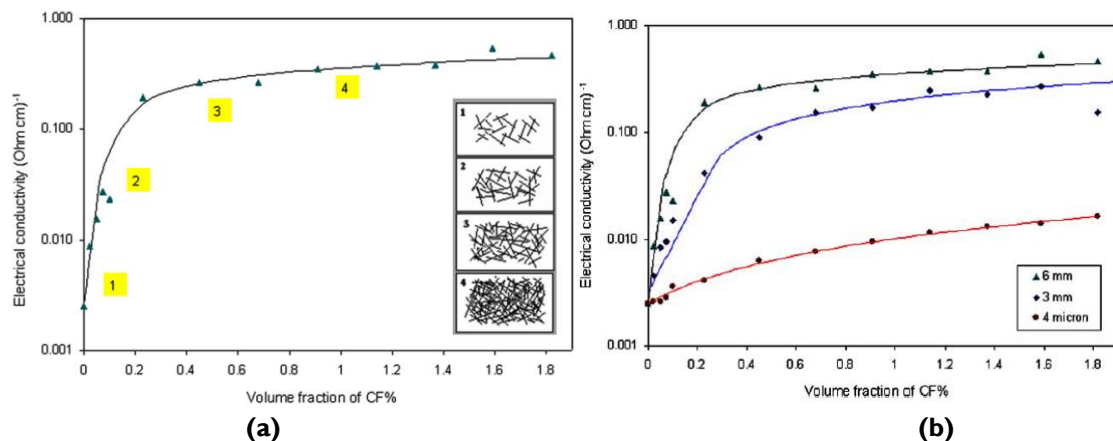


Figure 2-6: Increasing electrical conductivity with volume fraction of carbon fibres due to percolation phenomena (a) and effect of fibre length (b) at 1 day of hydration (Chiarello and Zinno, 2005)

Graphite powder has a layered, planar structure which is relatively soft due to its anisotropy and weak interplanar forces that make the planes slide in respect to one another when a force is applied (Han *et al.*, 2014). Graphite can conduct electricity and heat well, is resistant to chemical attack and is stable under standard conditions (Graphenea, 2017). The potential of using natural graphite powder as a functional filler has been investigated experimentally in this study and a critical analysis of the literature on the use of graphite as a functional filler is presented in Section 2.4.5.1. Conclusively, macroscale and microscale fillers have already been investigated for improving the electrical conductivity of cement composites. The steel-based fillers are prone to corrosion, whilst the carbon-based fillers are costly. Therefore, there is a need investigate how fillers at nanoscale can be used not only for improving the electrical conductivity but also for improving the composite's structural performance.

2.2.2. Nano-engineered concrete

The motivation for this research was to take advantage of nanomaterial advancements and develop a novel cementitious composite that would not only maintain or improve its structural performance, but it would also improve the electrical conductivity to allow for additional functionalities. The International Organisation for Standardization (ISO) defines a nanomaterial as a material that has any external dimension, any internal structure or surface structure in the nanoscale (1-100 nm) (ISO-18401:2017, 2017). The emergence of nanomaterials provides great opportunities for modifying the cementitious matrix at nanoscale (Figure 2-7) and generating multi-functional properties (Chuah *et al.*, 2014; Paul *et al.*, 2018; Xu *et al.*, 2018).

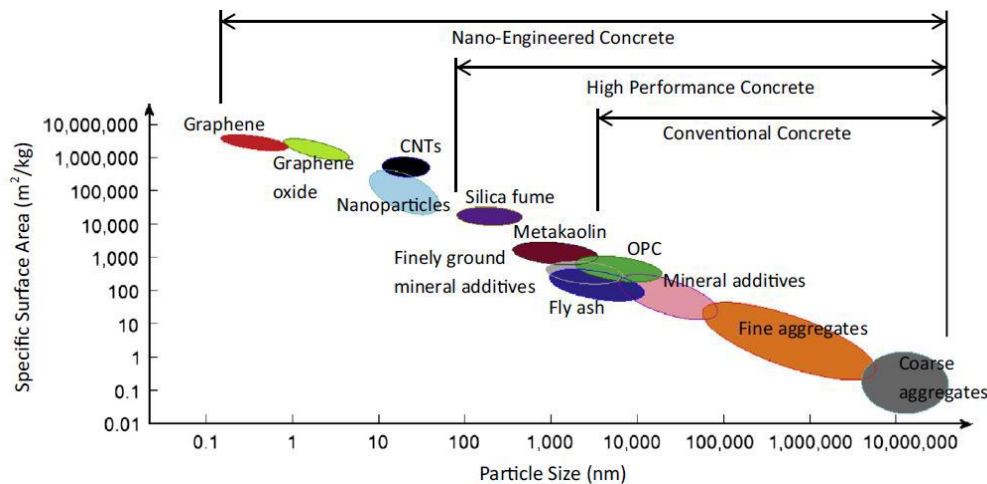


Figure 2-7: Options for cementitious composites with different materials based on their particle size and specific surface area (Chuah *et al.*, 2014)

Certain nanomaterials are already used in civil engineering applications such as nano-silica (nano-SiO₂) and nano-alumina (Al₂O₃) which are primarily employed to enhance the fresh properties of concrete and structural performance (Jones *et al.*, 2016; Bautista-Gutierrez *et al.*, 2019; Du *et al.*, 2019). Interest in biomimetic construction materials has led to some commercial concrete products with nano-titanium oxide (nano-TiO₂), which can induce a self-cleaning ability (Italcementi, 2010; Jones *et al.*, 2016; Krystek and Górski, 2018). However, in recent years, some nanomaterials have also been researched for their electrical conductivity and the biomimetic functionalities that they could induce in cementitious composites. The following section investigates in more detail one such family of materials - graphene-related materials (GRMs) - and their applications in cementitious composites.

2.3. Graphene-related materials (GRMs)

Over the past decade, there has been a proliferation of academic research and many breakthroughs with a newly isolated material called “Graphene” (Geim, 2009). Graphene was isolated in 2004 through graphite exfoliation by two researchers, Geim and Novoselov, who won the Nobel Prize in Physics in 2010 “for groundbreaking experiments regarding the two-dimensional material graphene” (NobelPrize.org, 2020). Graphene is a two-dimensional (2D) structure and comprises of a single layer of carbon atoms that are bonded together to form a perfect honeycomb lattice (Geim and Novoselov, 2007). Graphene has been called a ‘miracle material’ due to some unique properties that even reach theoretically predicted limits, as summarised by Novoselov *et al.* (2012): a Young’s modulus of 1 TPa; intrinsic strength of 130 GPa; thermal conductivity higher than $3,000\text{WmK}^{-1}$; impermeability to any gases, room-temperature electron mobility of $2.5 \times 10^5 \text{ cm}^2 \text{ V}^{-1} \text{ s}^{-1}$ (theoretical limit $2 \times 10^5 \text{ cm}^2 \text{ V}^{-1} \text{ s}^{-1}$) and a higher ability than copper to sustain extremely high densities of electric current. However, these properties refer to pristine, single layer-graphene, that is produced via direct mechanical exfoliation of graphite – a method that is not scalable for industrial applications (Kauling *et al.*, 2018). Therefore, different methods have been developed to fabricate GRMs. The following sections investigate the different GRM structures, production methods and the GRM properties and applications.

2.3.1. GRM structures

2D graphene is one atom thick and in this sense, graphene is considered the base material for GRMs of all other dimensionalities (such as 0D buckyballs, 1D nanotubes and 3D graphite), as illustrated in Figure 2-8 by Geim and Novoselov (2007). Here, the term “graphene” will only refer to the single layer material. Carbon nanotubes (CNTs) are allotropes of carbon with a cylindrical structure which have been successfully produced since 1991 (Iijima, 1991) and can be categorized as single-walled nanotubes (SWCNTs) and multi-walled nanotubes (MWCNTs). When many graphene layers are stacked, 3-dimensional (3D) graphite is formed (Figure 2-8), which has a crystalline structure and carbon atoms are strongly bonded together in 2D layers, but their interplanar bonding is weak (Do and Pham, 2010). For this reason, graphite has been used for hundreds of years and its weak interplanar forces allow it to be used for applications such as pencils. Based on the production method, there are other forms of GRMs that should be considered. When graphite is exfoliated to a multi-layer product, it results in what is called graphene/graphite

nanoplatelets or multi-layer graphene (GNPs). In this thesis, GNPs will refer to a material with less than 100 graphene layers. A summary of the nomenclature that is followed in this thesis is summarised in Table 2.1.

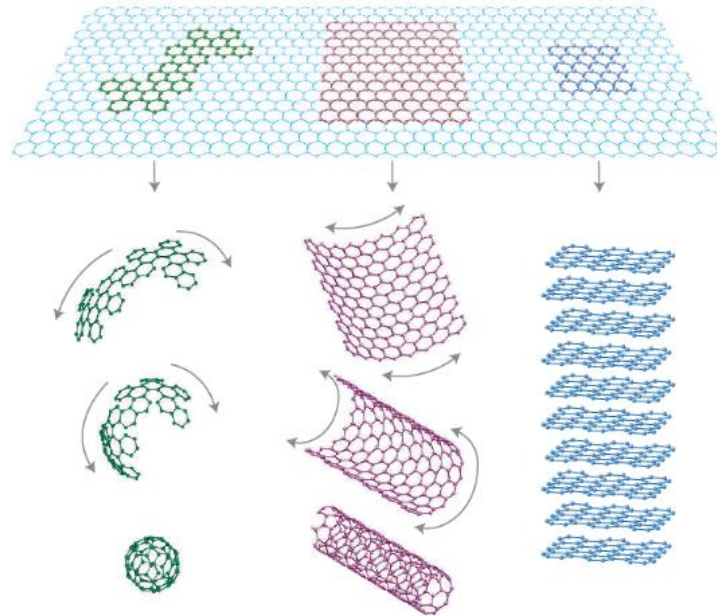


Figure 2-8: 2D graphene (top) can be wrapped in 0D buckyballs (bottom-left), rolled into 1D CNTs (bottom-center) or stacked in 3D graphite (bottom-right) (Geim and Novoselov, 2007)

Table 2.1: Nomenclature for GRMs in this thesis

Nomenclature in this thesis	Description
Graphene	The pristine, 2D single layer graphene
Carbon nanotubes (CNTs)	The 1D carbon nanotube including Single-wall CNTs (SWCNTs) and multi-wall CNTs (MWCNTs)
GNPs	Graphite/graphene nanoplatelets (or multi-layer graphene), referring to a product with less than 100 layers of stacked 2D graphene
GO	Graphene oxide comprising either a single or multi-layer graphene that has additional functional groups on its surface
rGO	Reduced graphene oxide
Graphite	3D material that comprises of many stacked 2D graphene layers (>100) and is characterised by weak interplanar forces

Two materials, graphene oxide (GO) and reduced graphene oxide (rGO) have also attracted great scientific interest due to the functional groups on their surface. A schematic of the GO and rGO structures along with the fabrication methods were illustrated by Amieva *et al.* (2016) in Figure 2-9. The oxidation of natural graphite leads to graphite oxide which when exfoliated, yields graphene oxide (GO). GO is usually synthesised following the

Brodie, Staudenmaier or Hummer's methods (Zhu *et al.*, 2010). It is a monolayer material¹ with different oxygen functional groups such as hydroxyl (–OH), carboxyl (–COOH), epoxide (C–O–C), and carbonyl (C=O) and is highly hydrophilic as the water is strongly bound to GO through hydrogen bonding interactions (Dreyer *et al.*, 2010; Zhu *et al.*, 2010). Reduction of GO (e.g. thermal or chemical reduction) leads to the formation of reduced graphene oxide (rGO), which partly restores the structure and properties of graphene by removing some of the oxygen-containing groups (Pei and Cheng, 2012). The main differences between GO and GNPs lie in the dispersibility potential and their electrical conductivity. The former is easier to disperse in water due to its oxygen groups, whilst GNPs do not possess any oxygen groups and are hydrophobic (Leenaerts *et al.*, 2009) with attractive forces between the layers that can lead to particle agglomeration (Shabafrooz *et al.*, 2018; Wang, Jiang, *et al.*, 2018). GO is electrically insulating due to the disrupted sp^2 bonding network and the oxygen-containing groups (Dreyer *et al.*, 2010; Du *et al.*, 2020). On the contrary, GNPs allow the passage of electric current, which makes them more suitable for functional applications.

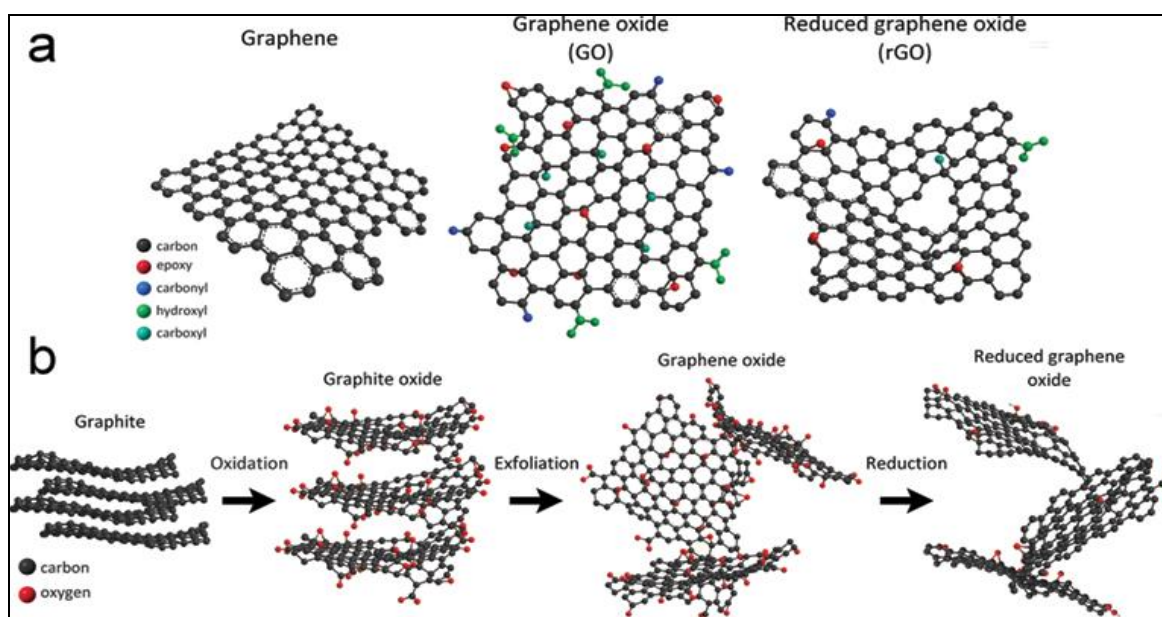


Figure 2-9: Oxidising and exfoliating graphite structure leads to graphene oxide (GO) which when reduced further leads to reduced graphene oxide (rGO) (Amieva *et al.*, 2016)

¹or multi-layer, in which case it is referred to as graphite oxide or graphene oxide nanoplatelets

2.3.2. GRM production methods and applications

Each GRM production method will result in varying fundamental properties (e.g. number of layers, average lateral size and carbon-to oxygen (C/O) atomic ratio) and it will also have an effect on cost and scalability (Novoselov *et al.*, 2012). There are generally two fabrication approaches; a top-down approach where graphene is exfoliated from graphite and a bottom-up approach where graphene can be assembled (Kauling *et al.*, 2018). Some of the production methods commonly employed include micromechanical cleavage, liquid phase exfoliation (LPE), chemical vapour deposition (CVD) and growth on silicon carbide (SiC) (Ferrari *et al.*, 2015; Phiri *et al.*, 2017). Raccichini *et al.* (2015) analysed the most common fabrication methods in terms of quality (G), cost aspect (C; a low value = high production cost), scalability (S), purity (P) and yield of the overall production (Y) as shown in Figure 2-10(a). For applications, such as advanced electronics, GRM quality and purity are very important and therefore, mechanical exfoliation, bottom up synthesis and CVD are more suitable. For bulk structural applications, large material volumes are required, whilst concrete is a commoditised product that only costs circa £85/m³ (Costain, 2020). Consequently, scalability and cost are of primary concern, and techniques such as LPE are more suitable. This was reinforced by Novoselov *et al.* (2012), who plotted quality versus price and showed that LPE resulted in lower costs than other methods and is therefore more suitable for applications in composites (Figure 2-10b).

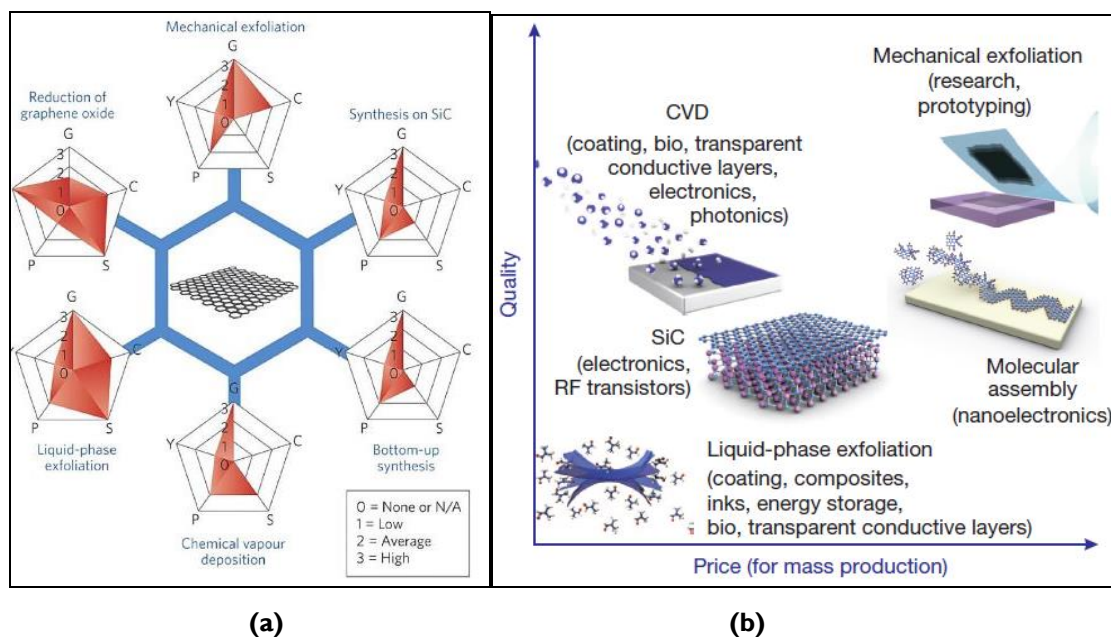


Figure 2-10: Evaluation of the different GRM fabrication methods (a) (Raccichini *et al.*, 2015) and quality versus price (b) (Novoselov *et al.*, 2012)

LPE exposes the starting material (graphite) to the combined action of a solvent and mechanical impact as a result of shear stress and sonication (Novoselov *et al.*, 2012; Wei and Sun, 2015; Monajjemi, 2017). The solvent is typically non-aqueous, as pure graphene layers are hydrophobic and it is difficult for them to be directly exfoliated and stabilised in water (Wei and Sun, 2015). During the sonication, the graphite starts splitting into platelets and a prolonged treatment will result in a greater fraction of monolayer flakes (Novoselov *et al.*, 2012; Phiri *et al.*, 2017). A schematic for the LPE methodology is shown in Figure 2-11. However, a study of over 60 producers found that the GRM quality is rather poor, and many companies produce “graphene” with over 100-layer thickness (Kauling *et al.*, 2018). Likewise, Kovtun *et al.* (2019) analysed 12 commercial products and found that the products with low defectivity (sp^2 bonds > 95%) had a low surface area, whilst when the GNPs were highly exfoliated, they had a lower sp^2 content, hence industrial scale exfoliation will introduce defects. Nonetheless, LPE is the most suitable fabrication technique for bulk applications.

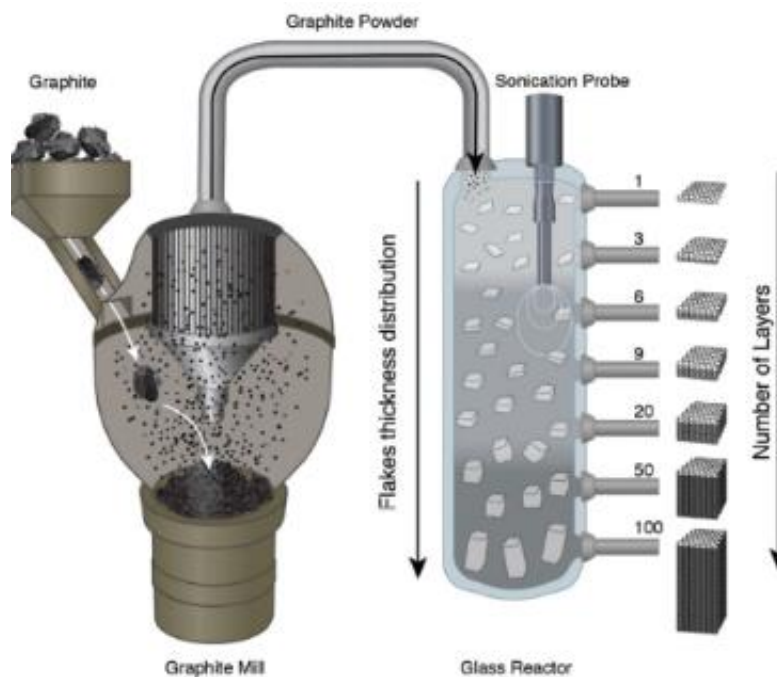


Figure 2-11: Liquid Phase Exfoliation (LPE) of graphite (Kauling *et al.*, 2018)

2.4. Graphene nanoplatelets (GNPs) in cement composites

In this thesis, GNPs fabricated via LPE, were investigated experimentally. The research interest in GNPs lies in the fact that the regular structure of the graphene layers permits an increase in the electrical conductivity of the cementitious matrix; therefore, allowing for additional functionalities, such as a self-sensing mechanism. This section analyses the relevant literature on the properties of cementitious composites that are modified by GNPs. Firstly, the dispersion techniques will be explored, followed by the effect of GNPs on the fresh properties, hydration, mechanical and durability performance of cementitious composites. Finally, the use of natural graphite and GNPs as conductive fillers will be discussed.

2.4.1. Dispersion studies

Reviewing the literature has revealed that the homogeneous dispersion of GNPs in the cement matrix was a key challenge (Korayem *et al.*, 2017; Du *et al.*, 2019), upon which the mechanical (Liu *et al.*, 2019); durability (Shamsaei *et al.*, 2018; Zhao *et al.*, 2020) and electrical conductivity (Chia and Huang, 2017; Tian *et al.*, 2019; Wang and Aslani, 2019) properties could depend. This is because of the large GNP surface area that leads to high van der Waals forces (attractive forces) between the individual particles (Du *et al.*, 2020) and because of their hydrophobic nature (Texter, 2014; Mehmood *et al.*, 2020). Dispersion of GNPs can take place both with mechanical and chemical methods (or a combination). The mechanical methods include high speed shear mixing, ball milling, magnetic stirring and ultrasonication (Bastos *et al.*, 2016; Wang and Aslani, 2019). The chemical methods include covalent or non-covalent functionalisation; the first involves chemical modification of the material using acids and oxidants; whilst the latter is based on a non-covalent interaction from surfactants that preserve the GNP structure (Wang and Aslani, 2019). This section reviews the dispersion methods that have been employed in the literature, with a focus on those that would be more suitable for cementitious composites. The techniques for assessing dispersion are also discussed.

2.4.1.1. Mechanical dispersion

Sonication of GNPs in an aqueous solution is one of the most common dispersion techniques in the literature (Korayem *et al.*, 2017). Sonication avoids damage to the material that could be induced through other mechanical methods (such as high shear mixing or ball milling) (Han *et al.*, 2015; Wang and Aslani, 2019). During sonication, mechanical vibrations

are transferred in the liquid which cause the formation and collapse of microscopic bubbles (cavitation) that in turn aid the dispersion of materials (Zhang and Chen, 2019). At high frequencies (>20 kHz) this process is called ultrasonication. The key sonication parameters include, frequency, power input, duration, type of sonication and temperature (Muthoosamy and Manickam, 2017). Sonication can be performed using either a bath sonicator or a probe/tip - the latter has a higher power output and would result in more efficient dispersion, however, it could also induce damage to the material (Zhang and Chen, 2019). Cavitation, however, leads to a temperature increase in the liquid due to the release of high energy levels (Konsta-Gdoutos *et al.*, 2010). Therefore, the temperature of the sonicated liquid must be carefully controlled to ensure that the water does not evaporate (which would affect the w/c).

In terms of sonication duration, Du and Pang (2018) found that at least 60 minutes were needed to deflocculate the GNP agglomerates and stabilise them in an aqueous solution for 24 hours. Using UV-Vis spectroscopy, it was found that to disperse carbon nanotubes (CNTs), which are also hydrophobic, a minimum sonication time of 30 minutes was needed, whilst no positive effect was observed after 120 minutes (Sobolkina *et al.*, 2012). Within 30 – 120 minutes however, the duration increase led to better dispersion. On the contrary, for the hydrophilic GO, the increase in the sonication duration had a negligible effect (Chuah *et al.*, 2018) as shown in Figure 2-12. This agrees with a study from Gao *et al.* (2018), who used a GO/CNT cement composite and found, through UV-Vis, that the degree of dispersion reached a plateau after 20 minutes of sonication. In the same study, however, it was shown that increasing the ultrasonication period from 1 to 60 minutes, reduced the average particle size of the GO/CNT suspension from 542 to 220 nm. Zhang and Chen (2019) also showed that increasing ultrasonic duration (1 - 5 hours) or power (at 720, 840, 960, 1080W), enhanced the GNP dispersion and exfoliation, however, the fragmentation degree also increased. Therefore, excessive sonication does not necessarily lead to better GNP dispersion, and suitable parameters must be chosen that balance the separating and scissoring effects of the ultrasonication (Gao *et al.*, 2019).

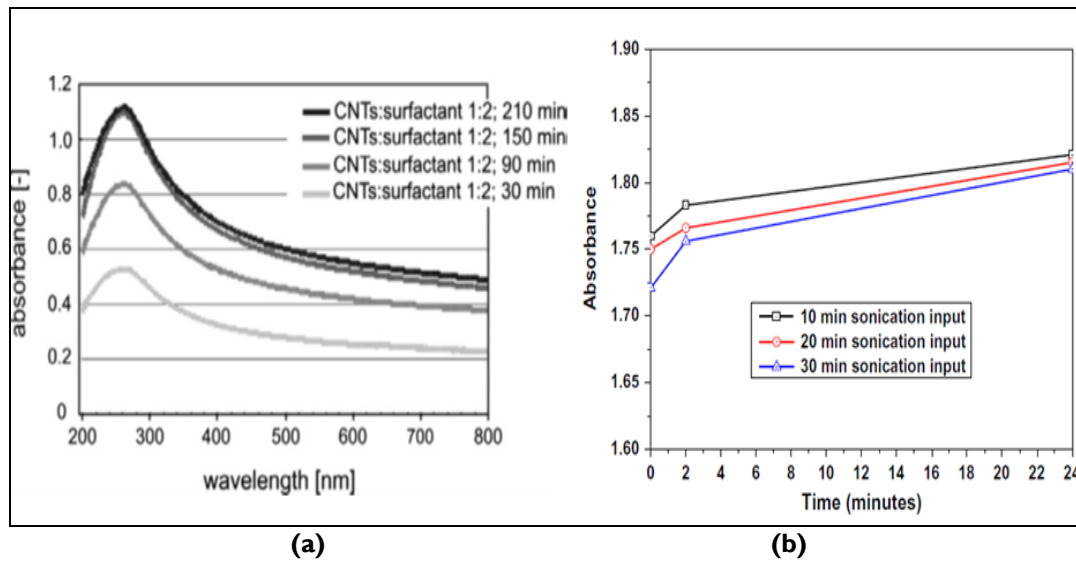


Figure 2-12: UV-vis showing an increase in sonication time resulting in better dispersion of hydrophobic CNTs (a) (Sobolkina *et al.*, 2012) whilst no pronounced effect is observed for the hydrophilic GO (b) (Chuah *et al.*, 2018).

2.4.1.2. Chemical dispersion methods

Chemical dispersion can include covalent or non-covalent functionalisation. Aggressive chemical functionalisation (e.g. the use of strong acids) could introduce defects in the material (Wang and Aslani, 2019). Instead, non-covalent functionalisation with commonly used surfactants and admixtures, would be a more appropriate solution for use in cementitious matrices. The dispersion capability of chemical admixtures is achieved by wetting, electrostatic repulsion and/or steric hindrance, while for mineral admixtures it is achieved by gradation, adsorption and/or separation (Han *et al.*, 2015). Starting from the latter, some authors have investigated the use of mineral admixtures, such as silica fume (SF), in dispersing GRMs, however, most studies are focused on the dispersion of the hydrophilic GO. Early studies showed that SF improved the GO dispersion in cement paste by mechanically separating the GO sheets and preventing aggregation, however, excess SF (at 5% and 10% by weight) had a negative effect on the compressive strength (Li *et al.*, 2016). However, this contradicts a more recent study from Lu *et al.* (2018), who showed that even though SF reduces the GO size and helped its disaggregation in water, it actually had a negative effect when the GO was dispersed in a cement pore solution. The authors explained that this could be due to the divalent cations (Ca^{2+}) in the cement pore solution that can interlock the SF and GO and lead to the re-agglomeration. For 0 - 15% SF and 0.1wt% and 2wt% GNPs, it was shown that moderate amounts of SF could aid the GNP

dispersion and refine the pore structure, however, excessive SF compromised the mechanical and electrical conductivity properties of the composite (Bai et al., 2018). Without SF, the GNP aggregations were up to 100 μm in size, which reduced to 20 μm when SF was added at 15wt%. However, the dispersion was only investigated by SEM and macroscale methods (strength testing and conductivity) and therefore it is difficult to confidently reach a conclusion that SF aids the dispersion of GRMs. The 28-day SEM images from this study show that the size of a GNP aggregation in Figure 2-13 (a) with no SF was much larger compared to when SF was introduced (Bai et al., 2018). With SF, the GNP agglomerates reduced, and they were broken apart (as shown by the circles).

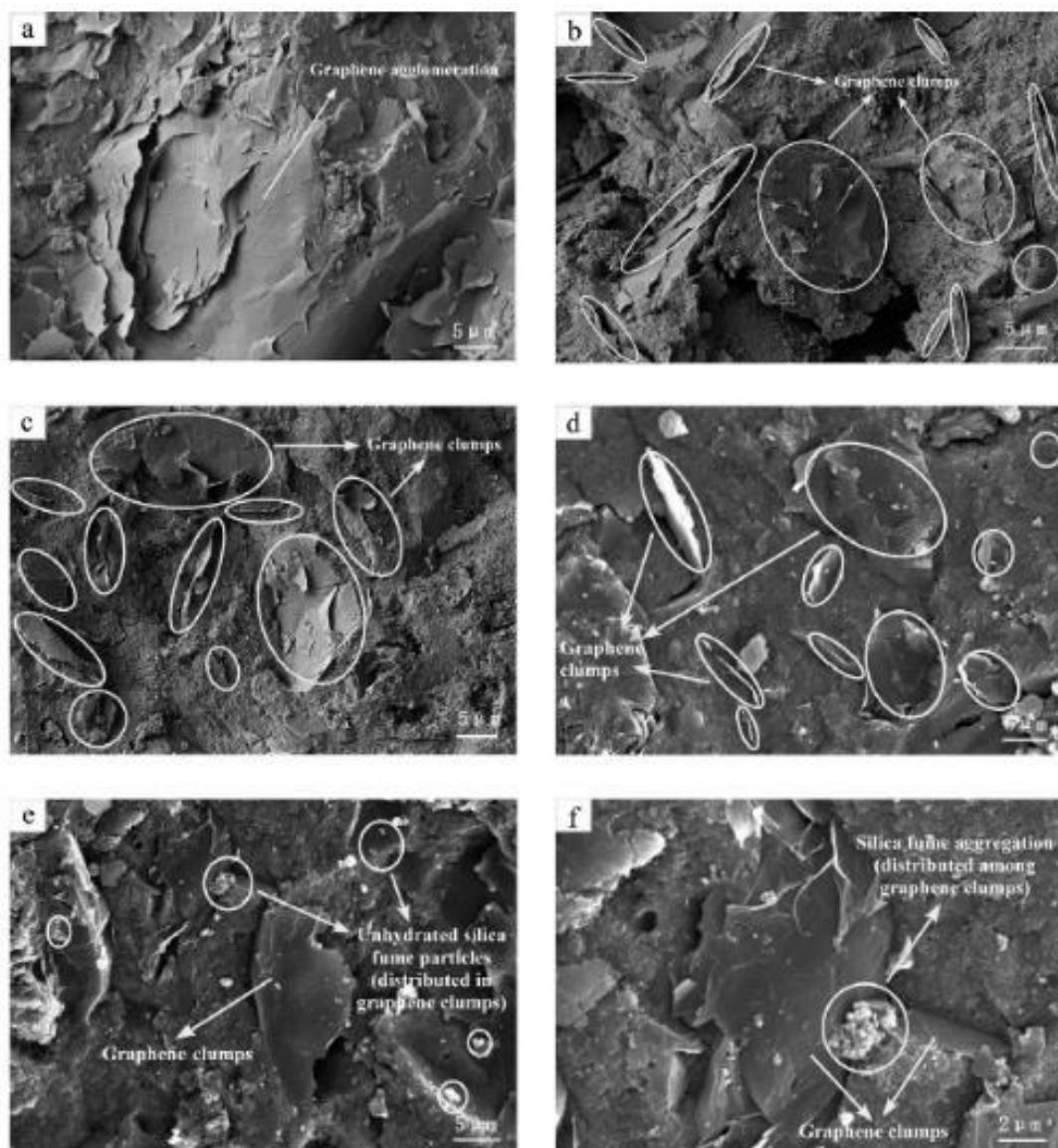


Figure 2-13: SEM of 28 days samples (a) No SF, (b) 5% SF (c) 10% SF, (d-f) 15% SF (Bai et al., 2018)

In terms of chemical admixtures, superplasticisers are water soluble organic polymers that act either as high range water reducers (for reducing the w/c) or as plasticisers (for improving workability). There are different types of superplasticisers, including lignosulphonates, sulphonated naphthalene-based and polycarboxylates. Lignosulphonates and naphthalene-based work by electrostatic repulsion; their negatively charged molecules attach to the positively-charged cement particles and make them repel each other (Figure 2-14a). Polycarboxylate dispersants are comb-like polymers that are composed of a polymer backbone and side chains (Sabziparvar *et al.*, 2019) and the length of polymer and chains can be engineered to provide the required workability or repulsion forces. Polycarboxylate-based superplasticisers work primarily by steric hindrance; the polycarboxylate polymers adsorb on to the cement particles and create a physical barrier between them to prevent agglomeration (Figure 2-14b).

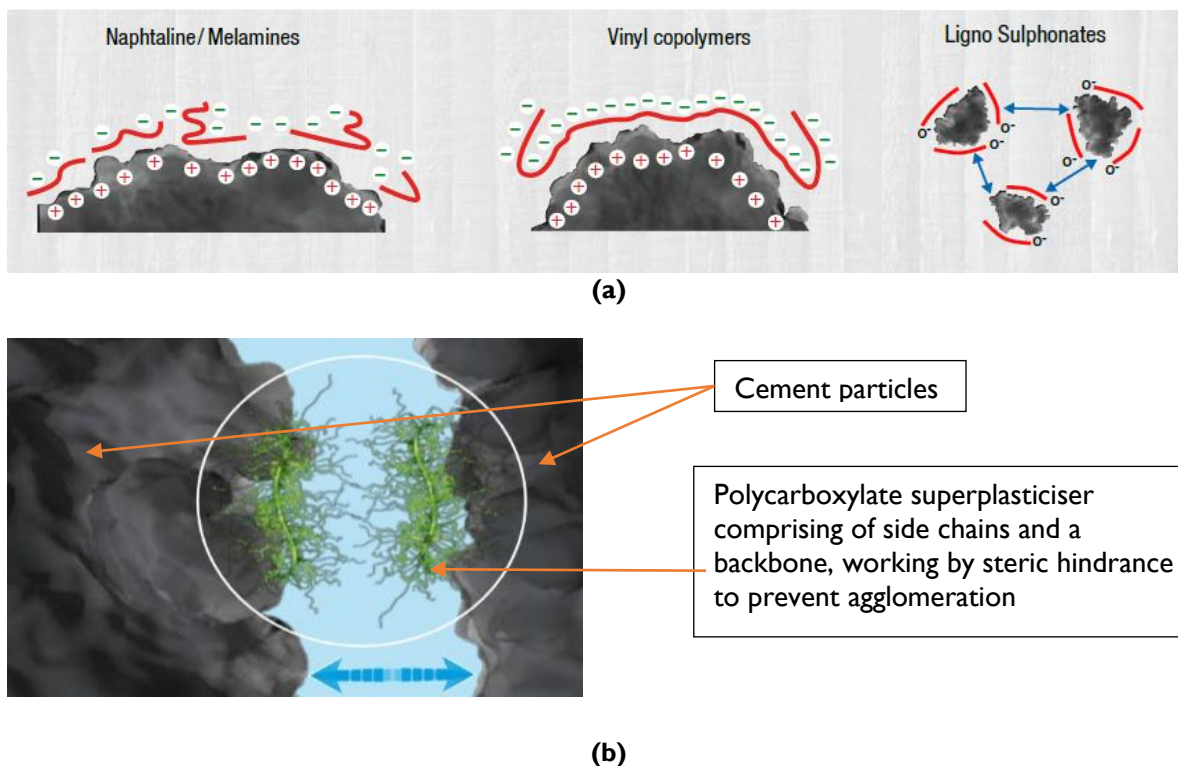


Figure 2-14: Electrostatic repulsion of naphthalene based superplasticisers and lignosulphonates (a) and polycarboxylate superplasticiser steric hindrance effect (b) (Sika Services, 2009)

Several studies focused on the use of superplasticisers for GRM dispersion, however, they primarily tested the hydrophilic GO. Different superplasticisers were tested for GO dispersion in a simulated cement pore solution by Zhao *et al.* (2018) who found that

polycarboxylates performed better over time, whilst the lignosulphonate and naphthalene-based ones led to GO sedimentation within 1 hour. Therefore, if the lignosulphonate and naphthalene-based plasticisers were not effective for dispersing the hydrophilic GO, then they might not be effective in dispersing hydrophobic GNPs. This agrees with another study that showed that the polycarboxylate had the best GO dispersion stability after 30 days compared to other commonly used surfactants such as a naphthalene based superplasticiser, a sodium dodecyl sulfate (SDS) and an alkylammonium salt of a high molecular weight copolymer (Sabziparvar *et al.*, 2019). Polycarboxylate polymer superplasticisers were also found to be more effective in uniformly dispersing GNPs compared to polycarboxylate ester (Metaxa, 2015). Looking at hydrophobic GRMs, such as CNTs and GNPs, the sodium dodecyl benzene sulfonate (SDBS) surfactant was found to be better for dispersing GNPs compared to other surfactants (Liu *et al.*, 2019). This agrees with Adresi *et al.* (2016) who found that the polycarboxylate superplasticiser dispersed MWCNTs worse than SDS but created less foam. However, SDBS is electrically insulating and even though it might disperse GNPs adequately, it will prevent the formation of electrically conductive paths, hence it will not be possible to use the composite for functional applications (Choi *et al.*, 2020). A recent study compared the efficiency of two polycarboxylate comb-type copolymers with different chemical backbone lengths to disperse CNTs and found that the longer backbone was more effective in filler dispersion (Liebscher *et al.*, 2020).

2.4.1.3. Combination of dispersion techniques

Both mechanical and chemical methods could be effective in dispersing GNPs, however, most studies follow a combination of these two techniques (Table 2.2). Konsta-Gdoutos *et al.*, (2010) found that the combination of a surfactant and sonication was more efficient in dispersing MWCNTs (which are hydrophobic) than the surfactant alone. The use of a polycarboxylate superplasticiser with sonication was found to be the best for dispersing GNPs, which was confirmed by a reduction in the electrical resistivity of the cement paste as shown in Figure 2-15 (Metaxa, 2015). A lower electrical resistivity indicated better dispersion as the GNPs were uniformly distributed and able to form a conductive network within the cement matrix. Recent studies have also combined ultrasonication with the use of

a polycarboxylate superplasticiser to ensure effective dispersion of hydrophobic GRMs (Ho *et al.*, 2020; Liebscher *et al.*, 2020; Wang, Dong *et al.*, 2020).

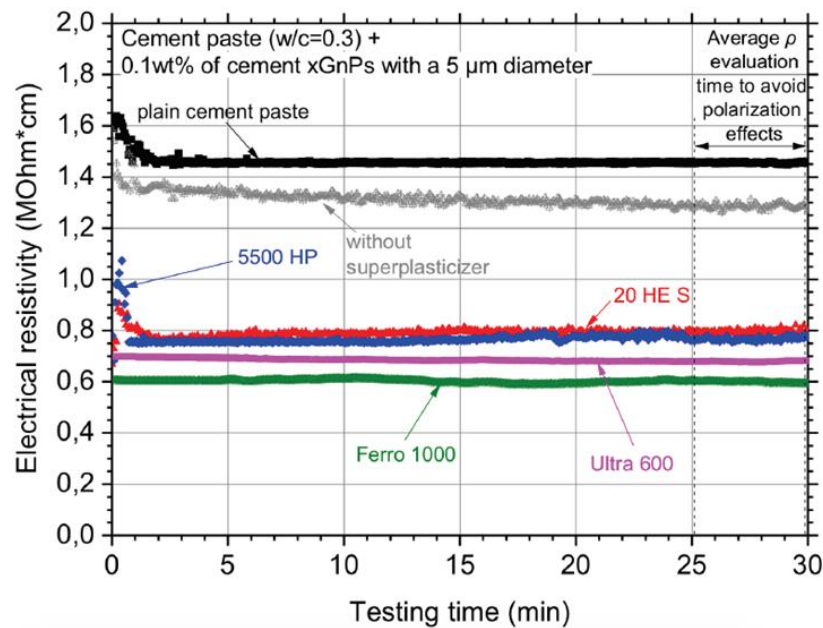


Figure 2-15: Typical electrical resistivity curves of GNP nanocomposites with different superplasticiser types (Metaxa, 2015).

Table 2.2 summarises the relevant literature on the GNPs dispersion. By observing the different columns, all but two papers, used a combination of sonication and a chemical treatment to disperse GNPs. The GNPs varied in terms of fundamental properties, such as specific surface area (SSA), size and thickness and the dosages were also varied so the findings cannot be directly compared. Furthermore, the sonication parameters (e.g. duration, power input, type), also varied between the studies. Just under half of the studies (9 out of 21) employed a polycarboxylate superplasticiser for dispersing the GNPs. Hence, a combination of dispersion techniques has been employed widely in the literature and it is expected to result in better mixing than one dispersion technique alone.

2.4.1.4. Effect of mixing sequence

The GRM mixing sequence in the cement paste has been investigated in some studies, however, the key focus was on GO (hydrophilic). To test the effect of the mixing sequence, Long *et al.* (2018) prepared two GO suspensions. In suspension 1, the GO was first mixed with cement (dry mix) and then the water and the polycarboxylate superplasticiser were added, whilst for suspension 2, the water and cement were mixed first (cement paste) and

the GO was added later along with the superplasticiser. In the first case the suspension re-agglomerated over time while adding the GO at the same time with the superplasticiser helped in ensuring the stability of dispersion. This was also confirmed in another study, where four different mixing sequences were trialled and it was found that that the optimum mixing sequence was to disperse GO and the polycarboxylate superplasticiser first and then add the suspension to the dry contents (Lu *et al.*, 2017). In a study that investigated the effect of mixing sequence on the GNPs dispersion, it was also confirmed that pre-mixing the GNPs in water and superplasticiser before adding to cement was more efficient than dry mixing of GNPs and cement (Ozbulut *et al.*, 2018). Therefore, a pre-dispersion of the GNP in a suspension containing water and superplasticiser is necessary before this suspension is added to the dry components (cement and sand).

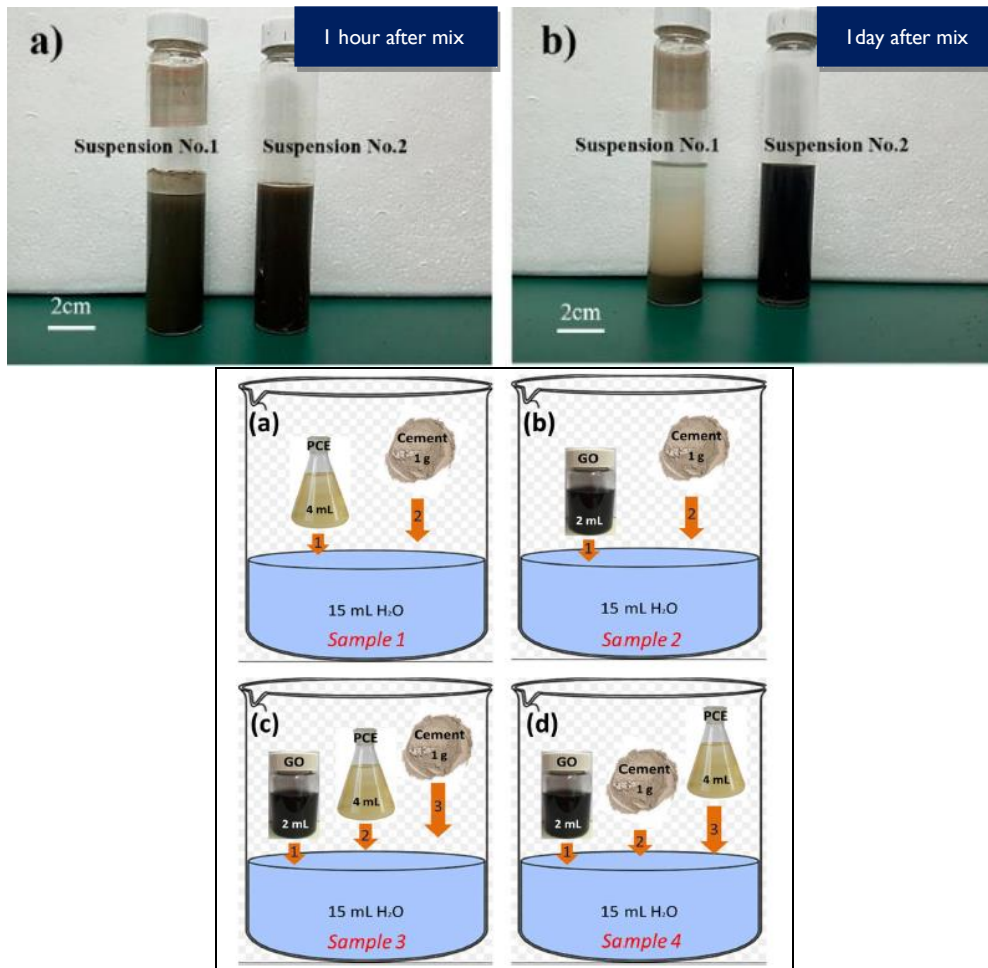


Figure 2-16: Effect of mixing sequence on the suspension stability over time as shown by Long *et al.* (2018) (top) and four different mixing methods as investigated by Lu *et al.* (2017).

2.4.1.5. Assessment of GRM dispersion

Various methods have been used either in isolation or in combination to investigate the GNP dispersion (Du *et al.*, 2019) and a summary is provided in Table 2.2. Looking at the “assessment technique” column, there was no single direct method of assessing the dispersion of GNPs and a combination of methods were employed. The studies used a minimum of two techniques to evaluate dispersion which was either assessed directly with microstructural techniques or indirectly via macroscale testing. Microscale observations are more direct as they look at the microstructure and assess the GNP dispersion in a suspension and the cement matrix. A commonly used technique is UV-Vis spectroscopy, that is based on the principle that the higher the absorbance, the better the GNP dispersion. This provides a method to check the dispersion stability in aqueous suspensions, however, it is not always representative of dispersion in the cement matrix. Some authors based their assessment on visual observations and zeta-potential measurements but again, these techniques focus on GNP dispersion in the water rather than the cement matrix. Scanning Electron Microscopy (SEM) and Transmission Electron Microscopy (TEM) are frequently used to investigate the interactions in the cement matrix, however, the main disadvantage is that only a very small area of the material is tested at a time and the results do not necessarily represent the bulk. However, most commonly, the authors assess the dispersion effectiveness indirectly via macroscale testing such as rheology, compressive and flexural strength tests, durability tests and electrical conductivity. Therefore, a combination of experimental techniques is necessary to understand the effectiveness of GNP dispersion.

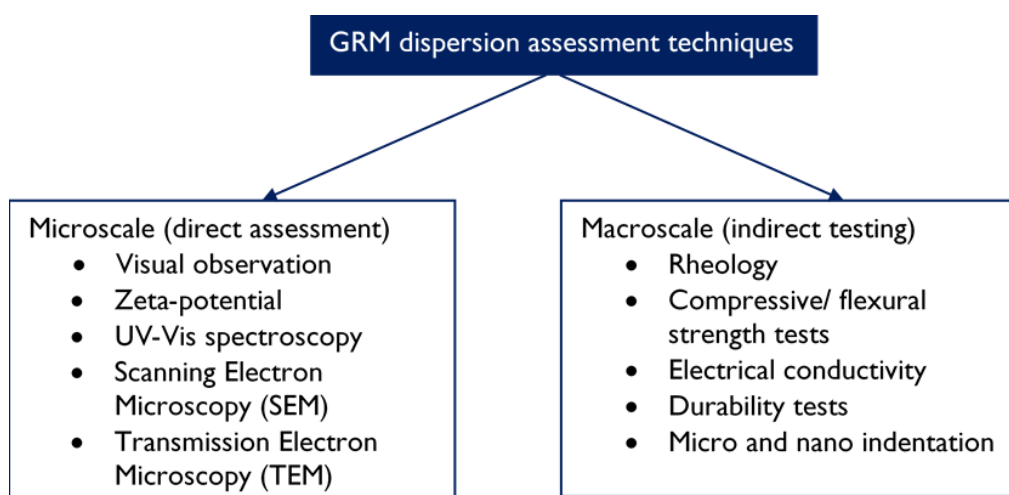


Figure 2-17: GRM dispersion assessment techniques

Table 2.2: GNP dispersion techniques in the literature and assessment method

GNP dosage (%bwoc)	Dispersion / mixing method and assessment technique			
	Sonication	Superplasticiser (dosage % bwoc)	Assessment technique	Ref.
352 m ² /g SSA, 2.6 nm thick; 2.6 μm; 5, 10%, 15, 20%	✓ 2 hours of ultrasonication in water and superplasticiser	✓ naphthalene sulfonate-based plasticiser	<ul style="list-style-type: none"> • SEM • Indirectly via electrical resistivity testing 	(Le <i>et al.</i> , 2014)
24 m ² /g SSA, 37 nm thick; 8 μm size; 2.5, 5.0 and 7.5%	✓ 1-hour ultra-sonication horn in a water bath	✓ naphthalene sulfonate-based plasticiser at 50% of the weight of GNP	<ul style="list-style-type: none"> • Visual observation • Indirectly – strength and durability 	(Du and Pang, 2015)
120-150 m ² /g SSA, 6-8 nm thickness; 5 μm; 0.1%	✓ probe ultrasonicator at 50 % of its power, at cycles of 0.5 s	✓ polycarboxylate ester (<i>ViscoCrete 20 HES</i>) and polycarboxylate polymers (<i>ViscoCrete Ferro 1000, ViscoCrete Ultra 600, ViscoCrete 5500 HP</i>).	<ul style="list-style-type: none"> • Visual observation • Indirect - Electrical conductivity 	(Metaxa, 2015)
120-150 m ² /g SSA, 6-8 nm thickness; 25 μm; 0.05%	✓ 20 min (frequency 40 KHz, power 180 W)	✓ methylcellulose as a surfactant + superplasticizer + defoamer	<ul style="list-style-type: none"> • UV-Vis • Optical microscope • SEM & TEM 	(Wang <i>et al.</i> , 2016)
3 different GNPs; 23 – 352 m ² /g SSA, 3 – 71 nm thick, 2.6 – 8 μm; 0.5, 1.0, 1.5, 2.0, 2.5%	✓ 2 hours with a high-power ultra-sonication horn in a water bath to control temperature	✓ naphthalene sulfonate-based high range water reducer (<i>Darex Super 20</i>)	<ul style="list-style-type: none"> • SEM • Indirectly - strength, RCPT, electrical conductivity 	(Du <i>et al.</i> , 2016)
192 m ² /g SSA, 5 nm thick, 6.8 μm. 0.025, 0.05, 0.1, 0.2, 0.4, 0.8, 1.6, 3.2, 6.4%	✓ 30 mins in water and superplasticiser	✓ Polycarboxylate superplasticiser	<ul style="list-style-type: none"> • SEM-EDS • Indirectly via strength, MIP, RCPT 	(Liu <i>et al.</i> , 2016)
500 m ² /g SSA, 1-5 nm thick, < 2μm. 0.2% vol.	✓ 1 h in water and superplasticiser	✓ polycarboxylate superplasticiser (<i>Sika Viscocrete</i>)	<ul style="list-style-type: none"> • SEM • Indirectly - strength 	(Han <i>et al.</i> , 2017)
120-150 m ² /g SSA, 2-4.2 nm thick. 0.02, 0.05, 0.10 and 0.15%	✓ ultrasonic processing (360W) for 30 min	✓ polyoxyethylene (40) nonylphenylether (<i>CO890</i>) decoration.	<ul style="list-style-type: none"> • AFM; XPS; SEM • Indirectly via chloride penetration test 	(Wang and Zhao, 2017)

24 m ² /g SSA, 37 nm thick, 8 µm. 0.25%, 0.5%, 1%, 2%, 4%	✓ ultrasonicator (19.1 mm tip). 300W and 20 kHz. ice bath. 0, 15, 30, 60, 120 mins.	✓ polycarboxylate superplasticizer (SP) (ADVA-181N, Grace Construction, 1.125 g/cc)	<ul style="list-style-type: none"> • UV-Vis • Zeta-potential • Visual observation • SEM 	(Du and Pang, 2018)
12 nm thick, 4.5 µm size; 0.03, 0.05 and 0.10%	✓ Ultrasonication used for 3 min	✓ Polycarboxylate ether-based superplasticizer	<ul style="list-style-type: none"> • Rheology • SEM-EDS 	(Rehman et al., 2018)
Different GNPs; 0 (reference) - 8 g/L ²	✓ High speed shear mixer - Silverson L5M laboratory mixer. 2 h at 5000 rpm.	✓ sodium cholate as a surfactant for functionalising GNPs	<ul style="list-style-type: none"> • Visual observation • SEM-EDS 	(Dimov et al., 2018)
120-150 m ² /g SSA, 6-8 nm thick, 25 µm; 0.1%, 1%, 2.5%, 5%, 7.5% and 10% bwoc	Three different dispersion techniques with a polycarboxylate superplasticiser: <ul style="list-style-type: none"> • GNPs + water + superplasticiser in a bath sonicator for 1.5 h first. • Dry mixing of GNP + cement + sand for 10 mins at 125 rpm. • GNPs + water+superplasticiser - high-speed shear mixer, 15 mins, 3000 rpm. 		<ul style="list-style-type: none"> • SEM • Indirectly via electrical resistivity testing 	(Ozbulut et al., 2018)
40 m ² /g SSA, 4-20 nm thick, 2-16 µm size; 0.01%, 0.025% and 0.05% bwoc	✓ probe ultrasonication (20 kHz, 300W, 450 W and 600W). 1-6 times and each stage was 5 minutes and placed in ice bath after each stage	<ul style="list-style-type: none"> ✓ anionic: sodium dodecyl benzene sulfonate (SDBS) and sodium dodecyl sulfate (SDS) ✓ cationic: CTAB ✓ non-ionic: Triton X-100 ✓ polycarboxylate superplasticiser 	<ul style="list-style-type: none"> • UV-Vis • Centrifugation • SEM-EDS • Slump test • Indirectly by strength and MIP 	(Liu, Fu, Yang, et al., 2019)
150-250 m ² /g SSA, 5-10 µm size; 0.05% and 0.1% bwoc	✓ probe ultrasonication. 100 cycles - 1 pulse (6 sec) & 3 sec rest + ice bath. Total energy 270,000 J.	✓ anionic type surfactant with hydrophilic groups	<ul style="list-style-type: none"> • SEM-EDS • Indirectly via strength, MIP, strength • Microindentation 	(Liu, Fu, Ni, et al., 2019)
32 m ² /g SSA, 3-10 nm thickness, 5-10 µm size; 0.05%, 0.1%, 0.5% and 1% bwoc	✓ ultrasonic rod for 5 min and a water bath for another 5 min. Repeated 3 times	<ul style="list-style-type: none"> ✓ polycarboxylic acid ✓ melamine – this was found to be the best (MELMENT F10, BASF) ✓ naphthalene sulfonate 	<ul style="list-style-type: none"> • Visual observation • SEM • Particle size analysis • Indirectly MIP, strength 	(Tao et al., 2019)

²the GNP dosage is not clear as the graphs show 0 – 0.8 g/L whilst the methods section says 0 – 8 g/L

Two GNPs by Nanesa - G2Nan ³ (30 μm , 14 nm thick) G3Nan (15 μm , 9 nm thick); 0.01% and 0.1%wt.	-	✓ pre-mixed dry mortars containing cement, sand and hydrated lime	• Rheology • Indirectly via strength	(Chougan <i>et al.</i> , 2019)
120-150 m^2/g SSA, 6-8 nm thick, 25 μm ; 0.03, 0.06 and 0.09% bwoc	✓ suspension with surfactant + water + GNP ultrasonically treated for 10 mins in probe sonicator (360W)	✓ Sodium dodecylbenzene sulfonate (SDBS) ✓ Sodium dodecyl sulfate (SDS) ✓ hexadecyl trimethyl ammonium bromide (CTAB) ✓ polyoxyethy-lene (40) nonylphenylether (CO890)	• UV-Vis • SEM • Indirectly via strength and MIP	(Wang and Deng, 2019)
120-150 m^2/g SSA, 6-8 nm thick, 25 μm ; 0.03, 0.06 and 0.09%	✓ horn ultrasonication & ice bath. Amplitude 40%, energy 750 J/ml. Duration varied for 0.5h, 1.5h, 3hr, 4.5hr and 6 hr	✓ polyacrylate surfactant at varying concentrations (optimum concentration found at 8mg/ml)	• UV-Vis • Visual observation • SEM • Electrical resistivity	(Zhu <i>et al.</i> , 2019)
134 m^2/g SSA, 6.9 nm thick, 25 μm ; 0.03, 0.06, 0.09, 0.12 %	✓ after stirring, ultrasonication for 30 min in a probe sonicator (power 360 W)	✓ polycarboxylate superplasticiser ✓ naphthalene superplasticiser ✓ melamine superplasticiser	• SEM • TEM and FTIR • Indirectly - strength	(Wang and Pang, 2019)
3-10 nm thick, 1-3 μm ; 0.03, 0.06 and 0.09%	✓ tip sonicator (20mm tip). Duration varied -1, 2, 3, 4 and 5 hours. Power varied - 720W, 840W, 960 W and 1080W	✓ Three solvents were tested; ethyl alcohol (EA), isopropyl alcohol (IPA) and tap water	• SEM • Viscosity • AFM/ Raman and FTIR	(Zhang and Chen, 2019)
GNP 1-3 nm thick, 56 μm . 0.01, 0.03, 0.05, 0.07, 0.1 and 0.3%	✓ sonication for 30 mins	✓ polycarboxylate superplasticiser mixed with water and stirred for 2 mins	• Visual observation • UV-Vis • SEM	(Ho <i>et al.</i> , 2020)

³ same as the experimental material in this thesis

In summary, different GNP dispersion methods have been employed, and often, a hybrid of a mechanical and a chemical technique is followed, as illustrated in Table 2.2. The literature agrees that creating a homogenous suspension of GNPs first, before adding to cement, is more efficient compared to dry mixing the GNPs with cement. Therefore, this mixing sequence is proposed for this thesis. In terms of mechanical mixing methods, sonication was frequently used, however, there is a disagreement around the optimum duration and power input. As shown in Table 2.2, most studies found that ~30 minutes were needed to disperse the GNPs and excessive sonication periods (longer than ~2 hrs) could induce damage to the material. From a chemical dispersion perspective, surfactants were very commonly employed. There is a wide consensus that polycarboxylates can aid the dispersion of GNPs, even though some studies found that other surfactants might be more efficient. Nonetheless, polycarboxylates are widely used in the construction industry and they would be more appropriate for scaling up the use of GNPs.

2.4.2. Early age performance and microstructure

Early age performance of concrete is of direct interest to the construction industry as it affects both the operations and the resultant strength and durability of the structure. This section investigates some key early age performance factors, including the effect of GRMs on fluidity, setting time and hydration, and microstructure.

2.4.2.1. Workability (fluidity) and rheology

A workable concrete is one that can be readily compacted, and the workability/ fluidity determines the ease of placement, the degree of compaction and the resistance to segregation and bleeding. There is a consensus in the literature that the GNP addition will result in a reduction in fluidity, as it is illustrated in Figure 2-18. This is mainly due to the large specific surface area of the GNPs that require more water to wet their surface (Paul *et al.*, 2018; Wang *et al.*, 2019; Ho *et al.*, 2020), leading to a decrease in the free water in the mix (Wang *et al.*, 2016). For example, in the case of G2NanPaste (GNPs product experimentally tested in this thesis), the specific surface area is 100 times larger than that of cement. As a comparison, the Elkem Microsilica® also has a similar surface area to G2NanPaste, which is ~30m²/g. The reduction of free water increases the inter-particle friction, hence, workability decreases (Chuah *et al.*, 2014). For a constant amount of water

in a mix (fixed w/c), increasing GNP concentration (up to a certain dosage) will promote denser packing which will also contribute to the increased inter-particle friction (Paul *et al.*, 2018). GNPs (which are hydrophobic), are also likely to aggregate in the cement matrix without any dispersion treatment, and these agglomerates will restrain the movement of cement particles and consequently reduce the fluidity further (Wang *et al.*, 2019; Guo *et al.*, 2020; Liu *et al.*, 2020).

Figure 2-18 shows that the GNP addition reduced the workability of the mix, which is indicated by a % reduction in the mini-slump test values. However, this reduction ranged from 2 - 40% depending on the GNP dosage, and generally higher GNP dosages, resulted in a greater reduction of the fluidity. However, the authors were not always in agreement on the workability % reduction. For example, for a GNP dosage of 0.05% bwoc, Guo *et al.* (2020) and Ho *et al.* (2020) found an approximately 9% reduction, whilst Wang *et al.* (2016) found a 31% reduction. These discrepancies do not seem to depend on the w/c (as a 9% reduction was found both for w/c = 0.16 and w/c = 0.485) but can depend on other parameters such as the GNP's properties (surface area, size and thickness), and the dispersion method employed. As can be seen from the notes on the figure, the authors used different GNPs and dispersion methods. For example, at 0.05wt% GNP content, one GNP had 56 μm size and the other 7 μm , however, both reduced fluidity by circa 9%. However, both authors used a polycarboxylate superplasticiser for dispersion, which could have been the dominant factor to affect the fluidity reduction. Due to the many different factors that could affect the fluidity of the cement composites, it is not possible to directly compare the findings, however, the main conclusion is that increasing GNP dosage is expected to reduce the fluidity of the mix, irrespective of the w/c, dispersion method or GNP properties.

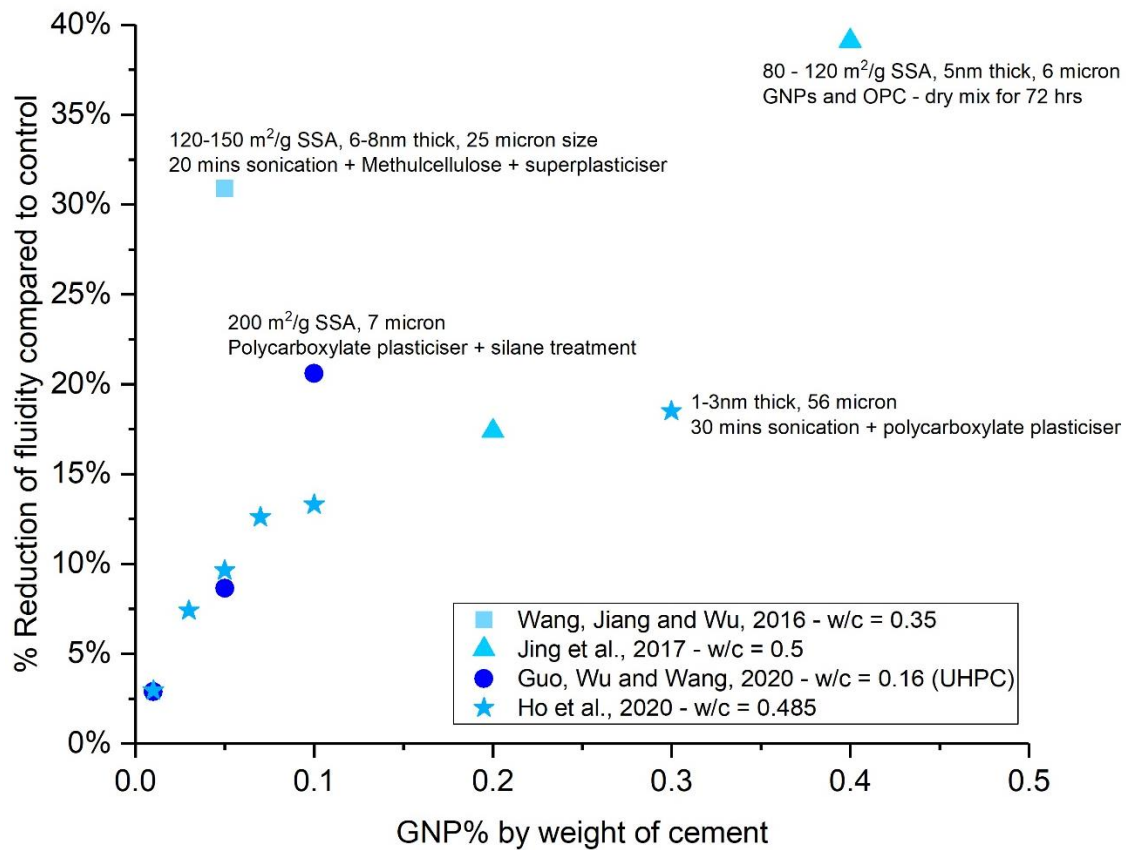


Figure 2-18: A summary of the literature on the % reduction of fluidity with the incorporation of GNPs as measured by mini-slump tests

Some authors also investigated the effect of GNPs on the rheology, which provides useful information on both the plastic viscosity (resistance to flow of the cement paste) and on the yield stress (the critical stress value below which the material does not flow) (Wallevik *et al.*, 2015). Rheology properties are measured using a rheometer and the results can be analysed using different models such as the Bingham model and the Herschel–Bulkley model (Papo, 1988; Jiao *et al.*, 2017). Rheology testing showed that the addition of 1% GNPs, with a SSA of 500 m²/g, 1-5 nm thickness and an average size < 2 μm, resulted in a 15% increase in plastic viscosity and a 23.2% increase in yield stress (Han *et al.*, 2017). This GNP product is very exfoliated with a low thickness and large surface area, whilst the authors used a polycarboxylate superplasticiser to aid the dispersion. Rehman *et al.* (2018) undertook a thorough investigation on the rheological properties of cement composites with GNPs and used some common rheological models (including the Modified Bingham and Herschel–Bulkley) for the analysis. The GNPs had a 12 nm thickness, 4.5 μm average size and were

added at 0.03%, 0.05% and 0.10% bwoc. They found that both the yield stress and the plastic viscosity increased with increasing GNP concentration, however, the superplasticisers had a positive effect on fluidity. In terms of rheometer geometry, concentric cylinders resulted in lower standard error compared to parallel plates rheometers, whilst the Herschel–Bulkley model was found to be the best-fitted (Rehman *et al.*, 2018). A recent investigation on the effect of G2Nan, which is the main GNP product tested in this thesis, found that the rheological behaviour was dramatically dependent on the G2NanPaste dosage, as shown in Figure 2-19 (Chougan *et al.*, 2019). G2Nan has a similar thickness (14 nm) to the GNPs used by Rehman *et al.* (2018), however, the average particle size is 30 μm , which was ~ 6 times higher. For the G2Nan mixes, the yield stress increased by 15.8% for 0.01% G2Nan whilst it decreased by more than half for 0.1% G2Nan and the plastic viscosity showed a similar trend (Chougan *et al.*, 2019). This was attributed to the large particle size of G2Nan, that when added at 0.1wt.% dosage, the packing density of the cement matrix was improved and had a lubrication effect that was more dominant than the thickening effect.

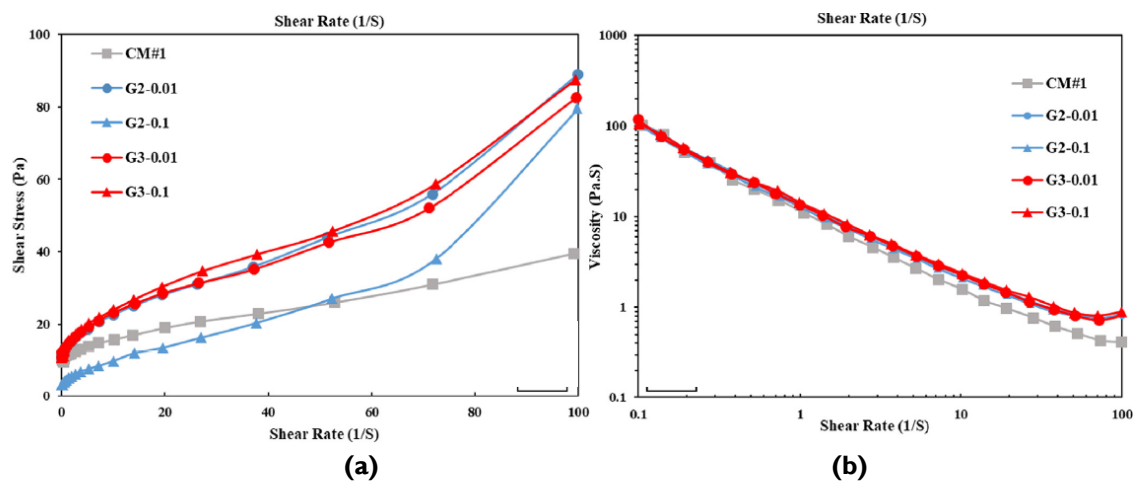


Figure 2-19: Rheology of the mortars modified with different contents of G2Nan and G2Nan (a) shear rate versus shear stress, (b) shear rate versus viscosity (Chougan *et al.*, 2019)

This finding around the lubrication effect is partly in agreement with a study that used pre-dispersed CNTs at 2.5, 5 and 10% bwoc, in high-early strength binder and found that moderate CNT additions reduced the viscosity (from 2% to 36%), whilst the 10 wt.% CNTs increased the viscosity by 17% (MacLeod *et al.*, 2020). This was due to an early interaction between CNTs and cement paste as well as the extended mix time (15 mins) which was beneficial in reducing bleeding (MacLeod *et al.*, 2020). CNTs are also hydrophobic so their properties are similar to GNPs and therefore the two studies can be compared. However,

these studies disagree with the rest of the literature that found a reduction in fluidity with increasing GNP content. The explanation for these discrepancies could come from an earlier study from Long *et al.* (2018), who investigated the fluidity with GO. Even though GO is hydrophilic and its dispersibility is different to that of GNPs, this study allowed for a better understanding of the mechanisms involved. It was found that the yield stress and plastic viscosity increased when GO was uniformly dispersed, whilst they were reduced when GO was agglomerated, as illustrated in Figure 2-20. For agglomerated GO, its surface area was reduced, and it required less water to wet its surface. Also, less polycarboxylate superplasticiser was needed to disperse the particles so the excess admixture was used as a superplasticiser to improve fluidity. With well-dispersed GO, both the superplasticiser and part of the free water were consumed to disperse the GO and therefore the fluidity of the cement paste reduced (Long *et al.*, 2018).

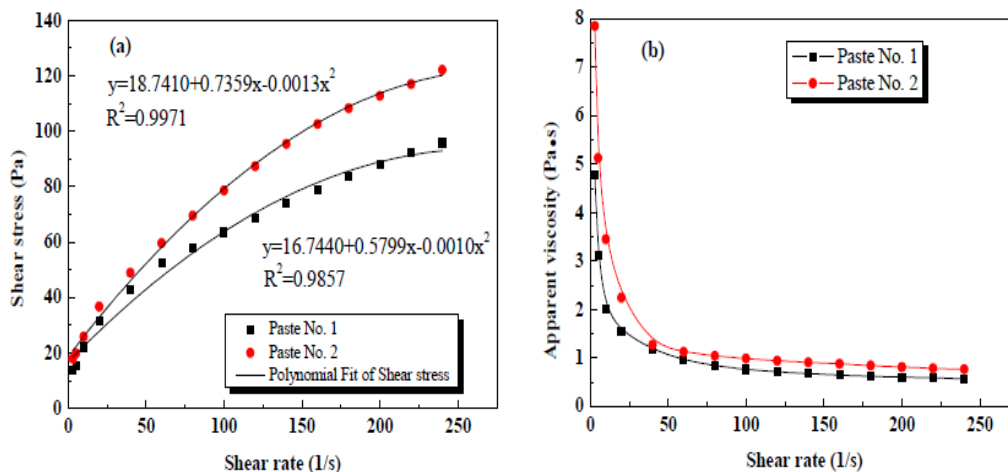


Figure 2-20: Rheological parameters of GO cement pastes with Paste No 1 containing agglomerated GO and Paste No2 containing well-dispersed GO (Long, Li, et al., 2018)

In summary, mini-slump tests showed that GNPs reduce the fluidity of the mixtures, however, the % reduction will be dependent on both the GNP properties and on the dispersion techniques. More detailed investigation in the rheological performance of cement composites modified by other GRMs has highlighted some discrepancies. Whilst some studies found a deterioration of the rheological properties with GRMs, others found an improvement and showed that GRMs could act as a plasticising admixture. These discrepancies could be explained by the dispersion state of the GRMs; however, further research is needed.

2.4.2.2. Hydration

Portland cement, in its anhydrous state, consists of four main compounds; tricalcium silicate (*alite*) (3CaOSiO_2 abbreviated as C_3S), dicalcium silicate (*belite*) (2CaOSiO_2 , C_2S), tricalcium aluminate (*aluminate*) ($3\text{CaOAl}_2\text{O}_3$, C_3A), tetracalcium aluminoferrite (*ferrite*) ($4\text{CaOAl}_2\text{O}_3\text{Fe}_2\text{O}_3$, C_4AF) as well as gypsum (calcium sulfate dihydrate, $\text{CaSO}_4 \cdot 2\text{H}_2\text{O}$) (Neville, 2011). When water is added to the cement, a hydration reaction takes place, where these four compounds (C_3S , C_2S , C_3A and C_4AF) react with water to form calcium silicate hydrates (known as C-S-H), calcium hydroxide ($\text{Ca}(\text{OH})_2$) and ettringite (AFt) and monosulfoaluminate (AFm) (Taylor, 1997). The hydration of cement is an exothermic reaction that releases heat and the rate of hydration decreases continuously (Neville, 2011). There are two main hydration peaks; an initial peak involving C_3A hydration which is very high and corresponds to the initial hydration at the cement surface, followed by a *dormant/induction* period, during which the hydration rate is very slow and the cement paste is workable. As the hydration of cement particles progresses further from the surface layer, the rate of hydration increases slowly (second peak) and setting occurs (the cement paste hardens) (Neville, 2011). The effect of GRMs on the hydration behaviour of cement composites has been widely investigated in the literature and it can be directly measured through isothermal calorimetry, thermogravimetric analysis (TGA) and X-ray diffraction (XRD). Wang and Pang (2019) tested different surfactants for dispersing GNPs and found that no new phases were formed, however, there was a change in the XRD peak intensities which could mean that GNPs have affected the crystallinity of hydration products (Figure 2-21a). The same finding (no new peaks but change in XRD peak intensity with GNP addition) has also been found in other studies by Baomin Wang (Wang and Zhao, 2017; Wang, Zhao, *et al.*, 2018; Wang and Deng, 2019). In all these studies, the authors observed the main crystalline products included calcium hydroxide (CH), ettringite (Aft) and monosulfide calcium sulphoaluminate (Afm). From Figure 2-21(a), the peak intensities for CH and AFt were enhanced with GNP addition (annotated as PS) which means they were better crystallised due to an accelerated hydration. In another study, the authors also found that the sample with 0.10% GNPs had a higher intensity peak for the $\text{Ca}(\text{OH})_2$ indicating a better crystalline degree and accelerated hydration (Figure 2-21b). Li *et al.* (2018) found that the amount of ettringite increased with the increase of GNP content (0.01- 0.05% bwoc), indicating that GNPs could promote the formation of ettringite. Testing 0.1wt% and 0.5wt%

GNPs and GO, Wang *et al.*, (2020) found no new peaks and no obvious changes in the intensities of the peaks with the GRM addition (Figure 2-21c), with the latter being in disagreement with previously mentioned literature. In summary, GNPs do not lead to the formation of any new hydration products however, they could affect the intensity of the XRD peaks and consequently the degree of hydration.

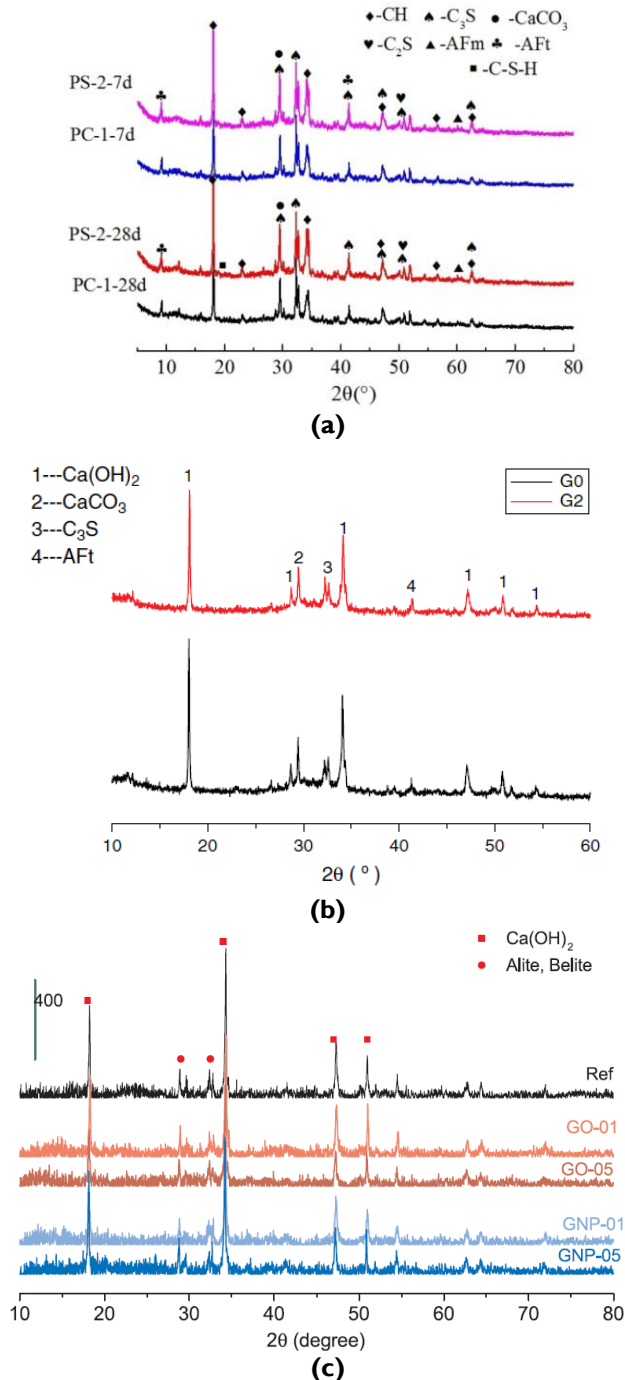


Figure 2-21: XRD patterns (a) 7 and 28 days for Portland cement (PC) and samples with polycarboxylate superplasticiser (PS) and GNPs (Wang and Pang, 2019) (b) PC sample (G0) and 0.1% GNP sample (G2) at 28 days (Wang, Zhao, et al., 2018) and (c) GO and GNPs at 0.1% and 0.5% dosages (Wang *et al.*, 2020)

An acceleration of the hydration rate at early ages was observed by isothermal calorimetry, however, it could be argued that the change was minimal, whilst TGA showed that there were no new phases (Wang *et al.*, 2016). This was further confirmed by Jing *et al.* (2017), who undertook a thorough investigation on the effect of GNPs on the hydration rate. Isothermal calorimetry showed that the major peaks were comparable for the plain cement paste and those incorporating 0.2% and 0.4wt.% GNPs, with only a slight shift to the left for the 0.4% GNP mix (Figure 2-22). This indicated a slight acceleration in the rate of hydration, however, it could also be attributed to the effect of baseline drift which is common in this experiment (Jing *et al.*, 2017). More weight loss of non-evaporable content compared to the control along with decomposition of calcium hydroxide and calcium carbonate were observed by TGA (Wang and Zhao, 2017). The latter indicates more hydration products and hence a greater hydration degree.

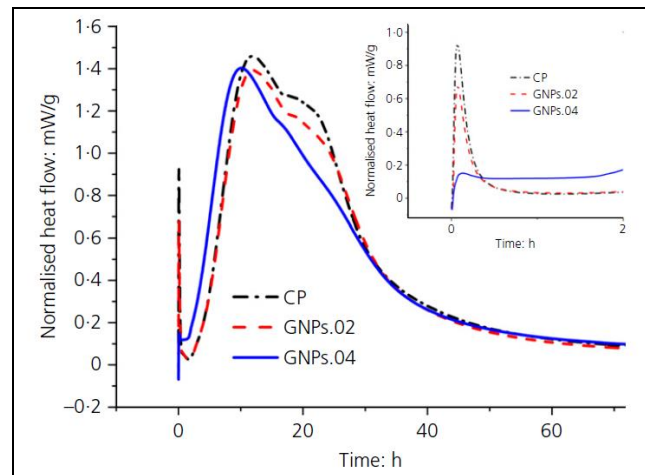


Figure 2-22: Isothermal calorimetry results showing that the major peaks occur almost at the same time with a slight acceleration for the 0.4% GNP content (Jing *et al.*, 2017)

A recent TGA study showed that the 1wt.% GNPs and control samples had similar amounts of free water (~7 wt%), physical bound water (~7.5 wt%) and they contained the same amount of Portlandite (15 wt%), indicating that GNPs did not affect the hydration of OPC (Goracci and Dolado, 2020). This agrees with Wang *et al.* (2020) who found that the addition of GO and GNPs at 0.1wt% and 0.5wt% had no obvious impacts on material minerals. However, a higher percentage of portlandite and non-evaporable water was found for mixes containing GNPs at 0.03%, 0.07% and 0.3%, that shows that GNPs could accelerate the cement hydration, as shown in Figure 2-23 (Ho *et al.*, 2020).

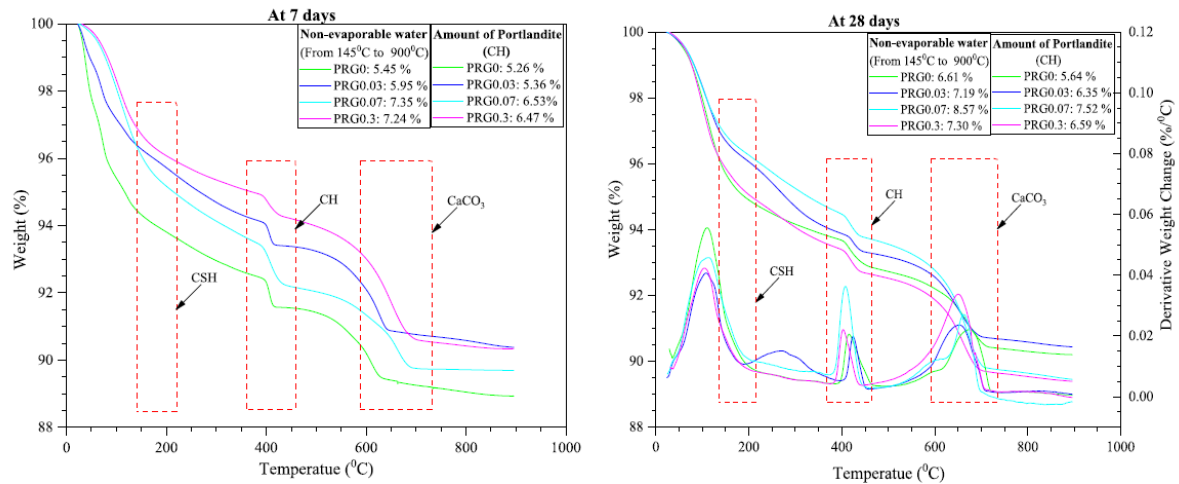


Figure 2-23: TGA results for GNPs at 0.03%, 0.07% and 0.3% bwoc (Ho et al., 2020)

2.4.2.3. Microstructure

Microstructural characterisation of GNP-cement composites has been carried out to understand the GNPs dispersion, their bonding with cement hydrates and the overall effect on the morphology. Atomic force microscopy (AFM) showed that the GNPs could reshape the microstructure of the cement paste and that a good interfacial bond was developed between the C-S-H gel and the GNPs (Tong et al., 2016). Ettringite, C-S-H gel and other hydration crystals were also found to be well-connected by GNPs which formed a 3-D structure that could bridge the cracks and fill the pores in cement matrix (Li et al., 2018). Figure 2-24, show that GNPs were wrapped by hydration products, whilst no agglomerates were observed which is an indication of good dispersion (Wang et al., 2016).

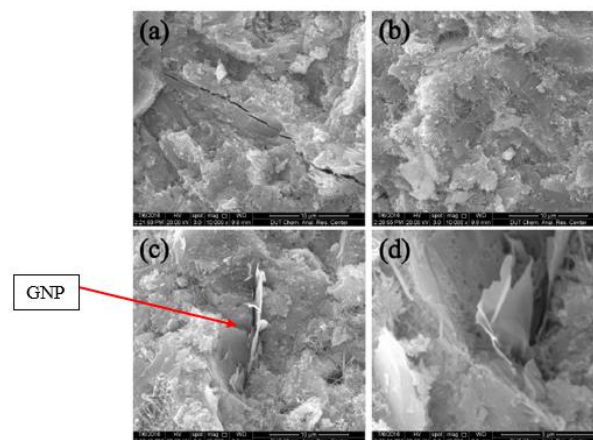


Figure 2-24: SEM images at 28 days (a) plain cement paste, (b) 0.05wt% GNP-cement (c-d) GNP inserted in the hydration products (Wang et al., 2016).

However, other studies observed GNP agglomerates with SEM testing. For example, partial GNP agglomerates were found by Jing *et al.* (2017), who also saw that the GNPs were almost unchanged and simply attached to cement hydration products with low interfacial bonding. On this study, the authors found that GNPs had little effect on hydration, which was further explained by the low interactions between GNPs and cement matrix. Tao *et al.* (2019) observed by SEM that GNPs were well dispersed at low dosages (0.05% and 0.1%), however, agglomerates were found for higher concentrations (0.5% and 1% bwoc). The primary limitation with microstructural observation with SEM, is that only a very small sample area is tested each time which is not necessarily representative of the bulk and also the image interpretation is subjective. For instance, from Figure 2-25, the authors claim that the mixes incorporating GNPs (c-h) were more compacted than the control and that poor dispersion at 0.3% GNPs impacted the hydration. However, the individual (or agglomerated) GNPs were not observed at all in the below SEM images so therefore it is difficult to confidently reach this conclusion. SEM for microstructural characterisation can be a useful complementary tool to understand the interactions at microscale, however, the subjectivity in the interpretation of the results and the small sample area can be limiting so caution needs to be exercised when authors base their conclusions on this test.

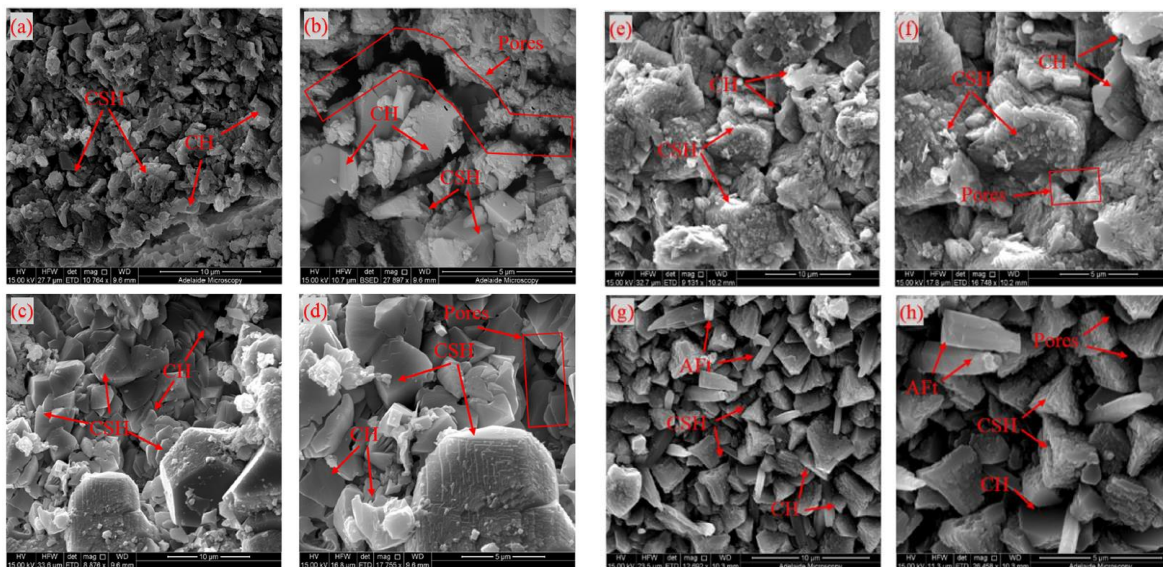


Figure 2-25: High magnification SEM images at 10 μm and 5 μm of GNP-cement mortar mixes at 28 days: (a, b) Control; (c, d) GNP0.03%; (e, f) GNP0.075; (g, h) GNP0.3% (Ho *et al.*, 2020)

To conclude, extensive experimental focus has been placed on the early age performance of cement composites with GNPs. However, there are still significant discrepancies in the literature with authors often finding opposing results. There is consensus that GNPs impair the rheological performance and workability of cement composites, but some studies found that GNPs could have a positive effect. In terms of hydration, some found acceleration while others found minimal or negative effects, however, the mechanism behind the effect of GRMs on hydration is not very well understood. Finally, microstructural observations showed good interactions with the cement hydration products in some studies whilst a poor interaction was shown in others. Due to the inconclusive nature of the literature in the aforementioned areas, the effect of GNPs on the early age performance of cement composites needs to be investigated further for the mechanisms to be understood.

2.4.3. Mechanical properties

The mechanical properties, including compressive and flexural strength, modulus of elasticity and resistance to cracking, are all critical parameters that will affect the structural performance of the GRM-cement composite. However, there is no agreement in the literature on whether the GNPs have a beneficial effect or if they impair the performance. Figure 2-26 summarises some of the key studies from the past four years, where GNPs have been added in cementitious composites. It is observed that the most common GNP dosages ranged from 0.05% - 0.1% bwoc. Generally, improvements in compressive strength were found when GNPs were added, however, there was no agreement on the % improvement and there was not an optimum GNP dosage. Almost a third of the data-points on the graph showed an improvement that was less than 5%, which could be statistically insignificant, depending on the number of tested samples and the resultant standard deviation. Some authors found a strength decrease, up to 10%. Limited studies found larger changes in strength; however, they have been excluded from the analysis due to lack of clarity on the material dosages and the dispersion protocol. The strength of concrete can be greatly affected by the w/c and the effective water in the mix (Neville, 2011) and therefore, the water content needs to be carefully controlled during the preparation of the specimens. Furthermore, other parameters could have also affected the findings, including the w/c and the curing technique for the specimens as they would affect the hydration and possibly the interaction with the GNPs. The intrinsic GNP properties could also have a pronounced effect, since according to Table 2.2, authors have used different GNP products which makes

it difficult to directly compare the findings. Nonetheless, these parameters are not discussed in detail here because the effect of GNPs on strength has been found to be statistically insignificant in most cases and the literature is not clear on the % change with GNPs.

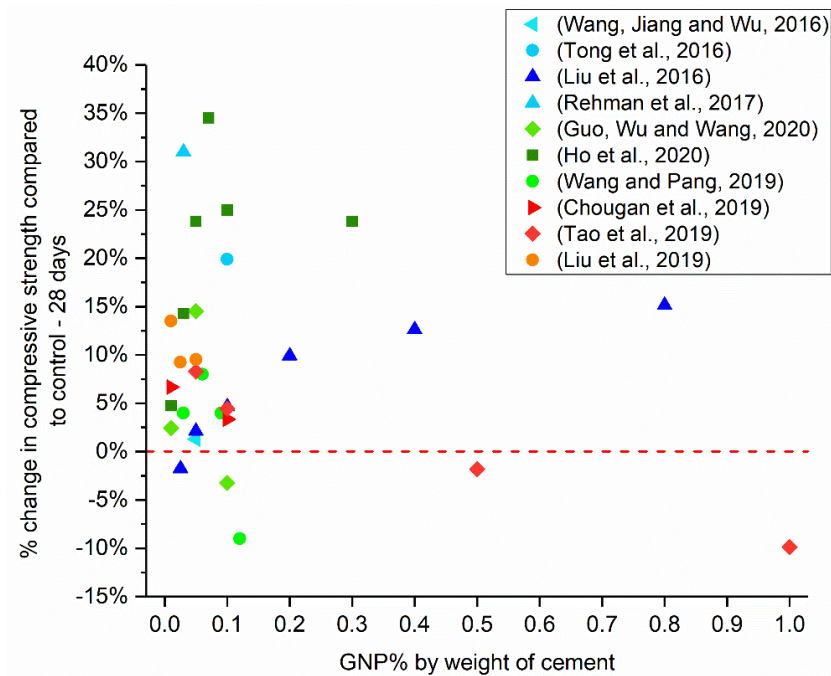


Figure 2-26: A summary of the literature on the effect of GNPs on the compressive strength of the cement composites at 28 days of curing

Similar trends in the flexural strength performance (usually measured by 3-point bending) have been observed (Figure 2-27), however, fewer studies carried out flexural strength testing. Improvements up to 20% have been reported, while some studies found a decrease of up to 10%. As in compressive strength, many data points were within 5% change, which could be statistically insignificant. Authors attributed the strength improvements to a refined microstructure (that led to improved bonding between GNPs and cement hydration products) and an accelerated rate of hydration (Ho *et al.*, 2020; Zhao *et al.*, 2020). However, as discussed in Section 2.4.2, there was no consensus on the effect of GNPs on the hydration behaviour and the microstructure of cement composites and therefore it is difficult to draw the conclusion that GNPs improve these properties. Others found an optimum dosage and explained that GNPs at low contents were well dispersed and beneficial, whilst high contents led to agglomeration and impaired the mechanical performance, such as Tao *et al.* (2019). Indeed, dispersion has been found to be a key limitation in the literature and effective dispersion will affect the resultant material

properties to an extent. Lee *et al.* (2019) found that the mixing method had an obvious effect on the mechanical properties of MWCNTs-mortars, with dry mixing being the least effective, whilst another study confirmed the same finding for GO (Lu *et al.*, 2019). Finally, another explanation is that due to the high Young's modulus of GNPs, the GNPs could reduce the stress concentrations when the specimen is under load and prevent the development of cracks (Wang *et al.*, 2016). This is also confirmed by Meng and Khayat (2016), that observed that GRMs (graphite nanoplatelets and carbon nanofibers) increased the cracking load due to a combination of the “*bridging effect*” and the “*filler effect*”. This means that the GRMs could act as a filler, hence reducing the overall porosity and improving the compactness of the structure, whilst also bridging some of the cracks that would normally be formed between the cement hydration products. However, the elasticity could depend on the GNP fundamental properties, such as the thickness and size, so it cannot be conclusively confirmed that the GNPs could have this effect. Very limited studies have also used micro-indentation to investigate the effect of GNPs on the hardness of cement composites. It was found that the high stiffness areas increased with the addition of 0.05% GNPs and the average microhardness increased by 8.9% compared to the control (Liu *et al.*, 2019). Vickers hardness testing showed found a uniform distribution of strength (and consequently GNP dispersion) with GNPs ranging from 0.5- 3% by volume (Liu *et al.*, 2018).

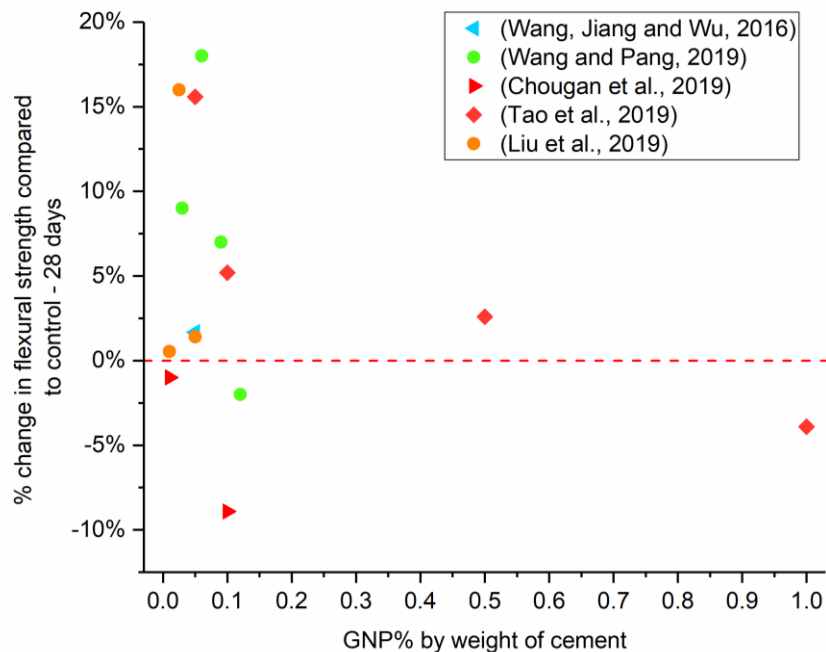


Figure 2-27: A summary of the literature on the effect of GNPs on the flexural strength of the cement composites at 28 days of curing

To summarise, the literature is very inconclusive on the effect of GNPs on the mechanical properties of cement composites. Some improvements were reported, however, the mechanism behind the interactions is not clear and many changes are not statistically significant. Dispersion is a key variable, however, even if good dispersion is achieved, there is no convincing argument as to why GNPs (chemically inactive) would interact with cement hydration products to accelerate the hydration and refine their microstructure. Therefore, further studies are needed to understand if the GNPs have a chemical benefit or if they act as inert fillers.

2.4.4. Permeability and durability

Durability of concrete structures is a key concern for the civil engineering sector, with permeability affecting the long-term performance, however, very few studies to date have investigated the effect of GNPs. Due to their small particle size, GNPs are expected to improve the packing density and reduce the overall porosity of the cementitious composites (Sbia *et al.*, 2015; Kirgiz, 2020). The larger pores and those that are connected are generally more harmful as they allow the flow of water and aggressive atoms (Neville, 2011); therefore, the finer the pores, the better the durability. Mercury intrusion porosimetry (MIP) showed that GNPs reduced the critical pore diameter and the average void diameter shrank by more than 40% with 1.5wt% GNPs (Du *et al.*, 2016). A 0.02% GNP addition decreased porosity by 39%, and it reduced the total pore area, median and average pore diameter (Wang and Zhao, 2017). Wang *et al.* (2016), also found a total porosity reduction from 18.4% to 17% for 0.05wt% GNPs. A recent study showed that both GO and GNPs could make the cement matrix denser by depressing the meso pores (Wang *et al.*, 2020). Figure 2-28 shows that GO nanosheets at 0.1% and 0.5% dosages, increased the coarse mesopores whilst GNPs reduced them; therefore GNPs with the larger size will narrow the pores whilst GO with the smaller size will coarsen them.

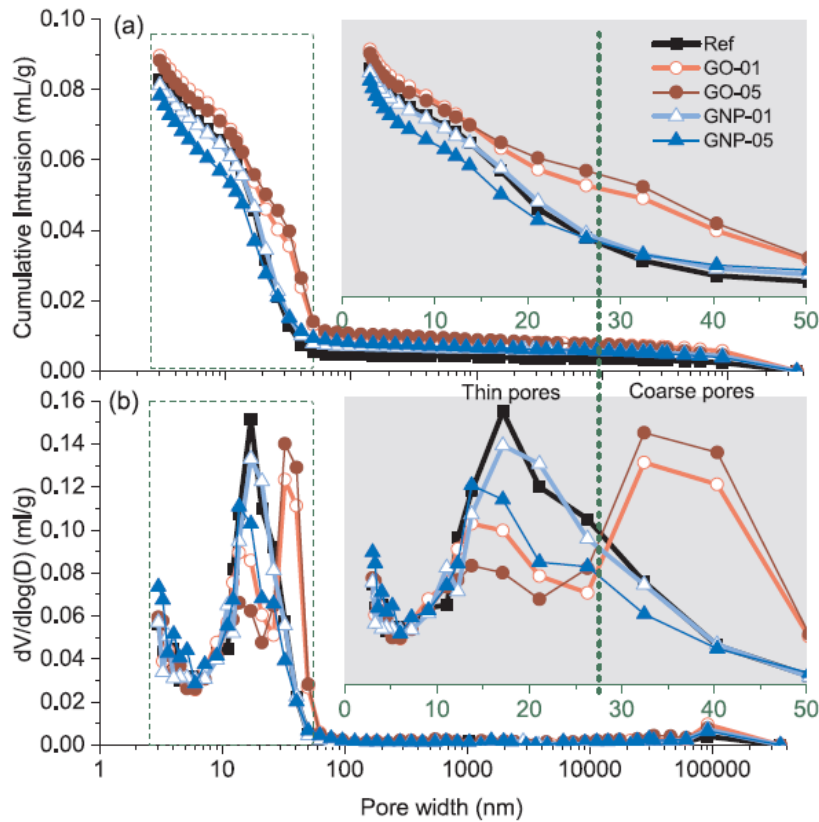


Figure 2-28: MIP results (a) cumulative and (b) differential of cement composites reinforced with GO and GNPs at 0.1% and 0.5% by weight of cement (Wang et al., 2020)

Few studies investigated the effect of GNPs on the chloride penetration and water permeability of cement composites. Chloride penetration depth decreased with 0.05%-0.2% GNPs, from circa 9mm to 5.7mm (Liu et al., 2016). In another study, with GNPs from 0.05% - 0.15wt%, the chloride migration coefficient also reduced, reaching a 34% reduction for 0.1% GNPs (Figure 2-29a shown as G2) (Wang et al., 2018). Much higher GNP dosages were tested by Du et al. (2016), who found the optimum GNP content to be 1.5% (Figure 2-29b). In terms of water permeability, a 75% reduction in water penetration depth (from 18.2mm to 4.4mm for 5% GNPs+2.5% superplasticiser) was found (Du and Pang, 2015). Another study by the same authors found that at low GNP content (<1.0wt.%), the water penetration depth was barely affected, however, at 1.5% GNPs it decreased by 80% (Du et al., 2016). Even though further literature on GNPs is scarce, studies on GO also showed that water permeability and capillary absorption reduces with GO or rGO addition (Devi and Ahmad, 2019; Gao, Jing, and Zhou, 2019; Prabavathy et al., 2019, Korayem et al., 2020). Finally, gas permeability is also relevant to the concrete durability under various exposure

conditions (Neville, 2011). Using liquid methanol as the gas source, Gao, Jing, Zhou, *et al.* (2019) found that the GO/MWCNTs addition reduced the permeability of cementitious composites. However, this has not been investigated to date for GNPs.

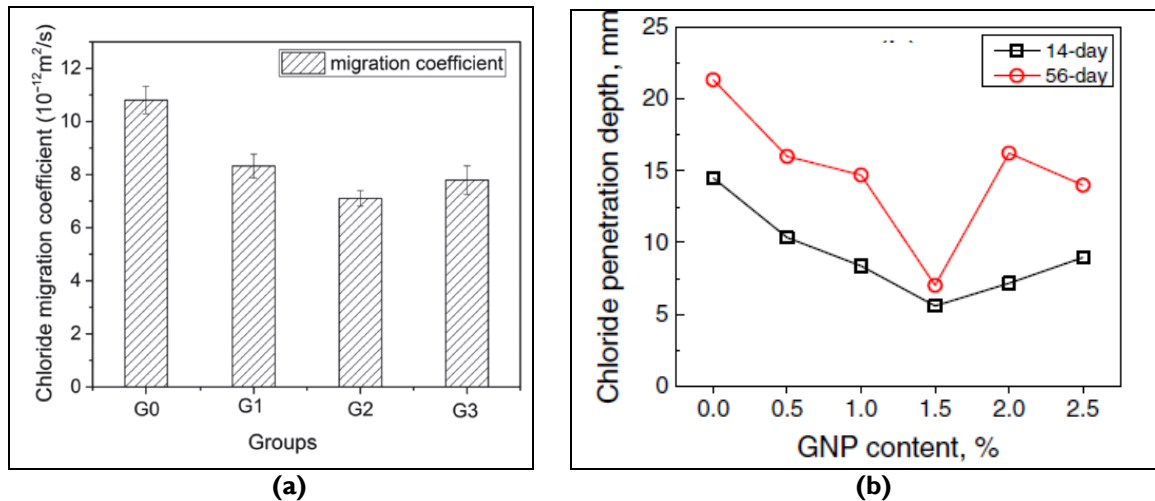


Figure 2-29: Decreasing chloride migration coefficient with GNPs (a) (Wang, Zhao, *et al.* 2018) and decreasing chloride penetration depth up to 1.5% GNP content (b) (Du *et al.*, 2016)

In summary, overall porosity and a pore refinement towards finer pores has been observed with the addition of GNPs. This has consequently led to a reduction in the chloride migration coefficient, water and gas permeability. However, the literature on durability is limited and further studies are needed.

2.4.5. Electrical conductivity

The effect of GNPs on the electrical conductivity of cement composites is of interest as it could allow the passing of current and induce a self-sensing mechanism as discussed in Section 2.2.1. Concrete offers high resistance to electric current and this depends on the water content, moisture state, hydration age, aggregates and cementitious materials as well as temperature and voltage (Neville, 2011). There are generally three different types of electronic conduction through the concrete; ionic conduction through the water in the pores, electronic conduction through the direct passing of the current through the conductive particles and tunnelling conduction through the conductive particles when in close proximity (Andrade *et al.*, 2015). Ionic conduction is very dependent on the water content, moisture state, temperature, presence of aggregates and hydration of the cement matrix, with cement paste at early curing ages being electrically conductive (Chung, 2002b; Davey *et al.*, 2019; Honorio *et al.*, 2020). However, as the hydration progresses, the water

available in the matrix reduces and therefore the possibility of ionic conduction reduces dramatically (Liu *et al.*, 2019); hence, most of cementitious matrices, and especially concrete (with aggregates) act as insulators (Neville, 2011). This means that the presence of conductive fillers is needed for advanced functionalities, such as self-sensing, so that electric current can be passed through the composite through either electronic or tunnelling conduction (or both) (Wen and Chung, 2006). This concept has been illustrated by Arabzadeh *et al.* (2019) and is shown in Figure 2-30. At low conductive filler content, no conduction paths form and any electric current would be transported through the free water in the pores by ionic conduction. As the conductive filler volume increases, a conductive path is formed which is the percolation threshold. Further increase in the filler content will improve these electronic conduction paths through the matrix.

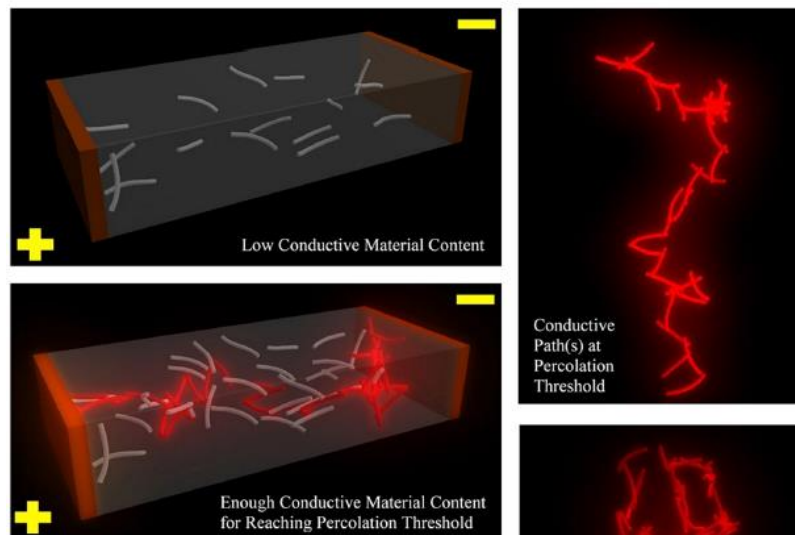


Figure 2-30: Schematic of the conductivity mechanism with carbon fibers (Arabzadeh *et al.*, 2019)

The electrical resistance is the fundamental property to be measured, as the inclusion of conductive fillers is expected to reduce the specimen's electrical resistance and is calculated using Ohm's law:

$$R = \frac{V}{I} \quad (\text{Eq. 1})$$

where R is the electrical resistance, I is the electrical current and V is the measured voltage .

The resistivity, ρ , can then be calculated:

$$\rho = R \frac{L}{A} \quad (\text{Eq. 2})$$

where L is the length between the inner electrodes and A is the cross-sectional area.

Other properties that are often measured are the electrical impedance (circuit opposition to a current) under AC⁴ and the capacitance - the ratio of change in an electrical charge to the change in the electric potential (Han *et al.*, 2014). To measure the volume resistance of concrete, the two-probe (2-probe) and four-probe (4-probe) methods are commonly used. The 2-probe method employs two electrodes to pass the current and simultaneously measure the voltage. The 4-probe method consists of four electrodes – the two outer contacts pass the electrical current and two inner contacts measure the voltage change. The 2-probe method gives less reliable readings than the 4-probe method, due to the error caused by the contact resistance (Chung, 2012). However, the 2-probe method is easier to implement and is preferred when a high level of accuracy is not required (Tian and Hu, 2012). Alternating current or direct current can be used for investigating conductivity (Chung, 2012). In choosing AC or DC voltage, Tian and Hu (2012) found that with the same specimen, the resistivity measured with AC was $\sim 1/3$ lower than the resistivity measured by DC. It was also shown that the resistivity decreased with an increase of the voltage irrespective of whether AC or DC is used, eventually it stabilised. AC resistance is generally more advantageous compared to DC as it avoids the polarisation effect, which can cause the measured resistance to increase above the true value (Meehan *et al.*, 2010). Nonetheless, DC measurements have a straightforward set up and the polarisation effect can be eliminated by passing current through the specimen for some time before the measurement until a steady state is reached. Finally, the choice of electrodes plays a key role in the measurement of self-sensing signal. The electrodes should have a very low resistance to allow the passage of current and a stable electrically conductive property (Han *et al.*, 2014). The most common materials are stainless steel, copper and aluminium and they can consist either of bars, wires or sheets with and without holes. The electrodes can be attached or embedded in the sample in different set-ups, as shown in Figure 2-31 (Han *et al.*, 2015).

⁴ In DC, there is no difference between impedance and resistance.

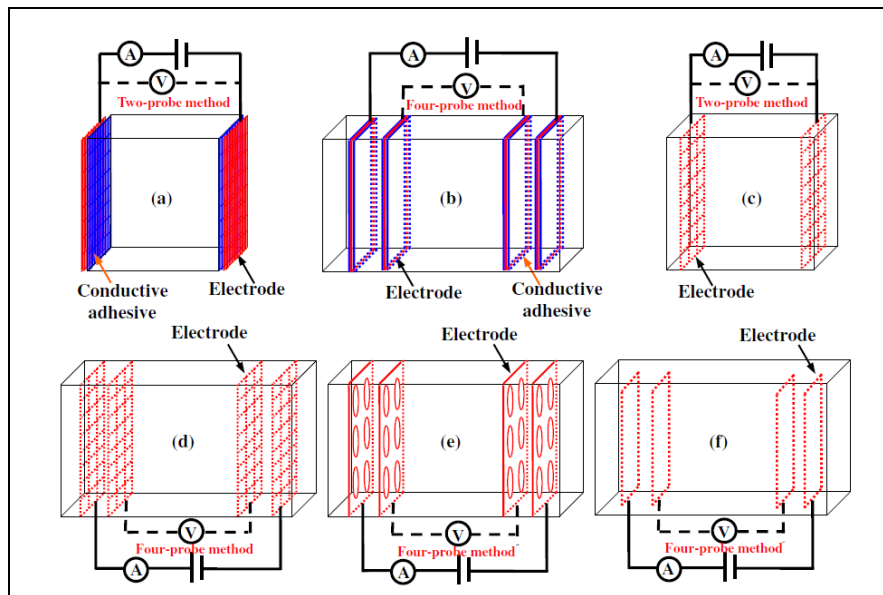


Figure 2-31: Common electrode layouts (a) attached for the 2-probe method, (b) embedded for the 4-probe method, (c) embedded for the 2-probe method, (d) – (f) embedded for the 4-probe method with different hole arrangements (Han et al., 2015)

2.4.5.1. Effect of graphite

Natural graphite comes in different forms - flake, amorphous and vein – and is categorised by its mesh size. Due to graphite's wide availability, low cost and promising properties, this section investigates its potential for self-sensing applications. Table 2.3 summarises the key properties of graphite.

Table 2.3: Summary of graphite properties (Poco Graphite Inc., 2015)

Property	Value/ Range	Comment
Density	2.26 g/cm ³	Most graphites have a density of 80% of the theoretical value
Hardness	1-2 (Mohs scale)	Decreases with increasing temperature
Compressive strength	69– 200 MPa	Brittle material – catastrophic failure
Flexural strength	7– 41 MPa	ASTM C651
Tensile strength	14 – 34 MPa	ASTM C656
Modulus of elasticity	-	Varies with graphite type and anisotropy
Electrical resistivity	400-1000 μΩ/in	Decreases with temperature and density increase

The literature showed that graphite did not react with the cement hydration products and thermogravimetric studies showed that the mass loss was minimally affected by the graphite content (Peinado et al., 1994). XRD testing on graphite-aluminate cement composites

demonstrated that graphite did not participate in the hydration process directly (Yuan *et al.*, 2012). A decrease in density from 2.42 to 2.3 g/cm³ with increasing graphite content was found by Sachdev *et al.* (2015) whilst a slight decrease in hardness with increasing graphite content was observed by Bhattacharya *et al.* (2008). The addition of graphite can significantly decrease the fluidity of the paste due to the low hydrophilicity of the material and agglomeration of the particles (Wang *et al.*, 2019). Flexural and compressive strength of graphite-cement composites were both found to reduce significantly with increasing graphite content (Yuan *et al.*, 2012). Graphite is a soft material so as the graphite dosage increased, the compressive strength of the composite decreased. Graphite addition led to a reduction in the pore volume and an increase in conductivity (Bhattacharya *et al.*, 2008). The graphite-cement composite became a conductor, however the mechanical and electrical properties depended on the water content and the setting process (Peinado *et al.*, 1994). When dry-mixing graphite and cement powder, a minimum threshold of 2wt.% graphite was needed, below which the insulating cement prohibited the formation of conductive graphite pathways and the conductivity levelled off at around 10 wt. % graphite (Sachdev *et al.*, 2015). Similarly, the DC electrical resistivity decreased rapidly between the percolation threshold at 2 wt.% and 10 wt.% where it plateaued (Figure 2-32(a)) (Bhattacharya *et al.*, 2008). However, a study by Frattini *et al.* (2017) found a conductivity threshold at ~30-40% of graphite (Figure 2-32(b)).

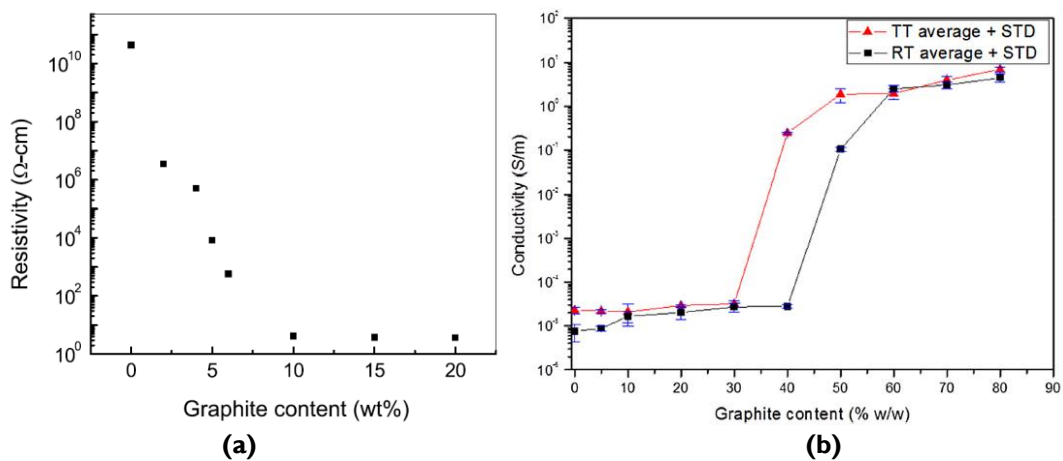


Figure 2-32: DC electrical resistivity with increasing graphite content (a) (Bhattacharya *et al.*, 2008) and electrical conductivity of cement pastes with graphite content (b) (Frattini *et al.*, 2017)

The percolation threshold and the electrical conductivity depend greatly on factors such as particle shape, size and origin of the graphite (Rew *et al.*, 2017). It was found that the higher the graphite aspect ratio, the lower the critical volume content that was needed for percolation and that better packing increased the probability of contact between the graphite particles (Nagata *et al.*, 1999). The smaller the graphite particles size, the more closely packed the graphite is in the matrix and therefore the percolation threshold is lower (Nagata, *et al.*, 1999). To summarise, graphite addition in the cement matrix can bring significant benefits in terms of electrical conductivity that could be advantageous for self-sensing. However, graphite is a soft material and acts as a filler and therefore, the mechanical and durability properties could be impaired at high graphite contents.

2.4.5.2. Effect of GNPs

GNPs have been investigated as an electrically conductive filler. Using 0.5wt.% GNPs in a cementitious composite that also contained silica fume, Haddad and Chung (2017) found that the resistivity increased by 68% from 5.77 $\Omega \times \text{cm}$ for the plain cement to 9.71 $\Omega \times \text{cm}$. The authors explained that this was because of the resistance associated with the interface between GNPs and cement when the GNPs were below the percolation threshold. This agrees with another study that found a marginal increase in resistivity with increasing GNP content for dosages less than 0.4wt.% due to the contact resistance at the GNP/cement interface, whilst the percolation threshold in this study was between 0.8% and 1.2wt% GNPs (Bai *et al.*, 2018). This percolation threshold was found to be independent of the w/c and only dependent on the electronic conduction via the GNP particles as illustrated in Figure 2-33. A recent study by Tao *et al.* (2019) found that for GNPs at 0.05wt% and 0.1wt%, the electrical resistance was almost unchanged whilst further increase to 0.5wt% and 1wt%, reduced the resistance by ~ 1 order of magnitude as conductive networks started to form.

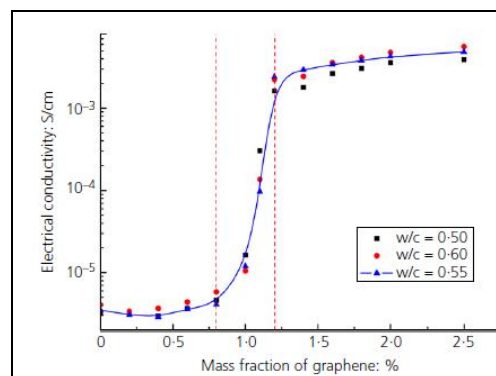


Figure 2-33: Effect of GNPs on the electrical conductivity of cement composites (Bai *et al.*, 2018)

GNPs were tested at higher dosages (5-20wt.%) and it was found that above a percolation threshold (between 10-15wt.%), the electrical conductivity was insensitive to moisture content and hence reliable for self-sensing (Le *et al.*, 2014). Above the percolation threshold, ionic conduction through the free water is minimal and electronic conduction through the GNP particles becomes the dominant mechanism. Mortars with 6.4wt.% GNPs had stable electrical resistance and accurate reaction to compressive stress whilst lower (3.2wt.%) or higher (12.8wt.%) GNPs dosages led to unstable electrical resistance and piezoresistivity (Liu *et al.*, 2016). Another study used GNPs (thickness 1-5nm, diameter <2 μ m, SSA = 500 m²/g) up to 10% by volume and carried out AC and DC tests (Sun *et al.*, 2017). As shown in Figure 2-34, as the content of GNPs increased, the electrical resistivity decreased and the percolation threshold was at ~2% by volume, irrespective of AC or DC measurements.

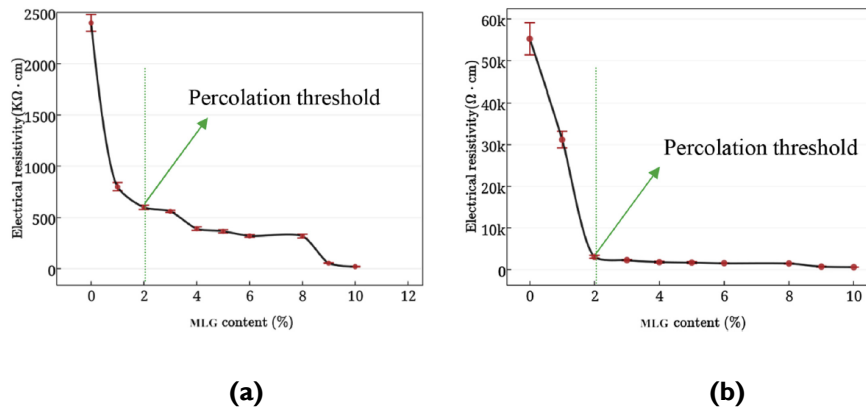


Figure 2-34: Electrical resistivity change with GNP % dosage increase (a) DC measurements (b) AC measurements (Sun *et al.*, 2017)

To understand the mechanism of GNPs conductivity in cement paste, Goracci and Dolado (2020) undertook a thorough impedance spectroscopy study with 1wt.% GNPs. The authors found that GNPs decreased the bulk resistivity and refined the pore structure that consequently enhanced water diffusion through the porous network (improvement in ionic conductivity). Therefore, the pore refinement due to GNPs was the main mechanism for higher conductivity for this GNP dosage. In summary, GNPs have been found to enhance the conductivity of cement composites by forming conductive networks above the percolation threshold whilst the pore refinement can improve the ionic conductivity below the percolation threshold. However, there are discrepancies around the dosages needed for the percolation threshold which could depend on the GNP properties, dispersion method and on the cementitious matrix.

2.5. Environmental performance of GRMs

As discussed in Section 2.1.1, concrete production and use is associated with several environmental challenges. This thesis investigates the potential of a new GNP-cement composite however, only scarce information is available on the environmental effect of GNP production and their consequent introduction in concrete. For this reason, a Lifecycle Assessment (LCA) study is proposed to be carried out in this work. An LCA is a systematic environmental analysis tool that aims to quantify the interactions between the investigated product and the environment by considering the inflows of energy and natural resources and outflows of emissions and waste in the system boundaries (Rashid and Yusoff, 2015). According to ISO standards (ISO-14040, 2006, ISO-14044, 2006), a LCA study comprises of four stages, as illustrated in Figure 2-35; goal and scope definition; inventory analysis; impact assessment and interpretation.

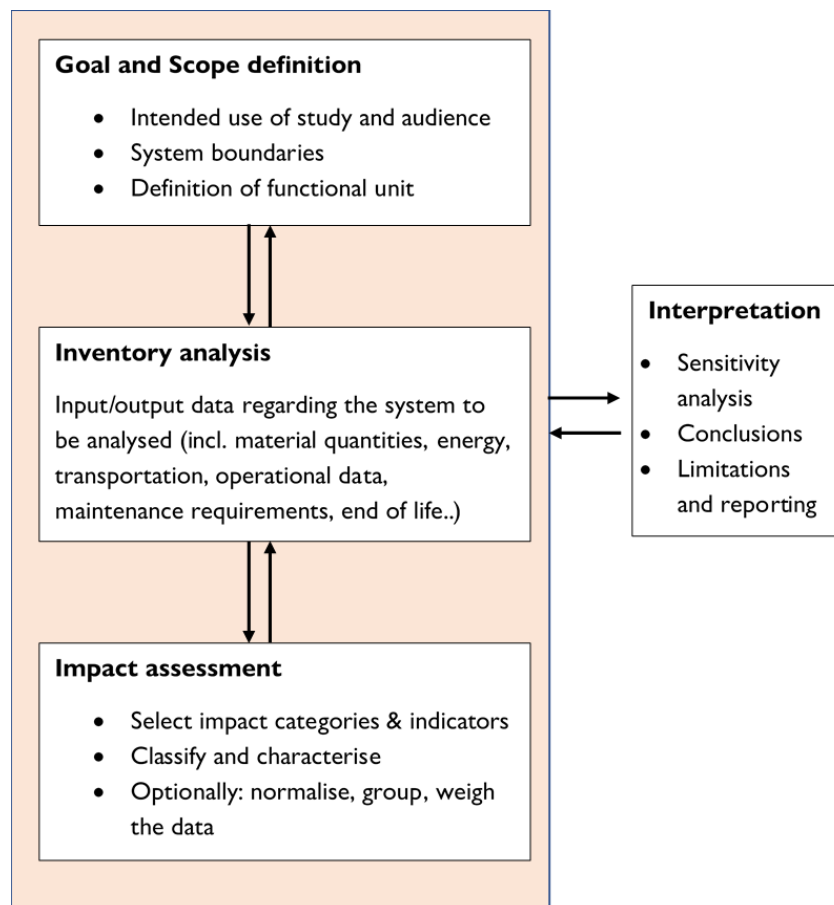


Figure 2-35: The LCA framework according to ISO 14040

Firstly, the aims and scope of the study should be defined. This includes the intended audience and purpose of the study, the system boundaries and a suitable functional unit that will make the LCA study easy to interpret and comparable to others. There are two common LCA types; “*cradle-to-gate*” which focuses on the production phase and “*cradle-to-grave*” which includes production, use and end of life of the material (Arvidsson, 2017). Also, at this stage, the methodology of impact assessment and the impact categories (eg. global, regional and local impacts) that will be analysed should be chosen. In terms of system boundaries, it is important to distinguish between the *Foreground* system (i.e. the processes directly considered in the study and that influence the results) and the *Background* system, which are the processes interacting with the foreground through energy and material flows (Arena, 2016). Secondly, inventory data are collected and quantified. The foreground data are usually primary (collected directly by the researcher), whilst the background data are secondary (collected from an inventory database that is provided in an LCA software package). In the impact assessment stage, the environmental burdens are classified, characterised, normalised and aggregated in a set of categories based on their potential impact on human health and environment. Some burdens relate to more than one impact categories and at this stage the results need to be allocated to their respective categories. At this stage, the results can be normalised, meaning that they will be presented as a fraction of the impacts of all human activities globally (person equivalent units). There are different approaches in analysing the impact categories, such as CML2001, Eco-indicator 99 and Impact 2002+. An example of the mid-point and damage categories (end-point) according to Impact 2002+, which is the chosen methodology in this study, is illustrated in Figure 2-36. The final stage of the LCA includes the identification of key issues associated with the LCA results, evaluation of the completeness and sensitivity of the LCA, identification of limitations associated with the study, and finally discussing the conclusions and recommendations (Hou, 2014).

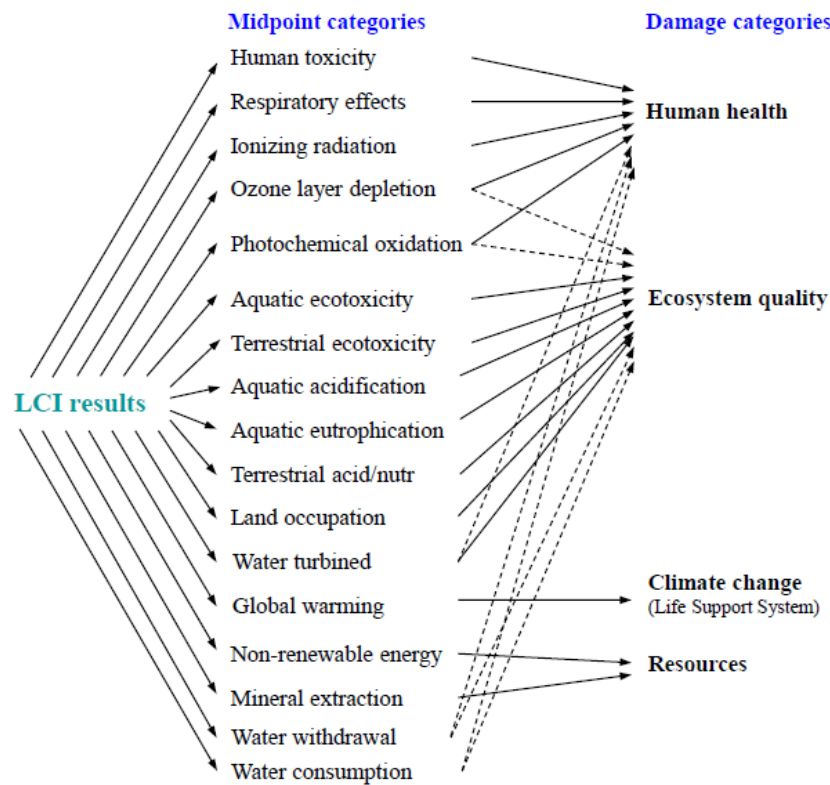


Figure 2-36: Lifecycle impact (LCI) results classified in midpoint categories and grouped in end-point damage categories according to Impact 2002+ methodology (Jolliet et al., 2003)

The use of LCAs as a sustainability tool in the industry has increased steadily since the 1990s (Rashid and Yusoff, 2015). However, many LCAs focus on a specific part of the building lifecycle but very few cover the whole life span (Ortiz et al., 2009; Ghattas et al., 2016). The built environment accounts for 39% of global energy related CO₂ emissions, however, a survey in the UK by Orr et al. (2019), found that embodied energy efficiency is not currently a high priority in structural design, whilst ease of construction is more valued. LCAs have shown that concrete has the highest embodied energy but the operational phase of buildings consumes most of the energy, and from a lifecycle perspective, concrete performs slightly better than timber buildings (Rashid and Yusoff, 2015). The Concrete Centre (2016b) showed that by taking advantage of the thermal mass of concrete, the operational emissions can reduce, and the concrete carbonation process can lead to CO₂ uptake. In terms of volume, concrete remains the building material of choice with global cement demand expected to reach 5,500Mt by 2050 (Allwood and Cullen, 2012). Therefore, LCAs for cementitious materials are important to understand the embodied energy and

environmental performance over the lifespan of the structure. Some studies have looked at replacing certain concrete components, such as sand and cement with recycled aggregates or with alternative binders. As an example, Turk *et al.* (2015) found that when part of the natural aggregate was replaced by waste concrete aggregate, the environmental impact was reduced to about 88%, however, their sensitivity analysis showed that the results were sensitive to the material transport distances. Another study found that the global warming potential was strongly related to the average amount of cement used and it was independent of whether the aggregates were natural or recycled; with CEMII performing better than CEMI (Braga *et al.*, 2017). Using GO, it was found that compared to mortars with natural aggregates, those with recycled fine aggregates and 0.2wt.% GO led to 6.7% CO₂ reduction for the equivalent mechanical strength (Long *et al.*, 2018), however their LCA analysis was not thorough and very limited results and data were presented. Therefore, despite the significance of LCAs for understanding the sustainability of structures, most studies to date have focused on buildings and on improving certain aspects of the building performance. The base case assumed is not always representative of the materials used in practice and therefore it is difficult to directly implement on infrastructure projects.

The LCA studies on graphene production methods are scarce and they have been summarised by Arvidsson (2017) with the most relevant ones being presented here. An early cradle-to-gate LCA was carried out to assess GNP production routes that were either based on ultrasonication or chemical reduction and it was shown that the ultrasonication route was better in terms of energy and water consumption but had higher human and ecotoxicity impact (Arvidsson *et al.*, 2014). Another cradle-to-gate LCA of three different GNP production routes; namely electrochemical exfoliation of graphite rods, graphite chemical oxidation with subsequent chemical or thermal reduction and chemical vapour deposition; has been carried out (Cossutta *et al.*, 2017). This study focused on GNPs produced by laboratory scale equipment and carried out a commercial scale simulation. It was found that the chemical reduction processes (with thermal or chemical oxidation) were the least impacting production methods for manufacturing large GNP quantities (Cossutta *et al.*, 2017). However, no LCA study to date has been published on the industrial scale graphene production.

2.6. Summary

Concrete is one of the most used infrastructure materials, however, it is associated with negative sustainability impacts, poor durability, and a need for structural monitoring, which in itself poses certain challenges. The emergence of biomimetic materials and nanotechnology allows for advanced functionalities to be instigated such as self-healing and self-diagnosing. Since graphene's isolation in 2004, there has been increasing interest in the use of GRMs in concrete structures. However, dispersion of GRMs is one key challenge in the literature and different dispersion methods are employed. A hybrid of chemical and mechanical techniques is usually followed and the homogenous dispersion of GRMs in a suspension of water and superplasticiser before adding to cement has been found to be an effective technique. Yet, there are discrepancies on the types of admixtures used, duration of sonication and there is also no direct technique to assess dispersion.

Following the dispersion challenge, extensive experimental focus has been placed on the early age performance of cement composites with GRMs. There is consensus that GRMs impair the rheological performance and workability, whilst there are disagreements in terms of hydration. Uncertainties persist on the effect of GRMs on the mechanical and durability properties of cementitious composites, with studies often reporting conflicting results. The electrical conductivity of GRM-cement composites has also been investigated, and it was found that GNPs can enhance the conductivity and could potentially instigate a self-sensing mechanism. However, there are differences on the dosages required to create a conductive path. Overall, the mechanism of interaction between GNPs and the cement matrix is still not well understood and the consequent effect of GNPs on the different structural properties of cementitious materials cannot be deducted with confidence. Finally, the sustainability of new composite materials is crucial, however, the literature on the effect of GNPs production is scarce and there is no study to date on the GNP impacts when added in cementitious composites. Based on this literature, this thesis aims to develop a dispersion protocol and consequently investigate the effect of GNPs on the properties of cementitious composites, including early age performance, mechanical and durability properties, and electrical conductivity. This thesis also addresses the sustainability concerns by carrying out a Lifecycle Assessment study for using GNPs in concrete.

Chapter 3. MATERIALS AND EXPERIMENTAL PROCEDURES

This chapter provides a detailed description of the materials, sample preparation and experimental procedures that were used in this study. Different graphene-related materials (GRMs) were employed to modify the cement pastes and mortars. Their effect on the early age, mechanical, durability and electrical conductivity properties of cementitious composites was investigated experimentally. Some of the experimental work in this thesis, was carried out as part of a secondment to the Italcementi – HeidelbergCement *i-lab* research facility in Bergamo, Italy, and this will be specified in the relevant chapters.

3.1. Materials

The main materials in this study were Portland cement (CEMI and CEMII), natural aggregates, GRMs, and surfactants (plasticisers and superplasticisers). The primary GRMs used in this study included three different products of natural graphite with varying sizes and properties as well as a graphite nanoplatelet (GNP) product. Four different chemical admixtures were used to aid the GNP's dispersion and were all supplied by BASF, Germany. Additional materials were used during the experimental testing that was carried out in *i-lab*. These include, graphene oxide (GO), carbon nanotubes (CNTs), two different types of cements, silica fume (SF) and a polycarboxylate superplasticiser. The chemical and physical properties of all the materials were either provided by the suppliers or obtained in the laboratory and are presented in the following sections.

3.1.1. Cementitious materials

Portland Cement CEMI 52,5N, supplied by Hanson Cement and conforming to BS EN 197-1:2011 was used for most of the experimental work, unless specified otherwise. A set of experiments were carried out with a blended Portland-limestone cement with 18% limestone (CEMII/A-L 32,5R) supplied by Tarmac (trade name Blue Circle). For the specimens prepared in *i-lab*, a Portland cement CEMI 52.5R, supplied by HeidelbergCement, was used. For a small number of samples prepared in *i-lab*, two additional cements and silica fume were also used, however the exact composition of these cements was not disclosed. The physical properties and chemical composition of the different cementitious materials used in this study are presented in Table 3.1.

Table 3.1: Physical properties and chemical composition of the cements used in the work presented in this thesis (provided by the suppliers)

		CEMI 52,5N	CEMII/A-LL 32,5R	CEMI 52,5R (<i>i-lab</i>)
Physical properties	Mean size (μm)	5 – 30	5 – 30	-
	Surface area (m^2/g)	0.3 – 0.4	0.4 – 0.6	0.48
	Density (g/cm^3)	2.7 – 3.2	2.7 – 3.2	3.14
	Loss on ignition LOI %	2.2	-	2.08
Oxides (%)	CaO	63.4	66.1	63.2
	SiO ₂	20.4	20	18.7
	Al ₂ O ₃	4.7	4.2	4.6
	Fe ₂ O ₃	2.7	2.7	4.6
	MgO	1.0	1.0	1.7
	K ₂ O	0.6	0.5	0.7
	SO ₃	3.1	3.1	3.5
	Cl	0.02	0.01	0.02

3.1.2. Aggregates

The aggregate used to fabricate cement mortars was fine sharp sand provided by Ridgeons, Cambridge. Its particle size distribution (Figure 3-1) was determined according to ASTM Standard C33 (2018), and the particles that were >2 mm were removed. For the mortars that were prepared in *i-lab*, sand was supplied in pre-packed bags of 1350 (± 5) g by NormenSand (Germany) conforming to BS EN 196-1 (2016), with a grain size distribution from 0.08 to 2.00 mm and a maximum moisture content of 0.2%.

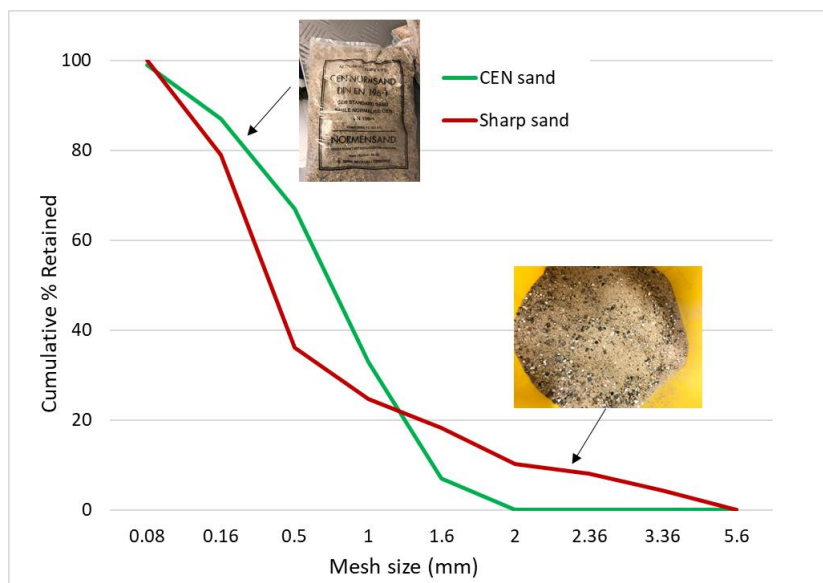


Figure 3-1: The particle size distribution (PSD) of the sharp-sand and the pre-pack CEN sand in *i-lab*

3.1.3. Graphene-related materials (GRMs)

The primary GRM used in this study was a GNPs product called G2NanPaste, supplied by Nanesa (Italy) in paste form. The paste contained 95% water and 5% active GNPs and the active content was measured at bi-weekly intervals by drying the paste in the oven at 105°C for 24 hours to evaporate the water. Three commercial products of natural graphite were also used. A coarse graphite powder (-10mesh) was supplied by AlfaAesar, (USA), and two finer graphite powders (-100 mesh and -325 mesh) were supplied by SigmaAldrich, UK. In *i-lab*, graphene oxide (GO), carbon nanotubes (CNTs) and a functionalised graphene (FG) were tested. The GO was supplied by Graphenea (Spain) in a water dispersion with 0.4 wt.% concentration whilst the CNTs were an experimental product supplied by a University (confidential). The information on FG was also confidential and it was an experimental product. The GRMs are shown in Figure 3-2 and some of their key properties that were provided by the suppliers are listed in Table 3.2. Additional characterisation work for some of the materials was carried out and is presented in Section 4.1.2.

Table 3.2: Key properties of GRMs used in the study (provided by the suppliers)

Property	GNPs (G2NanPaste)	Coarse graphite	Medium graphite	Fine graphite	GO (i-lab)	CNTs (i-lab)
Appearance	Black-grey colour, paste form	Black, steel-gray, powder	Grey, powder	Grey, powder	Yellow-brown water solution	Black powder
Carbon content	>97%	99.94%	99%	99%	49-56%, O = 41-50%	>93% purity
Aver. flake thickness	14 nm (40 layers)	-	-	-	Monolayer >95%	Not provided - confidential
Average particle size	30 μm (D50 = 25 μm)	-10mesh (2mm)	-100mesh (0.150mm)	-325mesh (44 μm)	< 10 μm	-
Additional info:	Surface area = 30 m ² /g	No additional information provided				Bulk density = 26-30 kg/m ³



Figure 3-2: Photos of GRMs used in this study (excluding the *i-lab* materials). From left to right: coarse graphite, medium graphite, fine graphite, graphite nanoplatelets (GNPs)

3.1.4. Chemical admixtures for dispersion

To aid the dispersion of GRMs in the cement matrix, four different chemical admixtures were tested: a lignosulphonate, a naphthalene-based and two polycarboxylate superplasticisers. The chemical admixtures used were plasticisers and superplasticisers that are often used in many modern concrete mix designs. All the admixtures were supplied by BASF and are shown dispersed in water in Figure 3-3 and their properties are listed in Table 3.3.

Table 3.3: Properties of the chemical admixtures used in the study (as supplied by BASF)

Type	Commercial product	Solid content %	Dosage (% weight of cement)	Appearance	Specific gravity (g/cm ³)
Lignosulphonate	MasterPozzolith 324N	0.4	0.24 - 0.71	Brown liquid	1.18
Sulphonated Napthalene	MasterRheobuild 1000	0.4	0.84 - 1.44	Dark brown liquid	1.20
Polycarboxylate ether	MasterEase 3820	0.29	0.32 - 2.16	Light brown liquid	1.08
Modified polycarboxylic ether	MasterGlenium C315	0.35	0.22 - 3.3	Off white opaque liquid	1.10

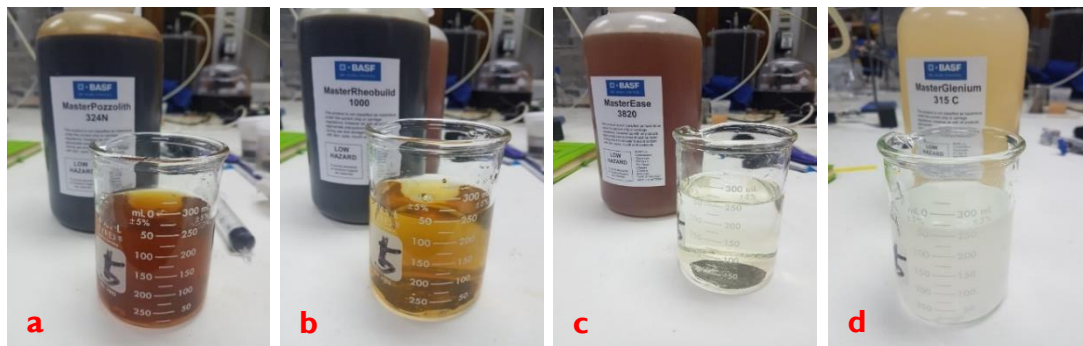


Figure 3-3: Chemical admixtures used for the dispersion of GNPs, supplied by BASF and shown dispersed in water – (a) MasterPozzolith324N (b) MasterRheobuild1000 (c) MasterEase3820 (d) MasterGlenium315C

For the *i-lab* mixes, a polycarboxylate superplasticiser (Driver31 by Sika), was employed and to determine its dry content (BS EN 480-8, 2012), a Mettler Toledo HR83 moisture analyser was used (Figure 3-4). 1g of the admixture solution was added and the superplasticiser dry content was determined as 24.37%.

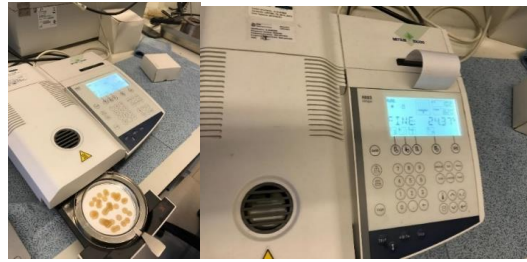


Figure 3-4: Mettler Toledo HR83 moisture analyser to determine the dry content of the Sika Driver3 I

A risk assessment and COSHH assessments were undertaken prior to working with the materials. The main risk arose from the use of nanomaterials and it was associated with the potential for inhalation. This was mitigated by wearing a FFP3 respirator face mask and using a fume cupboard when measuring and mixing the nanomaterials.

3.2. Sample preparation

This section presents the methodology followed for the preparation of the GNP suspension as well as the cement paste and cement mortar composite samples. The different methodologies that were followed in *i-lab* are specified in the text.

3.2.1. GNP suspension preparation

The GNP suspension preparation protocol builds on previous experimental work undertaken as part of the MRes thesis (Papanikolaou, 2017). The dispersion protocol included the use of a chemical admixture to improve dispersion and the use a bath sonicator, FBI1203 by Fisherbrand® operating at a sonication frequency of 37 Hz and power of 100W. The four different superplasticisers in Table 3.3 were tested. The GNPs were added in paste form (G2NanPaste) in a beaker containing water and the respective superplasticiser as illustrated in Figure 3-5.

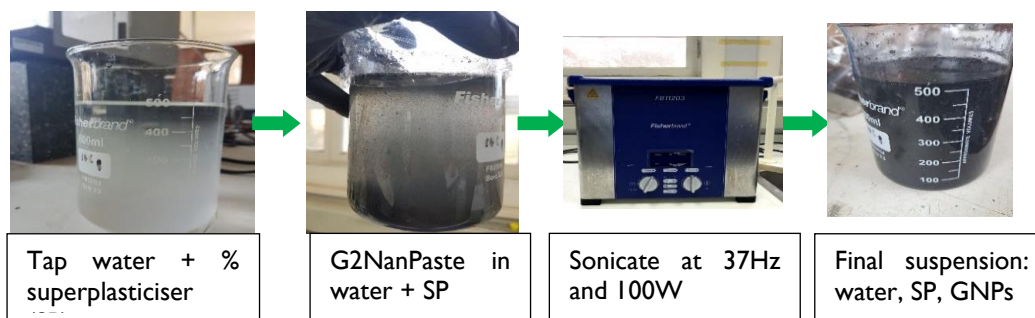


Figure 3-5: GNP suspension preparation using a bath sonicator and superplasticisers

During sonication, it was important to control the temperature increase of the suspension as it could result in damage of the GNP structure and to water evaporation which would consequently affect the w/c of the resultant mixture. For this reason, the temperature was controlled by replacing the water in the bath sonicator every 5 minutes. The sonication was stopped every 5 minutes for 30 seconds to replace the water in the bath sonicator and this helped in maintaining the sonication temperature between 20°C - 23°C for all suspensions.

In *i-lab*, a different solution preparation methodology was followed due to different equipment being available. Instead of the bath sonicator, a QSonica Q700 tip sonicator was used with a 12mm tip for 15 minutes (Figure 3-6). Mixing was paused every 5 minutes for 1 minute to control and measure the temperature. A cold-water bath was used to immerse the beaker to control the temperature increase in the solution.

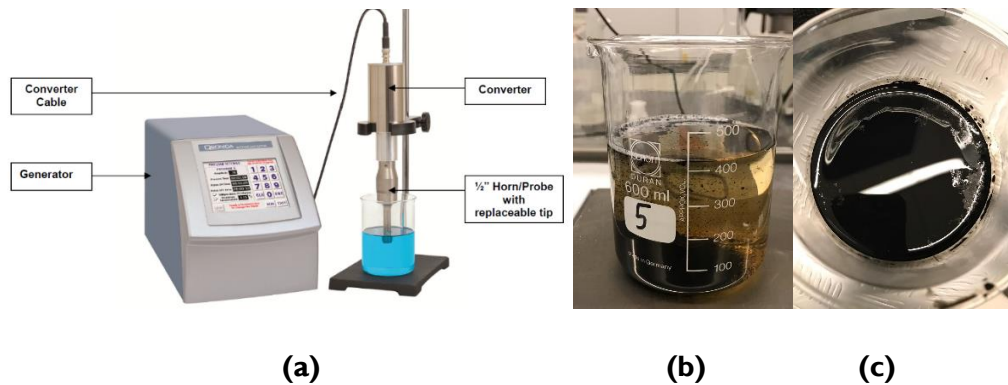


Figure 3-6: *i-lab* mixing (a) Qsonica Q700 tip sonicator - 12mm tip (b) a CNT suspension in water and superplasticiser before sonication and (c) after sonication

3.2.2. Cementitious composites

For the preparation of the cementitious composites, in the form of cement paste or mortar, BS EN 196-1 (2016) was followed. A laboratory bench-scale mixer, Kenwood I500 W, was used for all mixes. The cement powder was placed in the mixer bowl along with 60% of the total mix water. Immediately when the water and cement were brought into contact, the mixer was started at low speed for 10 seconds. Then the solution containing the sonicated GNPs, superplasticiser and the remaining 40% of the mix water was added and mixing continued at slow speed for another 50 seconds and at high speed for 30 seconds. Then the mixer was stopped for 90 seconds and during the first 30 seconds the paste/mortar adhering to the walls and bottom of the bowl was removed with a scraper and placed in the middle of the bowl. Then, mixing continued at high speed for 60 seconds. For preparing

cement mortars, the same methodology was used but sand was added slowly in the first 30-60 seconds. When mixing was completed, the fresh paste or mortar was cast in three layers of equal thicknesses in oiled stainless-steel moulds. A vibrating table was used for 10 seconds to ensure that each layer was properly compacted and that no air was entrapped. The specimens were demoulded after 24 hours and cured in a water tank at temperatures of $20^{\circ}\text{C} \pm 2^{\circ}\text{C}$ and a relative humidity 60% until testing. The overall mix preparation methodology is illustrated in Figure 3-7 and Table 3.4 summarises the specimen types and testing that was carried out. The 20x20x80mm prisms that were cast for electrical resistivity testing as well as the 10x50mm discs for gas permeability testing, were placed in a rubber mould instead of a stainless steel one.

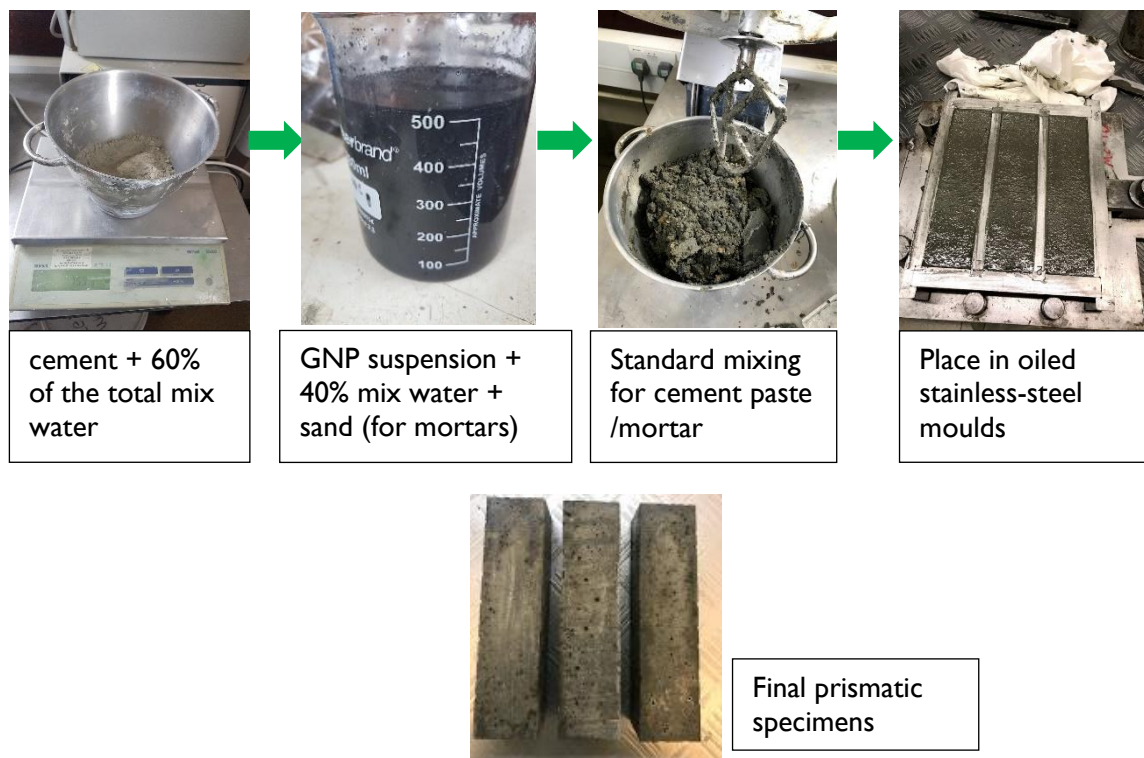



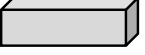
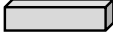


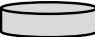

Figure 3-7: Cement paste and mortar preparation methodology

A different mixing protocol was followed for cement paste mixes with natural graphite. In this case, the graphite powder and cement were dry mixed for 2 minutes first before the water was added. Immediately when the water was added in the bowl, the mixer was started, and the same mixing and curing protocol was followed as for the rest of the samples. For certain tests, such as rheology testing and isothermal calorimetry, hand mixing of the cement paste was necessary due to the very small volumes that were required for the test. In this case, 30 g of cement were mixed with 13.5 ml of water ($w/c=0.45$) and varying

dosages of superplasticiser and GNP in a plastic cup. The suspension of water, superplasticisers and GNPs has already been mixed to ensure uniform dispersion. Hand mixing was carried out for 3 minutes using a plastic spoon and a vortex mixer.

Finally, some samples were prepared with a cement-based GNP coating. The coating contained cement paste, GNPs and superplasticiser, whilst the substrate comprised of cement paste only. The mixes were applied as two layers in 20x20x80 mm moulds, and each layer had the same depth, which was approximately 10mm and they were applied by hand using a spoon and trowel.

Table 3.4: Summary of specimen types prepared for each testing method

Specimen type	No	Test description	Age (days)				
			2	7	28	56	154
Prism (40x40x160mm) 	3	3-point bending (flexural strength). Cement paste and mortars	✓		✓		
Prism (40x40x160mm) 	3	Electrical conductivity (surface & embedded electrodes). 4-probe with DC current. Cement paste	✓	✓	✓	✓	✓
Prism (20x20x80mm) 	3	Electrical impedance spectroscopy (EIS). 2-probe method with AC current. Cement paste		✓	✓		
Cylinder (100 x 100 mm, slices) 	1	Micro-indentation. Cement paste	✓		✓		
Cube (40mm ³) 	6	Compressive strength	✓		✓		
Disc * (50 mm x 100 mm diameter) 	2	<ul style="list-style-type: none"> • Water sorptivity • Rapid Chloride penetration testing (RCPT) 	✓		✓		
Disc (10mm x 50mm diameter) 	3	Gas permeability	✓		✓		
Chipped pieces from broken surfaces	N/A	<ul style="list-style-type: none"> • SEM-EDS • MIP • TGA • XRD 	✓		✓		

*A 200mm height cylinder was cast for each test age and then four slices were cut out (50mm each)

3.3. Experimental procedures

3.3.1. Microstructure, dispersion and thermal characterisation

To assess the effectiveness of dispersion with different superplasticisers, zeta-potential, UV-Vis spectroscopy, visual observations and rheology testing were undertaken. To assess dispersion of natural graphite SEM and CT scan were used. To characterise the microstructure and early age thermal performance of the materials and the cement pastes/mortars, SEM-EDS, X-Ray diffraction analysis (XRD), thermogravimetric analysis (TGA), and isothermal calorimetry were carried out.

3.3.1.1. Zeta (ζ)-potential

Zeta-potential (ζ) testing was used to assess the dispersion of the GNP particles in the suspension of water and the different superplasticisers. When a solid particle ($>1\text{nm}$) is dispersed in water, an electrochemical double layer is created. A potential (ζ) at the slipping plane between the solid particle and the liquid medium is formed and its magnitude shows the degree of electrostatic repulsion between adjacent particles (Figure 3-8). A PA Field ESA device was used, where a high AC was applied, generating a sound wave response of the particles that corresponds to their dynamic mobility (ζ -potential). The ζ values depend on the pH and the conductivity of the dispersive medium (Caputo, 2015) and these values were simultaneously measured by the device. 20 measurements were taken for each test.

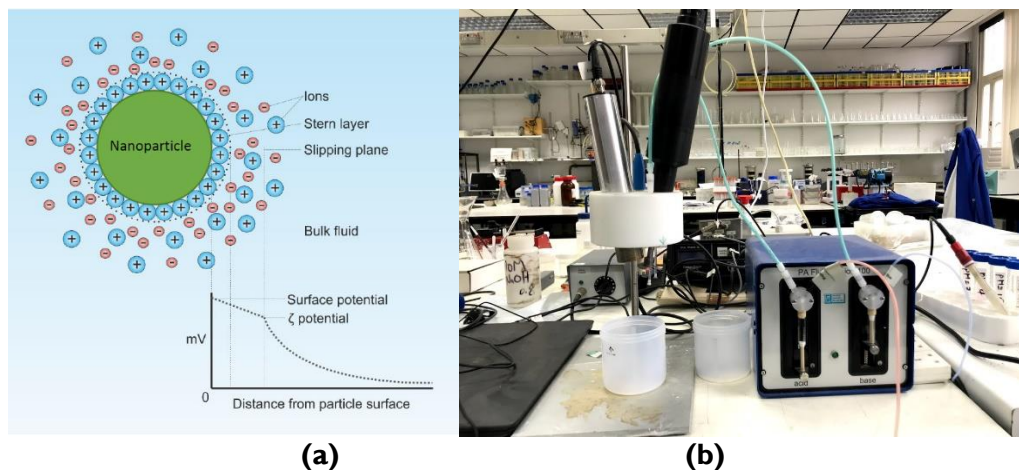


Figure 3-8: Zeta-potential (a) schematic of the electrochemical double layer (b) PA Field ESA device.

3.3.1.2. UV-Vis spectroscopy

The dispersion of GNPs and the effect of the chemical admixtures can be determined by UV-Vis spectroscopy. When electrons in atoms and molecules are excited, they can absorb visible and ultraviolet (UV) radiation. UV-visible spectrometers can measure the absorbance of UV or visible light by a sample at a wavelength spectrum range (UV region is 190-400nm, visible region is 400-800nm) (Royal Society of Chemistry, 2009). The absorbance versus wavelength curves will show a single wavelength that corresponds to the highest absorption (λ_{max}). The measurements are based on the Beer-Lambert Law which states that the absorbance is proportional to the concentration of the substance in the solution, so UV-Vis spectroscopy can be used to measure the concentration of sample.

$$A = ecl \quad (\text{Eq. 3})$$

where: A = absorbance, e= molar absorption coefficient (constant for a substance at a particular wavelength), c = concentration of solution, l = optical path length (cell/cuvette dimension). This law is true for dilute solutions but might not be applicable at higher concentrations and a plot of absorbance against concentration will be non-linear. Here, a Perkin Elmer Lambda 35 spectrometer was used (Figure 3-9) and 5 samples were tested for each concentration.

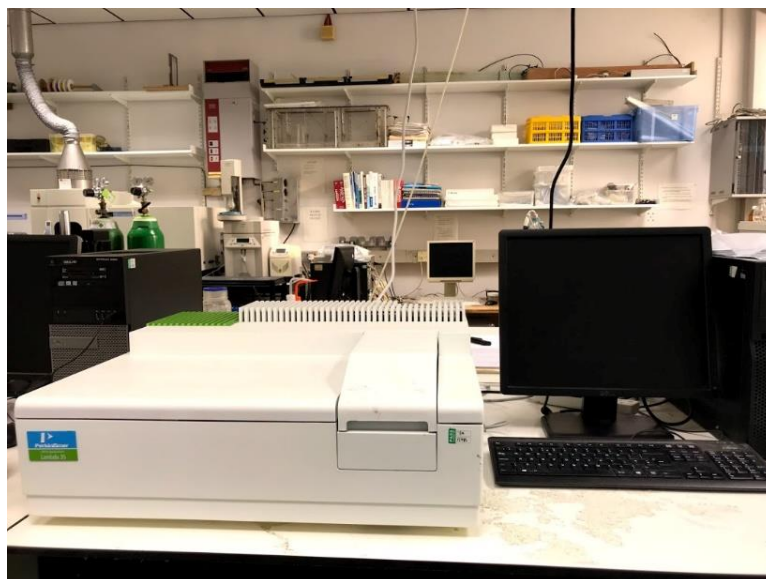


Figure 3-9: UV-Vis spectroscopy device for this study was a Perkin Elmer Lambda 35

3.3.1.3. Scanning Electron Microscopy (SEM) and Energy Dispersive Spectroscopy (EDS)

Scanning electron microscope (SEM) was used to obtain images of the microstructure of the GRMs and the cement pastes/mortars and to assess the dispersion of GRMs in the cement composites. Energy-dispersing X-ray Spectroscopy (EDS) analysis was also carried out to identify the composition of the material. A ZEISS EVO LS 15 SEM-EDX, was used (Figure 3-10). The GRMs were tested in a dry, powder form. For the cement paste/mortars, small chipped pieces were extracted from the cracked faces of the specimens. All cement paste and mortar samples were gold-coated before testing.



Figure 3-10: ZEISS EVO LS 15 scanning electron microscope (SEM-EDS) used for investigating the dispersion of the GRMs and the microstructure of the composites

3.3.1.4. X-ray computed tomography - micro CT-Scanning (μ CT)

X-ray computed tomography is a non-destructive test that can be used to visualise the composition of solid specimens. X-rays are projected onto the specimen (which remains in a fixed position) from 180°-360°. These projections are then used to reconstruct a 3D tomographic image where slices can be taken through the specimen. In this study, a XT H 225 ST CT scan device supplied by Nikon was used (Figure 3-11) to assess the dispersion of natural graphite in cement paste. A small sample (~5mm) was extracted from the cracked surface of the cement paste specimens containing natural graphite and analysed with X-ray computer tomography (μ CT). The resolution of this device was limited and therefore could not isolate the GNPs due to their very small size.



Figure 3-11: μ CT device (left) and sample positioning under the X-Ray source (right).

3.3.1.5. Fluidity characterisation

Fluidity of the fresh cement pastes and mortars was assessed for two reasons. Firstly, the fluidity of fresh mortars was characterised using a flow table as an adequate fluidity is required for mortars and concretes so that they can be pumped and poured on site, but a very high fluidity can result in bleeding and segregation of aggregates. Secondly, a rheometer was used to assess the compatibility of the different surfactants with GNPs during the development of the dispersion protocol and to establish the viscosity of the solutions. Rheology testing was undertaken either 5 minutes after the mixing of cement pastes/mortars has been completed in the benchtop mixer or 5 minutes after the samples were prepared in the vortex mixer specifically for rheology testing. In this study, a smooth-walled Brookfield DV3T Rheometer was used with a SC4-27 spindle (Figure 3-13). The spindle was inserted into the sample cup that was filled with the cement paste.

Measurements were carried out at room temperature and taken every 15 s. Each sample was firstly pre-sheared for 1 minute to account for any shearing that was experienced when the sample was mixed and transferred, and it was then left for a further 30 s to stabilise at 0 speed before the test started. The shear speed then increased progressively from 0 to 150 rpm in 25 rpm intervals (ascending rates). It was then kept constant at 175 rpm and then decreased progressively from 150 to 0 rpm again in 25 rpm intervals (descending rates). The Bingham rheological model was followed in this research, as it was found to provide a suitable fit for cement pastes with high w/c (up to w/c=0.42 tested in Papo (1988)). The Bingham model correlates the shear stress, shear rate and viscosity by (Shang *et al.*, 2015):

$$\tau = \tau_0 + \eta_p \dot{\gamma} \quad (\text{Eq. 4})$$

where τ is the shear stress (Pa), τ_0 is the yield stress (Pa), η_p is the viscosity (Pa s) and $\dot{\gamma}$ is the shear rate (1/s). In a graphical form (Figure 3-12), the plastic viscosity is given by the gradient of the best fit line of the descending shearing rates (because the thixotropic structure is broken down during the ascending rates and the results are simpler and more reproducible (Papo, 1988), whilst the yield stress is given by the y-axis intercept.

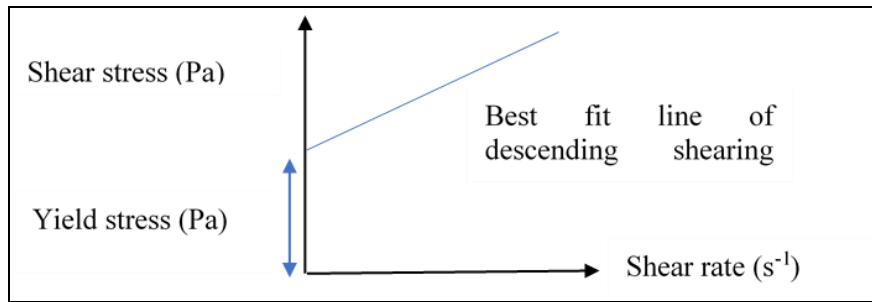


Figure 3-12: Calculation of yield stress and viscosity

The fluidity of the fresh mortars could not be assessed with the rheometer due to the very high friction that was developed between the spindle and the sand particles. Instead, the fluidity was measured as per BS EN 1015-3 (1999) with a flow table test (Figure 3-13). The fresh mortar was added in the bronze mould in two layers and tamped lightly to remove air and then the mould was quickly removed, and the table was vibrated 15 times (electrically operated). The fluidity of the collapsed mortar was measured in two perpendicular directions with an accuracy of ± 1 mm.

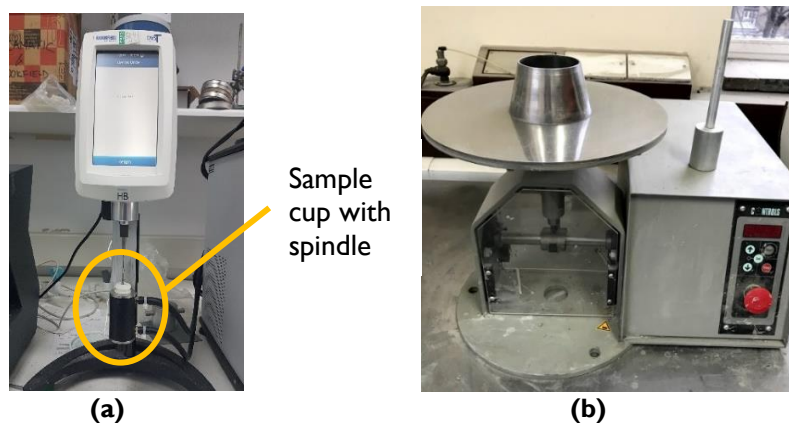


Figure 3-13: Brookfield DV3T Rheometer (a) and flow table used for workability evaluation (b)

3.3.1.6. X-Ray Powder Diffraction Analysis (XRD)

X-ray diffraction analysis (XRD) was utilised to identify the crystalline phases present in the cementitious specimens and to also characterise the GRMs. For the cement composites, chipped pieces were extracted from the cracked surfaces following strength testing and they were grinded to collect powder. The powder was then passed through a 25 μ m sieve before being used for XRD and thermogravimetric analysis (TGA) (described in Section 3.3.1.7). XRD was performed with a Siemens D500 X-ray diffractometer (Figure 3-14) with a CuK α source operating at 40kV and 40mA with the powder sample being mounted onto an aluminium sample holder. Scanning was carried out between $10^\circ < 2\theta < 60^\circ$ at a rate of 0.02 $^\circ$ /step and 1s/step. The peaks were found from the PDF-2004 database using X'pert Highscore software.

3.3.1.7. Thermogravimetric analysis (TGA)

Thermogravimetric analysis (TGA) shows the mass change of a sample with temperature and can be used for phase identification, reaction rate, investigating the sample purity and composition. TGA is more sensitive than XRD analysis and hence it can be used to quantify low amounts of hydration/carbonation products. It allows for identification of the amorphous phases and can be used to quantify the non-evaporable water and portlandite contents, which helps in tracking the degree of hydration. In this study, a STA6000 equipment was used (Figure 3-14). The temperature ranged from 40 $^\circ$ C to 1000 $^\circ$ C at a steady rate increase of 10 $^\circ$ C/min and the gas flow rate was kept constant at 30mL/min. The sample preparation was the same as for XRD testing.

3.3.1.8. Isothermal calorimetry

Isothermal calorimetry testing was used to measure the rate of hydration of the cement paste (exothermic reaction) over time when kept at a constant temperature. This test provides an insight in hydration behaviour, setting times and early strength gain and can be used to understand the effect of the GRMs on the hydration of cement. An isothermal calorimeter I-CAL 2000 HPC was used for the tests (Figure 3-14) and the ASTM C1679-08 (2008) standard was followed. The temperature in the calorimeter was set at 23 $^\circ$ C and was left to stabilise for 24 hrs before testing. The mixes were prepared by hand using a plastic spoon. The total test duration was 48 hrs.

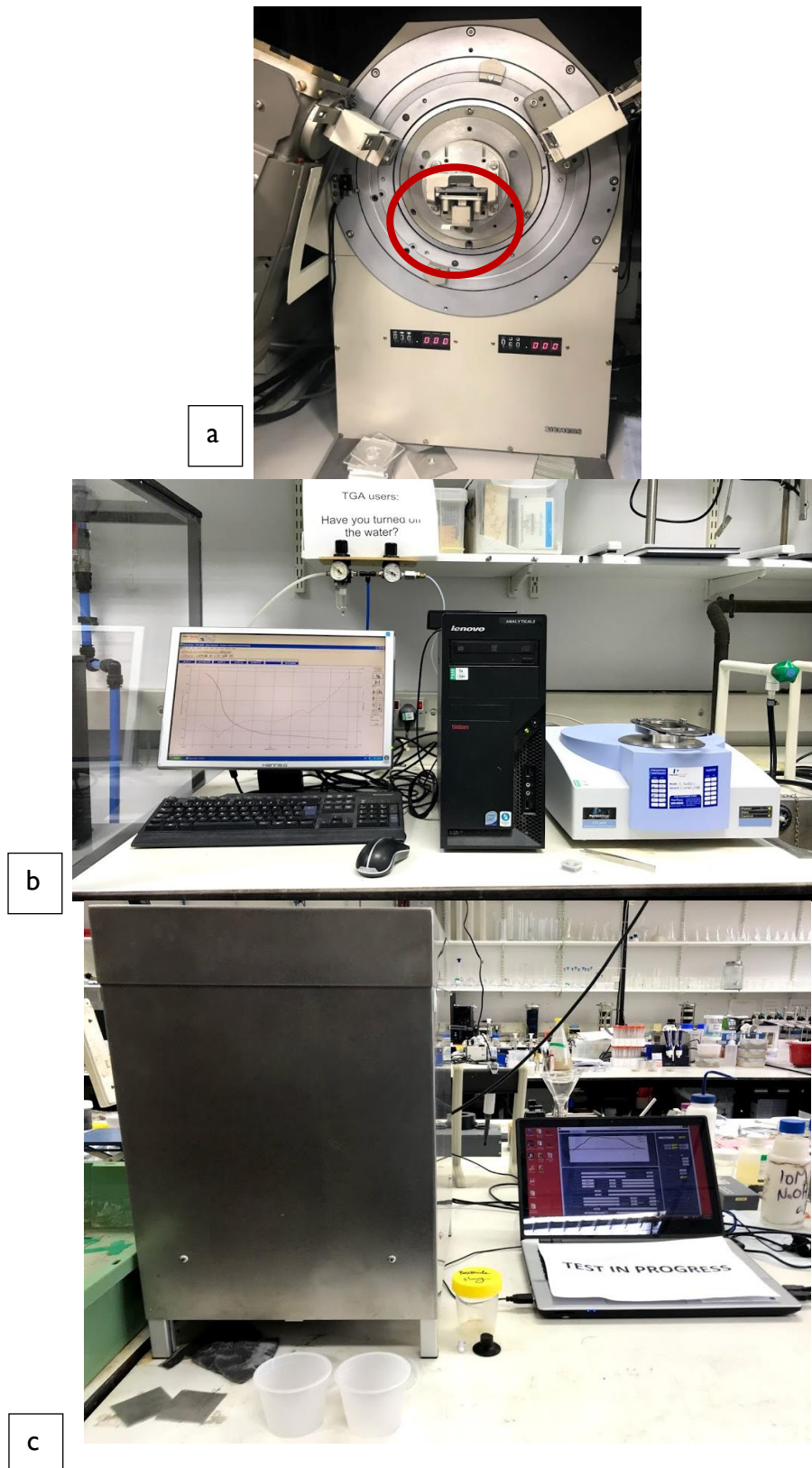


Figure 3-14: Equipment used for thermal analysis (a) XRD device Siemens D500 where the sample holder is circled in red (b) Thermogravimetric analysis (TGA) (c) I-CAL 2000HPC device for isothermal calorimetry testing

3.3.2. Mechanical characterisation

The effect of GRMs on the mechanical properties of cement composites was characterised by flexural and compressive strength testing as well as micro-indentation at specific time intervals.

3.3.2.1. Flexural strength test (3-point bending)

The flexural strength was determined with a 3-point bending test (Figure 3-15) on prismatic specimens with dimensions 40x40x160 mm. Triplicate testing was undertaken for every mix design. BS EN 196-1 (2016) was followed, and the tests were performed at 2 and 28 days of curing. A CONTROLS Uniframe machine was used at a loading rate of 50 N/s. The flexural strength was then determined based on:

$$R_f = \frac{1.5 \times F_f \times l}{b^3} \quad (\text{Eq. 5})$$

where R_f is the flexural strength (MPa), b is the width of the sample in mm, F_f is the maximum load that is applied to the middle of the prism (N) and l is the distance between the supports (mm).

3.3.2.2. Unconfined compressive strength (UCS)

The UCS of cement paste and mortar specimens was determined according to BS EN 196-1 (2016). Six repeat specimens were tested for each mix design at 2 and 8 days of curing and the cubic specimens with dimensions 40x40x160 mm were tested. A CONTROLS Advantest9 machine was used with a maximum capacity of 250kN at a loading rate of 2400 N/s (Figure 3-15). The UCS was calculated as:

$$f_c = \frac{P_{max}}{A} \quad (\text{Eq. 6})$$

where P_{max} is the ultimate compressive load at failure (kN) and A is the cross-sectional area of the sample. To calculate the area, the dimensions of the cubes were measured and recorded to the nearest mm prior to testing.



Figure 3-15: Flexural strength (3-point bending) (left) and compressive strength testing (right)

3.3.2.3. Micro-indentation

Micro-indentation testing was performed on cement paste samples to establish the hardness and elastic modulus of the specimens as well as to characterise the dispersion of GRMs. Successful micro-indentation was only possible in cement paste composites because the sand particles led to great inhomogeneity as shown in Section 4.3.4. Cylindrical specimens of 50mm diameter and 100mm height were prepared and cut into discs of approximately 25 mm thickness. The samples were tested at 2 and 28 days without any drying, however, their surface was polished as a very smooth surface is required for micro-indentation testing. A P240 silicon carbide (SiC) paper was first used for 30 s for both sides of the disc. One side was then polished progressively using P400-P800-P2500 SiC paper for 30 s in each stage. The polished discs were then tested with an Anton Paar MHT micro-indentation tester (Figure 3-16) with a Vickers tip. The indentation force in this machine can range from 100 mN - 30N. Based on previous work by the author, an indentation force of 8N was selected (Papanikolaou, 2017). The ASTM E384 – 16 (2016) was followed. During the entire test, the machine was protected from vibration and movement. The same process followed by Zhang *et al.* (2014) was used, where the loading and unloading time was 15 s each and the indentation time at maximum force was 20 s (this is different to the ASTM standard but more suitable for a cement paste). A Poisson's ratio of 0.25 has been assumed for all specimens with 15 indentation points measured. A typical load-displacement curve is shown in Figure 3-16 where h_p is the plastic depth and S is the measured stiffness of the unloading data (Zhu and Bartos, 2000).

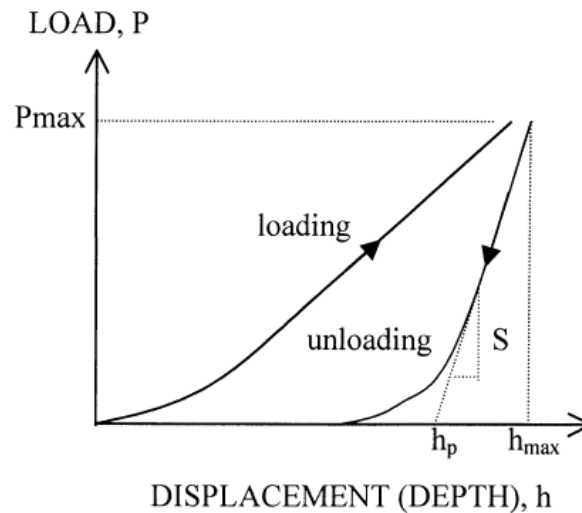
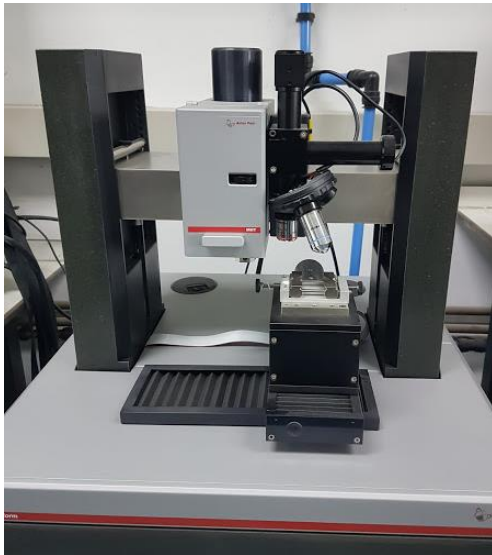


Figure 3-16: Anton Paar MHT micro-indentation testing machine and typical indentation load-displacement curve (Zhu and Bartos, 2000)

3.3.3. Permeability assessment

The permeability of mortars is an important factor for their long-term durability performance. Three different techniques were used in this study to assess the permeability of cement mortars reinforced with graphite nanoplatelets (GNPs) under exposure to water, gas and chlorides. These were water sorptivity by capillary absorption, gas permeability and rapid chloride penetration testing (RCPT). Furthermore, mercury intrusion porosimetry (MIP) testing was carried out as porosity and pore diameter are critical parameters that would affect the permeability of the specimens.

3.3.3.1. Water sorptivity (capillary absorption)

The liquid capillary absorption test was undertaken on mortar samples with different GNP dosages at 2 and 28 days to investigate the effect of GNPs on the sorptivity of the mortars. Disc mortar specimens were used for the testing with a thickness of 50 mm and 100 mm diameter. Duplicate testing was undertaken at each test age. The specimens were placed in an oven at a temperature of $50 \pm 2^\circ\text{C}$ for 3 days or until the mass change was less than 0.1% between 24-hour periods and then the specimens were put under vacuum for a further 24 hours for the temperature to stabilise. The discs were then removed from vacuum and their perimeter was sealed with adhesive tape. The mass of the sealed specimens was measured and was recorded as the initial mass for the specimens. The discs were placed in a tray in 5-10 mm of water (maintained at constant level) on two support pads. The timing device was

activated, and the mass change was recorded at predetermined intervals as per ASTM C1585-13 (2013). Measurements were taken at 60s, 5 min, 10 min, 20min, 30min, 60min, every hour up to 6 hr, once a day up to 3 days, 3 measurements 24 hrs apart from day 4 to day 7 and then 1 measurement from day 7 to day 9. The initial and secondary rates of absorption were then determined using:

$$I = \frac{m_t}{\alpha \times \rho} \quad (\text{Eq. 7})$$

where I is the absorption, m_t is the change in specimen mass (g) over time t , α is the specimen area that is exposed to water (mm^2) and ρ is the density of water (g/mm^3). The measurements from the first 6 hours were used to determine the initial rate of absorption and the remaining measurements to determine the secondary absorption rate.

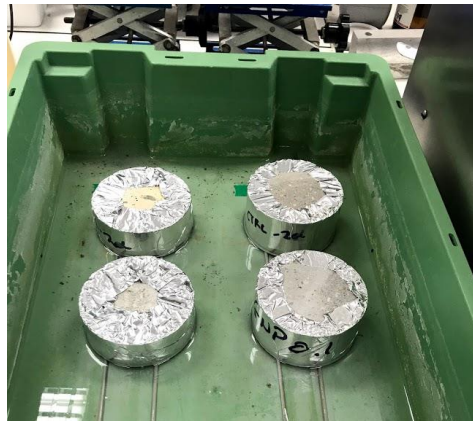


Figure 3-17: Water sorptivity testing with sealed mortar cylindrical specimens being immersed in water (5-10mm) at a constant depth

3.3.3.2. Gas permeability

Gas permeability testing was used in this study to determine the effect of GNPs on the gas permeation of cement mortars. This test is based on a protocol developed by Alshamsi and Imran (2002) where a liquid of known properties is used to measure the gas penetration. Methanol was selected as the permeating liquid in this study due to low boiling temperature (65°C) that allows tests to be run safely at a temperature less than the boiling. 10mm-thick cylindrical mortar discs with a 50mm diameter were prepared specifically for this test. Duplicate testing was undertaken at 2 days, however, due to large variability of the results, triplicate testing was carried out at 28 days. The discs were removed from water at the specified test age (2 and 28 days) and were vacuum dried in a desiccator for 24 hours to

ensure that uniform moisture conditions were reached as moisture content could affect the readings. The discs were then placed on the top of a pre-prepared cell filled with methanol liquid for 1/3 of the glass cell and were sealed with a silicone sealant to prevent leakage of methanol vapor. The initial weight of this whole cell was measured at the beginning of the test and this was recorded as the initial mass. The cell was then added to a water bath of a constant 40°C temperature and the mass change due to the vaporisation of methanol was recorded at 10-minute intervals until steady-state mass loss was reached. Using Darcy's law, the gas permeability coefficient K was determined as follows:

$$K = \frac{k\rho g}{\mu} \quad (\text{Eq. 8})$$

where K is the calculated intrinsic permeability coefficient, g (m/s^2) is the gravitational acceleration, ρ (kg/m^3) is the density and μ (Pa s) is the viscosity of methanol. The gas permeability set up is illustrated in Figure 3-18.



Figure 3-18: Gas permeability experimental set up with cells in the water bath at 40°C

3.3.3.3. Rapid chloride penetration testing (RCPT)

Rapid chloride penetration testing was used to assess the effect of GNPs on the depth of chloride penetration in the mortars and the tests were carried out at 2 and 28 days. Disc mortar specimens were used for the testing with a thickness of 50 mm and 100 mm diameter and duplicate testing was undertaken at each test age. Samples were conditioned based on an adjusted protocol from NT BUILD492 (1999) and the same conditioning method was followed for all samples. The conditioning protocol was as follows: the

specimens were removed from water at the specified test age, then they were surface dried with a towel and put in vacuum for 1 hour to ensure that both surfaces were fully exposed. With the vacuum pump still running, the container was filled (to cover the specimens) with saturated CaOH_2 solution and the vacuum was maintained for a further 20 minutes. Finally, air was allowed to enter the container and the samples were maintained in the solution for a further 2 hours. The migration test then commenced using a PROOVEit machine supplied by Germann Instruments (Figure 3-19(a)). Initially, a 30V voltage was applied to the specimens and the initial current was measured. Based on this value, an adjusted voltage was applied for a set duration, as specified by NT BUILD492. At the end of the test, the specimens were split in the middle and the sprayed with silver nitrate. The chloride penetration depth was measured with a calliper, and five measurements were taken across the length from each slice (Figure 3-19(b)).

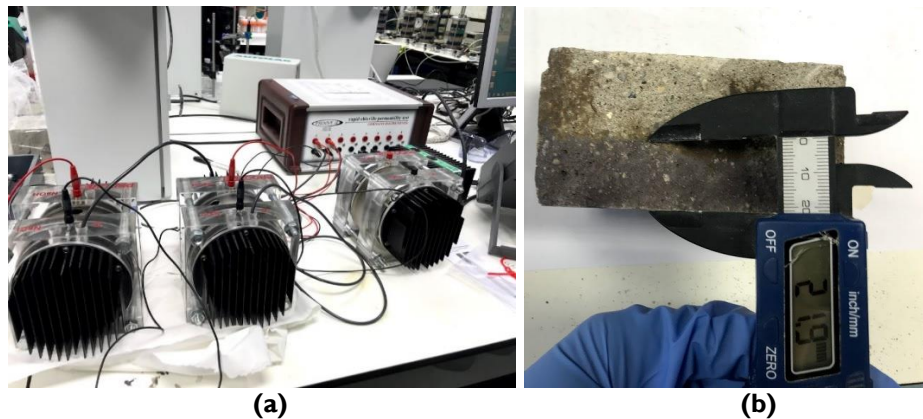


Figure 3-19: Rapid chloride penetration test (RCPT) setup (a) and chloride depth measurement with a caliper (b)

3.3.3.4. Mercury intrusion porosimetry (MIP)

Mercury intrusion porosimetry (MIP) is a technique used to assess the porosity and pore size distribution of cementitious composites. MIP testing was conducted at the Chongqing University in China, using a PoreMaster-60 porosimeter allowing a range of pressures from 0 to 414 MPa and the porosimeter ran on its own software "PoreMaster". Only the specimens from *i-lab* were tested there and one specimen was tested per mix design due to the equipment availability. Following compressive strength testing, broken pieces were collected from the samples and kept in isopropanol to stop hydration until the time of testing. Prior to MIP, the samples were removed from isopropanol and put in an oven at 50°C for 1 hour to dry. After that, they were crushed in smaller pieces (circa 1mm size) to

make sure that they fit in the MIP container and then they were put in vacuum for 1 day until MIP testing, as illustrated in Figure 3-20. A mercury with a density of 13.5g/cm^3 and a contact angle of 140° was used and the measurements were carried out at 20°C .

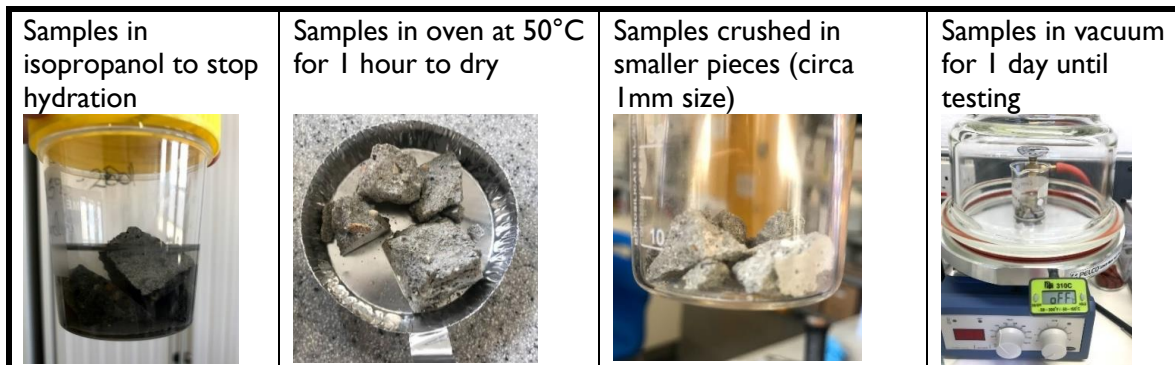


Figure 3-20: Sample preparation for MIP testing.

3.3.4. Electrical conductivity

The electrical conductivity of cement paste specimens was investigated to understand whether GRMs could be used to enhance the conductivity and consequently be used for self-sensing applications. Two different techniques were followed to determine the electrical resistivity (inverse of conductivity); one involved embedded electrodes in the specimen whilst the other measured the surface resistivity. The latter is non-destructive and could be used retrospectively in concrete structures that have already been built. Both techniques, follow a four-probe arrangement with DC current. In this set up, the outer two electrodes or probes are used to supply the electric current and the inner two electrodes/probes are used to measure the corresponding change in voltage. This method was chosen over the two-probe method or a bulk resistivity test, to improve the accuracy and eliminate the effects of the contact resistance between the electrodes and the specimen. Prismatic specimens with dimensions $40 \times 40 \times 160\text{mm}$ were prepared and testing was undertaken at 2, 7, 28, 56 and 154 days to establish the effect of hydration on the electrical resistivity performance. Only cement paste specimens were tested for electrical resistivity.

3.3.4.1. Embedded electrodes – 4-probe technique with DC current

The electrodes were a perforated steel sheet of a thickness 0.55mm and hole size 3 mm supplied by RS Components. As per Figure 3-21, the outer two electrodes (orange) were used to supply the direct current (DC) of 10V and the inner two electrodes (green) were used to measure the voltage, which was recorded with a datalogger every second and illustrated in the LABView software. The electrical resistance and the resistivity were

calculated as per Equations (1) and (2) and the value was then converted to the conductivity (σ), which is the inverse of resistivity:

$$\sigma = \frac{1}{\rho} \quad (\text{Eq. 9})$$

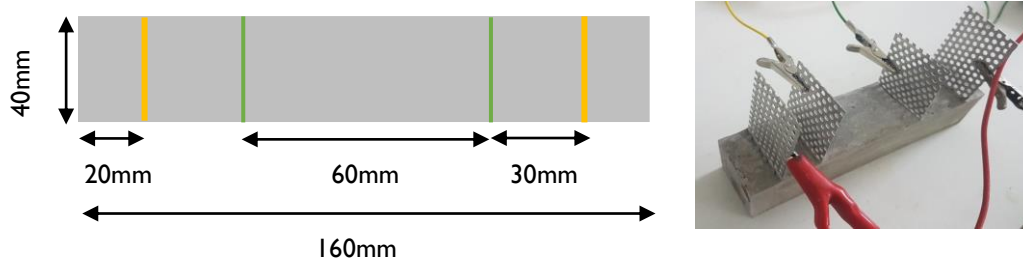


Figure 3-21: Four probe set up for electrical resistivity measurements. Outer electrodes supplied a DC = 10V and inner electrodes measured the change in voltage

3.3.4.2. Surface resistivity

Surface resistivity testing using a four-probe arrangement was carried out using a surface resistivity meter, called Resipod and supplied by Proceq (Figure 3-22). Prior to the test, the sample surface was wetted and the Resipod contacts were dipped in water to ensure a good connection between the sample and the machine. The Resipod was then firmly pressed down on the surface to be measured, until the outer two rubber caps (circled in Figure 3-22) rested on the surface.

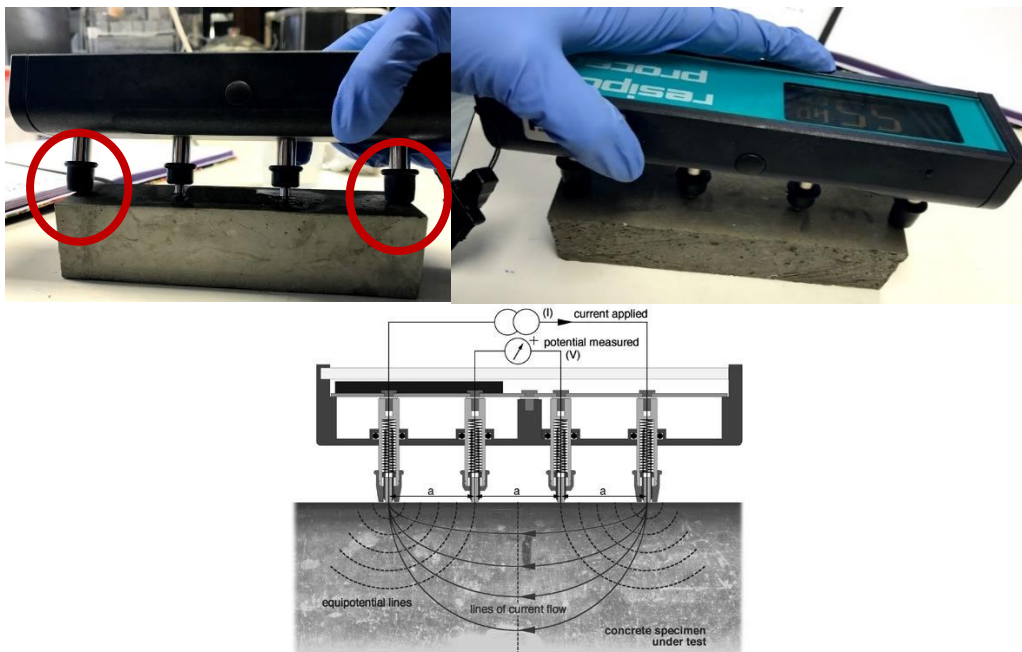


Figure 3-22: Surface resistivity measurements with Resipod, supplied by Proceq (top) and Resipod measurement principle (bottom) (Proceq, 2017)

3.3.4.3. Electrical impedance spectroscopy (EIS)

Electrical impedance spectroscopy involves the application of AC to the specimen that has a certain amplitude over a range of frequencies and the response of the specimen is then measured. This includes the magnitude and phase angle which is represented by a Nyquist plot (of the real impedance in the x-axis versus the negative imaginary impedance in the y-axis). In addition to the 4-probe tests, a 2-probe set up with AC current was used for EIS testing. The aim of the test was to understand the impedance response of the cement paste with functional fillers (the three different graphite products). Since AC current is applied instead of DC, there is no risk of polarisation and therefore a 2-probe set up can be used. This makes this experimental set up easier to implement in the field and for undertaking damage or load sensing measurements. For EIS testing, a potentiostat supplied by Autolab (Metrohm PGSTAT204) was used and small cement paste prisms were prepared (20x20x80 mm). The cement paste samples were cast in custom-made rubber moulds and two electrodes were inserted at 10mm from the edge of the specimen (60mm electrode spacing). Standard curing was followed for the samples and the tests were carried out at 7 and 28 days of curing. A frequency range of 1Hz – 1MHz was used with an amplitude of 0.5V and 10 points per decade were measured.

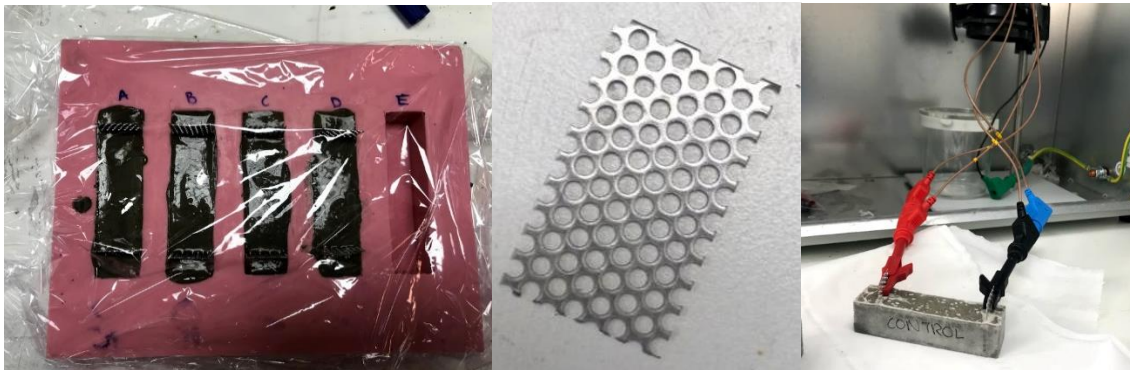


Figure 3-23: Samples for EIS testing (left), electrode used (middle) and 2-probe EIS testing (right)

Chapter 4. GRAPHENE-RELATED MATERIALS (GRMs) DISPERSION STUDIES

As discussed in Section 2.4.1, homogenous dispersion of graphene-related materials (GRMs) is a challenge and combined chemical and mechanical dispersion techniques, yielded better results than either technique individually. Dispersing GRMs in water and a dispersant also resulted in good dispersion. However, questions remain around optimum dispersion techniques specifically for GNPs and of the effect on the properties of cementitious composites. This chapter presents and discusses the experimental results from the development of a practical GNP dispersion protocol that was suitable for use in cementitious composites. Firstly, the different GRMs used in this study are characterised experimentally. This is followed by the development of a GNP dispersion protocol with different chemical admixtures and a protocol for dispersing natural graphite. Finally, the findings from the dispersion study that was carried out as part of a secondment to HeidelbergCement *i-lab* research facility in Bergamo, Italy, are also included.

4.1. GRM characterisation

4.1.1. Overview of the GRMs used

A number of GRMs were used (Section 3.1.3), including three different products of natural graphite, one GNP, one GO, one CNT and one functionalised graphene. The last three were not characterised further as they have only been used for a limited number of experiments in *i-lab*. Table 4.1 presents a summary of the information available and the characterisation tests conducted in this chapter. The three graphite materials and the GNPs were characterised via SEM, XRD and TGA. Further details on their properties were provided by the suppliers in Table 3.2 but also summarised in Table 4.1.

Table 4.1: Summary of GRMs used and characterisation tests

GRM	Info from suppliers (Section 3.1.3)	SEM	TGA	XRD
Graphene nanoplatelets (GNPs) - G2NanPaste	Black-grey colour, paste form; >97% carbon content; thickness 14 nm (40 layers); average size 30 μm ; SSA = 30 m^2/g	✓	✓	✓
Coarse Graphite - AlfaAesar – 10mesh	Black, steel-gray, powder; 99.94% carbon content; size -10mesh (2mm)	✓	✓	✓
Medium Graphite - SigmaAldrich – 100mesh	Grey colour, powder; 99% carbon content; size -100mesh (0.150mm)	✓	✓	✓
Fine Graphite - SigmaAldrich – 325mesh	Grey colour, powder; 99% carbon content; size -325mesh (44 μm)	✓	✓	✓
Graphene oxide (GO) - Graphenea	Yellow-brown water solution; 49-56% carbon, oxygen = 41-50%; Monolayer >95%; particle size: < 10 μm	-	-	-
Carbon nanotubes (CNTs) – Experimental product	Black powder; >93% purity; bulk density 26-30 kg/m^3	-	-	-

4.1.2. Characterisation of the different GRMs used

The SEM images of dried G2NanPaste are shown in Figure 4-1, where a wrinkled and folded morphology can be observed. Individual sheets are agglomerated together and form large clusters and therefore a treatment method is needed to break the GNP agglomerates and to disperse them homogeneously in the cementitious matrix. TGA testing was carried out to understand the behaviour and mineral decomposition of the materials with increasing temperature. Figure 4-3(a), showed that the G2Nan product completely decomposed, losing 100% of its weight at 1000°C, however, it remained largely stable until circa 600°C. XRD testing was carried out to characterise the crystalline nature and identify the main phases of the materials. XRD of G2Nan in Figure 4-3(b) showed a sharp and intense peak at $2\theta = 26.58^\circ$ which is characteristic of graphite as well as other weak peaks which represent the rhombohedral graphite phase, in agreement with Chougan *et al.* (2020). However, a further broad peak is observed at $\sim 2\theta = 12^\circ$, which could mean that there is some loss of crystallinity, probably due to some functional groups that are present and not completely removed during the G2NanPaste fabrication (Krishnamoorthy *et al.*, 2013). This is confirmed by Chougan *et al.* (2019) who found that after oxidation of pristine graphite, the graphitic peak shifts to $2\theta = 10.3^\circ$ due to sp^3 hybridisation of some carbon atoms. However, the

graphitic peak at $2\theta = 26^\circ$ is still very intense and therefore the sample possesses more graphitic than oxidised domains.

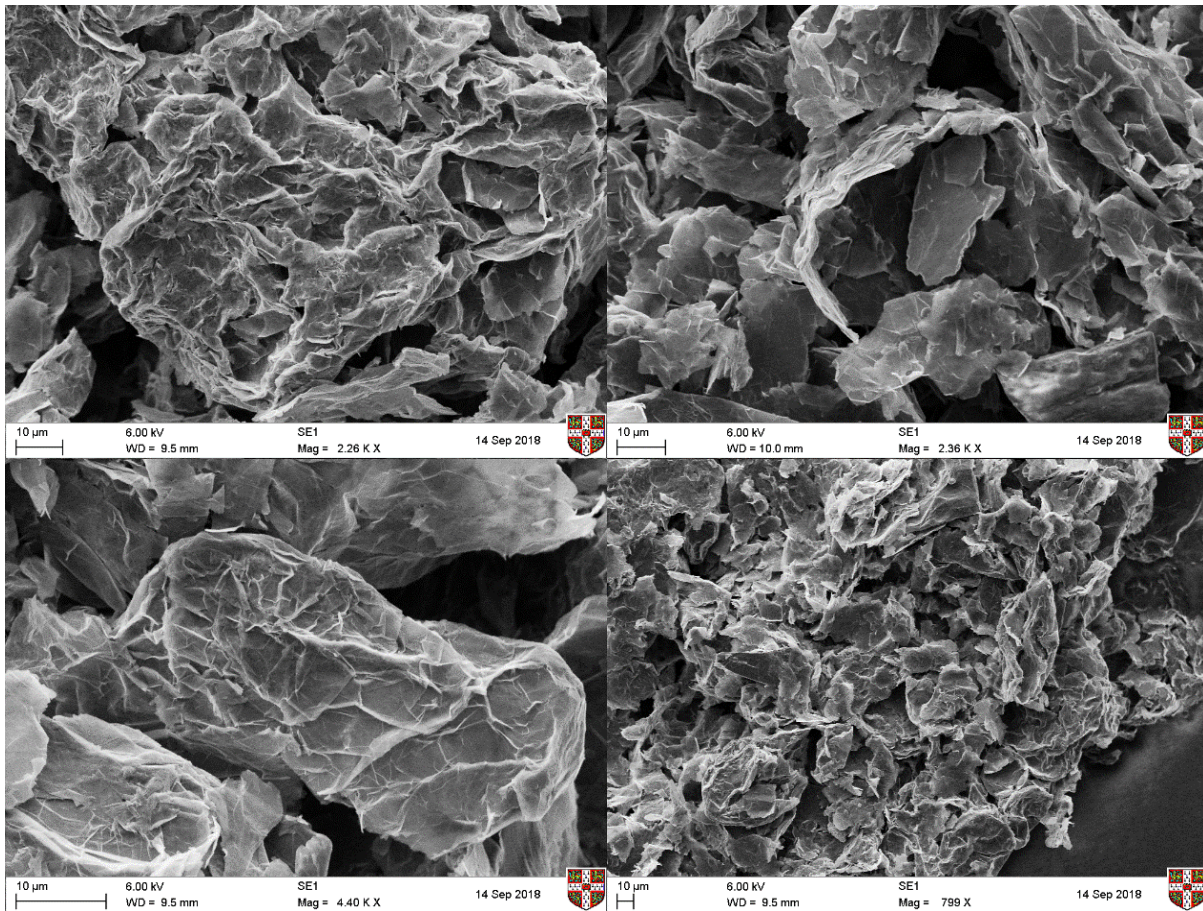


Figure 4-1: SEM images of dried G2NanPaste at 6kV accelerating voltage

The SEM images of the three different graphite products are shown in Figure 4-2. For the coarse graphite, large flakes can be seen with a size of at least 1mm. Some flakes are bigger than others, which is expected due to the inaccuracies when sieving. For the medium graphite, flakes are of varying sizes but all 150-200 μm. The bottom two images show the fine graphite, with a wrinkled and folded structure. As the flake size reduces, agglomerates can be seen, and it is difficult to isolate individual flakes.

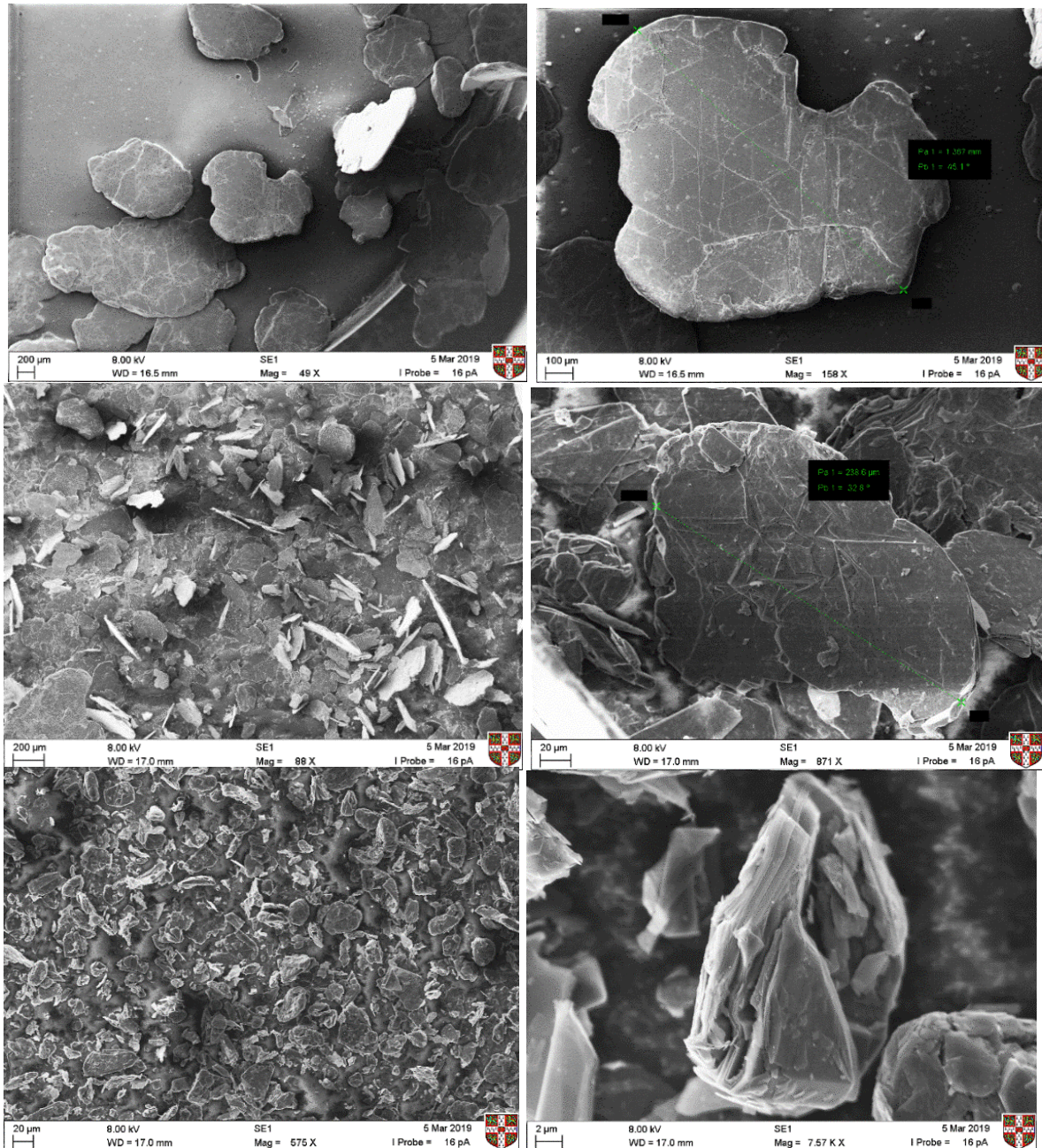
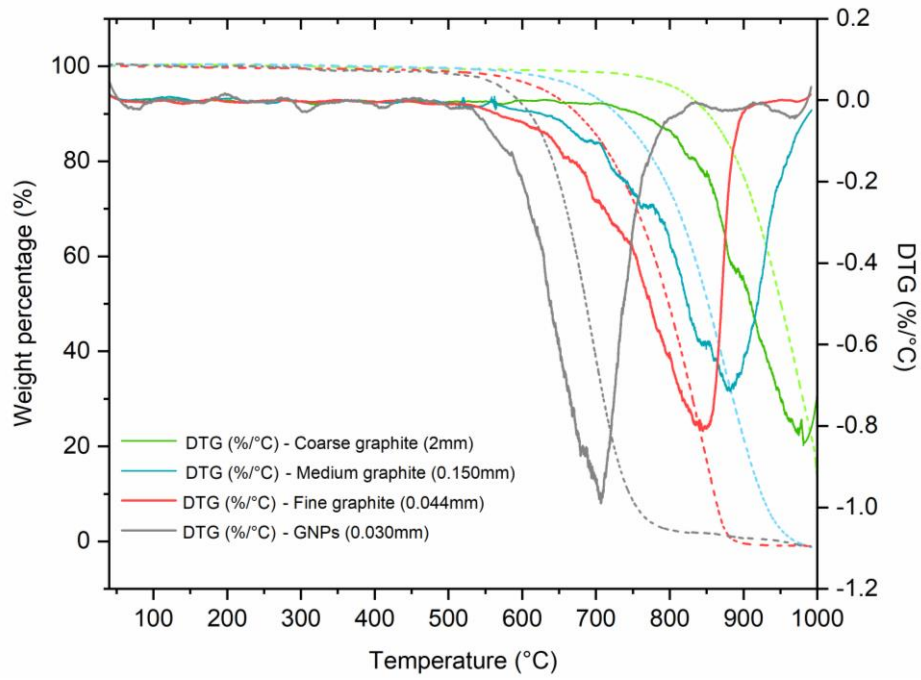


Figure 4-2: SEM images of the three different natural graphite products used in this study. From top to bottom (two different magnification images for each graphite): Coarse graphite, medium graphite, fine graphite

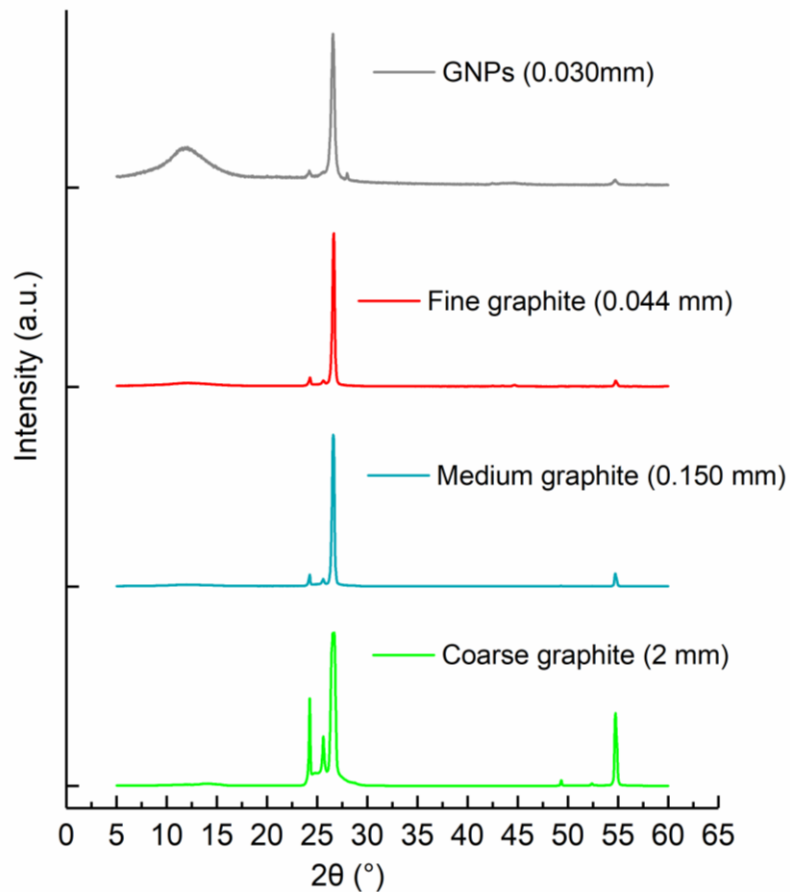
The TGA results in Figure 4-3(a), show that the coarse graphite did not decompose completely within this temperature range (40-1000°C) whilst the other two graphite types lost 100% of their weight. This could be due to the particle size of the coarse graphite (2mm), where the flakes were too large for all their minerals to decompose. In general, the smaller the particle size, the faster it loses weight with increasing temperature as the heat

decomposes the minerals more quickly. Therefore, the curves shift to the left (lower temperature) as the material size decreases. Furthermore, none of the materials show any mass loss before 100°C and therefore, they are all stable during cement mixing and hydration. From XRD testing in Figure 4-3(b), the same sharp and intense characteristic graphite peak is observed for the three graphites; at $2\theta = 26.7^\circ$ for the coarse graphite, $2\theta = 26.6^\circ$ for the medium graphite and at $2\theta = 26.64^\circ$ for the fine graphite. This characteristic peak for graphene-related materials has also been confirmed in other studies (Du and Pang, 2018; Li and Zhang, 2019). For the coarse graphite, some further graphitic peaks are also observed at $2\theta = 24.24^\circ$ and $2\theta = 54.74^\circ$.

In summary, the SEM revealed the morphology of the GRMs studied, whilst TGA revealed their mineral decomposition behaviour with temperature, with all materials (other than the coarse graphite) decomposing completely after $\sim 800^\circ\text{C}$. XRD confirmed that all materials have an intense and sharp graphitic peak $\sim 2\theta = 26^\circ$ whilst a weak and broad peak at $\sim 2\theta = 10.3^\circ$ is observed for GNPs which could indicate that the crystallinity is partially lost and some oxygen functional groups might be present.



(a)



(b)

Figure 4-3: Characterisation of the main GRMs used in this study (a) weight loss by thermogravimetric analysis (TGA) from 100°C to 1000°C (b) X-ray diffraction peaks

4.2. GNPs dispersion in water

The aim of the first phase of experiments was to develop a practical protocol of dispersing GNPs in cement. The dispersion of GNPs in water was investigated first as Section 2.4.1.4 showed that it was more effective for GNPs to be dispersed in water before mixing with the dry cement. Preliminary testing on the mixing sequence was carried out during the MRes thesis (Papanikolaou, 2017) using hydrophilic GO, where its dispersion in water was expected to be sufficient. However, it was found that a superplasticiser was needed to achieve homogeneity. Since GNPs are hydrophobic, their dispersion in water was not expected to be adequate and to confirm this, zeta potential testing was carried out. Colloidal particles with $|\zeta| > 15\text{mV}$ are expected to be moderately stable, although higher values ($\geq 30\text{ mV}$) are required to ensure the long-term stability of the colloidal suspensions (Gholampour *et al.*, 2017). A single dosage of 0.015wt% GNPs in suspension was sonicated for 60 minutes, and the dosage was calculated based on an equivalent w/c = 0.45. This is a small GNP dosage compared to what was tested in the literature (Section 2.4), however, the aim here was to understand the behaviour of GNPs in water. The ζ value was found to be equal to -2.15 mV and is shown as a red dashed line in Figure 4-5b. This value was measured at a temperature of 23°C. Sonication of the suspension can lead to an increase in temperature and here, the temperature was controlled by pausing the sonication for 1 minute every 5 minutes. However, to understand the effect of temperature on the zeta value, one experiment was carried out where the sonication temperature was not controlled, and it reached 31°C. A decreasing trend in zeta potential was found with increasing temperature. At 27°C, a 7% reduction in the zeta value was observed (-1.99 mV) whilst a -11% reduction was found for 31°C (-1.91 mV). Even though this variance with temperature is small, it still shows that GNPs tend to agglomerate more easily with increasing temperature. Nonetheless, for all measurements, the ζ value was very close to zero, indicating an extremely strong tendency of the particles to agglomerate in water. This confirms that GNPs do not disperse sufficiently in water without any chemical treatment.

This dispersion of GNPs in water was visually observed (Figure 4-4), where GNPs were added in water at 0.015wt%. From Figure 4-4(a), it can be seen that the GNPs settled at the bottom of the beaker and no dispersion was achieved. When a polycarboxylate superplasticiser (1.76wt% MasterGlenium C315) was added (Figure 4-4(b)), a more homogeneous dispersion of the GNPs was observed, as indicated by the darker colour of

the suspension. However, the colour at the bottom of the beaker was much darker, meaning that most of the GNPs were agglomerated and settled at the base. Instead, after applying sonication treatment for 1 hour, the GNPs appeared visually to be more uniformly dispersed as shown in Figure 4-4(c) by a homogenous dark colour across the beaker. This uniformity was maintained for at least 1 hour after sonication although the long-term stability of the suspension should be investigated further. These preliminary visual observations agree with the literature and show that GNPs dispersion in water was not sufficient and that a combination of chemical and mechanical treatment is indeed needed. This will be tested in more detail in the following sections.

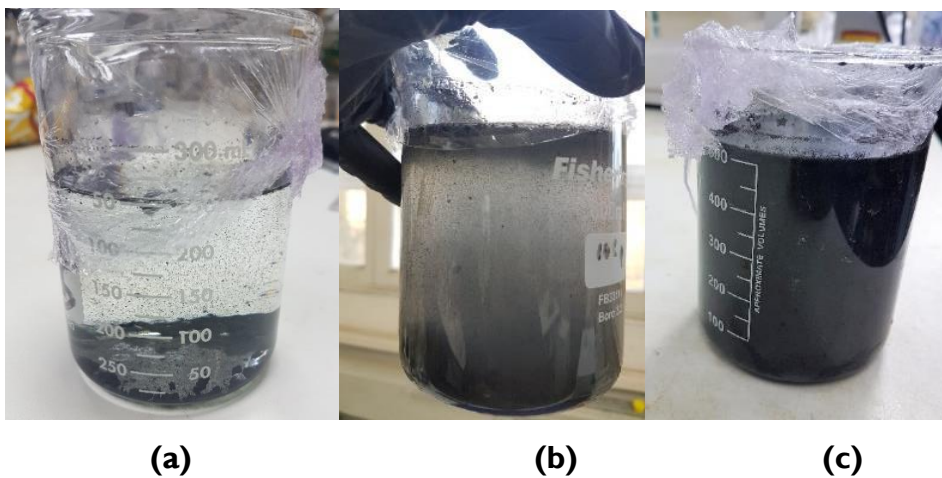


Figure 4-4: Visual observation of the GNPs (a) in water only, (b) with polycarboxylate superplasticiser and (c) with polycarboxylate superplasticiser and 1 hour of sonication

4.3. Effect of chemical admixtures on the dispersion of GNPs

This section investigates the effect of chemical admixtures on the dispersion of GNPs with 1 hour of sonication being used in all cases. Four superplasticisers were tested within the dosages recommended by the supplier as illustrated in Table 4.2 and these dosages are expressed as percentage by weight of cement. The dosages in water were calculated based on a $w/c = 0.45$. These four plasticisers were selected as they are commonly used in industry and are compatible with concrete components (Section 2.4.1.2) and therefore if found effective, they would result in a practical method of dispersion without the need for further addition of chemical admixtures.

Table 4.2: Overview of the chemical admixtures tested for GNP dispersion

Commercial name	Type	Tested dosages (% bwoc)
MasterPozzolith 324N	Lignosulphonate	0.24% - 0.71%
MasterRheobuild 1000	Sulphonated Napthalene	0.84% - 1.44%
MasterEase 3820	Polycarboxylate ether	0.32% - 2.16%
MasterGlenium C315	Modified polycarboxylic ether	0.22% - 3.3%

4.3.1. Dispersion using zeta-potential testing

Zeta-potential, Section 3.3.1.1, is a measure of electrostatic repulsion between nanoparticles and is a useful tool for characterising the dispersion efficiency. Initially, the four superplasticisers were tested in water without any GNPs to understand their dispersion behaviour. The superplasticiser dosages from Table 4.2 were used, and the minimum, median and maximum was tested from each dosage range. As illustrated in Figure 4-5 (a), the zeta value of lignosulphonates was very high because they work by electrostatic repulsion. However, the naphthalene-based superplasticiser showed a low zeta value which means that it might not have an effective electrostatic repulsion mechanism. The steric hindrance mechanism is not shown clearly with this test and as expected, the zeta value of the two polycarboxylates (MasterEase and MasterGlenium) was low (<20), as they work primarily by steric hindrance. These results agree with Srinivasan *et al.* (2010) who found that cement suspensions had zeta values around -10 mV with a lignosulphonate superplasticiser, circa -25 mV with naphthalene-based superplasticisers but it reduced to -10 mV for polycarboxylates that work primarily by steric hindrance rather than electrostatic repulsion.

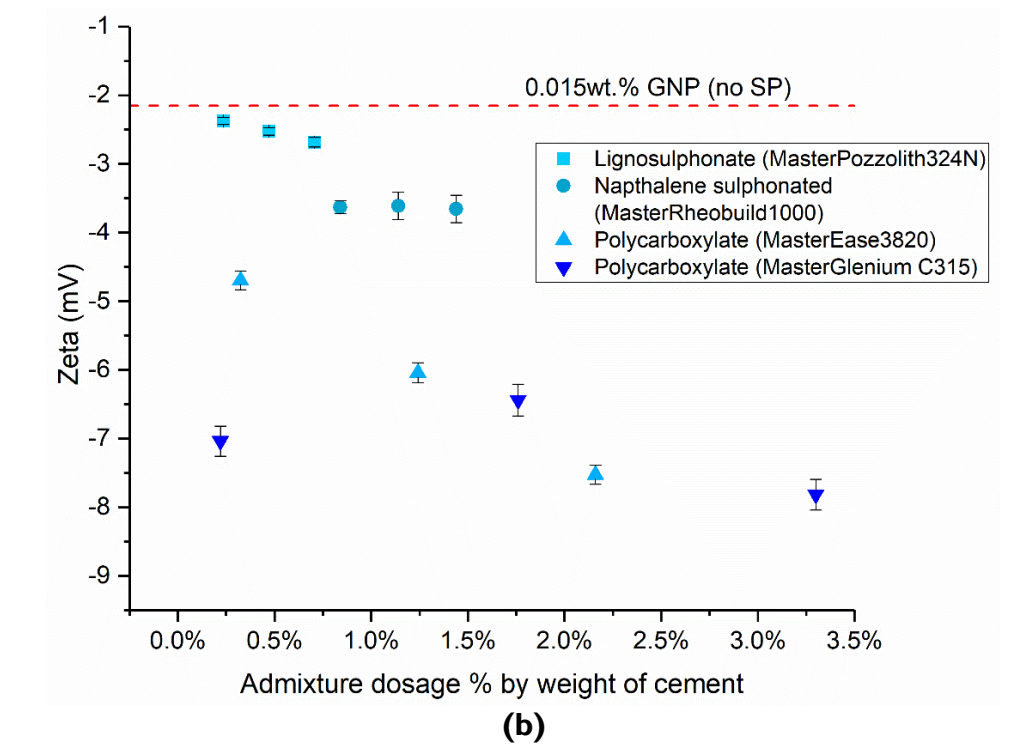
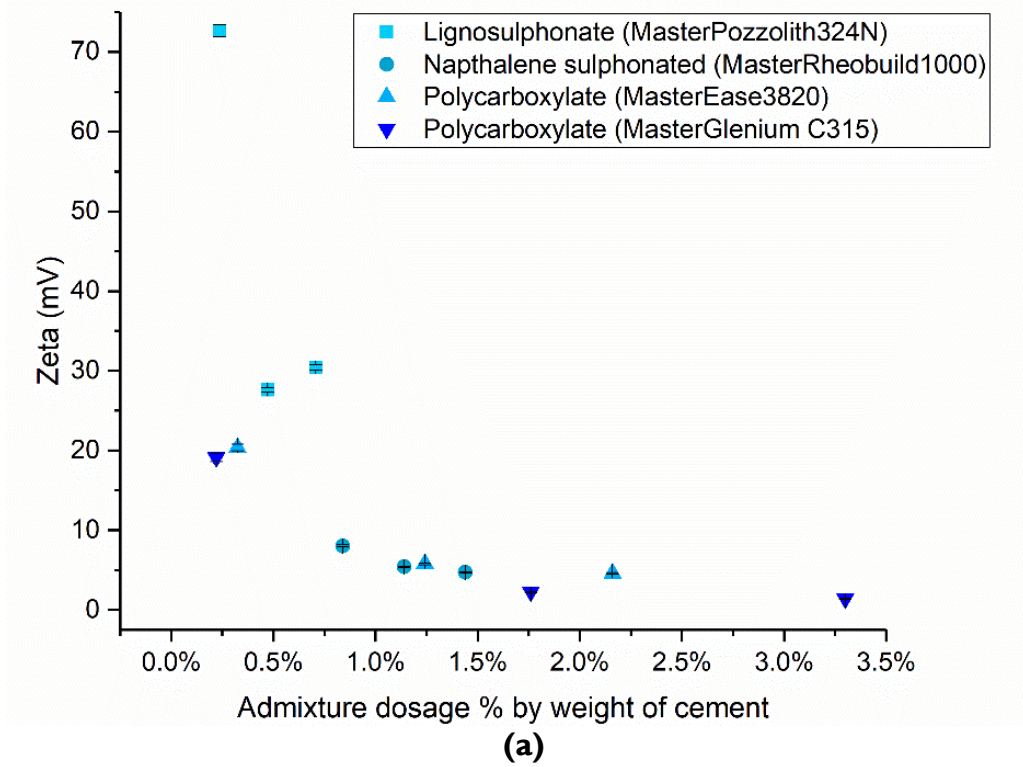


Figure 4-5: Zeta potential values of (a) admixtures in water only and (b) admixtures with 0.015wt% GNPs (by weight of cement for $w/c = 0.45$) in water

The effectiveness of the four superplasticisers in dispersing GNPs was then tested. A single dosage of 0.015wt% GNP was used. As discussed in Section 4.2, dispersing GNPs in water only (without any superplasticiser) resulted in a zeta value of -2.15 mV which means that GNPs had a strong tendency to aggregate. Figure 4-5(b) shows that the lignosulphonate and naphthalene-based superplasticisers are very ineffective in dispersing the GNPs. These two types of superplasticisers work by electrostatic repulsion, so their zeta-value should have been the highest. Yet, the lignosulphonate superplasticiser only improves the ζ value by 11%-25% and keep it under -3 mV, whilst the naphthalene-based superplasticiser improves the value by circa 70% (to around -3.6 mV). None of these changes are significant enough to ensure that the GNPs are well dispersed. On the contrary, because polycarboxylates work by steric hindrance, it was not expected to see a high ζ value. However, both polycarboxylate dispersions with GNPs have a value >5 mV indicating that they are more effective in dispersing the GNPs. The low zeta value (<30 mV) is not an indication of low dispersion capacity; rather it is because they work by a strong steric hindrance mechanism that is not shown clearly in a zeta-potential measurement. Between the two products, MasterGlenium has higher zeta values at all three dosages.

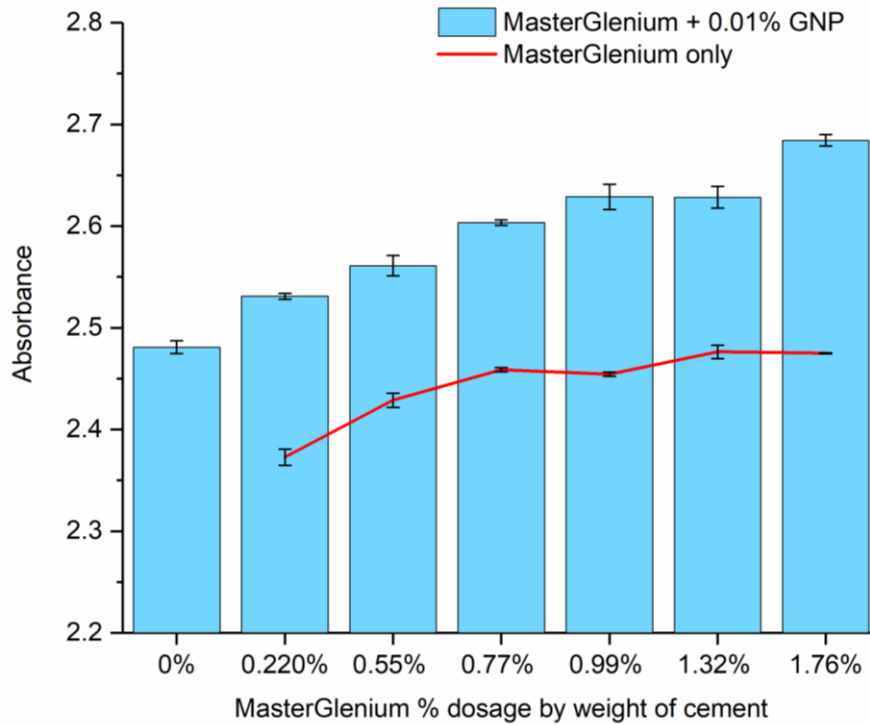
Limited studies have undertaken zeta-potential measurements as a method to establish dispersion of GRMs. Du and Pang (2018) investigated the dispersion stability of GNPs in water (37 nm thickness, 8 μm diameter and 24 m^2/g SSA) with the aid of a polycarboxylate superplasticiser. The authors found that the zeta of GNPs in water was less than 10 mV, which indicated a strong tendency to agglomerate and agrees with this study. When superplasticiser was added, the zeta-potential increased to around 20-40 mV, depending on the sonication duration and it was around -35 mV for 60 minutes sonication, which is the same duration as used here. These are higher values compared to the findings of this study, which could depend on the sonication parameters (for example, frequency and power output), specific properties of the superplasticiser (such as polymer backbone length) and on the differences between the GNP products (such as thickness and surface area). In another study, when reducing GO to rGO with hydrazine, it was found that the zeta-potential reduced from -70.9 mV for GO to less than -30 mV when hydrazine was added and reduction time increased, which shows that the GO had lost its oxygen functionalities (Gholampour *et al.*, 2017). rGO has comparable properties with GNPs due to the lack of

oxygen functional groups and therefore from a dispersibility perspective, their zeta values would be similar.

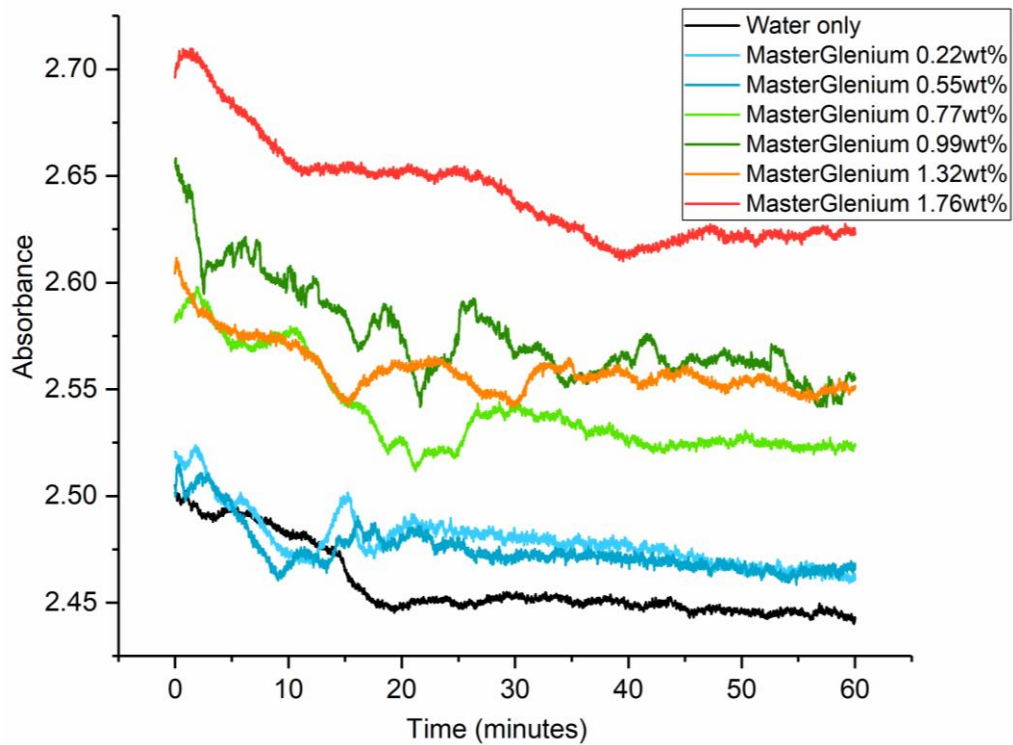
From the zeta potential results, it was found that the lignosulphonate and naphthalene-based superplasticisers had a worse performance than expected and that the electrostatic repulsion was not enough to disperse the GNPs. The polycarboxylates, that work by a combination of electrostatic repulsion and steric stabilisation (chemical and physical mechanisms), performed better and between the two products, MasterGlenium had a stronger mechanism of repulsion that was shown in zeta-potential. Therefore, some further testing is necessary to understand the effect of MasterGlenium for the dispersion of GNPs in water.

4.3.2. Dispersion using UV-Visible spectroscopy (UV-Vis)

UV-Vis spectroscopy was carried out to establish the effect of the different MasterGlenium dosages on the dispersion of G2NanPaste. Section 2.4.1.5 showed that UV-Vis has been widely used to assess the dispersion of GRMs in aqueous solutions and the principle behind the testing is that the higher absorbance indicates a better dispersion. Initially, the effect of increasing MasterGlenium dosage (from 0% - 1.76wt%) for dispersing a single GNP concentration (0.01% bwoc for w/c = 0.45) was tested. It should be noted that a maximum concentration of 1.76wt% superplasticiser was tested with UV-Vis as it would not be feasible to use higher dosages due to bleeding if the dispersions were then added in cement paste. This was followed by the effect of varying GNP content (from 0.01wt% - 1wt%) and finally, the absorbance over time was measured to assess the stability of the dispersion. The absorbance tests were carried out at a single wavelength of 220 nm with five tests for each concentration. This wavelength was selected based on an initial wavelength scan test from 200-700 nm that showed that the highest absorbance was around 220 nm. The results are illustrated in Figure 4-6.



(a)



(b)

Figure 4-6: UV-Vis absorbance of 0.01% active G2NanPaste with varying MasterGlenium contents (a) at single wavelength $\lambda = 220 \text{ nm}$ and (b) at single wavelength $\lambda = 220 \text{ nm}$ over time

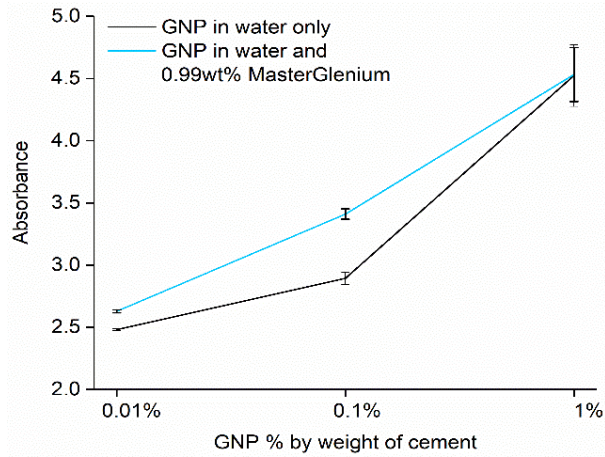
From Figure 4-6(a) and the blue bars it is clear that the absorbance of 0.01wt% GNP is higher in all cases when the polycarboxylate superplasticiser is added compared to the control (0% MasterGlenium). The higher absorbance indicates better dispersion of the GNP particles in the aqueous solution. Looking at the effect of the superplasticiser content, and comparing the difference between the red line (control superplasticiser measurement) and the blue bars, the absorbance shows an increasing trend with higher superplasticiser content; however, a plateau is reached around 0.99% - 1.32% of superplasticiser. Increasing the superplasticiser further to 1.76% leads to better dispersion, however, at this dosage issues like bleeding could occur when this dispersion is added in a cementitious composite. A single wavelength scan was also performed at 328 nm and 500 nm which are away from the peak absorbance value. At these wavelengths, the higher absorbance was found for 0.99% MasterGlenium and increasing the superplasticiser content further, did not aid the dispersion as shown in Table 4.3. The stability over time was also evaluated for the different superplasticiser contents (Figure 4-6(b)). The superplasticiser dosages of 0.22 % and 0.55% seem to increase the absorbance only slightly compared to the GNP in water only, indicating that they are not enough to disperse the GNPs. The plateau is observed again for dosages between 0.77% - 1.32%. In all cases, absorbance reduces slightly over time. Hence, the dispersion will not be stable for a long period and the GNP dispersion needs to be added in the cementitious matrix as soon as possible after mixing.

Table 4.3: UV-Vis absorbance of 0.01wt% GNP with increasing MasterGlenium content at wavelengths 328nm and 500nm

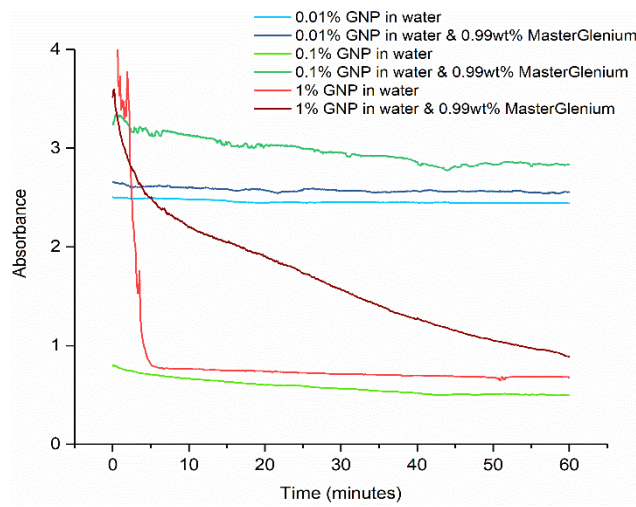
MasterGlenium wt%	$\lambda = 328 \text{ nm}$	$\lambda = 500 \text{ nm}$
0.22%	0.141	0.143
0.55%	0.150	0.144
0.77%	0.186	0.183
0.99%	0.196	0.194
1.32%	0.155	0.150
1.76%	0.189	0.181

The effect of increasing the GNP content was then investigated. Three GNP contents of 0.01wt%, 0.1wt% and 1wt% were chosen, to cover the GNP dosages that were covered in the literature. A single 0.99wt% MasterGlenium dosage was selected and the stability of the dispersion over 60 minutes was tested. The samples were prepared by adding the required superplasticiser dosage in water, followed by GNP addition. The suspension was then

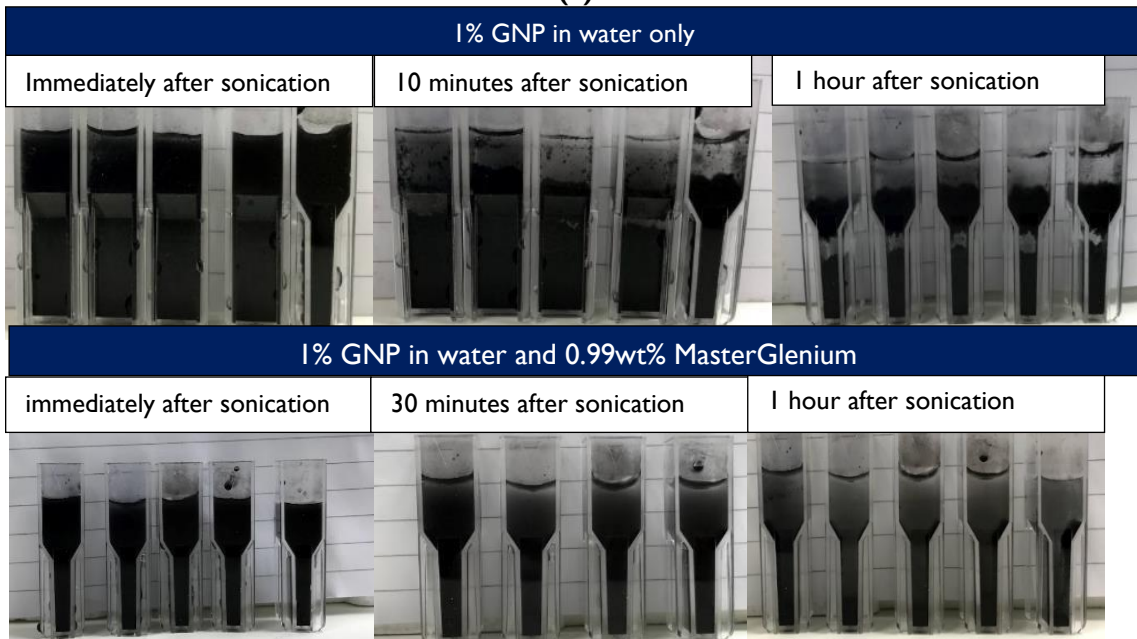
sonicated for 60 minutes and paused every 5 minutes for 1 minute to control the temperature. As shown in Figure 4-7(a), the addition of 0.99wt% MasterGlenium led to a small improvement for 0.01wt% GNP, with the effect being more pronounced for the 0.1wt% GNPs. This means, that a superplasticiser/GNP ratio of approximately 9:1, can significantly improve the GNP dispersion and keep it in suspension over 1 hour (Figure 4-7(b)). For a higher GNP dosage of 1%, the addition of superplasticiser was found to be effective in keeping it in suspension in the first 5-10 minutes, but then the absorbance decreases significantly. Nonetheless, the addition of superplasticiser even at this high dosage, helped the absorbance to decrease less abruptly compared to when GNPs were dispersed in water only. The beneficial effect of the superplasticiser for the 1% GNP concentration is also confirmed by visual observation (Figure 4-7(c)). Without the superplasticiser, the GNP particles started settling and segregating almost immediately after 10 minutes of sonication. Instead, when the superplasticiser was added, the settling of GNPs over time was more progressive, shown by the more uniform colour of the dispersion across the depth of the cuvette.



(a)



(b)



(c)

Figure 4-7: Effect of increasing GNP dosage on the absorbance (a) with 0.99wt% MasterGlenium (b) over 60 minutes (c) effect of 0.99wt% MasterGlenium on the dispersion of 1% GNP in water

The suspension stability over time was assessed by Du and Pang (2018), who found that one hour of sonication and 15wt% of polycarboxylate superplasticiser was sufficient to stabilise a 1% GNP addition for 6 hours. Liu, Fu, Yang, *et al.* (2019) carried out extensive UV-Vis testing to understand the effect of different surfactants and of the sonication time on the dispersion of GNPs (40 m²/g SSA, 4-20 nm thickness, 2-16 µm size) in water. These GNPs have comparable properties with the GNP product tested here (G2NanPaste). The authors found that the UV-Vis absorbance had higher values for a sonication output power of 450 W and a duration of 15 minutes after which it reached a plateau. Amongst the surfactants, sodium dodecyl benzene sulfonate (SDBS) at a concentration of 6:1 to GNPs performed better compared to the polycarboxylate superplasticiser. This agrees with another study by Wang and Deng (2019) who also found that SDBS performed better than other surfactants. On the contrary, a recent UV-Vis study by Ho *et al.* (2020) found that the combination of polycarboxylate superplasticiser and sonication resulted in a stable dispersion within the first 4 hours of sonication. Hence, the combined effect of a surfactant and sonication is indeed an efficient way to homogeneously disperse GNPs in water. Even if SDBS performed better in some studies, these surfactants are not commonly used in cementitious materials and could result in incompatibilities. Therefore, the use of a polycarboxylate superplasticiser that is already widely used in concrete results in a more practical dispersion protocol.

4.3.3. GNPs dispersion in cement

Rheology testing using a rheometer (Section 3.3.1.5) was performed to establish the effect of the four different superplasticisers (Table 4.2) on the dispersion of GNPs in the cement paste and to observe if this interaction might be different compared to when GNPs were dispersed in water only. Rheology testing can be used to ensure that a balance is maintained between good fluidity and dispersion. Initially, the effect of GNPs on the rheology of neat cement paste (w/c = 0.45) was investigated with no superplasticiser. The GNPs were added in water and sonicated for 1hr before being added in the dry cement. From Figure 4-8, it can be observed that low dosages of GNPs (up to 0.03wt%) did not affect the fluidity of fresh cement paste. However, increasing the GNP dosage had a significant effect on fluidity and 0.1wt% GNP addition increased the viscosity by 75% compared to the control. These results were expected as GNPs are hydrophobic and have a large surface area which needs

additional water to wet their surface and results in inter-particle friction as discussed in Section 2.4.2.1.

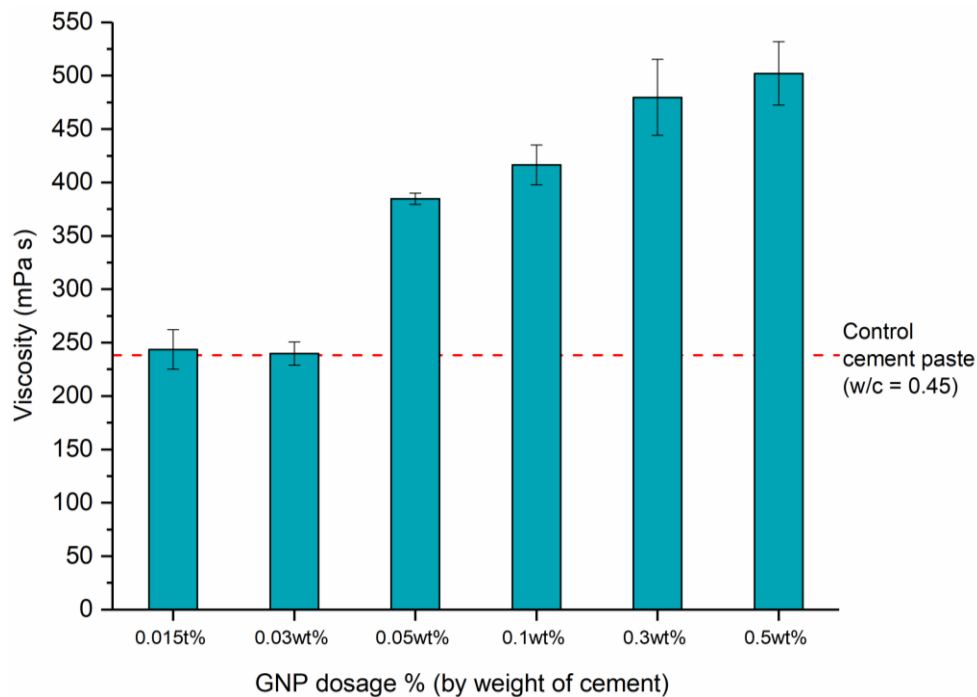


Figure 4-8: Effect of increasing GNP dosage on the viscosity (mPa s) of cement paste

Comparing these findings with the literature, a more significant reduction in fluidity was found in this study. As illustrated in Figure 2-18, several papers showed a reduction in fluidity with GNPs that ranged from 2.5% - 40%. For example, for 0.1wt% GNPs, the literature showed a circa 15% reduction in fluidity as measured by the mini-slump test. However, the results are not directly comparable since they are not only dependent on the GNP content but also on the fundamental properties of GNPs used and the dispersion technique (while w/c did not have a pronounced effect). It should be noted that no surfactant was used for dispersion here, whilst the studies in Figure 2-18 had used a different dispersion protocol. Therefore, further studies are needed to understand the effect of these parameters on the fluidity of cement composites with GNPs.

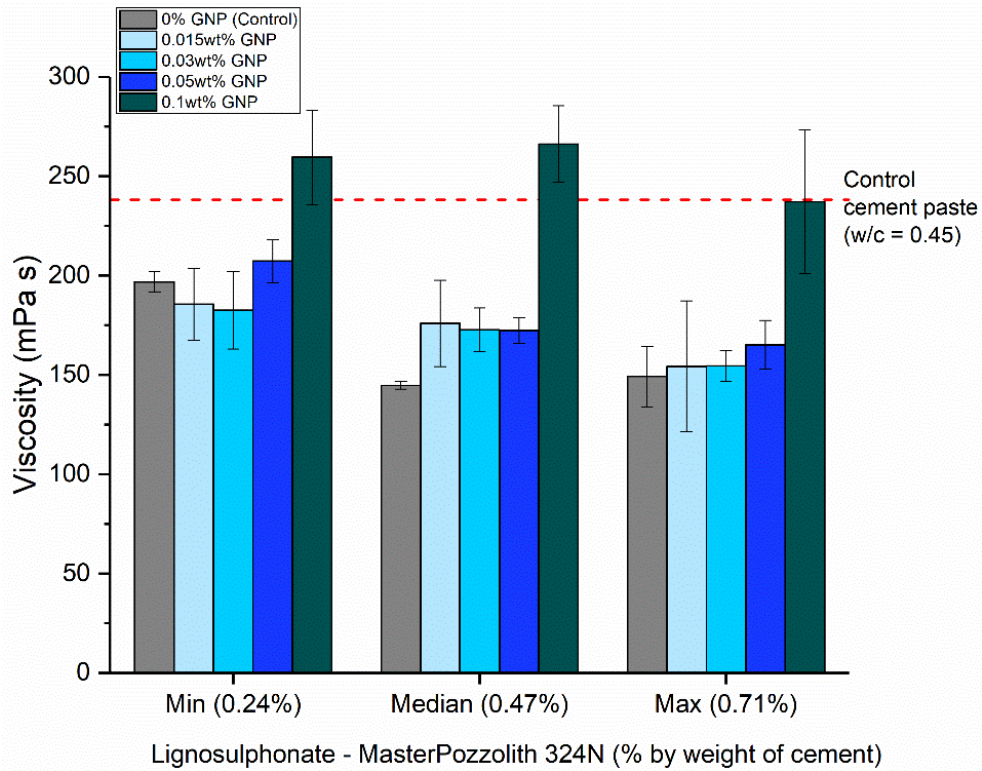
The effect of the four different plasticisers (at three concentrations each) on the viscosity of GNP-cement paste was then investigated. GNP dosages varied from 0% to 0.1% bwoc to establish the effect of the increasing GNP dosage on the dispersion efficiency of the superplasticisers. From Figure 4-9(a) and looking at the control measurements (0wt% GNP),

it can be seen that the lignosulphonate plasticiser was only somewhat effective in improving the fluidity of the neat cement paste whilst increasing the dosage from 0.47% to 0.71% had a minimal effect. When GNPs were added, there was only a minimal change in viscosity (within statistical error) which could mean that the GNP dosage was very small and could be fully dispersed. Increasing the GNP dosage to 0.1wt%, affected the viscosity more significantly and therefore the plasticiser was not able to disperse the higher GNP content and maintain an optimum balance between dispersion and fluidity. Furthermore, lignosulphonates are old technology and not used widely in the UK anymore, but they are still in use in other countries (BASF, 2017), hence their use is less relevant.

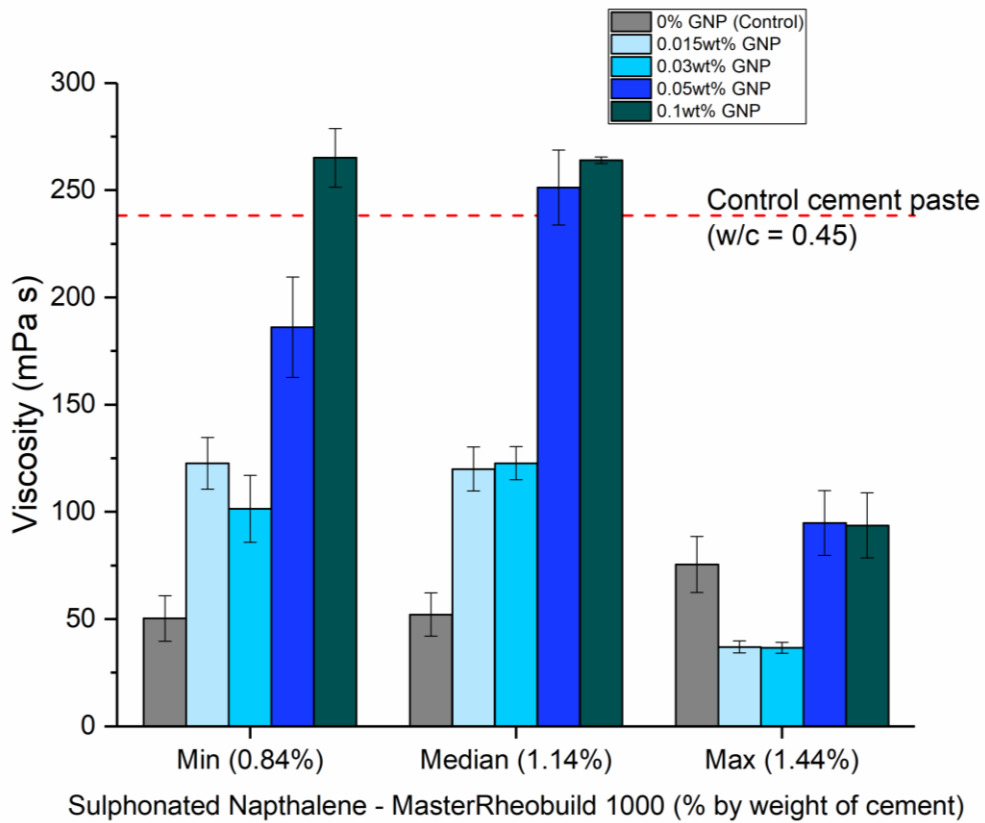
By observing the control measurements in Figure 4-9(b), it can be seen that the sulphonated naphthalene-based plasticiser reduced the viscosity of the cement paste by circa 79%. With GNP addition, the viscosity increased significantly, especially for higher GNP concentrations (0.05wt% and 0.1wt%). The rapid increase in viscosity with high GNP concentrations could restrict its usability for practical applications since it would not allow for adequate compaction and it could make pumping of the cement composite difficult. Furthermore, at maximum plasticiser concentration (1.44wt.%) an incompatibility is observed with the cement which means that plasticiser micelle concentration is too high for use in cement paste. It should be noted that this admixture was specifically produced for this experiment by BASF, who have also limited their manufacture of naphthalene-based products (BASF, 2017). Therefore, both the lignosulphonate and naphthalene-based plasticisers could have a limited ability in dispersing GNPs. However, their future use, in the UK at least, is expected to be limited and therefore they are not recommended as a practical dispersion method. Furthermore, both lignosulphonates and naphthalene-based plasticisers work by electrostatic repulsion and the above experimental results indicate that this mechanism is not sufficient to homogeneously disperse GNPs.

The two polycarboxylate plasticisers were tested next. From Figure 4-9(c), a clear trend in reducing the viscosity with increasing plasticiser dosage can be observed. When the GNPs were added at low dosages, there was no statistical change in the viscosity, which meant that the superplasticiser content was sufficient to fully cover all GNPs at these concentrations. Increases of 39% - 126% were observed for the 0.1wt% GNPs compared to the control, which was less than the increases observed with the two previous superplasticisers. This means that MasterEase was more effective in dispersing GNPs whilst

also maintaining a good rheology compared to the lignosulphonate and naphthalene-based one. According to the supplier, this is a new product that comprised of three different polymers which means that it is a complex formulation (BASF, 2017). Finally, Figure 4-9(d) shows that MasterGlenium C315 was more effective than MasterEase in reducing the viscosity of the neat cement paste (reduction ranges from 67% to 75% whilst for MasterEase it ranged from 31% to 69%). The minimum dosage at 0.22wt% appeared ineffective in dispersing the increasing contents of GNPs and therefore it was not considered further. Increasing the superplasticiser dosage from 1.76% to 3.3% also did not appear to influence the viscosity with increasing GNP content and therefore using the higher concentration is of little benefit. Furthermore, the maximum superplasticiser dosage (3.3wt%) resulted in significant bleeding of the cement paste after 24 hours and therefore it was not possible to use this concentration. As mentioned in Section 4.3.2, however, higher MasterGlenium dosages resulted in excessive bleeding and therefore, the maximum dosage that could be used without resulting in bleeding was 0.99wt%. MasterGlenium C315 is a single polymer technology that is extensively used in the construction industry for ready mix concrete and it is one of BASF's most powerful superplasticisers (BASF, 2017). Overall, it was observed that the polycarboxylate-based plasticisers that primarily work by steric hindrance (the polymers adsorb onto the cement particles and create a physical barrier between them, so they prevent agglomeration) were more effective than lignosulphonates and naphthalene-based products that work by electrostatic repulsion. Therefore, the physical mechanism of GNP dispersion that was provided by steric hindrance is more effective than the electrochemical mechanism.



(a)



(b)

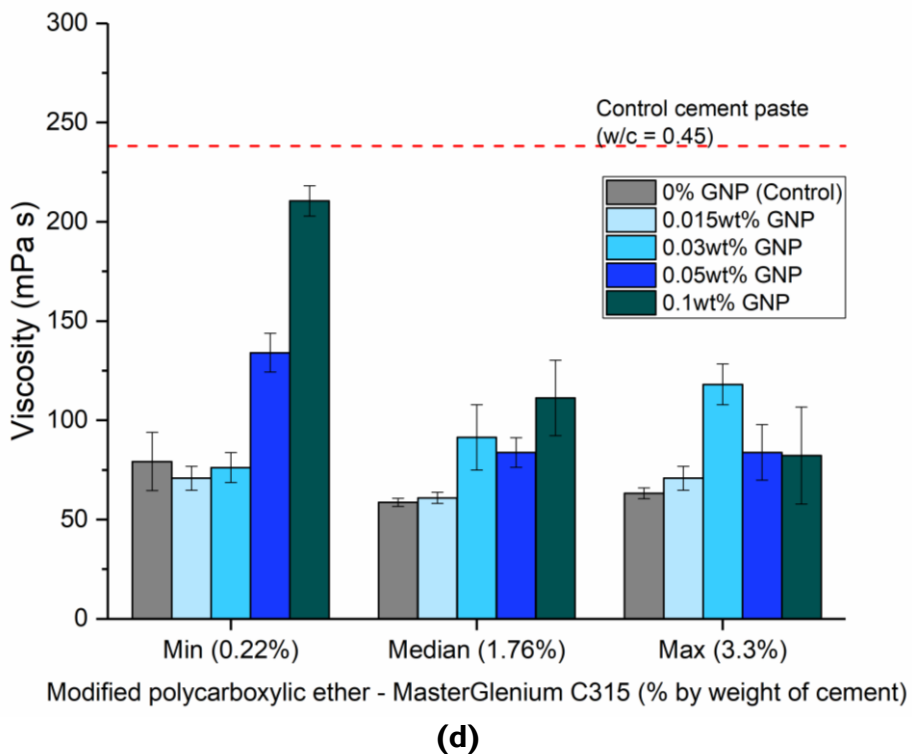
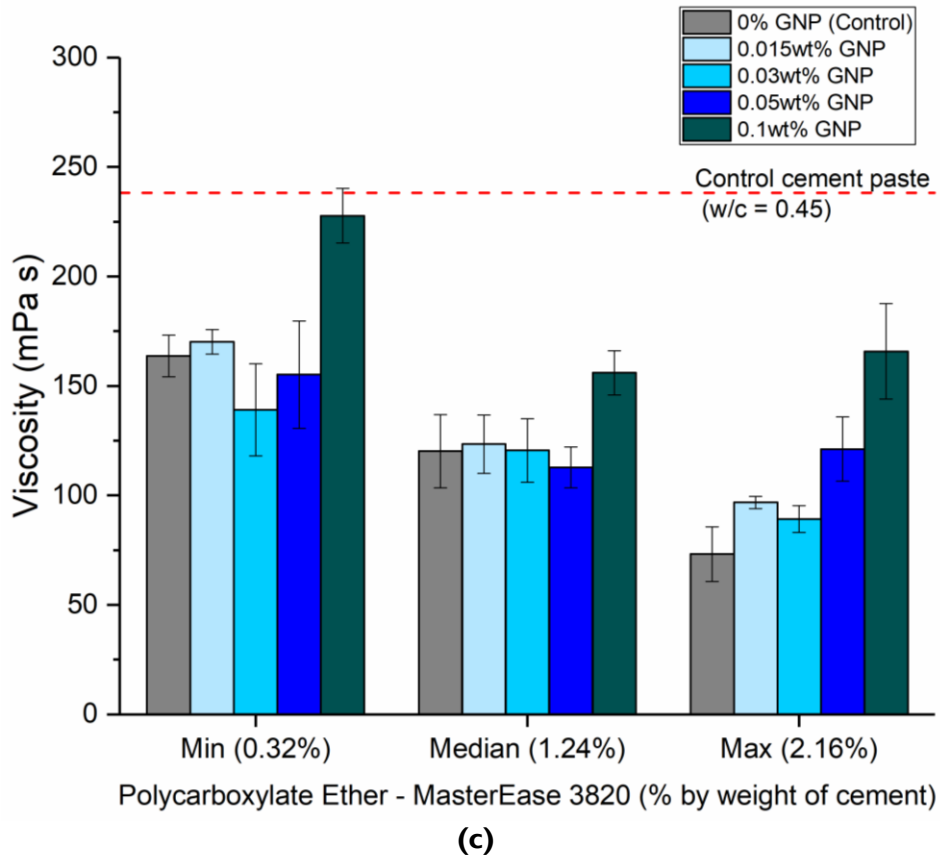


Figure 4-9: Effect of increasing GNP dosage and different plasticisers on the viscosity of cement paste ($w/c = 0.45$) (a) lignosulphonate (b) sulphonated naphthalene (c) polycarboxylate ether (d) modified polycarboxylic ether

4.3.4. Other dispersion studies

Another technique to assess the dispersion of GNPs in cement paste could be via micro-indentation testing. Micro-indentation was used in this study to establish the effect of GNPs on the microhardness and elasticity of cement paste and the detailed results will be provided in Chapter 5, along with a commentary on dispersion. The principle behind using micro-indentation to assess the dispersion is that if the Vicker's tip hits 15 different locations in the sample and the variance in values is small; then the GNP dispersion can be assumed to be homogeneous. Micro-indentation was successfully used in cement paste (Section 5.1.4), however, when scaling up to mortars, this test was not effective and could not be carried out. Mortars were tested because they represent structural applications more closely compared to cement paste and it is important to understand whether dispersion of GNPs is maintained in the presence of aggregates. GNPs were added at 0.1wt% in mortar and a micro-indentation test was carried out. As illustrated in Figure 4-10, the presence of sand particles (white particles) meant that the indenter would either hit a sand particle or it would be in the interfacial transition zone between aggregate and cement paste. This has led to either inaccurate or 0 measurements, where the indenter could not measure a response. Therefore, micro-indentation cannot be used effectively to assess the dispersion of materials in mortars and concrete due to the presence of aggregates. Instead, indirect macroscale testing could be employed to assess the dispersion. However, this remains a key challenge in the literature and in this study, it is assumed that if GNPs are homogeneously dispersed in cement paste, then the same dispersion protocol will also result in a good dispersion in mortars.

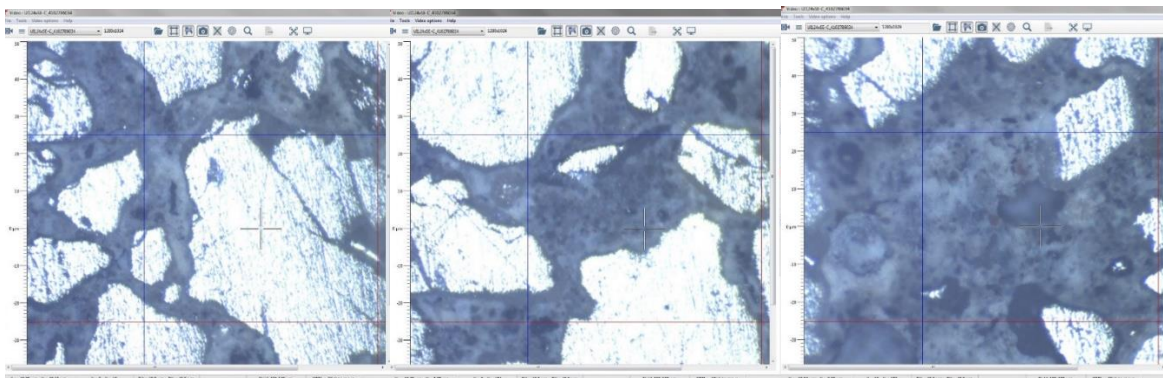


Figure 4-10: Micro-indentation results on GNP-cement mortars (white particles represent sand)

Other techniques to assess dispersion of GNPs include SEM and CT-Scan. SEM tests were carried out here to investigate the microstructural performance and the results are presented in Chapter 5. However, the dispersion cannot be assessed with accuracy due to the very small sample size. Nonetheless, it was still a useful tool and a commentary on the dispersion of GNPs is also provided when the microstructural performance of cement composites is discussed. μ CT-scan could also be used to isolate the different phases and understand the dispersion. However, the resolution of the μ CT-scan was not enough to identify the individual GNPs. Instead, μ CT-scan was used to assess the dispersion of natural graphite where the particles are much larger in size and this is discussed in the following section.

4.4. Dispersion of natural graphite

Natural graphite materials were dry mixed with cement before the aqueous components were added (Section 3.2.2) based on a dispersion protocol that was developed and is presented here. Preliminary experiments were performed to establish the optimum mixing sequence for graphite. As graphite is not a nanomaterial, it was expected that it would disperse more easily compared to GNPs. Firstly, the same protocol as the one developed for GNPs was investigated. Water, 0.99wt% MasterGlenium and the coarse graphite (2mm) were mixed together and sonicated for 1 hour before mixing with dry cement (Figure 4-11). This was not an efficient method, as the graphite particles settled at the bottom of the beaker and did not mix uniformly in the solution even after sonication.

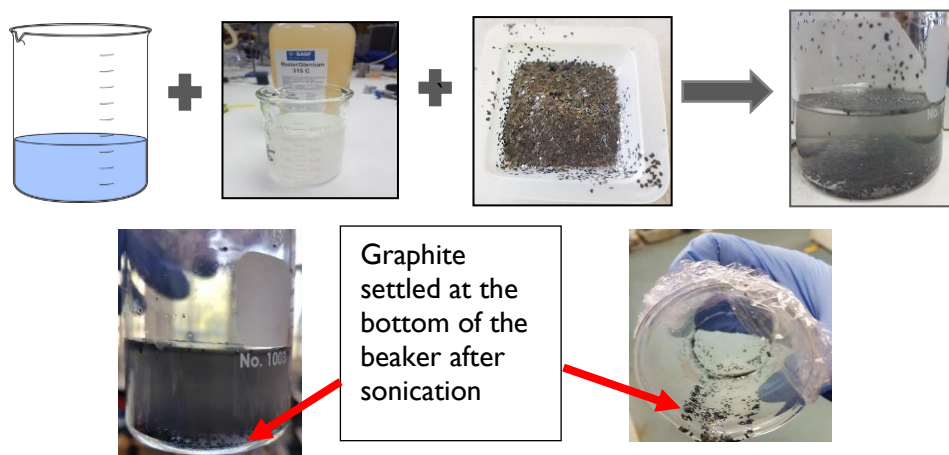


Figure 4-11: Preliminary procedure for graphite mixing showing the initial addition of graphite in solution first and then mixing with dry cement

Instead, dry mixing of graphite powder with cement paste was tested, followed by the addition of water after 2 minutes of dry mixing following similar work in the literature (Bhattacharya *et al.*, 2008). This mix protocol produced a more homogeneous mix as shown in Figure 4-12. The dispersion of graphite in the cement matrix was also assessed by SEM-EDX, 28 days after mixing. The graphite flake particles are shown as green in Figure 4-13(a), whilst the remaining cement paste matrix is shown as pink. The EDS analysis of the area illustrated in Figure 4-13(a) is then shown in part (b) of the same figure and it confirms that the main elements present in the sample are carbon and calcium, which was expected due to the presence of graphite and because calcium silicate (C-S-H) is the main reaction product of cement hydration. Other typical elements from cement hydration such as sodium, silicon, oxygen, sulphur, and magnesium were also present. From Figure 4-13(c-d), the interaction between a graphite flake and the cement hydration products can be observed. A compact microstructure was found around the graphite flake, which was due to the ongoing hydration of cement paste that had been cured for 28 days. The graphite flake, which can be distinguished by its wrinkled morphology, was ~1 mm which is less than the expected 2 mm size, and it appeared to be integrated within the cement hydration products. No voids were present at the interface between the graphite flake and the remaining microstructure. However, this finding will be investigated further in Chapter 5 to understand the effect of natural graphite on the microstructure of cement composites.

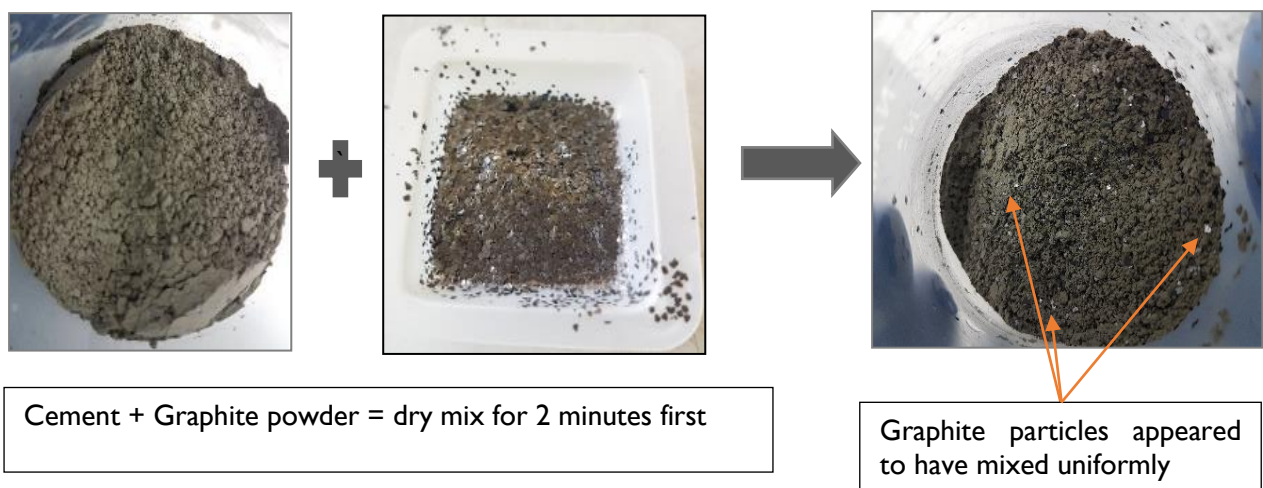


Figure 4-12: The mixing protocol for the graphite material used.

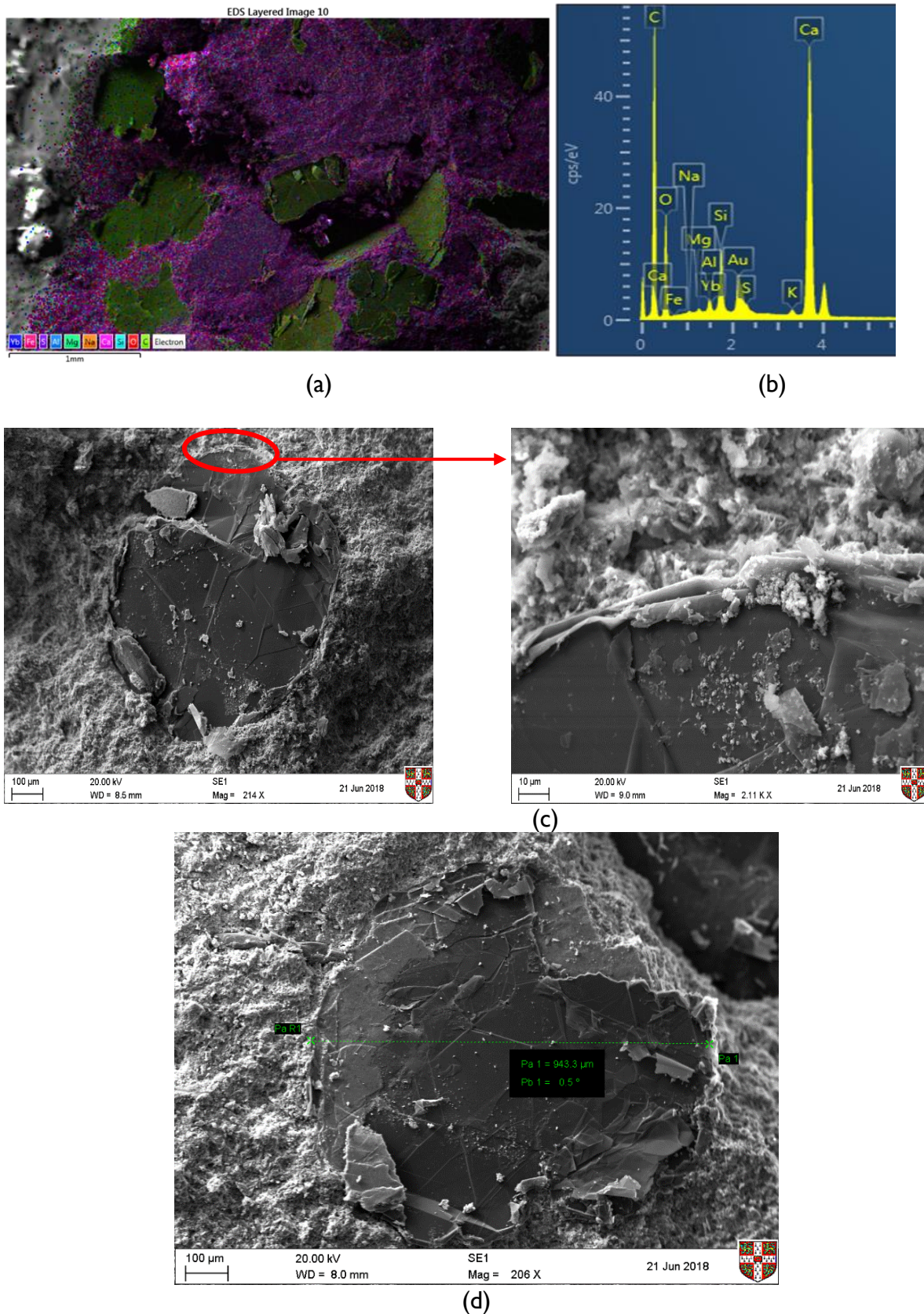


Figure 4-13: Microstructural verification of the effectiveness of the graphite dispersion (a-b) SEM-EDX images confirming dispersion of graphite flakes (c-d) SEM-EDX showing graphite flake bonding and interaction with cement paste at 28 days of hydration

μ CT-scan was also used to assess the dispersion of a 30wt% coarse graphite dosage in the cement matrix. This high concentration was selected based on what would be needed to achieve a stable electrically conductive network for this graphite type. The dry mixing protocol described above was followed and no superplasticiser was used. The test was carried out after 28 days of curing the sample in a water tank and a 5 mm specimen was chosen to allow for a better resolution of the images (the smaller the sample size, the better the resolution of the μ CT-scan). Figure 4-14(a-b), shows the 3D reconstructed image of the 5mm graphite-cement paste sample and Figure 4-14(c) shows a slice through the 3D image. To isolate the different phases that make up the image, a grey-scale analysis is used that can detect the different substances based on their density. Three distinct peaks were observed in the μ CT-scan, each representing the different elements including air, bulk cement paste and graphite particles. In Figure 4-14, the graphite is represented with a pink colour whilst the bulk cement paste is shown as black. The graphite flakes were well dispersed within the matrix and near each other which was due to the high graphite concentration (30wt%). The orientation of the flakes appeared to vary, even though some clusters were oriented in the same way. The effect of mixing on the orientation of the graphite flakes was not investigated in detail and further research would be needed in this area. The key finding from the μ CT-scan was that graphite flakes were well dispersed with the dry mix method even at a high graphite concentration no agglomerates were observed. Therefore, dry mixing of graphite and cement was found to be the most effective method, and this protocol was followed in the experimental work carried out in this thesis.



(a)

(b)



(c)

Figure 4-14: X-ray computed tomography (CT-scan) of an approximately 5mm cement paste specimen, showing the graphite flakes (pink) being dispersed in the matrix (grey) – this is at a graphite dosage of 30% by weight of cement

4.5. Dispersion studies at the HeidelbergCement *i-lab*

The work described in this section was carried out in the HeidelbergCement Italcementi research facility, *i-lab*, in Bergamo (Italy) as part of a secondment in 2019. The aim of the experimental work was to undertake a systematic study of additional parameters and to expand on the use of other carbon nanomaterials. The following parameters were tested:

- ✓ High-speed shear mixing
- ✓ Hydrophobic mixing of carbon nanotubes (CNTs)
- ✓ Effect of GNPs, GO and CNTs on the properties of standard CEMI mortar
- ✓ Two alternative cements; P2 (hydrophobic-treated) and P3 (hydrophilic-treated)
- ✓ Effect of silica fume on the dispersion of carbon nanomaterials
- ✓ Effect of a functionalised graphene (experimental product) on the CEMI mortar

Due to the available equipment, the dispersion was characterised either directly – using SEM and visual observation - or indirectly through workability and strength testing of mortars. The following sections present the results from these additional dispersion methodologies.

4.5.1. High-speed shear mixing

A Silversone L5M-A high-speed shear mixer was used as an alternative to the bath sonication technique used in all the previous experiments described above. This shear mixer comprised of one spindle and one ring with square holes (Figure 4-15(a)). The shear speed of this mixer can range from 0-8000 rpm, however, at high speeds (>5000 rpm), the spindle could get blocked. Therefore, speeds between 3000 – 5000 rpm were tested for 10 minutes to disperse a suspension of 2.6wt% CNTs (for w/c = 0.45) in a solution of 400 ml water and 1.35wt% polycarboxylate superplasticiser. However, as can be seen from Figure 4-15(b), at the end of the mixing, part of the suspension remained stuck to the different parts of the mixer such as on the spindle and on the ring. Since some of the suspension was stuck on the machine, this meant that the effective concentration of CNTs in the resultant cement mixture could be less than estimated. This challenge was not present with bath sonication since all the suspension was in the beaker during mixing and there were no external parts. This could be overcome to an extent by keeping some of the mix water out of the beaker and cleaning the shear mixer. However, this would still not ensure full recovery of the material. Furthermore, the high shear speed could affect the integrity of the nanomaterials by resulting in breakage and further exfoliation due to the shear forces, although this was

not tested in this study. Thus, this mixing technique is not recommended as it is difficult to clean the equipment and recover the GRM from the spindle, which would consequently affect the resultant dosages in the cement composite.

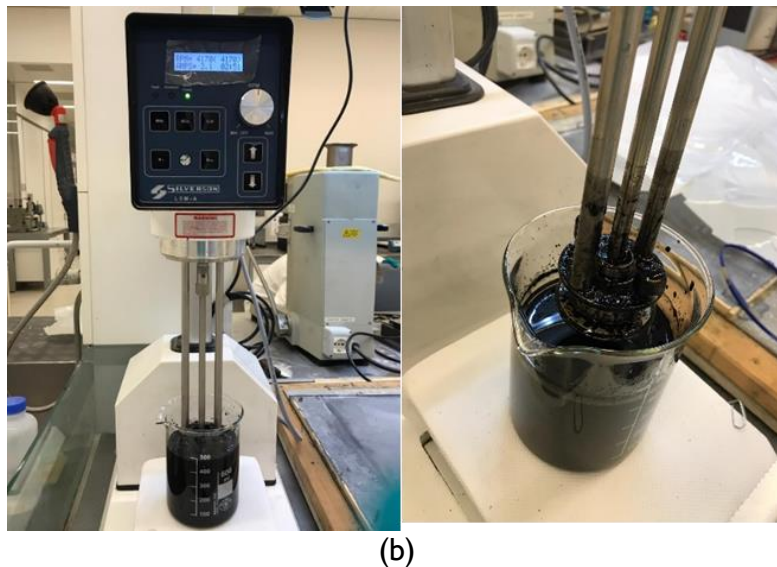
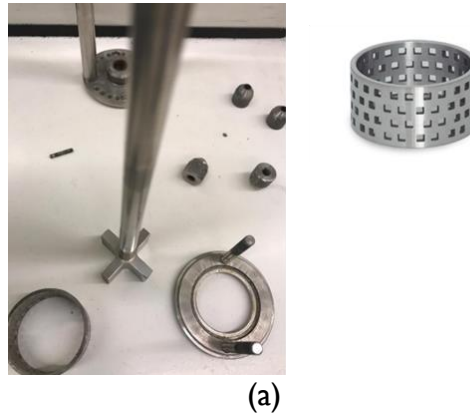


Figure 4-15: Silversone L5M-A high shear mixer (a) square hole ring and spindle (b) high speed shear mixing of CNTs after 10 minutes

4.5.2. Hydrophobic mixing of carbon nanotubes (CNTs)

Hydrophobic mixing, used for dispersing hydrophobic chemicals (such as organic pollutants) in soils, was investigated here to assess its feasibility in dispersing hydrophobic GRMs, such as CNTs, in cement. The principle behind the hydrophobic mixing of CNTs was that if hydrophobic materials were dispersed in a non-soluble (hydrophobic) admixture first before being added in cement, then they could adsorb onto the cement particles. In this way, partially hydrophobic properties to the cement would be instigated – since the hydrophobic mixture can only cover part of the cement particles. When the cement and the mix of the

hydrophobic agent and CNTs would come in contact with water, the fluidity would be initially maintained due to water repulsion. After a while, the cement hydration would start. This mixing methodology could help both with maintaining fluidity and dispersion. GRMs would be adsorbed on the cement particles first rather than making clusters with each other hence they are much more dispersed.

To test this hypothesis, a hydrophobic admixture (defoamer) was used, whose formulation was based on modified polyalkoxyesters. The defoamer was selected because it is commonly used as an admixture in commercial cement mixes to reduce the creation of foam due to superplasticisers. The commercial name of the defoamer was Degressal® PLB 847, supplied by BASF, Germany. The defoamer comprised of 100% active content (no water present) and it came in a liquid form with a viscosity of 650 mPa s. The CNTs were a proprietary experimental product supplied by a third party and hence limited information was available (Table 3.2). The process of dispersing the CNTs in the hydrophobic defoamer is illustrated in Figure 4-16. Initially, a CNT concentration of 0.2wt% by weight of the hydrophobic admixture was added and as seen in Figure 4-16(a), it floated at the top and there was no immediate mixing. A QSonica Q700 tip sonicator was then used to mix the two components (CNTs and defoamer) due to equipment availability in the *i-lab*. Initially, tip sonication for 5 minutes with a power of 96W (automatically set by the machine) was followed to understand whether any mixing between the two hydrophobic components is possible. As shown in Figure 4-16(b), the colour of the suspension across the beaker became very dark, indicating that mixing of the two hydrophobic components was indeed achieved with the tip sonication. However, in the 5 minutes, the temperature increased from 21.1°C to 30°C and this could damage the material. In following steps, the CNT concentration progressively increased by 0.2wt% intervals until it reached a dosage of 1% of the hydrophobic admixture weight and at each interval it was sonicated for 5 minutes. The aim was to understand the impact of the increasing CNT dosage and whether higher CNT dosages could be effectively dispersed. However, with increasing sonication time and dosage, the temperature of the suspension reached 42°C and the suspension became very viscous and it was difficult to mix by hand.

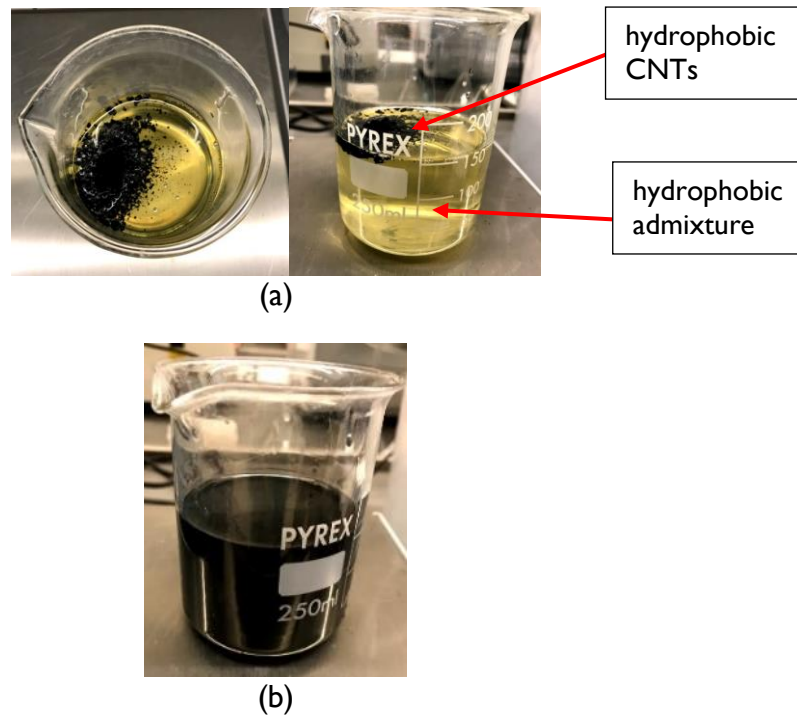


Figure 4-16: Mixing of hydrophobic carbon nanotubes (CNTs) in a hydrophobic admixture

The hydrophobic mixing was stopped when the CNT content reached 1wt% concentration (1.5g of CNTs in 150g of admixture). If this concentration was to be mixed in one of the standard mortars that were prepared in *i-lab* (comprising of 450g cement), it would equate to 0.3% CNT by weight of cement. However, adding the 150g of the defoamer in the 450g of cement would not be practical and it would diminish all the structural performance of the resultant cement mix. Furthermore, the temperature increase due to sonication could lead to damage of the CNT structure. Therefore, even if the hydrophobic mixing of CNTs was successful, it would not be feasible to consequently mix this hydrophobic suspension in a cement composite due to the high dosages of admixture that were needed. This mixing technique for dispersing CNTs had not been tested in the literature and therefore, these findings could not be compared. However, this work was only preliminary and further work could include different types of hydrophobic admixtures, different GRMs and different dispersion techniques to better understand whether hydrophobic mixing could be feasible under certain parameters.

4.5.3. Effect of GRMs on the properties of CEMI mortars

The effect of three different GRMs on CEMI mortars was investigated as an indirect measure of dispersion. Visual observations and microstructural characterisation were also carried out. The three GRMs that were tested in mortars in *i-lab* were as follows (Table 3.2): 0.3wt% GNPs (G2NanPaste), 0.3wt% CNTs, 0.03wt% and 0.06wt% GO and 0.03wt% of a functionalised graphene (FG). The FG is an experimental material from Politecnico di Milano prepared as a water dispersion with 0.075wt% active concentration. No further information was provided but it was assumed that functionalisation induced oxygen functional groups and hence this mix was treated as GO. These GRM concentrations were selected based on the commonly used values in the literature for each respective GRM. Different cements were investigated including a standard CEMI 52,5R, a hydrophobically-treated cement (named P2), a hydrophilically-treated cement (named P3) and a blended cement with 10% silica fume, with the latter three cements being described in Section 4.5.4. The blended mix with SF was tested as some studies suggested that SF could aid the dispersion of GRMs in cement composites (Section 2.4.1.2). For all mixes a polycarboxylate superplasticiser, Driver31 by Sika, was used and its content remained the same (0.23% bwoc) and w/c was fixed at 0.48 for all the mortar mixes that were prepared in the *i-lab*. The plasticiser content and the w/c were determined following preliminary tests to achieve a target fluidity for the mortars of 130mm. As described in Sections 3.2.1 and 3.2.2, all GRMs were mixed in a suspension of water and superplasticiser first and then a QSonica Q700 tip sonicator was used with a 12mm tip for a total of 15 minutes followed by BS EN196-1 mixing and curing to prepare the mortars. Table 4.4 summarises the various GRMs and the cements used in the mortar mixes that were prepared in *i-lab*. Testing for all the mixes was undertaken at 7 days, other than those included in the red box that were run at 2, 7 and 28 days.

Table 4.4: Summary of all the mortars prepared in i-lab. The red box indicates the mortars tested at 2, 7 and 28 days

	0.3% GNPs (G2NanPaste active)	0.3% CNTs	0.03% GO (Graphenea active)	0.06% GO (Graphenea active)	0.03% FG
CEMI	✓	✓	✓	✓	✓
P2 (hydrophobic)	✓	-	✓	-	-
P3 (hydrophilic)	✓	-	✓	-	-
CEMI + 10% SF replacement	✓	-	✓	-	-

As shown in Figure 4-17, the addition of all GRMs resulted in a significant decrease in the fluidity of the mortars (measured by mini-slump test) which was expected due to their large surface area and also because some of them – GNPs and CNTs – are hydrophobic. The only exception was the addition of functionalised graphene (0.03% FG) that resulted in a 6.4% increase in the fluidity. The mechanism cannot be explained as limited information was available about this material and therefore, it will not be investigated further. Doubling the GO dosage decreased the fluidity, however, the decrease was not linear. GNPs (G2NanPaste) and CNTs, that were both hydrophobic, reduced the fluidity dramatically by approximately 30%. This was expected both due to their high surface area and hydrophobicity and because they were used in a dosage that were 10 times higher than GO. Due to the very low fluidity of the CNTs mix, the specimens were vibrated for 10 seconds to ensure compaction. The fresh density of the samples is presented in Table 4.5 and it remained very stable, indicating that the GRM addition did not result in any air entrapment in the mix.

Table 4.5: Fresh density of CEMI mortars

	Fresh density (g/cm ³)	% change to control
Control (CEMI)	2.240	0%
0.03% GO	2.257	0.69%
0.06% GO	2.237	-0.20%
0.3% G2NanPaste (GNPs)	2.259	0.79%
0.3% CNTs	2.245	0.14%
0.03% FG	2.281	1.78%

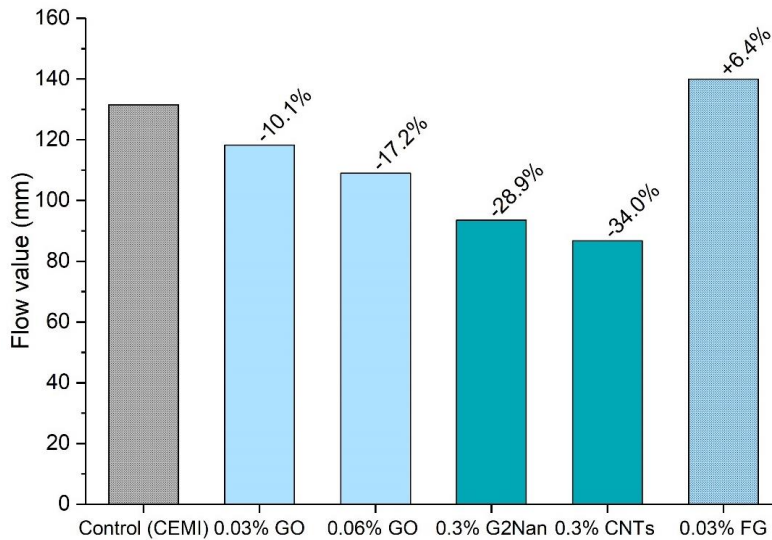
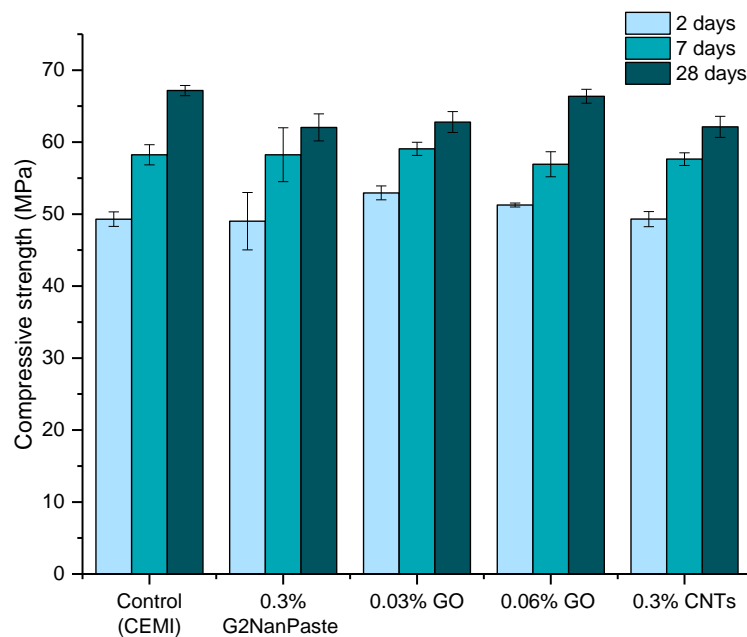


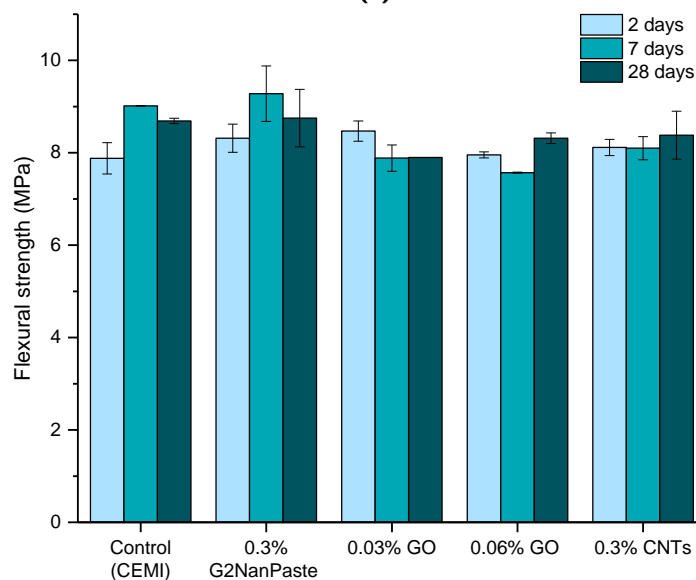
Figure 4-17: Fluidity of CEMI mortars with different carbon nanomaterials

The effect of GRMs on the compressive strength of CEMI mortars is illustrated in Figure 4-18(a). The addition of GNPs showed almost no effect at 2 and 7 days but resulted in a 7.6% reduction at 28 days. The hydrophobic CNTs also showed an insignificant change in strength at 2 and 7 days. On the other hand, GO showed an acceleratory effect at 2 days as it increased the compressive strength by 7.4% and 4% (0.03 wt.% and 0.06 wt.% respectively). However, at 7 days this effect was insignificant and at 28 days a reduction in strength was observed, with strength reducing from 67.2 MPa for CEMI control to 62.8 MPa for 0.03% GO. In terms of flexural strength, a slight enhancement was found at the early age performance (2 days) of the CEMI mortars with all GRMs (Figure 4-18(b)). GNPs improved the 2-day flexural strength by 5.5%, CNTs improved it by 3% whilst GO improved it by 7.5% and 1% at 0.03 wt.% and 0.06 wt.% respectively. This is an indication that the lower GO content provided better performance whilst the higher dosage worsened the performance, however, this needs to be investigated for more dosages to understand the pattern. Having said that, changes within 5% could be statistically insignificant if the error bars are considered. However, at 7 and 28 days this strengthening trend changed. Although, the addition of GNPs resulted in a slight enhancement of 2.9% and 0.7% at 7 and 28 days, the addition of GO was found to compromise the flexural strength at these higher curing ages. The addition of 0.03% GO led to a 12.5% reduction at 7 days and a 9.1% reduction at 28 days. Therefore, a slight acceleratory effect was observed at 2 days with the addition of these GRMs which however, led to a regression of flexural strength as the curing

progressed. The strength results of the CEMI mortars showed that the addition of GRMs had a negligible effect on both the compressive and flexural strength. A detailed analysis of how GRMs affect the mechanical performance of CEMI mortars is included in Chapter 5 along with a comparison with the relevant literature. Here, the primary interest was to understand the dispersion and whether the different GRMs behave differently when dispersed with the same protocol in CEMI mortars. Given that the error bars are small in all cases, dispersion of GRMs between samples is assumed to be homogeneous.



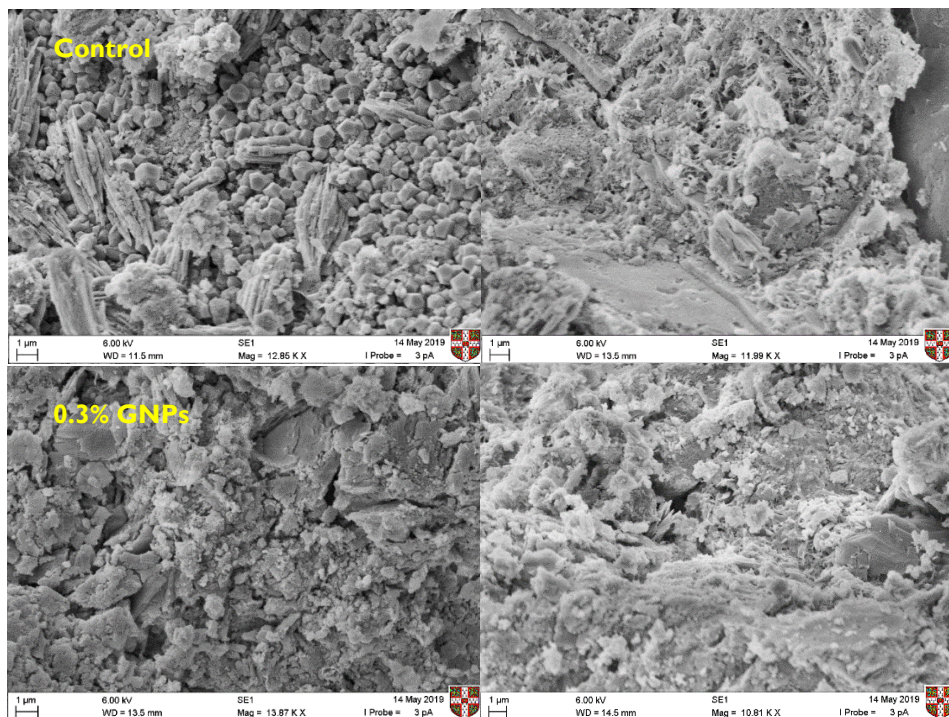
(a)



(b)

Figure 4-18: The effect of different GRMs on the strength of CEMI mortars at 2, 7 and 28 days in terms of (a) compressive strength and (b) flexural strength.

The microstructure of the samples was observed at 2 days. Two points were chosen for each sample to be investigated and the SEM images are presented in Figure 4-19. Overall, the microstructure of the mixes did not appear to depend on the GRM addition. Some cracks and open pores were present which was due to the early hydration age. In the control mix, the cement hydration products were clearly seen in the form of hexagonal portlandite crystals (left) and needle-shaped ettringite on the right. The fact that the morphologies remained largely unaltered justifies the negligible effect that was observed on the strength of the mortars. The individual GRM particles could not be identified in SEM and therefore it was difficult to assess their dispersion in the mortar. At the 1µm scale, some individual CNTs can be observed (yellow arrows in the last image of Figure 4-19). The CNTs can be distinguished from the ettringite crystals because of their smaller size and because they can bend in many different directions. Some CNT clusters can be seen which could be an indication of agglomeration. However, CNTs appeared at different points during the SEM test so it can be assumed that their dispersion in the mortar was sufficient.



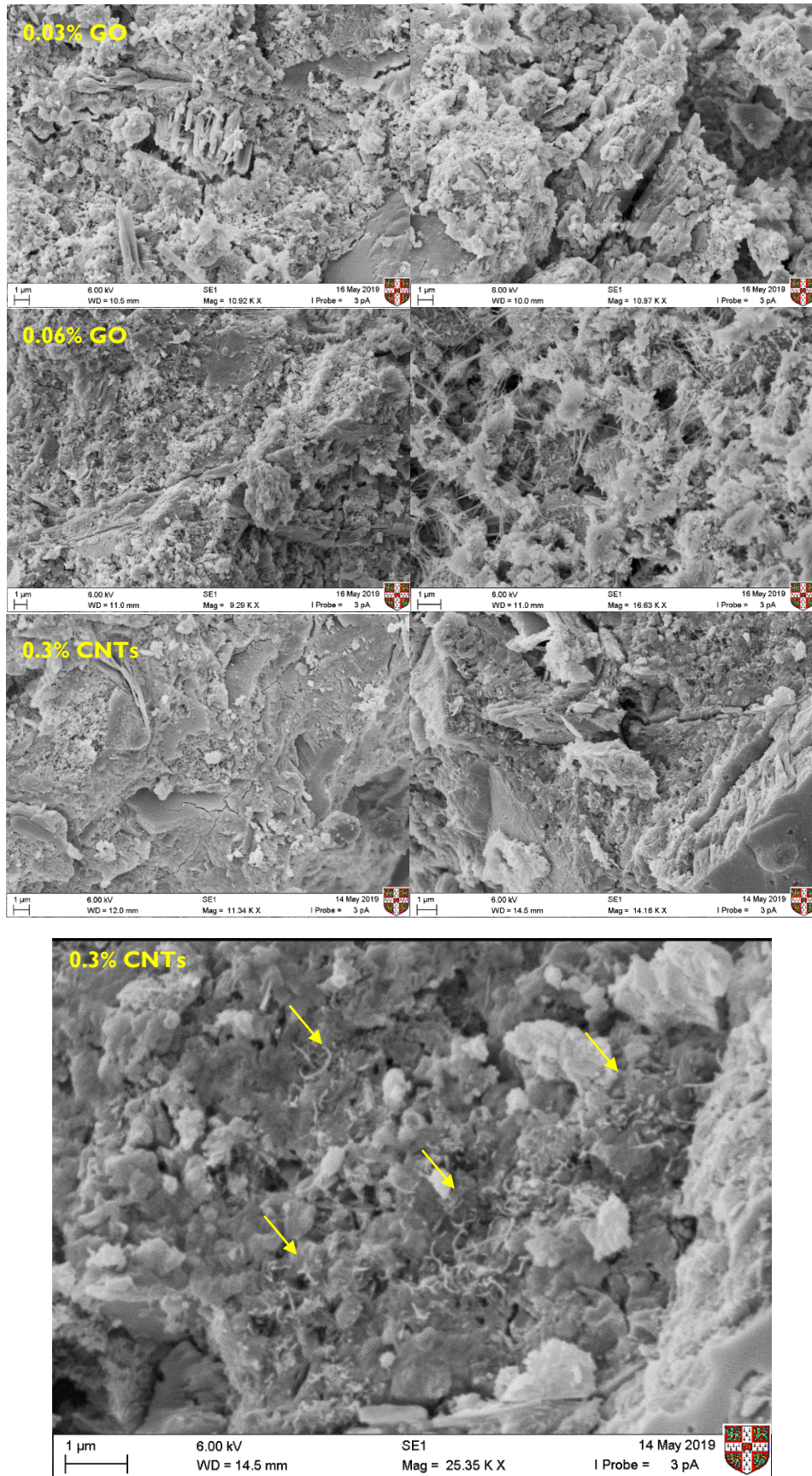


Figure 4-19: SEM images of CEMI mortars at 2 days of hydration

Some of the samples were also investigated further using SEM at 7 days with two points analysed per sample (Figure 4-20). As expected, the hydration had progressed, and less open pores and cracks were observed at 7 days compared to the samples at 2 days. Likewise, the effect on strength was insignificant with the addition of GRMs, which could be justified by the fact that the microstructure between the samples was largely unchanged.

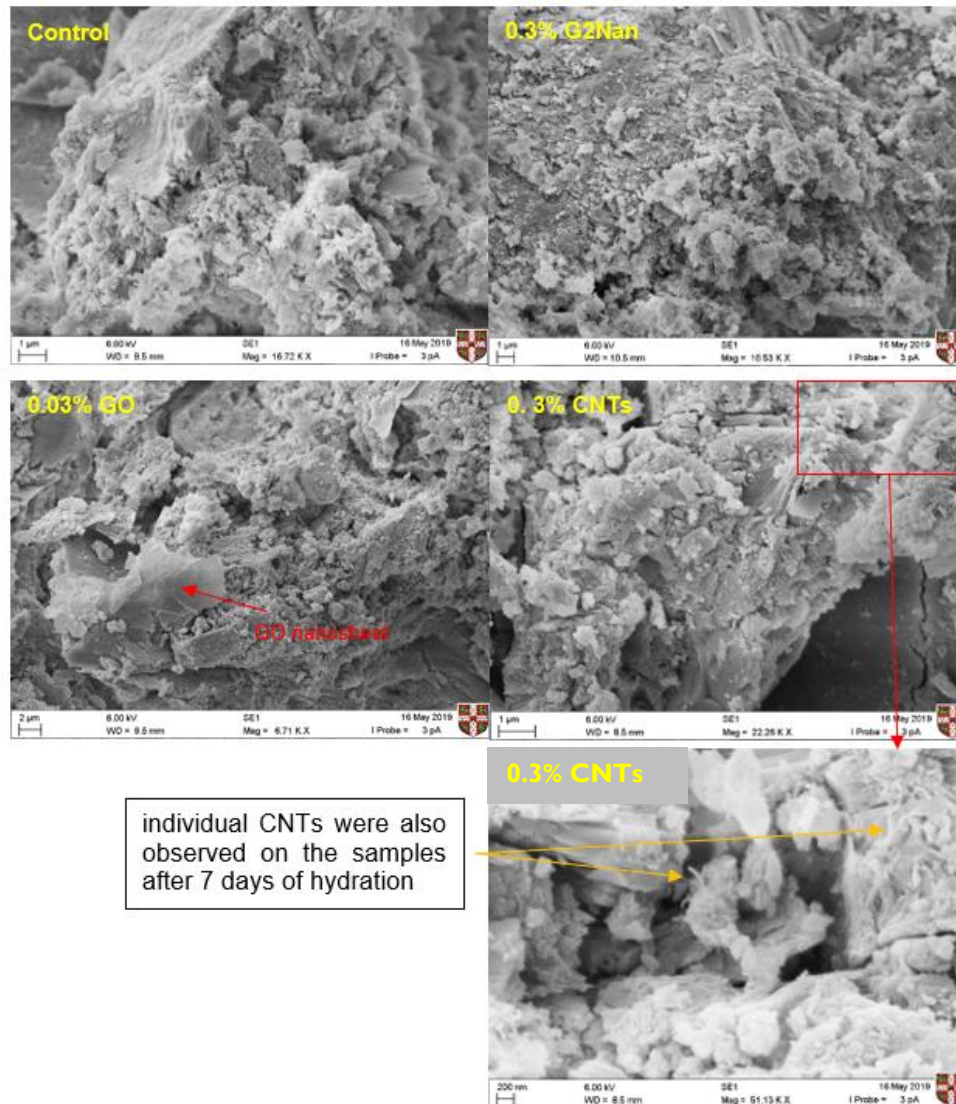


Figure 4-20: SEM images of CEMI mortars at 7 days of hydration

The effect of GRMs on the porosity of the mortars at 2 days of hydration was assessed by MIP (Section 3.3.3.4) by Chongqing University. Only one sample per mix design was tested due to the equipment availability and the intruded volume and pore diameter (from 5-500 nm only) are illustrated in Figure 4-21. The addition of 0.3% GNPs and 0.03% GO reduced

the total porosity of the sample slightly (by 2%) and shifted the pore size range to the right (towards a smaller size). On the other hand, the total porosity increased by 19.5% and 22.3%, and the pore size also increased (therefore became more harmful) when 0.3% CNTs or 0.06% GO was used. These experimental results are preliminary because the measurement of a relevant porosity parameter proved to be difficult in cement-based materials. The results obtained will depend not only on the measuring parameters but also on the drying method used prior to the porosity measurements (Chen *et al.* 2013).

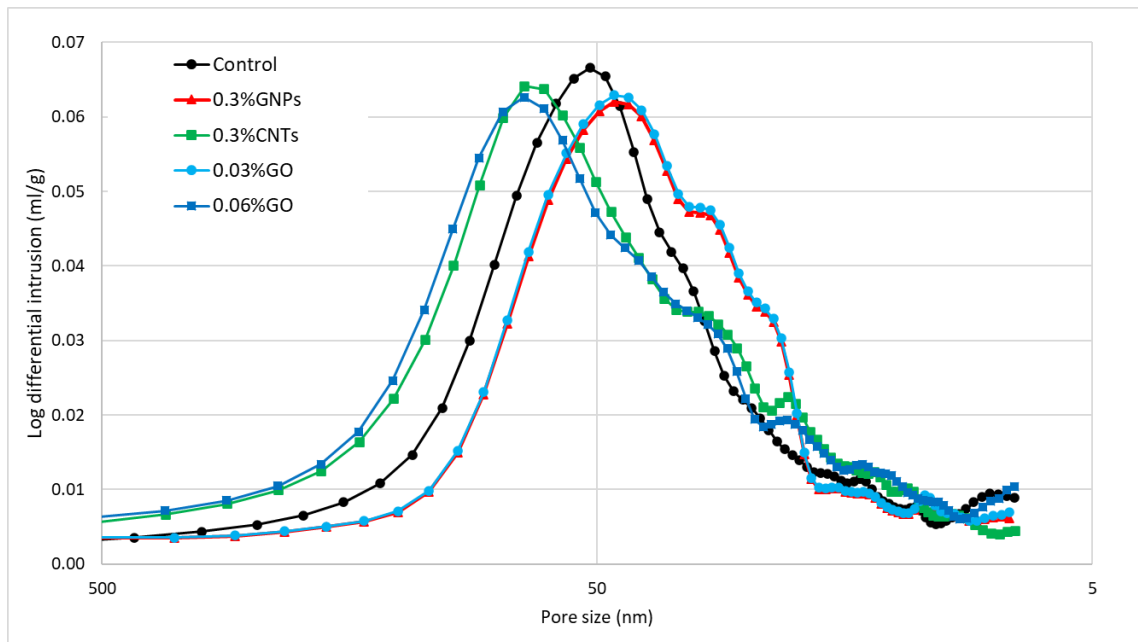


Figure 4-21: MIP results for the *i-lab* CEMI mortars containing GRMs at 2 days of hydration

4.5.4. Alternative and CEMI blended cementitious binders

Three alternative binders were tested to assess their effect on GRM dispersion; namely, P2, P3 and a mortar mix with CEMI that incorporates 10% SF replacement. The silica fume (Elkem Microsilica® Grade 940U, bulk density of 200 – 350 kg/m³) was supplied by Elkem. P2 was a treated cement with partially hydrophobic properties whilst P3 was treated with partially hydrophilic properties. These two cements were commercially sensitive to the *i-lab* and hence no further details on their composition were provided. All tests were carried out at 7 days only and three specimens were tested for flexural strength by 3-point bending and six specimens were tested in compression. GNPs (G2NanPaste) and GO were the only GRMs tested for dispersion, the former being hydrophobic and the latter hydrophilic.

Figure 4-22 illustrates the fluidity of the two alternative binders with GNPs and GO. Both binders resulted in a lower initial fluidity than CEMI (131.5mm). However, when compared to Figure 4-17, it is shown that P2 and P3 were better in maintaining fluidity when the GRMs were added. GO in both cases had a higher fluidity compared to the GNPs (which was also the case for CEMI). The fresh density with GRM incorporation remained largely unchanged.

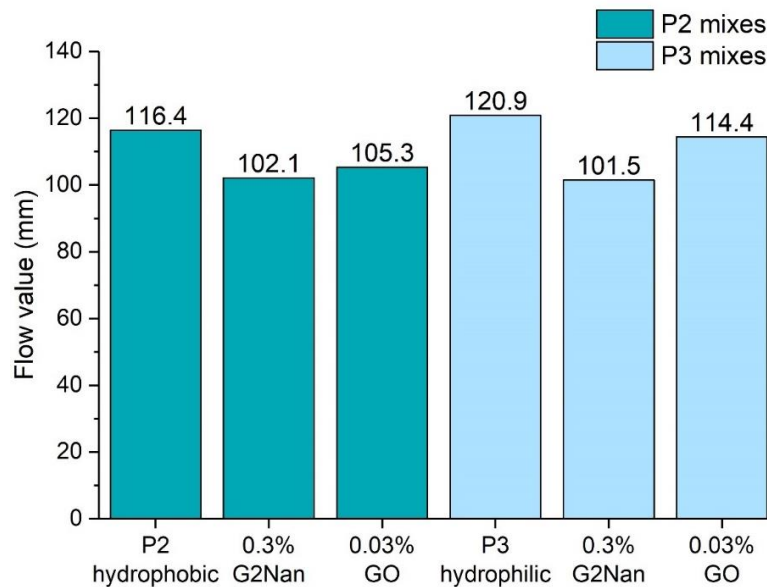
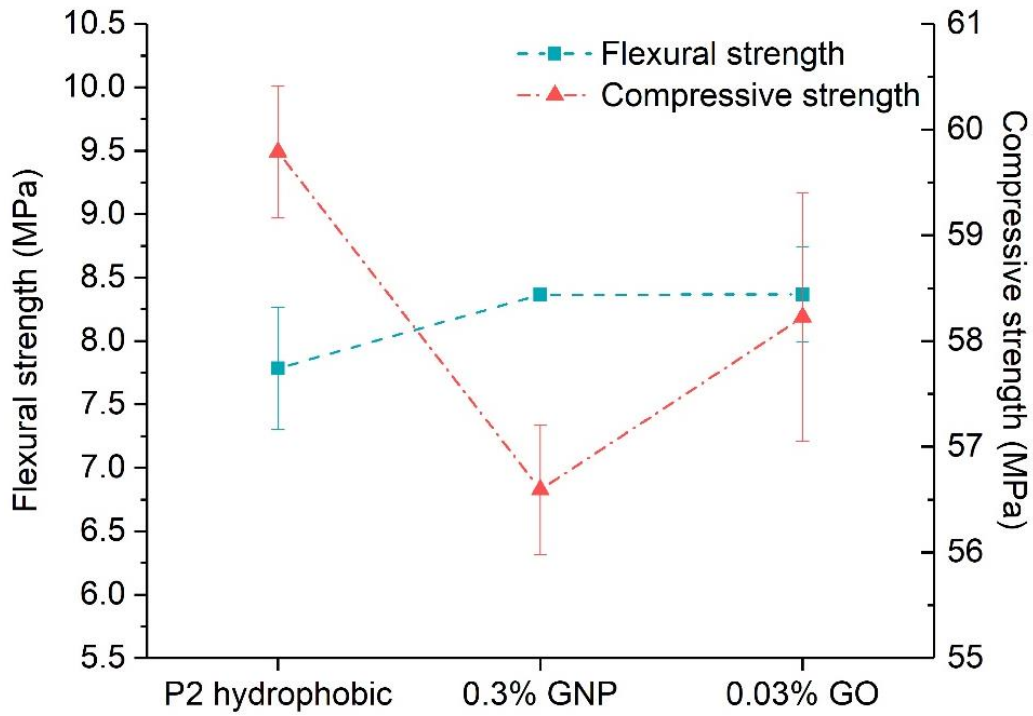
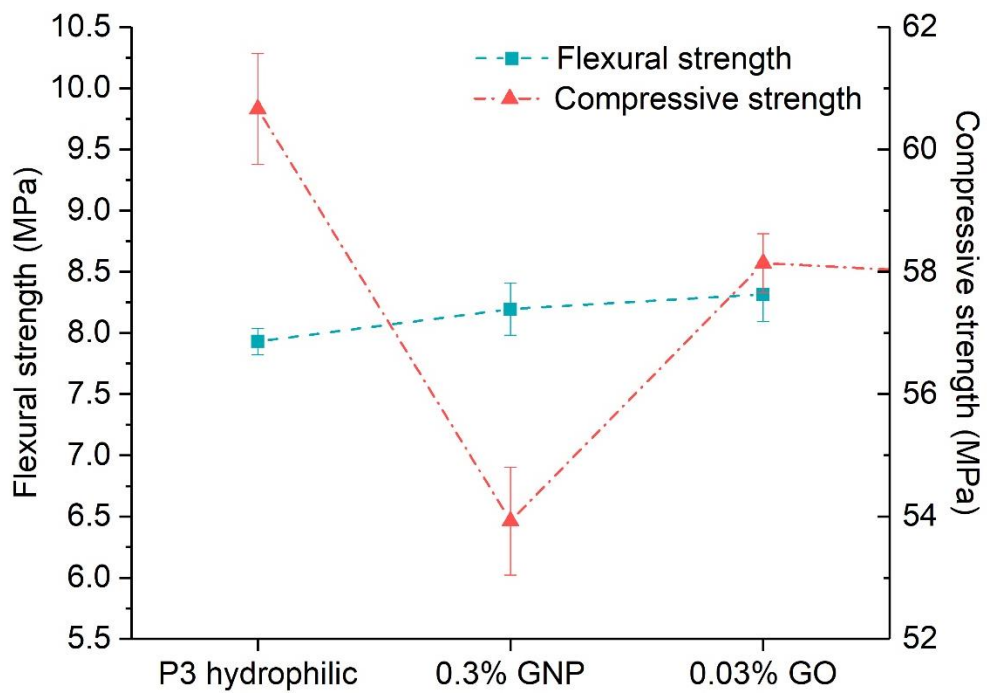


Figure 4-22: Fluidity of P2 and P3 mortars with G2Nan and GO

Figure 4-23 presents the effect of the GRMs on the strength of the two alternative cements. For both cements, the GNPs reduced the compressive strength (red line) significantly whilst the reduction of GO is more moderate. On the contrary, the flexural strength was found to improve for both cements with the addition of either GNPs or GO. This is discussed further later when comparing with the CEMI mortar.



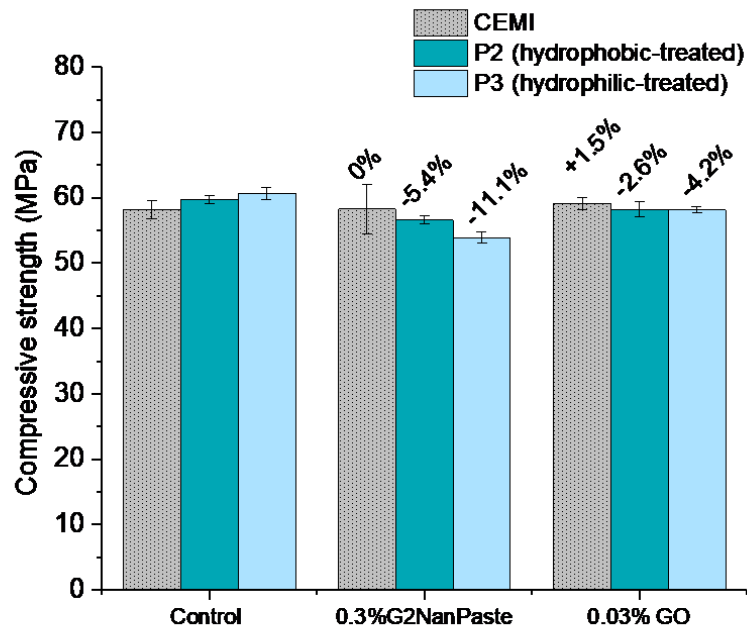
(a)



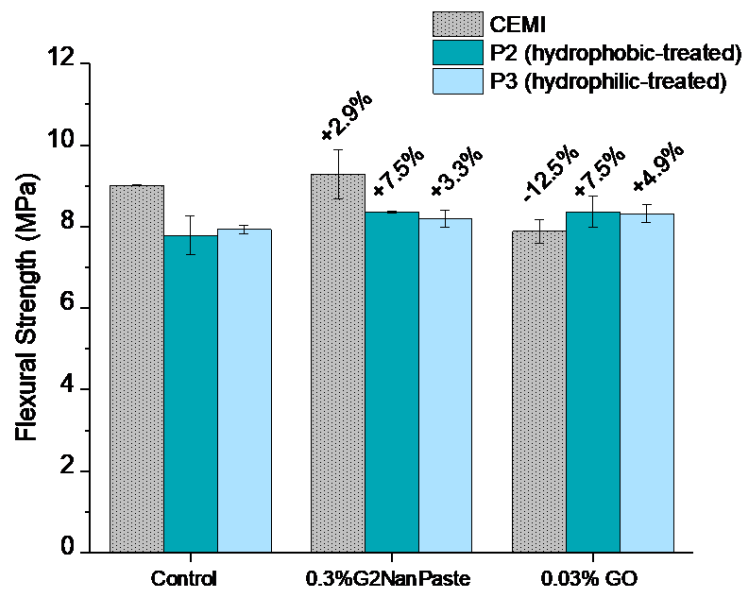
(b)

Figure 4-23: Effect of 0.3wt% GNPs and 0.03wt% GO on the compressive and flexural strength of (a) P2 (hydrophobic-treated) cement and (b) P3 (hydrophilic-treated) cement at 7 days.

For comparison, Figure 4-24 includes the effect of GNPs and GO on all three binders; namely CEMI, P2 and P3. Both P2 and P3 led to a slight enhancement of compressive strength at 7 days. When using CEMI, no effect was observed with the addition of GNPs, whilst GO showed only a slight increase. However, when replacing CEMI with either P2 or P3, the compressive strength reduced clearly. It can be observed, that with P2, GNPs reduced the strength by 5.3% and GO by 2.6% whilst for P3, the reduction was much more pronounced (-11.1% and -4.2% respectively). Therefore, even though both cements reduced the compressive strength, P2 led to a less reduction compared to P3. Therefore, hydrophobic treatment of the cement is a more effective method of dispersing the GRMs compared to the hydrophilic treatment of cement and will result in better macroscale properties. Flexural strength however, showed opposing trends (Figure 4-24(b)). Replacing CEMI with either P2 or P3 reduces the flexural strength of the mortar. The addition of both G2Nan and GO appear to improve flexural strength at 7 days and the effects are more pronounced when the hydrophobic cement is used. For P2, both G2NanPaste and GO improved the flexural strength by 7.5% compared to the reference mortar. With CEMI, GO decreased the flexural strength significantly whilst the use of P3 showed moderate improvements. Therefore, the improvement in flexural strength is much more pronounced with the hydrophobically treated cement (P2). Overall, nanomaterials with P2 improve the flexural strength but the compressive strength is slightly compromised, whilst CEMI shows a decrease in flexural strength and maintenance of the compressive strength. These results cannot be directly compared with the literature as similar cements have not been tested before. Furthermore, not enough information on their composition has been provided by HeidelbergCement so it is not possible to understand and compare the mechanism with others.



(a)



(b)

Figure 4-24: Comparison of the effect of GNPs and GO on the (a) compressive strength and (b) flexural strength of CEMI, P2 and P3 mortars at 7 days. % indicates the change compared to their respective control.

The combined effect of SF and the GRMs was investigated. CEMI mortars with 10% SF as a cement replacement were prepared, so the total binder content remained the same. The effects on fluidity and fresh density are shown in Table 4.6 and the values for the CEMI are also included for comparison. When 10% SF was added, the fluidity reduced significantly from 131.5 mm to 111.5 mm. This is expected as SF is much finer than PC and has a high

surface area, so it requires more water to hydrate (Siddique, 2011). Both GNPs and GO reduced the consistency of the mixes but resulted in a less relative reduction in the SF mixes. Nonetheless, due to the low initial fluidity of the SF mortar, GNPs resulted in a very low consistency and the mix was vibrated for 10 seconds to ensure compaction. The fresh density of the mixes with SF was slightly less than the CEMI mortars but in both cases the effect of GRM addition is insignificant. This indicates that neither GNPs nor GO introduced air in the mix.

Table 4.6: Fluidity and fresh density of CEMI and CEMI+10%SF mortars

	Fluidity (mm)		Fresh density (g/cm ³)	
	CEMI	CEMI + 10% SF	CEMI	CEMI + 10% SF
Control	131.5	111.5	2.24	2.22
0.3% G2NanPaste	93.5	85.6	2.26	2.22
0.03% GO	118.3	101.9	2.26	2.20

Figure 4-25 shows the effect of GNPs and GO on the strength of the SF mortars, whilst the CEMI results are included for comparison. The compressive strength was slightly reduced by ~2% for both GNPs and GO (Figure 4-25(a)). The compressive strength values are all very similar to the CEMI mortars. Likewise, the SF mix resulted in a lower initial flexural strength compared to CEMI. The addition of GNPs and GO both led to a further reduction by 4.9% and 2.1% respectively (Figure 4-25(b)). For GNPs, this mix performed worse than the equivalent CEMI, however, GO resulted in a better strength compared to CEMI. Nonetheless, GRMs reduced the flexural strength. Overall, both CEMI and CEMI+10% SF mortars with GRMs showed an insignificant change compared to the control. Therefore, it is very difficult to reach a conclusion about the effect of SF on the dispersion of GNPs and GO. The positive effect that was expected from the addition of SF was not observed. As found by Li *et al.* (2016) and Bai *et al.* (2018), SF could be used to mechanically separate the GO aggregates and reduce their particle size. Lu *et al.* (2018) also showed that SF helped the disaggregation of GO in water even though this trend was then reversed in the cement pore solution. Therefore, it is not clear if SF helps in the dispersion of GRMs, however, it is commonly used as a cement replacement and therefore its compatibility with GRMs needs to be tested.

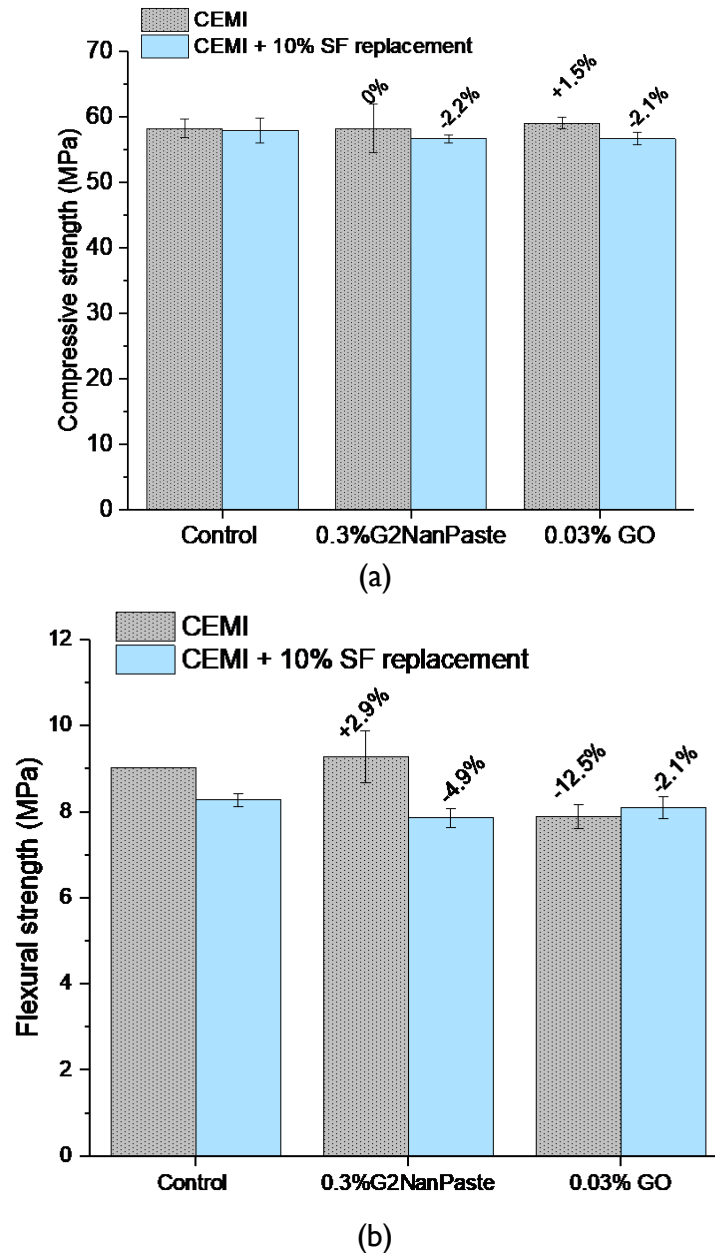


Figure 4-25: Comparison of the effect of GNPs and GO on the (a) compressive strength and (b) flexural strength of CEMI and SF mortars (CEMI with 10% SF replacement) at 7 days. % indicates the change compared to their respective control.

4.6. Summary

Dispersion of GNPs in the cement matrix was identified as a key challenge in the literature as detailed in Section 2.4.1. The primary objective of this chapter was to establish a dispersion protocol that would ensure the GNP dispersion in cement. Firstly, based on the literature findings, the dispersion of GNPs in water was investigated. Through zeta-potential, UV-Vis spectroscopy testing and visual observations, it was found that polycarboxylate

superplasticisers along with sonication were effective in dispersing GNPs in water. This was then tested for cement matrices via rheology testing and it was confirmed that MasterGlenium was the most suitable polycarboxylate superplasticiser. This is widely in agreement with the literature, that has shown a good dispersion when a combination of a polycarboxylate superplasticiser and mechanical treatment (e.g. sonication) is used. Other techniques to assess dispersion, such as micro-indentation, have also been discussed.

Next, the dispersion of natural graphite was tested. The aim of using natural graphite in this study is to improve the electrical conductivity of cement composites so that they could be used for self-sensing applications (presented in Chapter 6). The protocol that was developed and will be followed in the rest of the thesis for natural graphite involved dry mixing the graphite with cement for 2 minutes before adding the water and following BS EN 196 standard mixing, whilst no superplasticiser is needed to mix the natural graphite. The dispersion of natural graphite did not prove to be challenging, unlike GNPs, and its dispersion was confirmed by visual observation, SEM and μ CT scan testing.

Finally, the findings from the dispersion work carried out as part of a secondment in *i-lab* were presented. Different dispersion techniques were investigated, some of them for the first time. The use of a high-speed shear mixer was not effective for dispersing GRMs. Hydrophobic mixing of CNTs (which are also hydrophobic) has been tested for the first time in the context of dispersing CNTs in cement. Unfortunately, the mixing was not successful due to the high admixture dosages that would be added in cement and could compromise the performance. Next, the effect of a hydrophobic and a hydrophilic treated cement was tested, and it was found that the hydrophobic treated cement resulted in better performance with GRMs. However, not enough information was disclosed on their composition and therefore it is difficult to draw conclusions as to the mechanism of dispersion and why improvements were observed. However, this indicated that research in hydrophobic mixing is promising and should be investigated further in future work. Finally, the effect of silica fume as a partial cement replacement was also tested, however, no improvement in the properties was observed, on contrary to what was expected from the literature review.

Overall, the experimental work carried out in this chapter, provided a dispersion protocol for GRMs on which the remaining of the thesis is built upon. This involves pre-mixing the

GRM with water and a polycarboxylate superplasticiser (0.99wt% MasterGlenium by BASF) in a bath sonicator for 1 hour, before adding the suspension in the dry cementitious contents and then following standards BS EN 196-1 mixing. From the work that was carried out in the *i-lab*, it was found that the interactions of GRMs with other types of cements and admixtures (such as silica fume and hydrophobic admixtures) is not clear and their use does not necessarily result in better dispersion. Hence, the dispersion protocol that was developed at Cambridge will be followed for the remaining experimental work. Further research is needed on the effect of mineral admixtures and of alternative cementitious materials (e.g. GGBS and fly ash) on the dispersion of GRMs. Furthermore, research on the effect of other commonly used chemical admixtures (such as accelerators, retarders etc.) on the GRM dispersion and resultant properties when the GRMs are added in a cement matrix is needed.

Chapter 5. GRM-CEMENT COMPOSITES PERFORMANCE

This chapter investigates the effect of GRMs, namely GNPs and natural graphite, on the early age and mechanical properties as well as the durability performance (GNPs only) of cement composites. The dispersion protocols developed in Chapter 4 for dispersing these GRMs in cement are used here. Firstly, cement pastes, using two different cement types, were tested to examine the effects of cement type and the interaction with GNPs. This was followed by extensive testing on CEM I mortars, where the effect of GNPs on the fresh, mechanical and durability properties was investigated. Natural graphite-cement paste composites were tested. The developed cement pastes could have applications as coatings to improve the electrical conductivity (discussed in Chapter 6) and/or durability, whilst mortars would be used for structural applications. An overview of the experimental work for this chapter is provided in Figure 5-1.

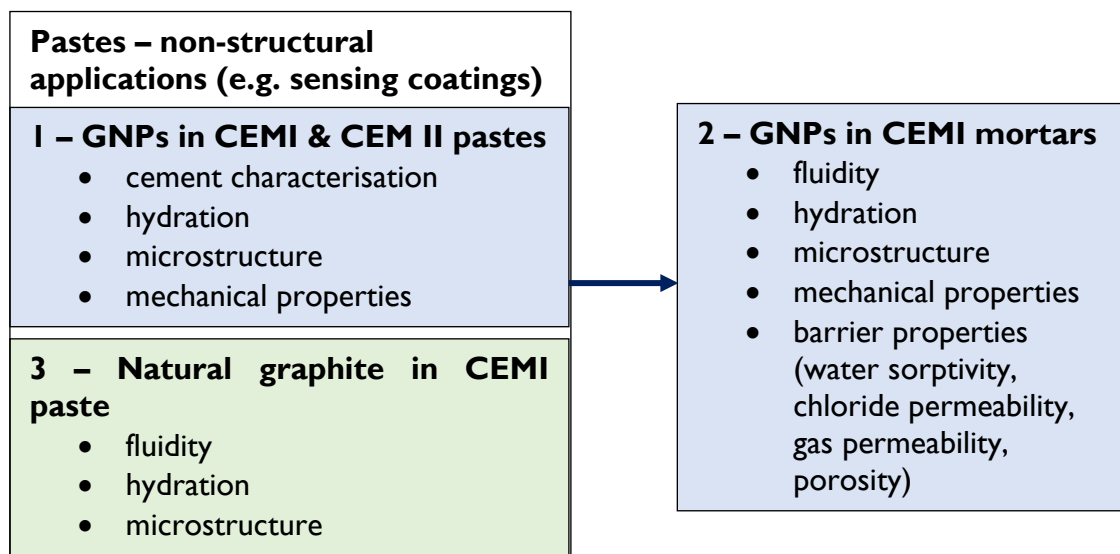


Figure 5-1: Overview of experimental work for Chapter 5

5.1. GNPs in cement paste

The effect of GNPs was partly investigated earlier in Section 4.3.3, showing reduced fluidity of cement pastes irrespective of the use of a superplasticiser. Other important properties such as hydration and mechanical performance are investigated here. These provide the basis for understanding the interaction between GNPs and cement and they must be considered if GNP-cement pastes are to be used in coating applications in the future. Two cements were selected in this study, CEMI 52,5N, referred to thereafter as CEMI, which was used for most of the experimental work in this thesis and is currently used in many infrastructure applications including tunnels and bridges, and CEMII/A-LL 32,5R, referred to thereafter as CEMII, which is commonly used for lower strength applications such as housing. To understand the effect and interaction of GNPs with the cement hydration products, a single dosage of 0.3wt% GNP was selected. Recent literature showed that GNP dosages (~0.1% - 1% bwoc) were investigated for structural applications in mortars and concrete. All mixes had a w/c = 0.45 and the same GNP dispersion protocol was followed, involved the use of 0.99wt% MasterGlenium and 1 hour of bath sonication. The control mixes (without GNPs) still had the superplasticiser, so the only variables were the GNP addition and the cement type.

5.1.1. Cement characterisation

Initially, the two cements were assessed by TGA and Figure 5-2 illustrates the weight loss with increasing temperature curve and the DTG curve. To understand the hydration degree, the weight loss curves were compared as they show the decomposition of the different minerals with temperature. The DTG curves can be used to identify the different phases in the material. It can be observed that CEMII (green lines) decomposed more compared to CEMI (red lines) as more weight loss was observed overall. At 1000°C, CEMII lost almost 8% of its total mass whilst CEMI lost less than 6%⁵. However, up to ~600°C, CEMI lost more weight and the decomposition of CEMII started after this temperature. This is because, CEMII contains 18% limestone (CaCO₃) which decomposes at 700°C, to CO₂ and CaO. By observing the mass loss in the graph, only ~7% of the CO₂ was evaporated at this temperature.

⁵ The limestone content of CEMI was much higher than expected as a mass loss was observed at 700°C, where limestone decomposes to CO₂ and mass is lost due to the CO₂ evaporation

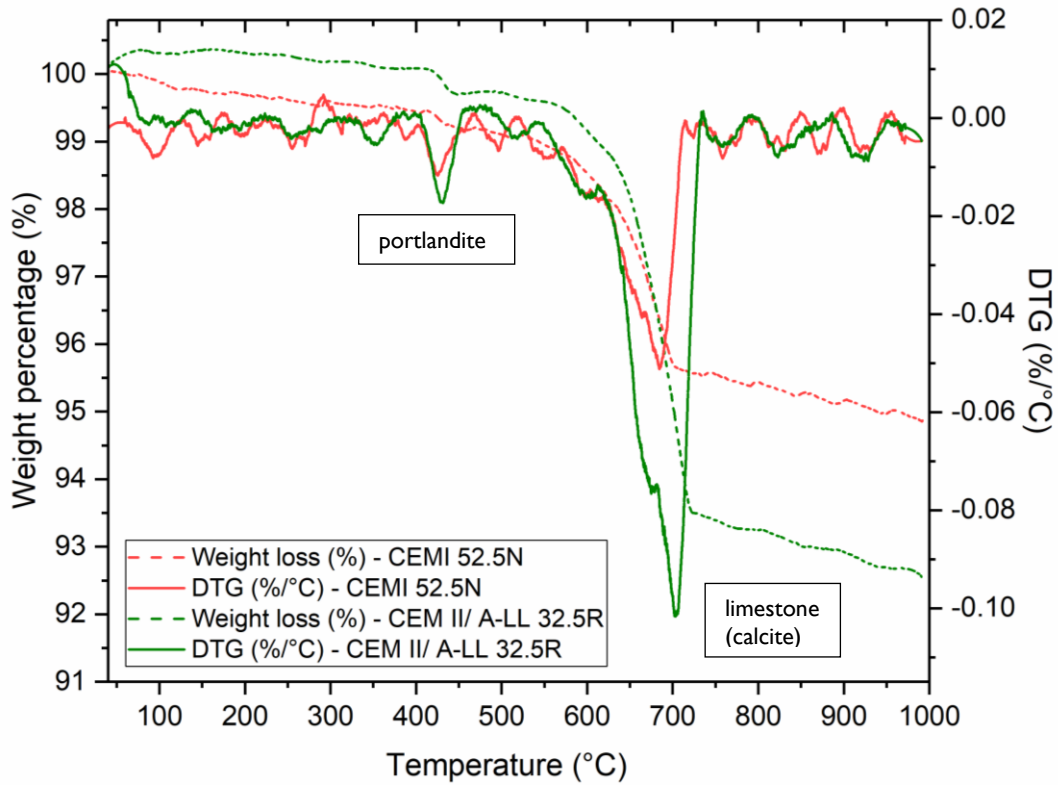


Figure 5-2: TGA/DTG curves of CEMI 52,5N and CEM III/A-LL 32,5R cements used in this study

5.1.2. Effect on hydration

The effect of the 0.3wt% GNP dosage on the cement hydration was investigated by TGA. Tests were carried out at 28 days as well as 2 days to understand the effect on the early age hydration. Mechanical and durability testing was carried out at the same test ages and therefore the hydration results could also inform the findings from the remaining experiments. For CEMI, the TGA/DTG curves for 2 (top) and 28 days (bottom) are shown in Figure 5-3.

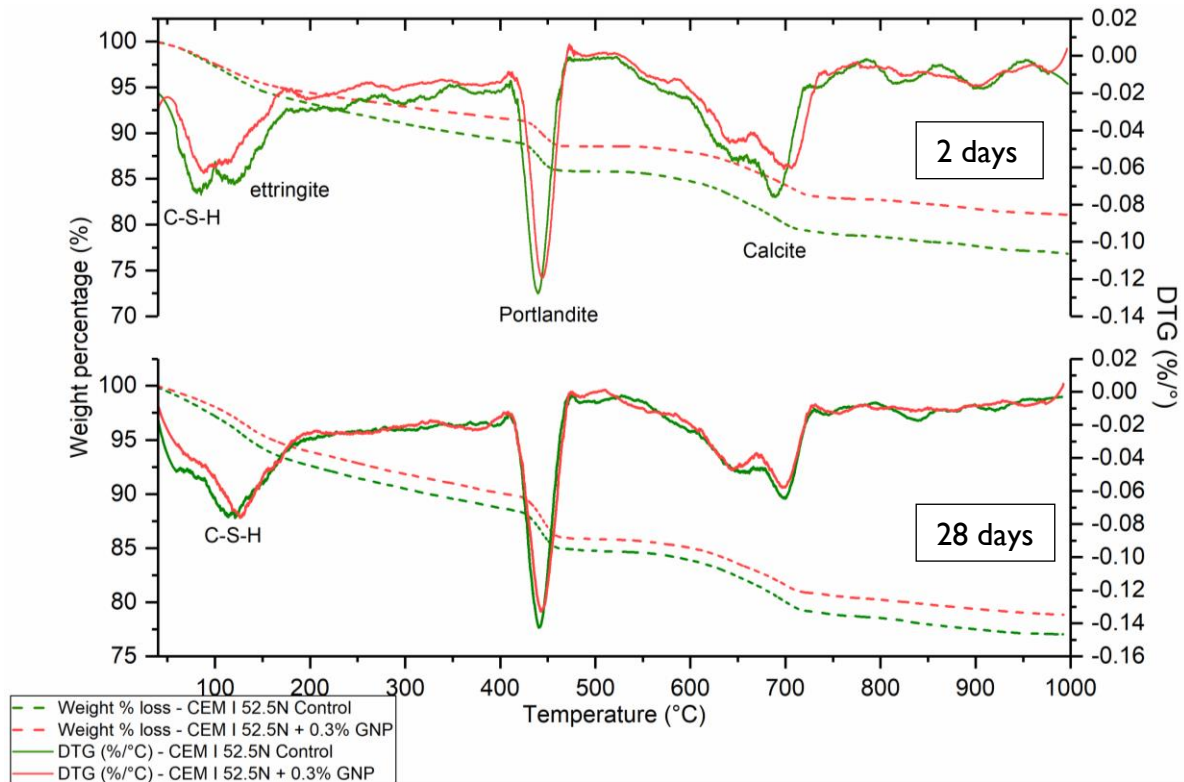


Figure 5-3: TGA/DTG curves of CEM I 52,5N with 0.3wt% GNP at 2 and 28 days.

At both test ages, the GNP samples were found to lose less weight compared to the control which means that the hydration was slightly reduced with GNP addition. The effect was more pronounced at 2 days compared to 28 days. To ensure that the findings were comparable, only the weight loss curves from 40°C to 400°C were considered. This is because the raw cement and GNP materials showed almost no weight loss in this temperature range whilst the cement paste (C-S-H and ettringite) did. At higher temperatures, the raw cement materials had portlandite and limestone that decomposed (as shown in Figure 5-2) and therefore, the effect of GNPs on the hydration could not be deducted. The DTG showed that the rate of mineral decomposition remained unchanged. GNP addition did not affect the mineral decomposition as in all cases the DTG curves were very similar and no additional decomposition of cement hydration products occurred. At both test ages, three distinct peaks could be observed: C-S-H at ~100°C, portlandite (CaOH₂ decomposition) at ~450°C and calcite (CaCO₃) at ~700°C. Next, the effect of GNPs on the hydration of CEMII was investigated and the results are illustrated in Figure 5-4 for 2 and 28 days.

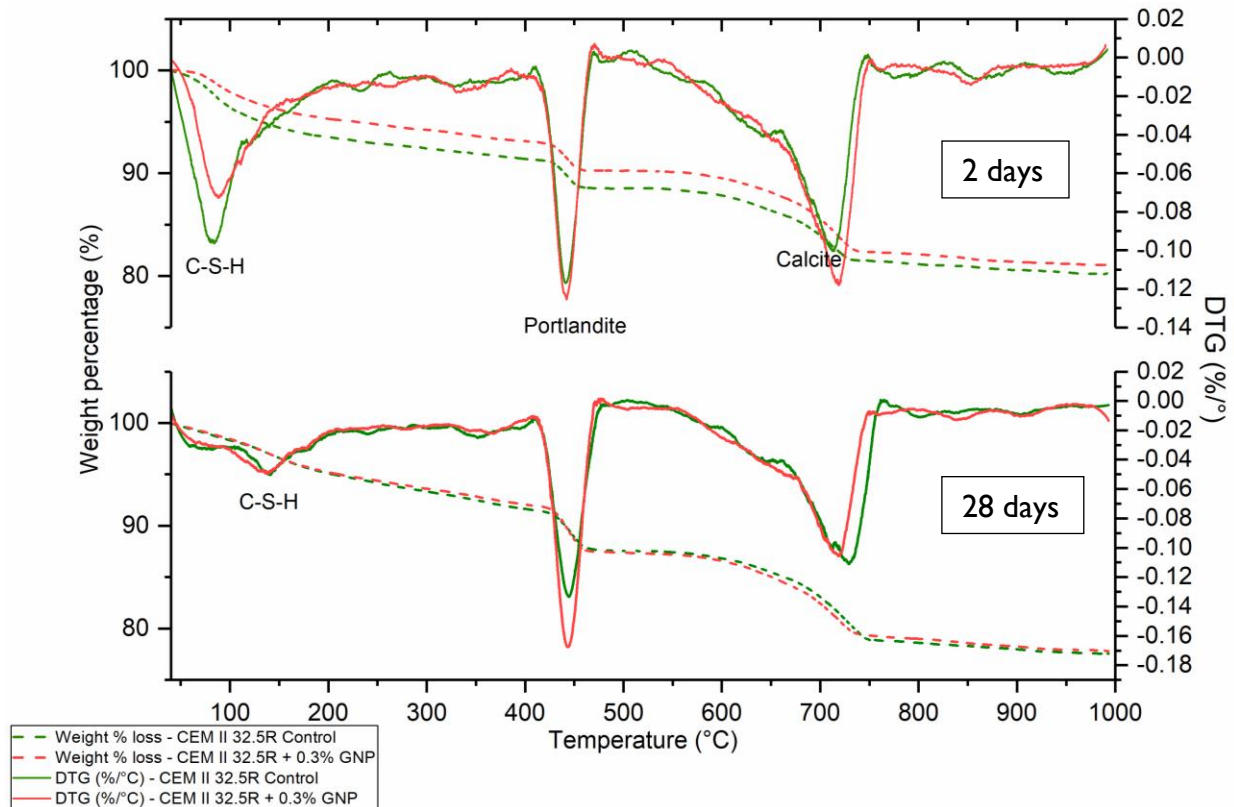


Figure 5-4: TGA and DTG curves of CEMII/A-LL 32,5R with 0.3wt% GNP at 2 and 28 days.

The weight loss curves from 40°C to 400°C were observed and it is seen that the GNP sample (red line) lost less weight at 2 days compared to the control, but at 28 days, the curves were identical. Hence, GNPs slightly reduced the hydration degree of CEMII paste at 2 days, but they had no effect in the long term. The DTG curves were very similar, indicating that the rate of mineral decomposition with temperature was not affected by GNP addition. However, a new major DTG peak was introduced around 750°C which was not as pronounced when CEMI was used. This was due to the presence of limestone in CEMII, which decomposed at this temperature as shown in Figure 5-2.

In addition to the comparison of the weight loss curves, two further parameters were used to assess the effect of GNPs on the hydration behaviour of cement paste; non-evaporable content and loss on ignition (LOI) weight. Non-evaporable water is the water that is released when the temperature exceeds 105°C and is due to the loss of water from the cement hydration products rather than water evaporation (which happens at 100°C). The non-evaporable water was measured from 105°C to 400°C. This temperature range was

selected because the raw materials (cement and GNPs) did not lose any weight. On the contrary, a great weight loss due to portlandite and calcite decomposition at higher temperatures was observed for the raw materials and therefore, any comparisons above 400°C would not be representative. LOI weight represents the total weight loss due to the decomposition of cement hydration products from 105°C - 1000°C and the greater the weight loss, the higher the cement hydration. From Figure 5-5 and Table 5.1, it is seen that GNP addition reduced both the non-evaporable water content loss and the LOI. The effect was more pronounced for CEM I at 2 days where, LOI reduced from 20.8% to 16.7% when GNPs were added, and non-evaporable water loss reduced from 8% to 5.8%. At 28 days the percentage change of these two parameters was less pronounced, however, GNP addition still led to a reduction. When CEM II was used, both the non-evaporable water loss and the LOI were only slightly reduced at 2 days whilst there was almost no change at 28 days. This agrees with the TGA/DTG curves that were shown in Figure 5-4.

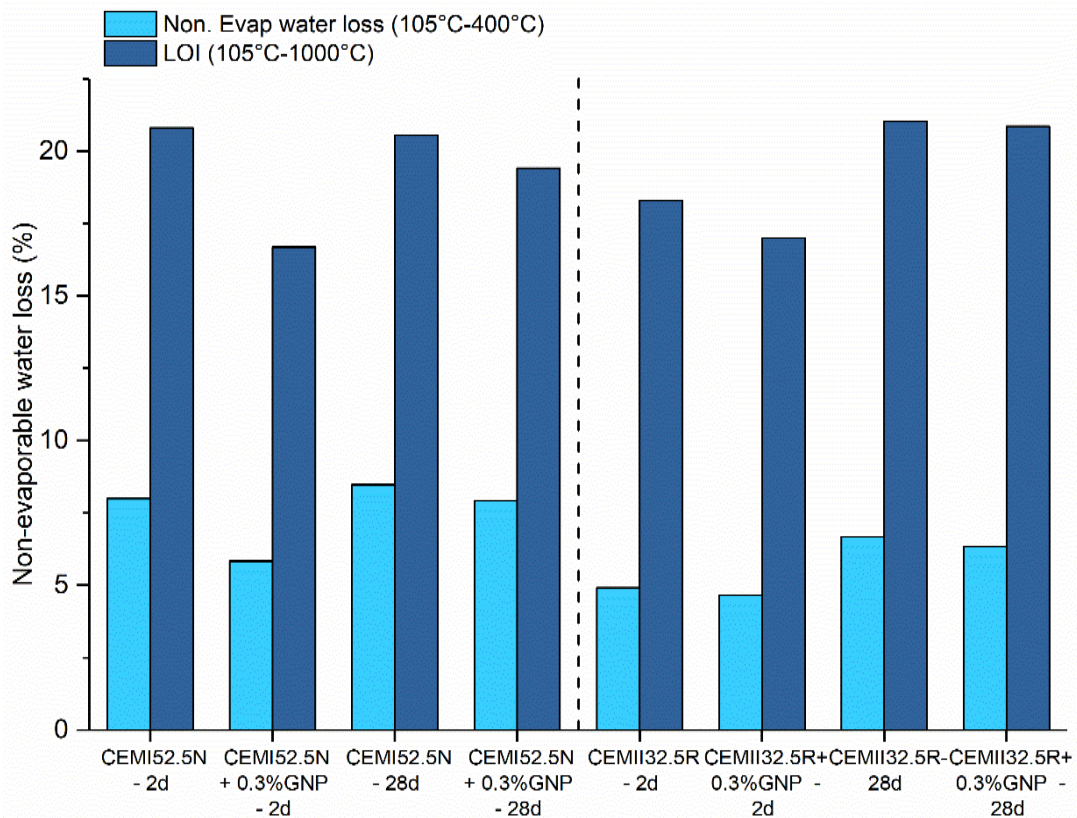


Figure 5-5: Non-evaporable water loss and loss on ignition (LOI) weight for CEM I and CEM II paste samples with 0.3wt% GNP

Table 5.1: Non-evaporable water loss and LOI weight of the CEMI and CEMII control and GNP samples.

Mix / Temperature	Non. Evap water loss (105°C-400°C) (%)	LOI (105°C-1000°C) (%)
CEMI52.5N Ctrl - 2d	8.0	20.8
CEMI52.5N + 0.3%GNP - 2d	5.8	16.7
CEMI52.5N Ctrl - 28d	8.5	20.5
CEMI52.5N + 0.3%GNP - 28d	7.9	19.4
CEMII32.5R Ctrl - 2d	4.9	18.3
CEMII32.5R+ 0.3%GNP - 2d	4.7	17.0
CEMII32.5R Ctrl - 28d	6.7	21.0
CEMII32.5R+ 0.3%GNP - 28d	6.3	20.9

Isothermal calorimetry was also used to examine the effect of GNPs on the hydration and data was collected for the first 48 hours (2 days). The control measurements refer to $w/c = 0.45$ and 0.99wt% MasterGlenium, therefore, the difference between the curves is due to the 0.3wt% GNP. Cement hydration is an exothermic reaction, characterised by the following; a first peak which is very high and corresponds to the initial hydration at the surface of cement particles (within one hour), followed by a dormant/induction period during which the material is workable, and finally a second peak at around 10 hours during which the individual cement grains come in contact with water and final setting occurs (Neville 2011). As shown in Figure 5-6, the second hydration peak occurred at a much later age than expected – at ~18 hours for CEMII (blue lines) and 22 hours for CEMI samples (green lines). The delay was attributed to the superplasticiser which was present in all samples and retarded the hydration. CEMII samples hydrated at an earlier age compared to CEMI and a more depressed and broader peak was found, meaning that the rate of heat of hydration was lower for the CEMII compared to CEMI. When 0.3wt% GNP was added, the hydration curves remained almost unchanged and the same peaks could be seen. Therefore, GNP addition did not affect the hydration behaviour of cement paste and did not participate in the hydration directly, irrespective of which cement was used. CEMII had a much higher cumulative heat of hydration in the first 26 hours which was due to the reactions with the limestone cement. After ~26 hrs, this trend reversed and the cumulative hydration heat of CEMI increased more rapidly. A slight reduction of the cumulative heat with 0.3wt% GNPs was found for both cements, meaning that the hydration was slightly compromised with

GNP addition. These findings agree with the earlier TGA results that showed that the control samples hydrated more compared to the GNP samples.

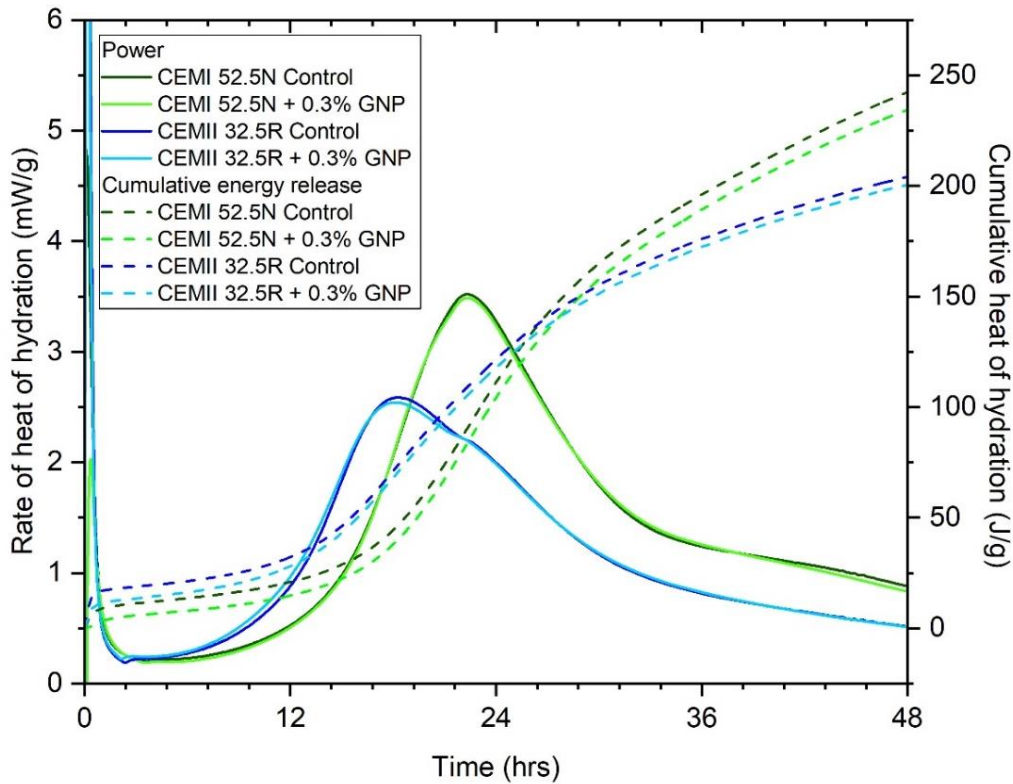


Figure 5-6: Isothermal calorimetry results of CEMI and CEMII cements with 0.3wt% GNP

Isothermal calorimetry can also be used as an indirect measure of the initial setting time which occurs approximately at 1/3 of the second peak (Calmetrix, 2016). Table 5.2 shows that for CEMI pastes, setting time occurred at ~15.7 hrs and the effect of GNP was negligible. For CEMII pastes, the initial set happened at an earlier age at ~11.5 hrs, and again, the effect of GNP addition was negligible. This initial setting time is only an approximation, and the method is not very accurate, therefore, further setting time testing would be needed to establish the precise setting time of the different pastes.

Table 5.2: Initial setting times and peak power values for CEMI and CEMII pastes with 0.3wt% GNPs

	Peak power (mW/g)	Initial set (hr)
Control CEMI 52.5N	3.52	15.7
CEMI 52.5N +0.3wt% GNP	3.49	15.8
Control CEMII 32.5R	2.59	11.9
CEMII 32.5R + 0.3wt% GNP	2.54	11.4

Finally, XRD analysis was carried out at 28 days to identify the crystalline phases and the spectra of the four samples are shown in Figure 5-7. The spectra looked very similar, irrespective of GNP addition and cement type. The typical Portland cement hydration products were detected in all cases; portlandite (CH) peaks at $2\theta = 18.1^\circ$, 34.2° and 47.2° ; ettringite at $2\theta = 18^\circ$, 42° ; C-S-H at $2\theta = 29.1^\circ$ which could also be attributed to calcite due to carbonation of calcium hydroxide; and residual tricalcium silicate (C_3S) at $2\theta = 23.1^\circ$, 32.2° , 51.8° . The peak intensities for the different samples remained largely unchanged with GNP addition, however, the peaks of the controls were slightly higher. The characteristic peak of graphite at $2\theta = 26^\circ$ was not observed in the samples which could be due to the very small dosages of the material. Overall, GNP addition had an insignificant effect on hydration after 28 days, in agreement to TGA.

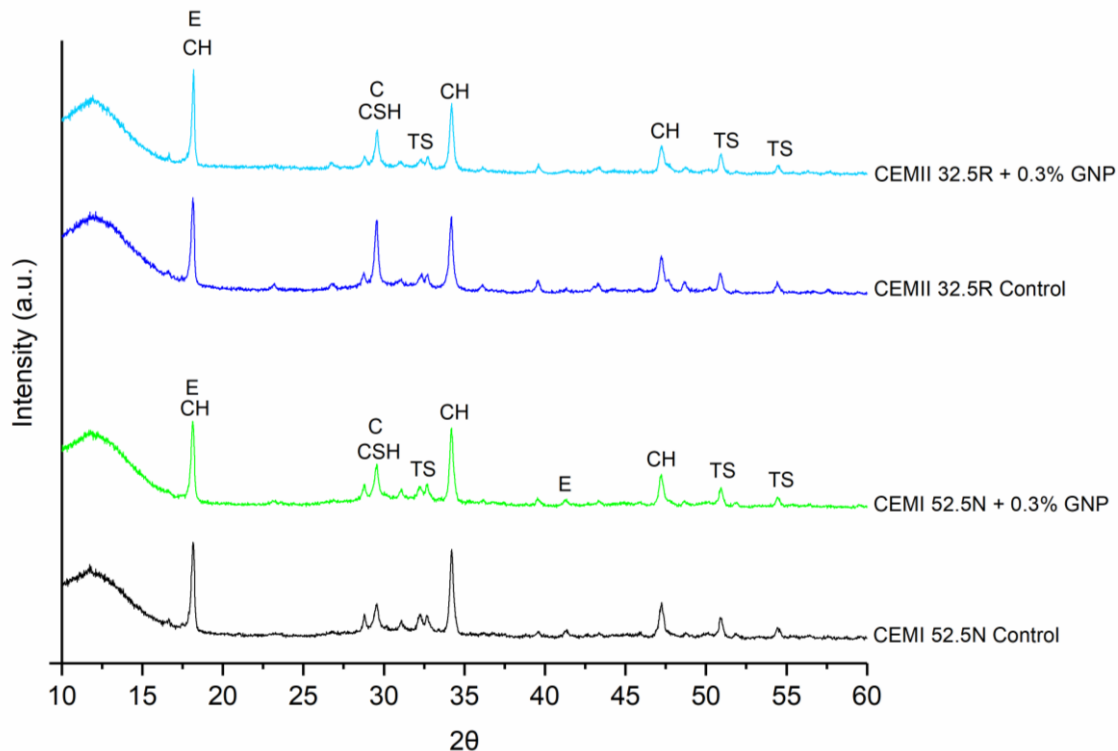


Figure 5-7: XRD spectra of CEMI and CEMII cement paste controls and with 0.3% GNP at 28 days (CH – portlandite, E – ettringite, C – calcite, CSH – C-S-H, TS is C₃S)

It can be concluded that GNPs slightly reduced the cement hydration at 2 days, which was confirmed by TGA and the reduction in the cumulative heat of hydration in the isothermal calorimetry. At 28 days, TGA along with XRD confirmed that GNPs had a negligible effect

on hydration. These hydration results can be explained by an inert filler mechanism. GNPs do not directly affect the hydration of cement pastes, irrespective of which cement type is used and therefore, there is no chemical mechanism involved. However, the very small GNP particles, can act as fillers in the cement matrix by filling some of the pores in the mix and bringing the cement hydration products closer. At the same time though, GNPs could be blocking some of the cement particles from hydrating by using some of the free water in the mix to wet their surface. Therefore, a slight reduction in weight loss was observed in the TGA results. The control mixes in both cases, had more water available for hydration, whilst the GNP mixes used some of that water to wet the surface of GNPs and disperse them in the mix. The effects on hydration were not pronounced because the GNP dosages used are very small and overall, the effect on hydration is negligible.

These results agree with the literature that showed that GNPs had a negligible effect on hydration of PC. TGA showed that no new phases were created with the addition of GNPs (Wang *et al.*, 2016; Wang *et al.*, 2020) whilst similar amounts of free water, physical bound water and portlandite were found with GNP addition (Goracci and Dolado, 2020). Isothermal testing also confirmed that GNPs had a minimal effect on cement hydration, as the curves were very similar and minimal movements could be attributed to baseline drift (Wang *et al.*, 2016; Jing *et al.*, 2017).

5.1.3. Effect on microstructure

The effect of GNPs on the microstructure of CEMI and CEMII pastes was investigated by SEM at 28 days. The SEM micrographs for the CEMI samples are presented in Figure 5-8. In Figure 5-8(a-b) of the CEMI control, some un-hydrated crystals could be observed along with a slightly porous microstructure and some needle-shaped ettringite crystals. Figure 5-8(c-f) shows that with the addition of 0.3wt% GNPs, some individual GNP particles can be found (indicated by yellow arrows); characterised by a wrinkled morphology. However, in most cases these GNPs were not well incorporated within the cement hydration products. The samples often broke around the GNPs which means that they could have created an interfacial transition zone that resulted in planes of weakness in the mix.

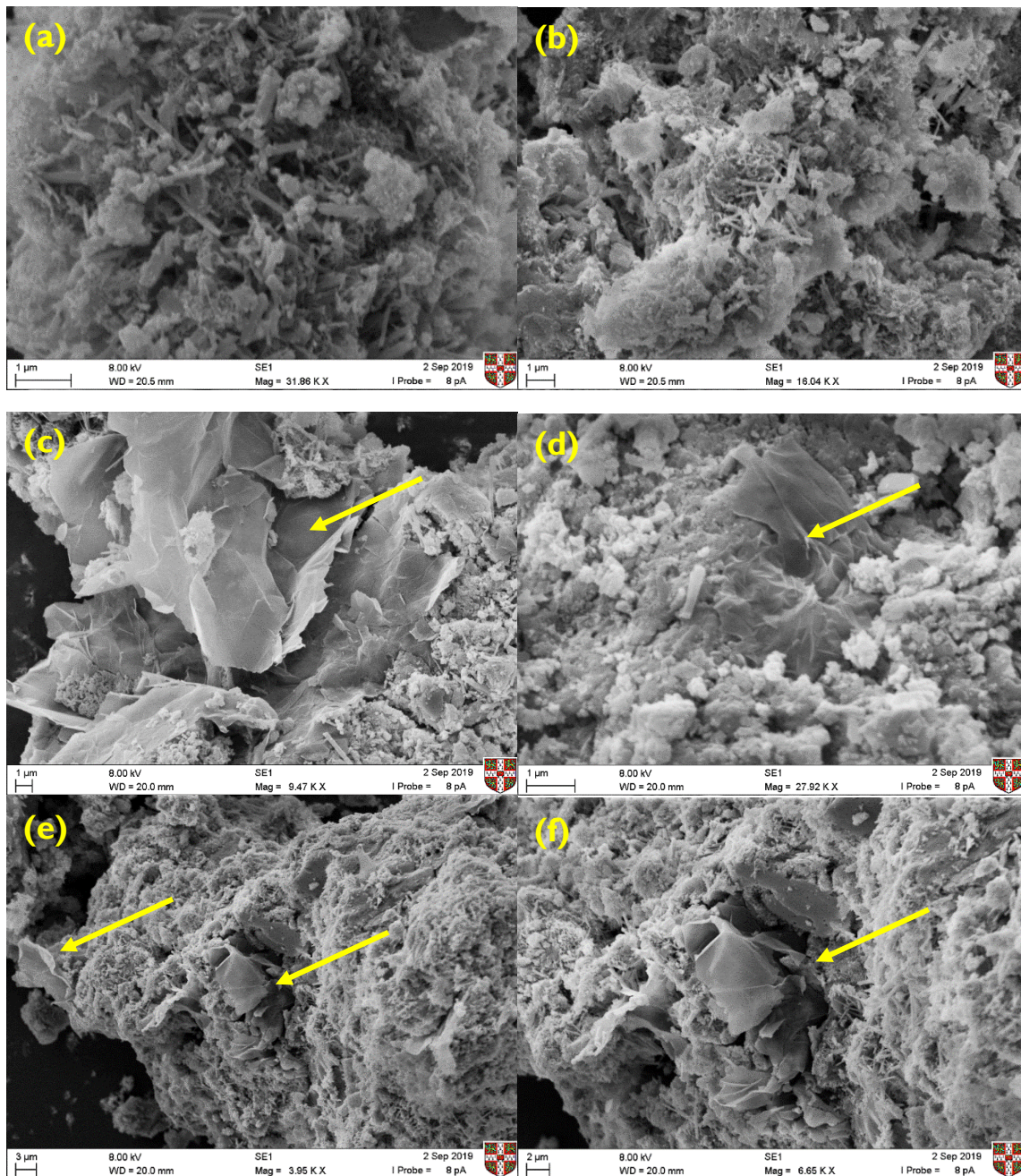


Figure 5-8: SEM of CEMII mixes (a-b) control, (c-f) with 0.3wt% GNP

The SEM micrographs for the CEMII mixes are shown in Figure 5-9. In Figure 5-9(a-b) the control samples looked similar to the CEMII micrographs; some un-hydrated crystals could be seen even at 28 days. By looking at Figure 5-9(c), some cement hydration products and crystals can be seen clearly, however, a GNP sheet is shown next to them and is not well integrated (yellow arrow). This could mean that the GNPs are not well linked with the cement hydration products and very little interaction can be assumed. Also, it should be

noted that the GNP sheet might have formed a plane of weakness, as the particle has cracked in this location, whilst the GNP structure seemed to remain intact. By taking a closer look in Figure 5-9(d), it is clear that the cement hydration structure had broken around the GNPs. Therefore, the presence of the GNPs might create an interfacial transition zone within the hydrated cement structure; similar to the zones that can be introduced by aggregates. This could consequently impact the mechanical performance of the cement composites. If the GNPs create planes of weakness, then these zones could act as defects within the composite. The effect on the mechanical performance is investigated in more detail in Section 5.1.4.

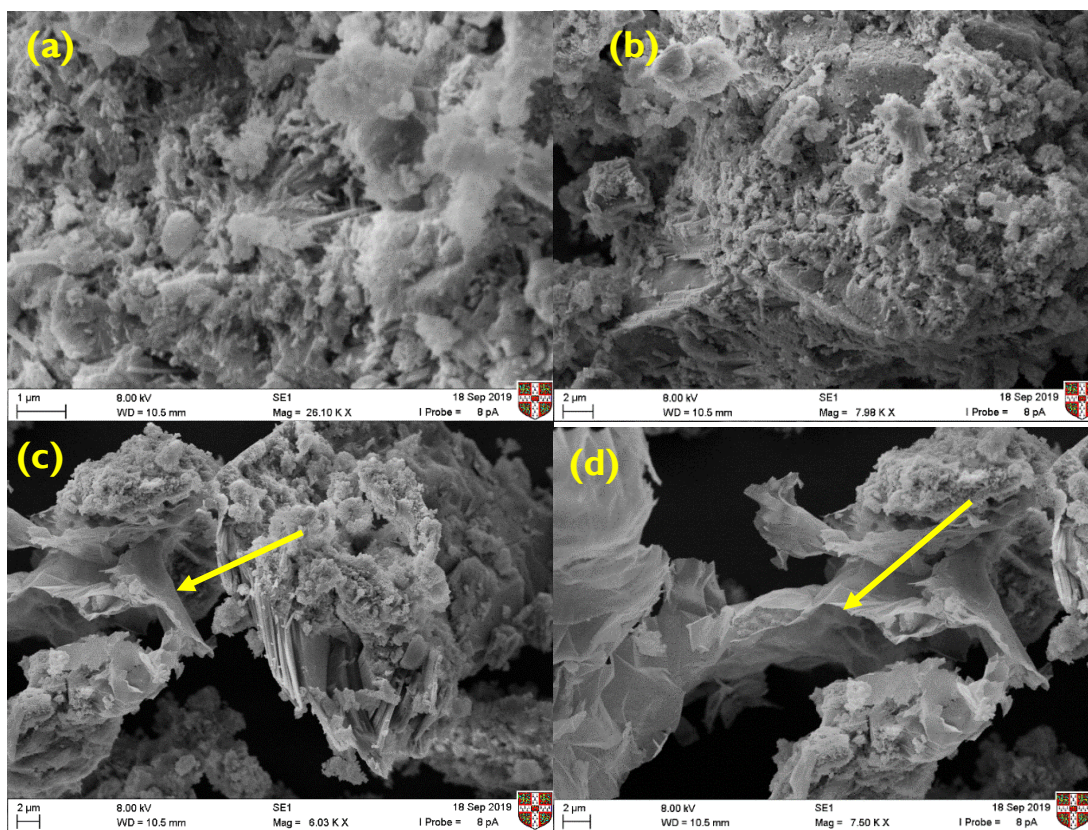
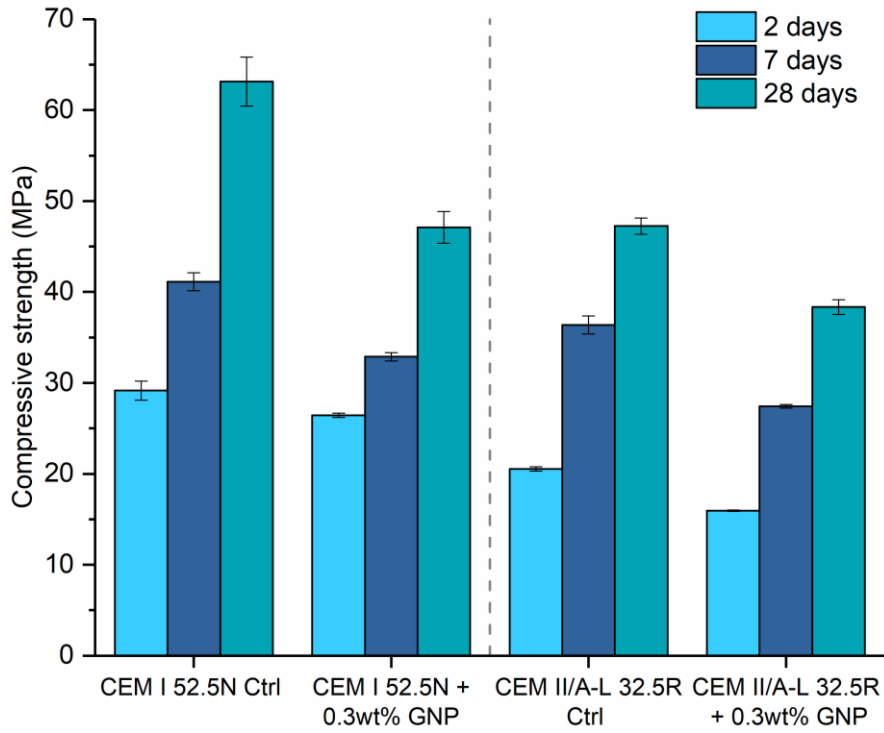


Figure 5-9: SEM of CEMII mixes (a-b) control, (c-d) with 0.3wt% GNP

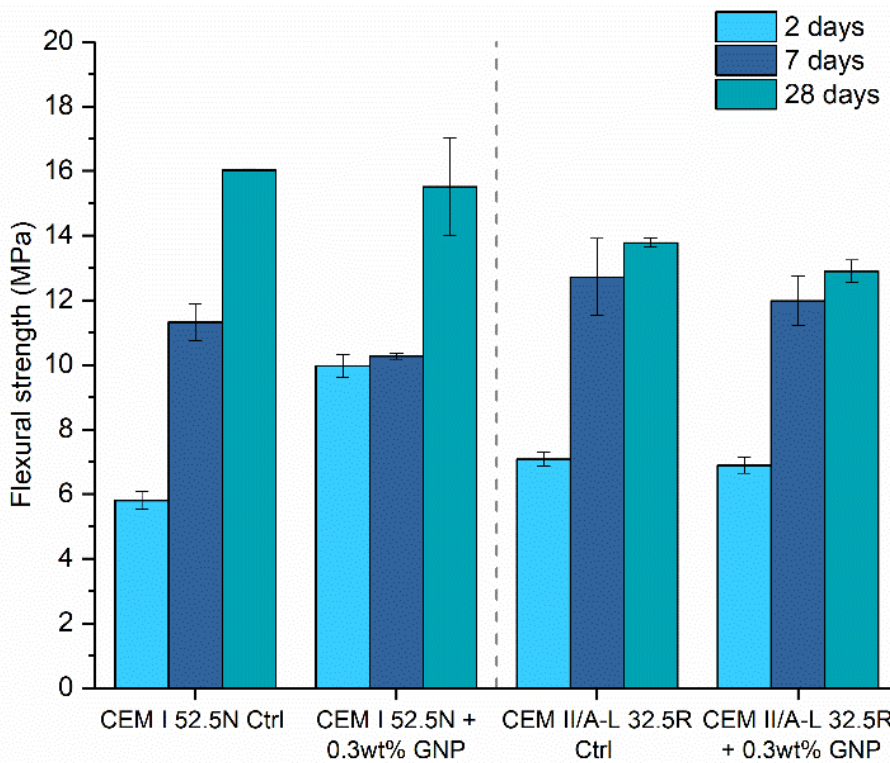
Overall, the GNPs appear to have dispersed within the cement matrix and no agglomerates were observed. However, the interaction with the cement hydration products is poor and some weakness planes can be seen, where the microstructure broke around the GNP particle. The microstructure and cement hydration products remained largely unaltered, meaning that GNPs did not induce any chemical and microstructural changes in the cementitious composites. Instead, GNPs seemed to be acting as fillers.

5.1.4. Effect on mechanical properties

The effect of GNPs on the mechanical properties of cement pastes was investigated by testing both CEMI and CEMII with a single dosage of GNPs (0.3wt%) at 2, 7 and 28 days. As presented in Table 3.4, six 40 mm cubes were tested in compression and triplicate prisms of 40x40x160 mm were tested under flexure. The density of all mixes remained unchanged with GNP addition which could be due to the small GNP dosages. Figure 5-10 (a-b) illustrates the effect of 0.3wt% GNPs on the compressive and flexural strengths, together with the error bars. In all cases the strengths increased with curing age, whilst CEMII resulted in lower compressive strength compared to CEMI, as expected. Starting with the compressive strength, it was found to reduce in all cases with GNPs, and the effects were pronounced at 28 days. GNPs reduced the compressive strength of CEMI by 25% and of CEMII by 19% at 28 days. On the contrary, by observing the flexural strength, a large increase was seen at 2 days for the CEMI mix when GNPs are added, however, this trend was reversed at 7 and 28 days, where strength reductions were observed. For the CEMII pastes, the flexural strength reduced slightly with GNP addition by 2%, 5% and 6% at 2, 7 and 28 days compared to the control. As shown in Figures 2.26 and 2.27, while some authors found an improvement in the compressive and flexural strengths with the addition of GNPs, some found a reduction. Hence the reduction in strength that was observed here, was not surprising and is consistent with relevant literature. The strength improvements were attributed to an improved hydration and microstructure with GNP addition and none of these properties improved with GNPs in this study. On the contrary, cement hydration slightly reduced with GNPs, which could partially explain the strength reduction. During compressive loading, GNPs could be acting as weak points within the cement hydration products, where fracture paths could be initiated and therefore, reducing the compressive strength and resulting in a more brittle failure.



(a)



(b)

Figure 5-10: The strength performance of the CEMI and CEMII pastes with 0.3wt% GNP at 2, 7 and 28 days in terms of (a) compressive strength and (b) flexural strength.

The hardness and Young's modulus of the samples were also determined by micro-indentation testing and the results are illustrated in Figure 5-11. For the control samples, both the hardness and Young's modulus increased as hydration progressed. However, the change was minimal from 7 to 28 days for the CEMII control. The hardness was lower with CEMII, reaching a 60% reduction compared to CEMI at 2 days. This was expected as the CEMII mixes were of lower strength compared to CEMI. Due to a problem with the samples, the 28-day test of CEMI + 0.3wt%GNP and the 2-day test of CEMII +0.3wt% GNP were not carried out. For the CEMI mixes with 0.3% GNP, the hardness increased by 4% and 25% at 2 and 7 days. The effect at 2 days was insignificant, however the effect at 7 days could be due to two reasons; firstly, GNP particles could be stronger than cement hydration products and secondly, due to a possible reduction in porosity, the overall hardness of the composite increased. For CEMII, a small change was observed at 7 days, whilst the hardness increased by 21% at 28 days with 0.3wt% GNPs.

Overall, the hardness results are not in agreement with the compressive strength and whilst a reduction in compressive strength was found with GNPs, the hardness was either maintained or slightly improved. This could be due to local and global effects. Hardness (by micro-indentation) is usually measured for more homogeneous materials, such as plain cement paste and steel, whilst for composite materials the local effects could play a role. For example, the local effect of stronger GNP particles would translate in higher hardness measurements. The porosity reduction with GNPs that acted as nano-fillers, also affected the micro-hardness measurements. However, at a global level (compressive strength results), there was an interfacial transition zone between GNPs and cement paste which created areas of weakness and resulted in a lower compressive strength.

The use of CEMII reduced the Young's modulus by 19%, 27% and 38% at 2, 7 and 28 days compared to the CEMI. CEMII mixes were less stiff and more flexible, which agrees with the flexural strength results. This finding was expected for lower strength cements that usually result in higher porosity due to smaller hydration products that occupy less volume. Adding 0.3wt% GNPs had a negligible effect on the Young's modulus for the CEMI mortars. However, a small reduction was found for CEMII at 7 days, with no effect at 28 days. Micro-indentation testing has not been common in the literature and therefore, it is difficult to directly compare the results from this study. Liu et al. (2019) also found that micro-hardness increased by ~9% with the addition of 0.05wt% GNPs and agrees with the findings here.

Nonetheless, further research is needed to understand the hardness and elasticity behaviour of GNPs when incorporated in a cement matrix.

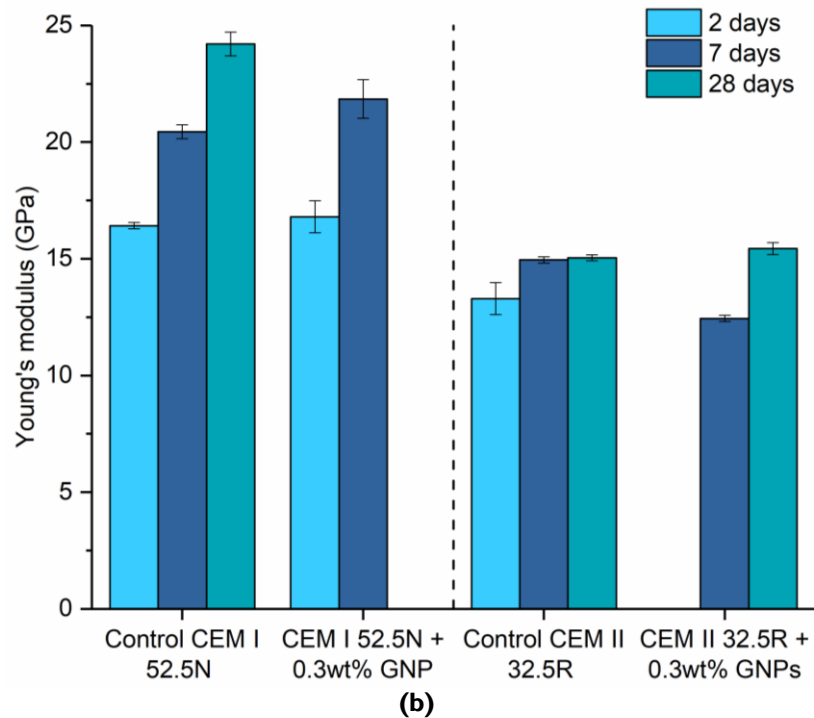
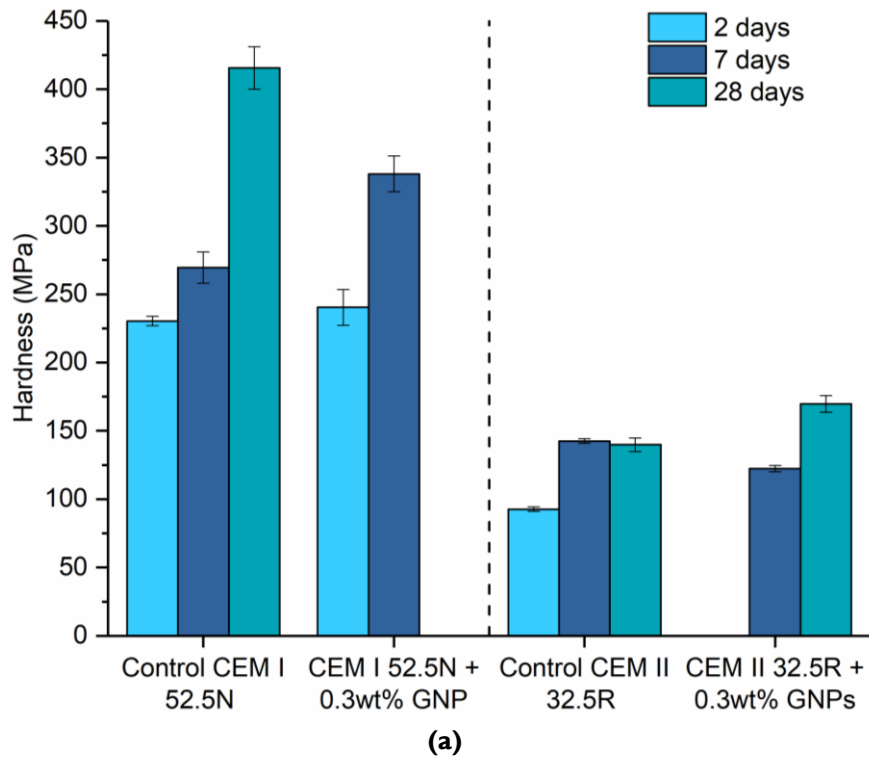


Figure 5-11: Effect of GNP addition on the hardness (a) and Young's modulus (b) of CEMI and CEMII pastes at 2, 7 and 28 days.

Micro-indentation was employed here to assess the homogeneity of GNP dispersion by observing the error range in the micro-hardness measurements for each sample, where a higher error indicated a higher degree of inhomogeneity. Fifteen measurements were carried out for each sample and some clear outliers were removed as they could have been due to the Vicker’s tip hitting a pore or unhydrated cement, although a minimum of 10 measurements were kept for each sample. From Table 5.3, the CEMII controls had a lower error than CEMI samples, which was expected due to the more brittle nature of high strength cements. When GNPs were added, a very small increase in error was found, with the effect being more pronounced in CEMI mixes. This means that GNPs induced a certain degree of inhomogeneity in the cement paste, as it would have been expected for any additive. However, the standard error remained small and comparable to the controls, and therefore it can be deduced that GNPs were homogeneously dispersed in the cement paste since no large variances in the measurements were observed.

Table 5.3: Standard error of micro-hardness measurements as a way of GNP dispersion assessment

Sample	St Error (MPa)
Control CEM I 52.5N - 2d	3.43
Control CEM I 52.5N - 7d	11.44
Control CEM I 52.5N - 28d	15.50
CEM I 52.5N + 0.3wt% GNP - 2d	13.10
CEM I 52.5N + 0.3wt% GNP – 7d	13.02
Control CEM II 32.5R - 2d	1.73
Control CEM II 32.5R - 7d	1.66
Control CEM II 32.5R - 28d	5.04
CEM II 32.5R + 0.3wt% GNP – 7 d	2.35
CEM II 32.5R + 0.3wt% GNP – 28 d	6.12

5.2. GNPs in CEMI mortars

This section presents the effect of GNPs on the early age properties, mechanical and durability performance of CEMI mortars by varying the GNP dosage. The GNP dosage range was selected based on the literature and ranged from 0.05% to 0.5% by weight of cement (therefore including the 0.3wt% dosage that was tested for cement pastes). The dispersion protocol developed in Chapter 4 was used throughout this section and mortar mixing was detailed in Section 3.2.2.

5.2.1. Fluidity of mortars with GNPs

The fluidity of mortars was tested with a mini-slump test and three repeat measurements were carried out for each GNP concentration. All samples had a w/c of 0.45 and the same amount of MasterGlenium, whilst the results show the average of 3 tests. Figure 5-12 shows that the fluidity reduced with increasing GNP concentration, and at 0.5wt% GNP it was less than half compared to the control. Mixing higher GNP concentrations would not be possible without increasing the w/c or the superplasticiser content. These findings were expected since GNPs have a high surface area and also promote a better packing density, which causes inter-particle friction and reduces the free water, in turn, reducing the overall fluidity. Jing *et al.* (2017) used more exfoliated GNPs (diameter <6 µm and <5 nm thickness) but slightly different dosages and found that the mini-slump values reduced significantly with GNP addition. Their control mix had a similar flow value to this study (~230 mm), which reduced by 17.4% for 0.2wt% GNPs and by ~39% with 0.4wt% GNPs. Ho *et al.* (2020) used GNPs of similar size but smaller thickness (average size = 56 µm, thickness = 1-3 nm) and found that 0.3wt% GNPs reduced the fluidity by ~18%, which is smaller compared to this study where it was reduced by ~34%. A study by Chougan *et al.* (2019) who used the same GNP product found that 0.1wt% GNPs reduced the viscosity of mortars by ~49% which is more dramatic compared to the 15% reduction found here for the same concentration. Therefore, the effect on fluidity is not only influenced by the different GNP properties. The differences could also be attributed to the different mixing methods employed, the measurement technique and the properties of the other constituents such as the cement and sand used. Nonetheless, GNPs reduced the fluidity of the cement mortars, with the effects becoming pronounced after 0.3wt% concentration. Hence, this is a practical limitation when using GNPs in mortars and the mixing method should be adjusted to ensure that sufficient fluidity is maintained if higher dosages are to be used.

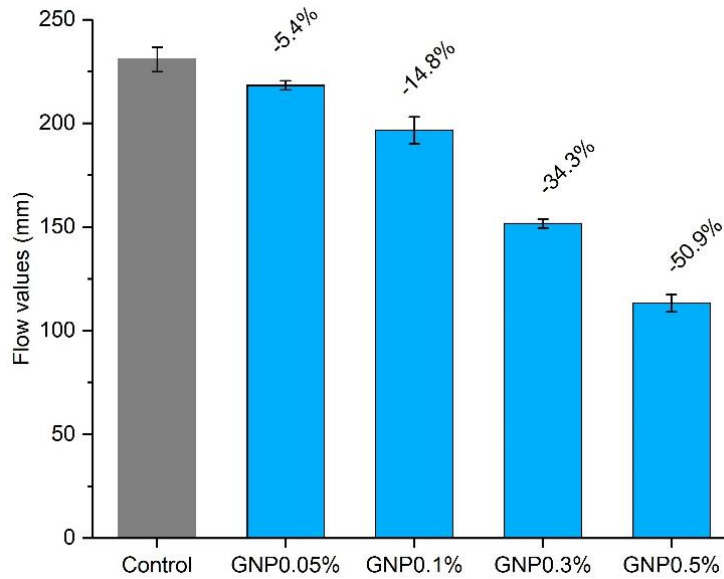


Figure 5-12: Fluidity of CEMI mortars with GNP addition as measured by a mini-slump test

5.2.2. Effect on hydration

The effect of GNPs on the hydration of CEMI mortars was investigated using TGA and XRD testing. Earlier tests on cement pastes showed that hydration was only slightly impacted by 0.3wt% GNPs at 2 days whilst no effect was observed at 28 days, and the cement hydration products remained the same. TGA results in Figure 5-13 show a more pronounced effect at 2 days compared to 28 days. At 2 days, the control mix lost more weight compared to the GNP samples, and an increasing GNP dosage led to a reduction of weight loss, indicating a delay in the hydration process. It should be noted that a test with the 0.05wt% GNP sample was not possible due to a problem with the sample. Nonetheless, there is a clear trend that increasing GNP dosage led to a reduction in weight loss and therefore reduced the hydration rate. At 28 days the effect was less clear, and all the curves were almost identical, therefore GNP addition did not affect the long-term hydration, which agrees with the findings from the cement paste tests presented earlier. The DTG curves at both 2 and 28 days looked almost identical, irrespective of GNP concentration. Hence, no new phases were created with GNP addition in the mix. The slight retardation observed with GNPs at 2 days can be attributed to GNPs high specific surface area that needs more water to hydrate and therefore, reduces the free water available for cement hydration. As the cement

hydration progresses, the GNPs are admixed and the water is slowly released and used again for cement hydration, therefore, no long-term impact is observed.

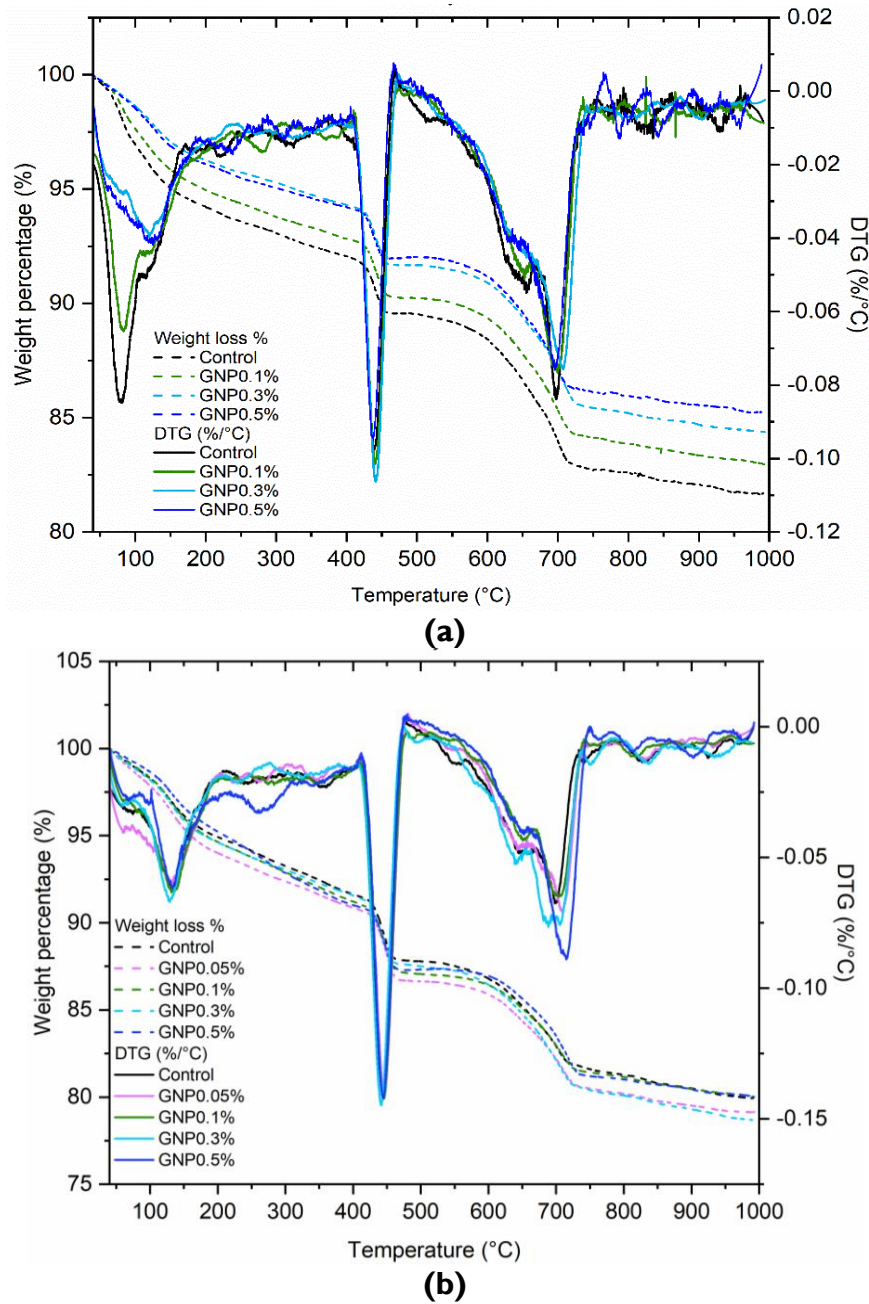


Figure 5-13: TGA/DTG curves of CEMI mortars with varying GNP contents at (a) 2 days and (b) 28 days.

The non-evaporable water loss (105°C - 400°C) and the LOI (105°C - 1000°C) from the TGA data are illustrated in Figure 5-14. At 2 days, the increasing GNP dosage resulted in a slight decrease in the non-evaporable water loss (light blue bars) with the decrease being

~10% for GNP0.3% and GNP0.5%. The LOI also showed a decreasing trend with increasing GNP dosage indicating that GNP samples lost less weight and therefore, hydrated less compared to the control. However, at 28 days, the non-evaporable water loss and LOI showed some contradicting results. The change in LOI compared to the control is insignificant (<2% variance) with the exemption of 0.3wt% GNP where a 6% increase was observed. Instead, the non-evaporable water loss showed a slight increase with GNP addition (again, with the exemption of the 0.3wt% sample), meaning that a slight acceleration was observed at 28 days with GNP addition. As explained earlier, some of the water that would otherwise be used for cement hydration, was used to wet the surface of GNPs at 2 days and as hydration progressed, this water was slowly released back in the mix. Therefore, the slight increase in the non-evaporable water loss in the GNP samples at 28 days could be due to the delayed hydration and water release that hydrated the cement at a later age than normal.

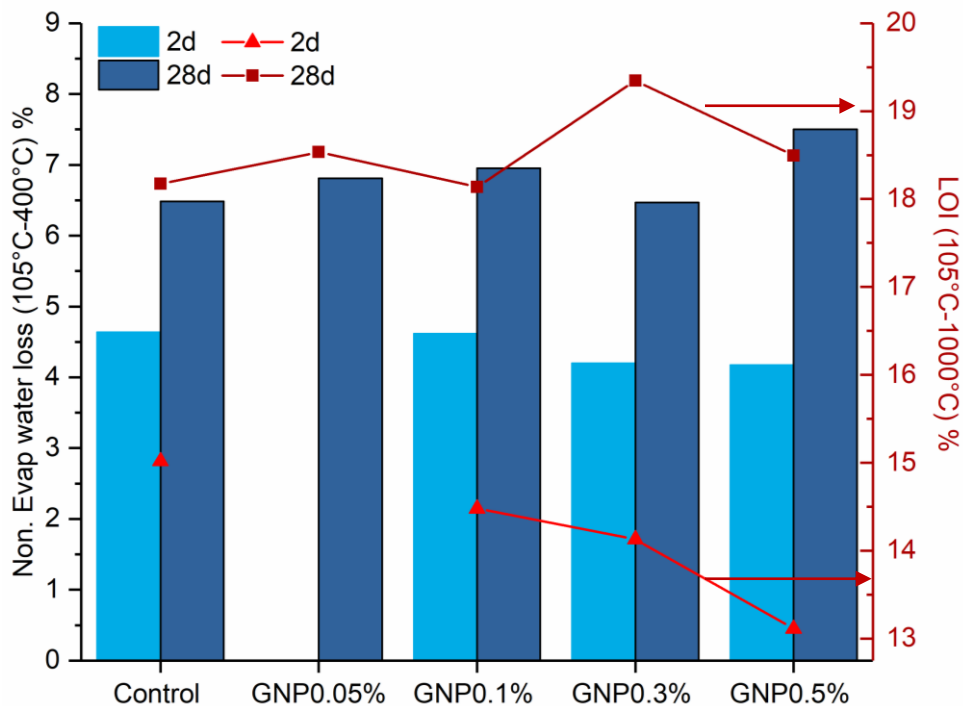
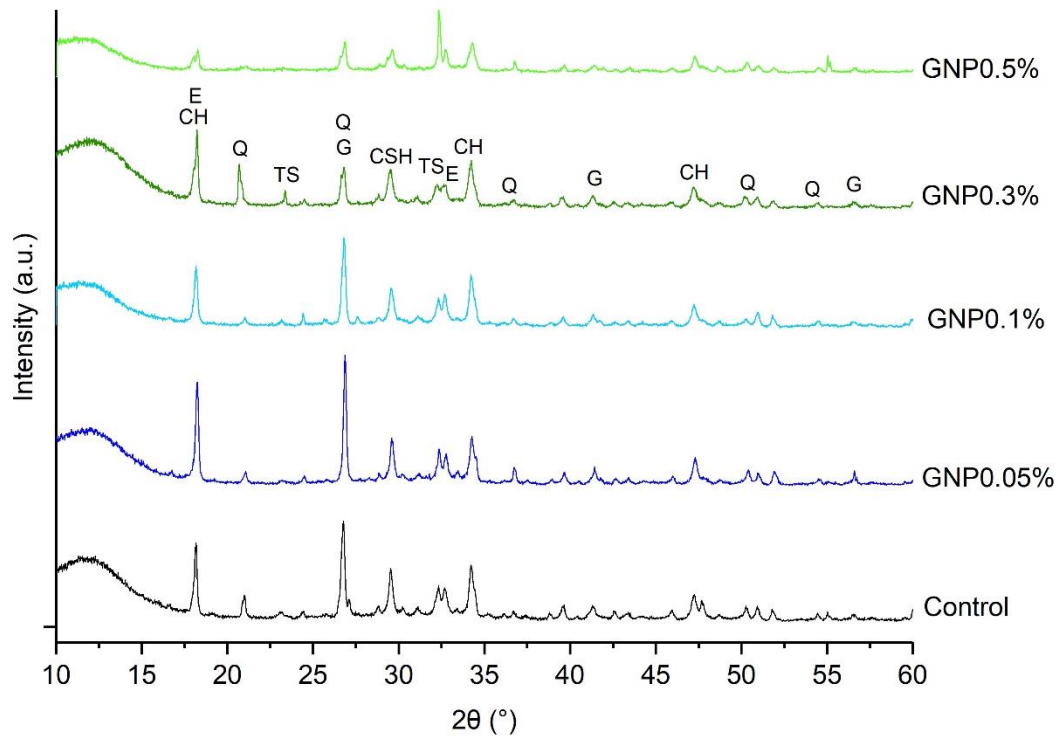


Figure 5-14: Non-evaporable water loss and loss on ignition (LOI) weight for CEMI mortars with varying GNP dosages at 2 and 28 days

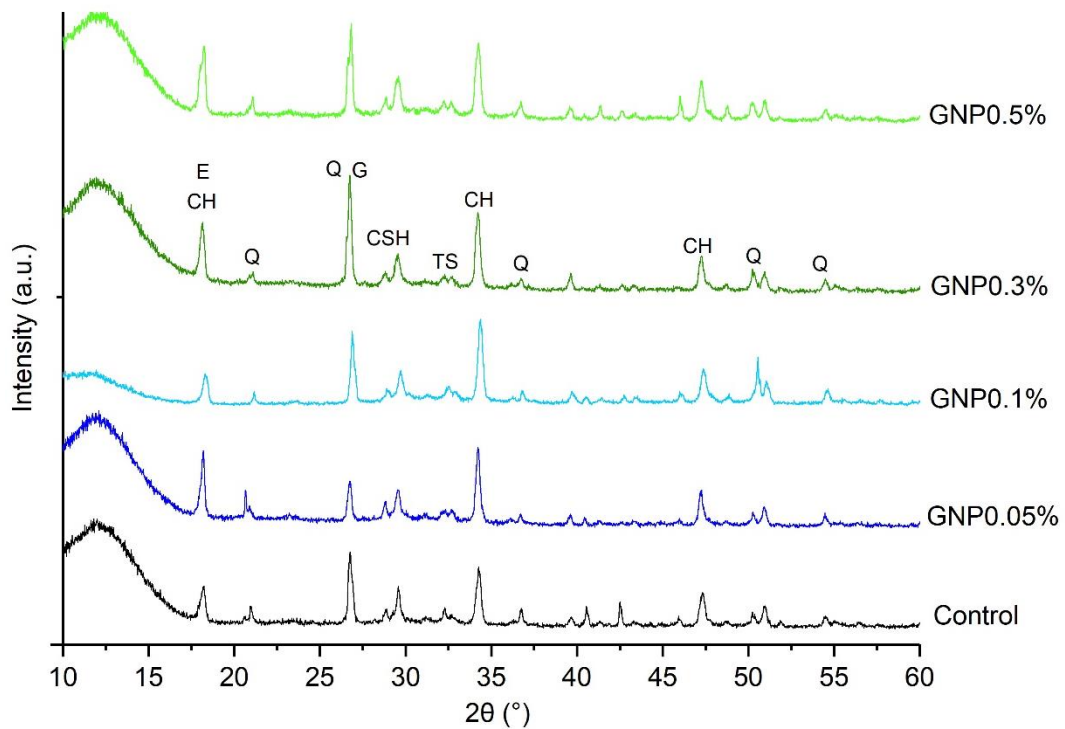
XRD testing was used as a complementary to TGA analysis and the results are shown in Figure 5-15. GNP addition did not result in any new mineral phases in the mix as all curves

look very similar. However, the intensity of some peaks was depressed, especially for higher GNP concentrations at GNP0.3% and GNP0.5%. The typical cement hydration peaks were found in all samples at both 2 and 28 days. At 2 days (Figure 5-15 (a)), portlandite (CH) peaks were found at $2\theta = 18.2^\circ$, 34.2° and 47.2° , and were clearly depressed for 0.5wt% GNP which is an indication that hydration was delayed at that GNP dosage. Ettringite was found at $2\theta = 18^\circ$, 42° and C-S-H at $2\theta = 29.5^\circ$ which can also be attributed to calcite from the carbonation of calcium hydroxide. Residual tricalcium silicate (C_3S) was found at $2\theta = 23.1^\circ$, 32.3° , 51.8° . A strong peak at $\sim 2\theta = 26^\circ$ can be seen which could be due to the presence of carbon (due to GNPs), as the typical graphitic peak is found at $\sim 26.7^\circ$. However, quartz also has a peak at almost the same location, so it is difficult to distinguish between quartz or graphite there. Other typical graphitic peaks were also observed at $2\theta = 42.6^\circ$ and 57.6° . A strong characteristic peak of quartz (Q) at 21.0° was found for all samples but the intensity varied based on the amount of sand present in each sample. It should be noted that all samples were ground and sieved before XRD testing so large sand particles were removed from the specimens. Further quartz peaks of smaller intensities can be seen at $2\theta = 36.7^\circ$, 39.6° , 50.3° , 55.06° . Overall, at 2 days, no new phases were created and the peak intensities remained largely unchanged for the low concentrations of GNPs (0.05wt% and 0.1wt%) whilst a slightly reduced intensity was found for 0.3wt% and 0.5wt% GNPs. Thus, the higher GNP dosages reduced the hydration rate, which agrees with the TGA results.

Similar observations can be made for the samples at 28 days (Figure 5-15 (b)). Much stronger peaks were found compared to 2 days, due to the progress of hydration. Strong peaks can also be seen for the GNP0.5% sample, meaning that the high content of GNPs did not affect the long-term hydration. As for 2 days, the mineral peaks for portlandite (CH), ettringite (E), C-S-H, tricalcium silicate (TS), quartz (Q), and graphite (G) were found. No new phases were noticed with GNP addition and the peak intensities were similar, indicating that at 28 days, GNPs had a negligible effect on hydration which agrees with the TGA findings.



(a)



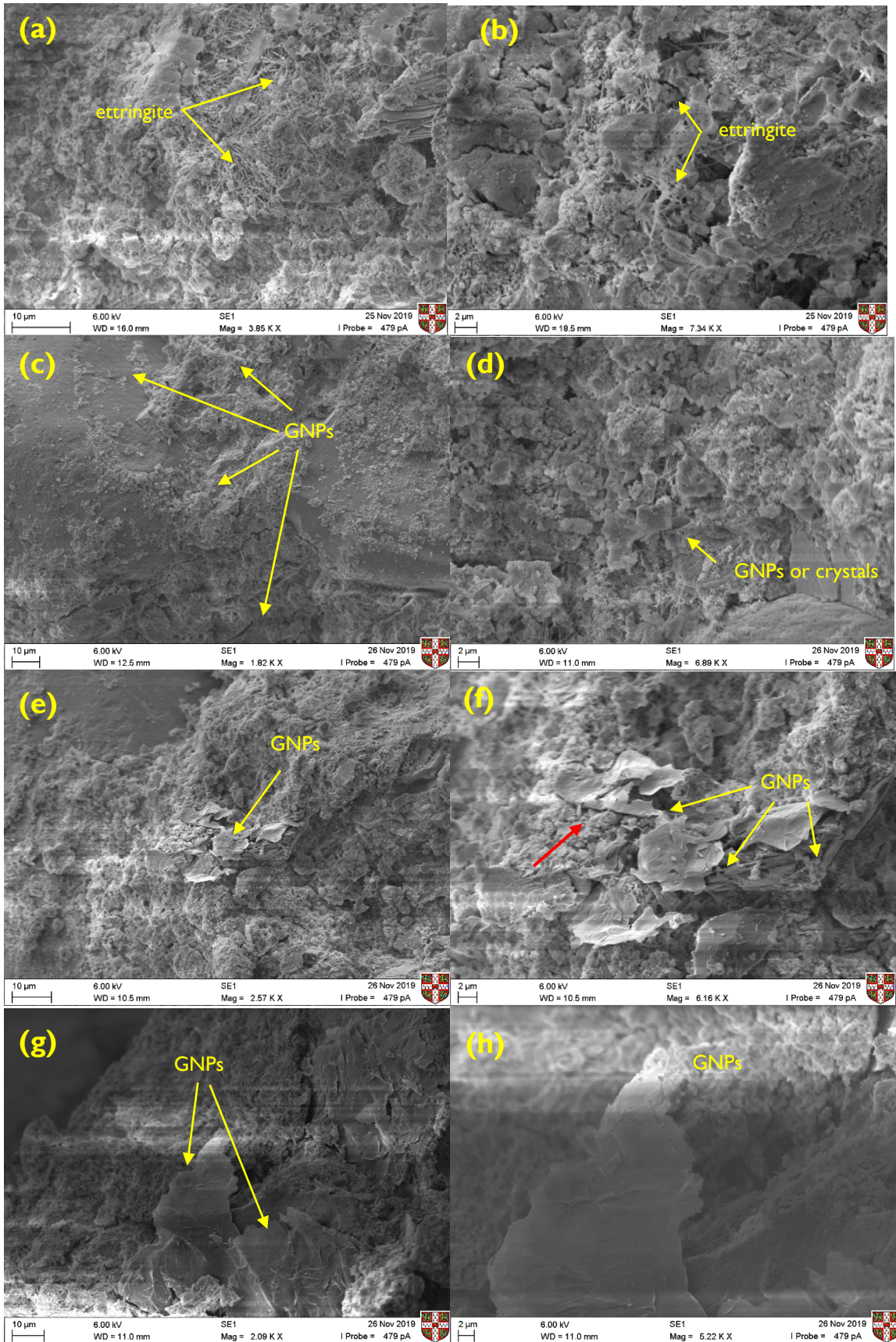
(b)

Figure 5-15: XRD spectra of CEMI mortars with varying GNP concentrations at (a) 2 days and (b) 28 days (CH – portlandite, E – ettringite, C – calcite, CSH – C-S-H, TS is C3S, G – graphite, Q - quartz)

The above hydration results are similar to the findings for when GNP was added in cement paste (Section 5.1.2). The GNP addition, irrespective of dosage, did not result in any new hydration phases. However, increasing GNP dosage depressed the hydration peaks at 2 days, resulting in a slight delay of the hydration degree. At 28 days, no such effect was seen, meaning that there is no long-term impact of GNPs on the hydration performance of cement composites.

5.2.3. Effect on microstructure

The microstructure of the mortars containing GNPs was investigated by SEM-EDX testing at 2 and 28 days. Two representative images are shown below for each concentration, one at 10 μm (left) and one at 2 μm (right). The SEM results for 2 days are shown in Figure 5-16, however, due to a problem with the machine during gold coating, the images at 2 days are not very clear. For this reason, EDX was not carried out on these samples. For the control mix (Figure 5-16(a-b)), ettringite crystals and pores were seen because the hydration was still at an early stage and therefore, high porosity and a loose hydration structure was expected. A similarly loosely compacted structure was observed with 0.05wt% GNP (Figure 5-16(c-d)), but, it was difficult to identify individual GNPs. As the GNP content increased further, GNPs were present in all samples. For 0.1wt% GNPs (Figure 5-16(e-f)), a small cluster of GNPs was found, however, it is not clear if this is an agglomerate of many particles or one GNP particle that was broken in smaller pieces. Given that the size of each GNP is $\sim 30 \mu\text{m}$ and the GNPs in this figure appeared to be less than $30 \mu\text{m}$, the latter theory is supported. At higher concentrations of 0.3wt% (Figure 5-16(g-h)), and 0.5wt% GNPs (Figure 5-16(i-j)), some aggregation of the flakes was present. It can be deduced that these are agglomerates rather than individual broken flakes, due to the very large size of the particles that are near each other. The flakes were not well integrated in the cement hydration products due to difficulties in mixing these high concentrations. In some cases, GNPs also created a slipping plane of weakness which could explain the reduction in compressive strength. This is clear in Figure 5-16(f and j) and it is illustrated by red arrows, where the GNP flakes were not integrated with the cement hydration products.



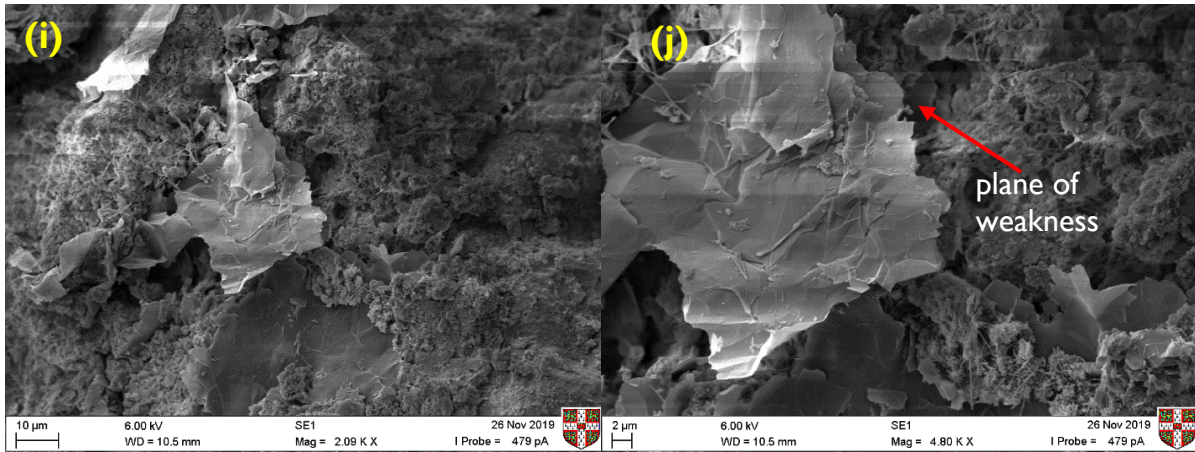
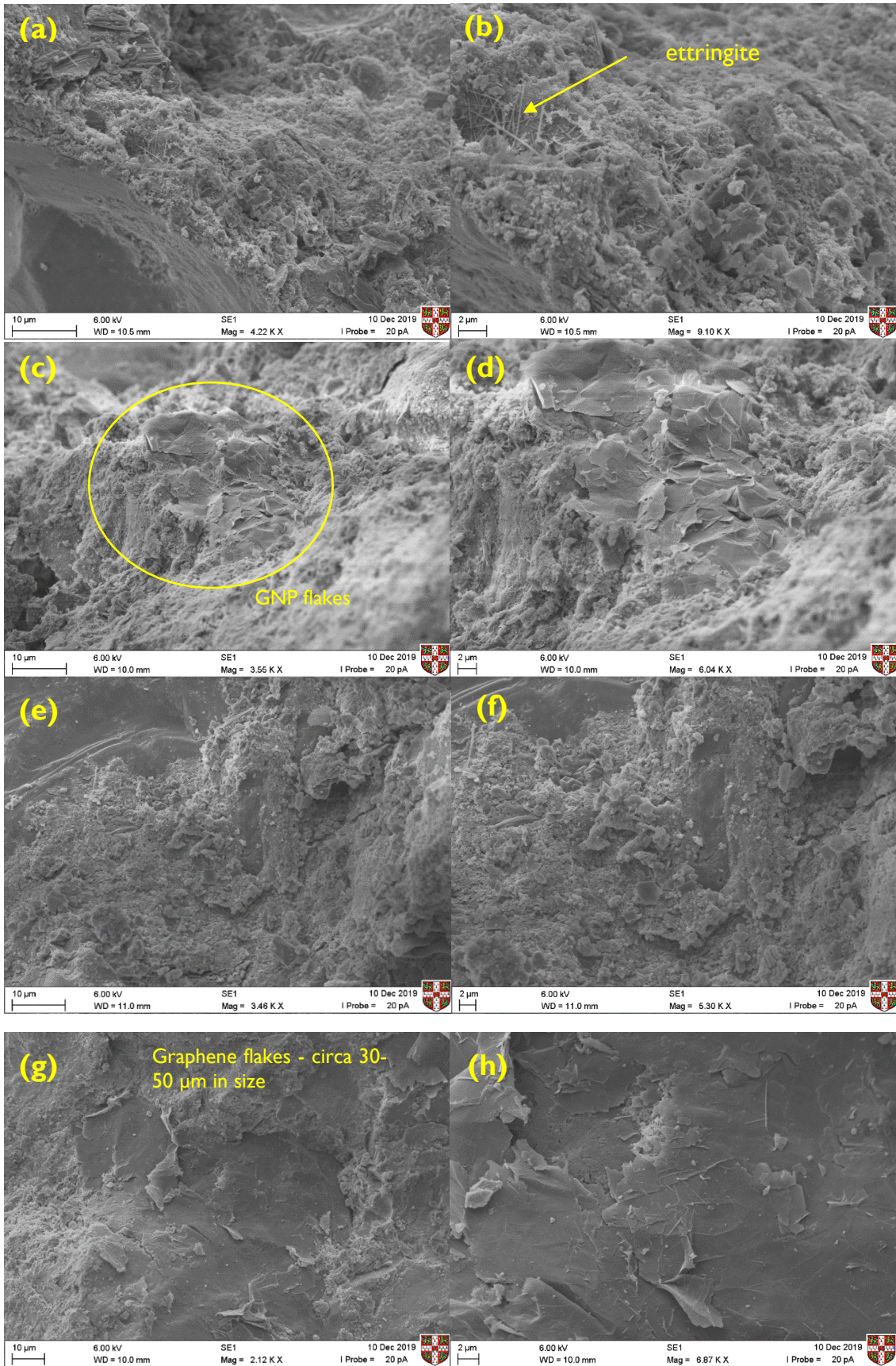


Figure 5-16: SEM of CEMI mortars at 2 days (a-b) control (c-d) 0.05wt% GNP (e-f) 0.1wt% GNP (g-h) 0.3wt% GNP (i-j) 0.5wt% GNP

The SEM images at 28 days are illustrated in Figure 5-17. Overall, typical cement hydration products such as needle-shaped ettringite, hexagonal portlandite crystals and layered and rhombohedral calcite can be observed in all images. A more compact structure with less pores was found in the control samples (Figure 5-17(a-b)) compared to 2 days. However, some ettringite crystals were still present, meaning that the cement hydration was still ongoing. GNPs could be found in the 0.05wt% GNP sample and are shown with a yellow circle in Figure 5-17(c), characterised by a wrinkled and folded morphology. Each GNP was $\sim 30\mu\text{m}$ in size therefore, this could be a small cluster of 1-2 GNPs rather than just one flake. For the 0.1wt% GNP sample, it was difficult to isolate individual GNPs, however, a very compact structure was observed, similar to the control. As the GNP content increased further to 0.3% and 0.5%, the GNP flakes could be seen clearly. The GNPs (Figure 5-17 (g-j)), were better integrated with the cement hydration products compared to the samples at 2 days. Overall, the GNP addition was not found to affect the morphology of the microstructure.



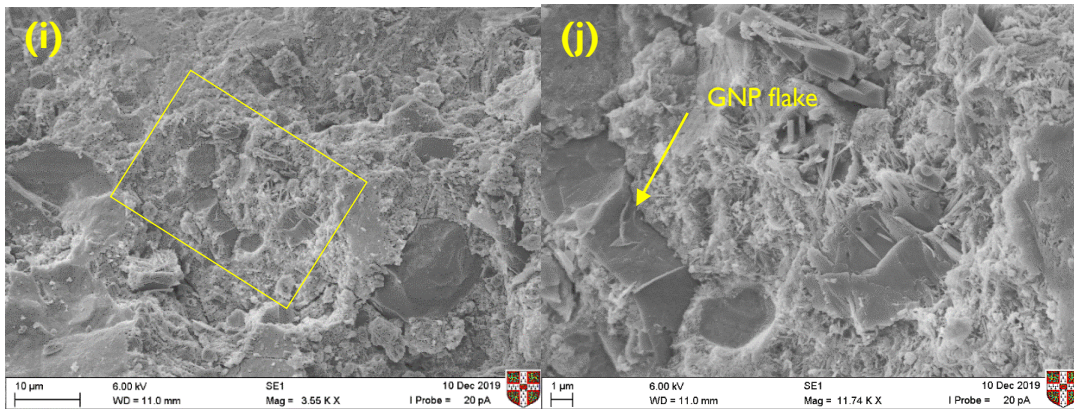


Figure 5-17: SEM of CEMI mortars at 28 days (a-b) control (c-d) 0.05wt% GNP (e-f) 0.1wt% GNP (g-h) 0.3wt% GNP (i-j) 0.5wt% GNP

The 28 day EDX analysis results are shown in Figure 5-18, with the elemental sample composition summarised in Table 5.4. In all cases, oxygen is the main element present in the samples, followed by calcium and silicon. These elements were expected due to the cement hydration products and the presence of sand in the mortars. As GNPs were introduced in the mix, carbon was also present. No carbon was seen in the 0.05% GNP sample which could be due to the small GNP dosage. However, as the GNP dosage increased to 0.1%, carbon became one of the main elements and represented around 12% - 16% of the total weight of all elements. However, the presence of carbon could also be attributed to the superplasticiser, so it was not purely due to GNPs. This elemental composition is expected to vary slightly between different locations in the samples.

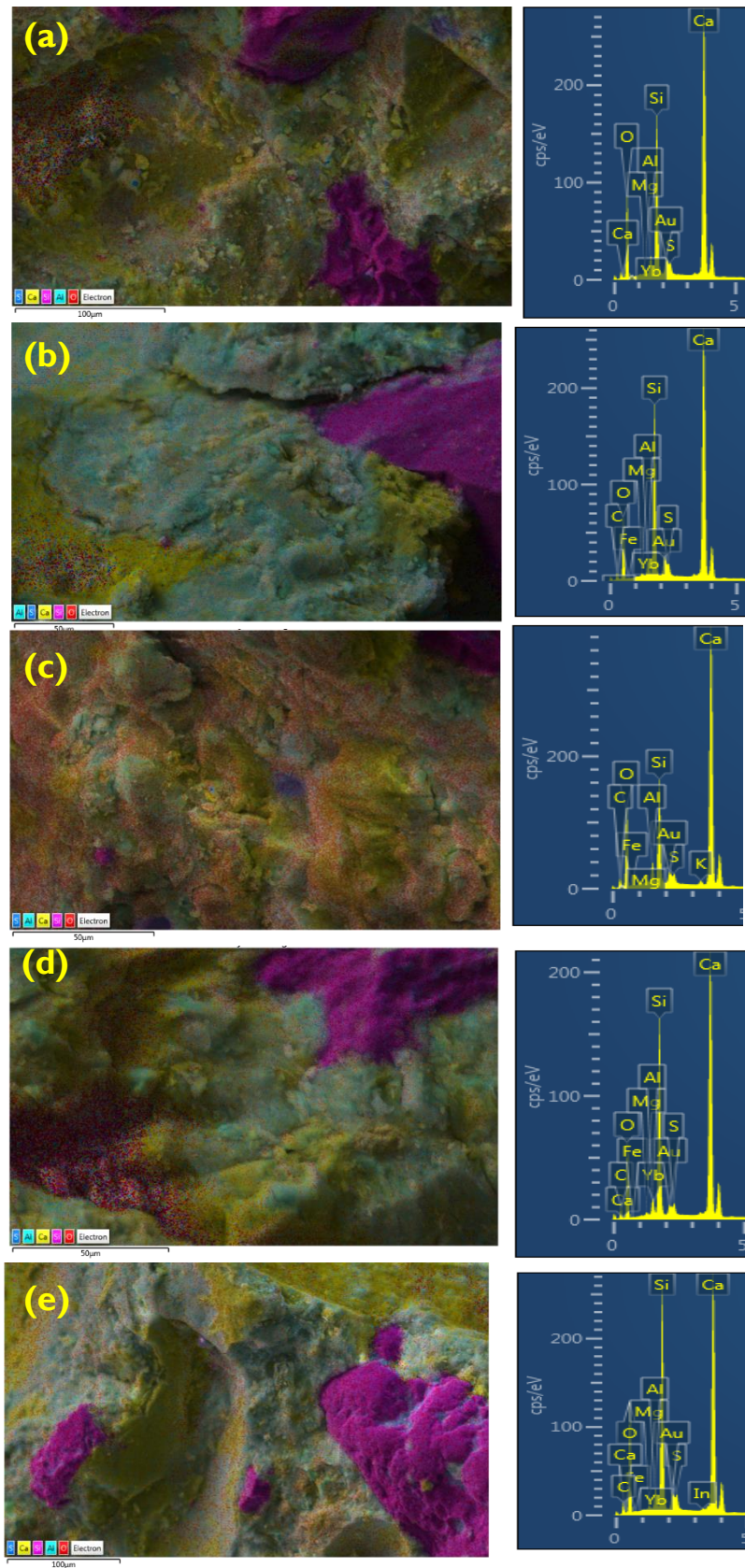


Figure 5-18: EDX of CEMI mortars at 28 days (a) control (b) 0.05wt% GNP (c) 0.1wt% GNP (d) 0.3wt% GNP (e) 0.5wt% GNP

Table 5.4: EDX of CEMI mortars at 28 days showing the different elements

Element	Weight %				
	Control	GNP0.05%	GNP0.1%	GNP0.3%	GNP0.5%
O	65.7	47.28	61.04	55.18	60.84
Al	1.22	1.49	1.27	0.85	0.93
Si	9.08	13.05	5.14	8.62	8.67
Ca	21.14	28.12	18.02	16.64	13.20
Au**	-	6.21	-	-	-
C	-	-	12.61	16.29	14.02
Yb	0.86	1.08	-	0.72	0.50
S	0.78	1.11	0.59	0.63	0.72
Fe	0.92	1.29	0.68	0.85	0.61
Mg	0.31	0.38	0.38	0.23	0.24
Other	-	-	K = 0.28	-	In = 0.25
Total	100.00	100.00	100.00	100.00	100.00

** The samples were gold coated and therefore Au should have been added as a baseline. This was an error when collecting the EDX images.

These results are not directly comparable to the literature due to the different dispersion methods, cement mixes and GNPs used by other researchers. Rather the microstructural results were used to inform the findings of the remaining experimental work carried out in this thesis. In summary, SEM-EDX showed that GNPs could form planes of weakness with the cement hydration products, especially at 2 days. This could subsequently lead to a reduction in the mechanical properties. No obvious refinement in microstructure with GNPs was found, and the microstructures of all samples appeared similar at 2 and 28 days. The 28-day samples had a more compact microstructure compared to 2 days which can be attributed to the progress of hydration.

5.2.4. Effect on mechanical properties

The effect of GNPs on the mechanical properties of CEMI mortars was examined using compressive and flexural strength testing. From earlier tests on pastes, Section 5.1.4, an overall reduction in compressive strength is expected, with similar results for flexural strength. Compressive strength results are shown in Figure 5-19 and six specimens were tested for each concentration. The 28-day strength was almost double the 2-day strength in all cases, which was due to the ongoing hydration of cement. Irrespective of the curing age,

the higher GNP dosages caused a noticeable reduction in compressive strength. A reduction of less than 10% was observed for GNP 0.05% and 0.1% contents, however this increased to over 20% for both 0.3% and 0.5% GNP at all curing ages. Especially, 0.5wt% GNP reduced the 28-day strength from 59.4MPa to 43.3 MPa.

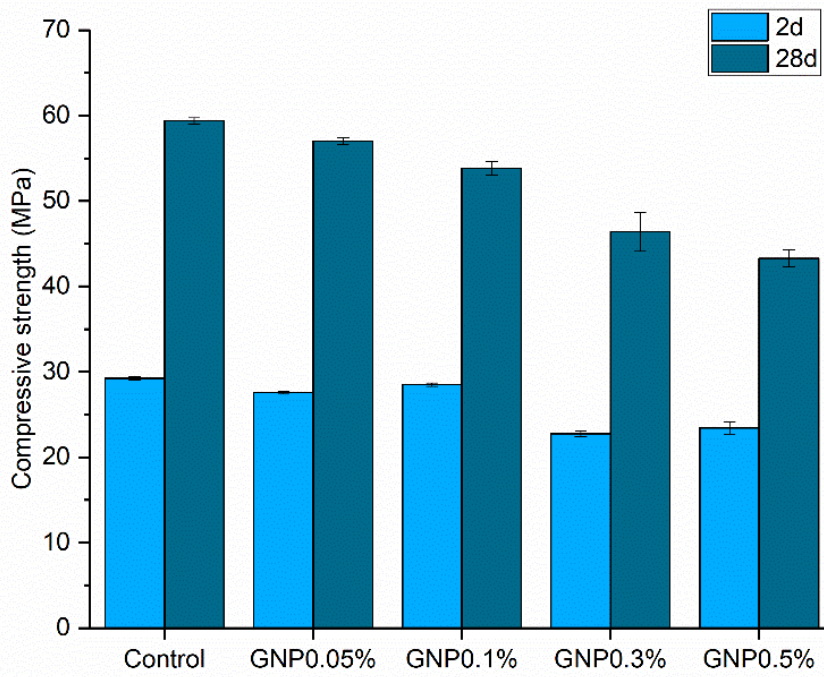


Figure 5-19: Compressive strength of CEMI mortars with varying GNP contents at 2 and 28 days

Flexural strength testing (3-point bending) was carried out to understand the effect of the varying GNP concentration and triplicate testing was carried out. Figure 5-20 illustrates the flexural strength results for 2 and 28 days. As expected, the 28-day strength was higher than then 2-day strength for all mixes as the cement hydration had progressed. However, a reduction in strength with GNP addition was found at both test ages which was more pronounced at 2 days. For 2 days, the flexural strength was slightly reduced for 0.05% GNP addition, however, it reduced by 10.8% for 0.1% GNP and by ~20% when GNP content increased to 0.3% and 0.5%. A lesser effect was observed at 28 days, with 0.05% GNP and 0.1% GNP having an insignificant effect, whilst 0.3% GNP and 0.5% GNP reducing the flexural strength by ~5% and ~9% respectively. Overall, the error bars were small, indicating that the GNPs were equally present in the different specimens.

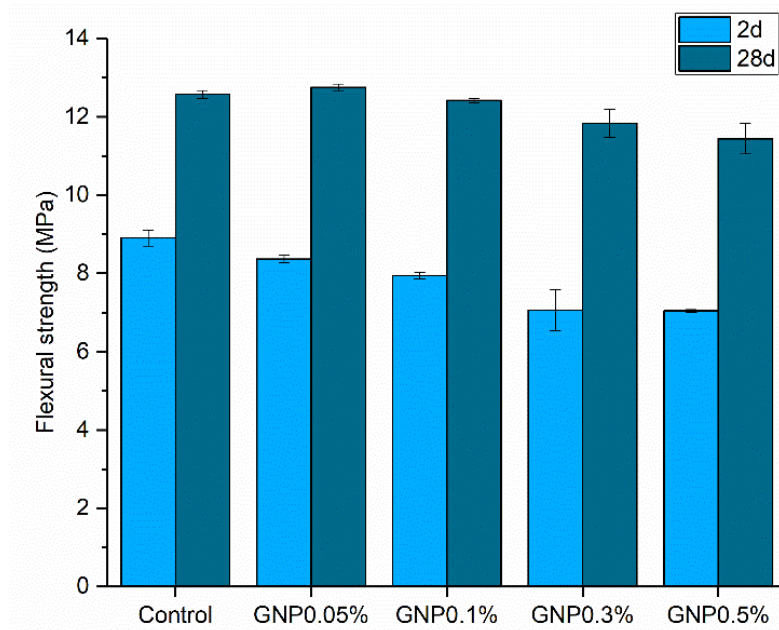


Figure 5-20: Flexural strength of CEM I mortars with varying GNP contents at 2 and 28 days

Due to a malfunction of the device, the load-displacement curves could not be directly exported. Instead, photos of the plots were taken and then processed with a data collection software, GetData – GraphDigitiser, so all the data points had to be processed manually which could inherently lead to some errors in the results presented in Figure 5-21. Furthermore, the Young's modulus was calculated from the gradient of curve within the elastic range of response and the results are shown in Table 5.5. From the results, it can be observed that at 2 days, the GNPs addition led to a reduction of the flexural stiffness. The same finding was observed in Section 5.1.4, where micro-indentation testing showed a reduction in Young's modulus with CEMII whilst the 0.3wt% GNP addition showed a negligible effect. At 28 days, the trend is not as clear, with low GNP dosages (up to 0.1wt%) making the material stiffer however, this behaviour reversed with the GNP dosage increased to 0.3wt% and 0.5wt%. Due to the inherent errors in the data collection and processing though, this trend cannot be confirmed with confidence and further testing would be needed in future work to understand the effects of GNPs on the flexural and tensile behaviour of mortars.

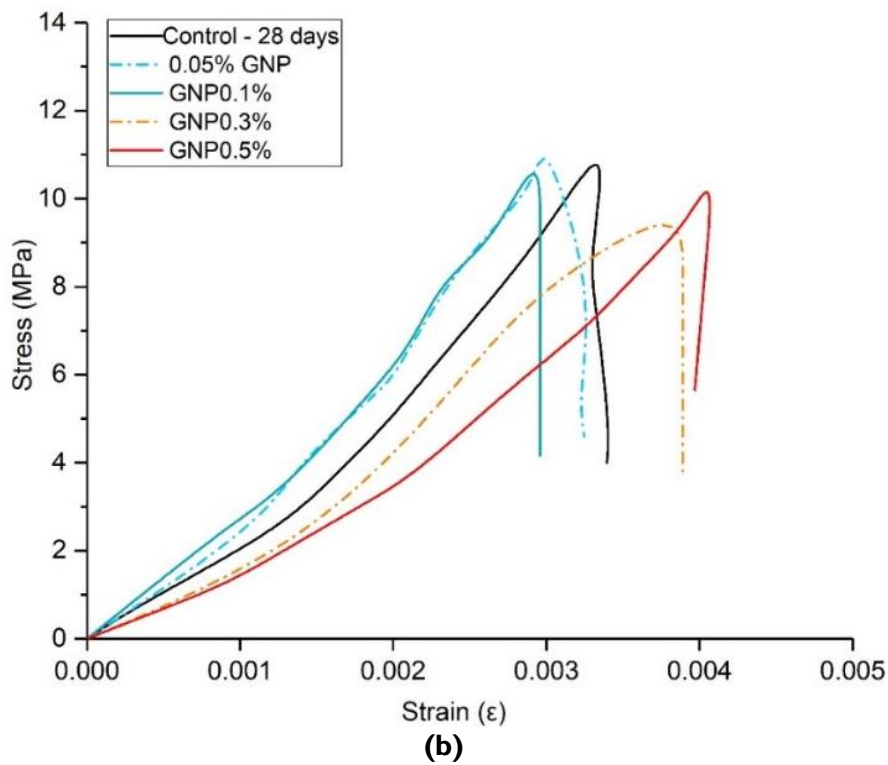
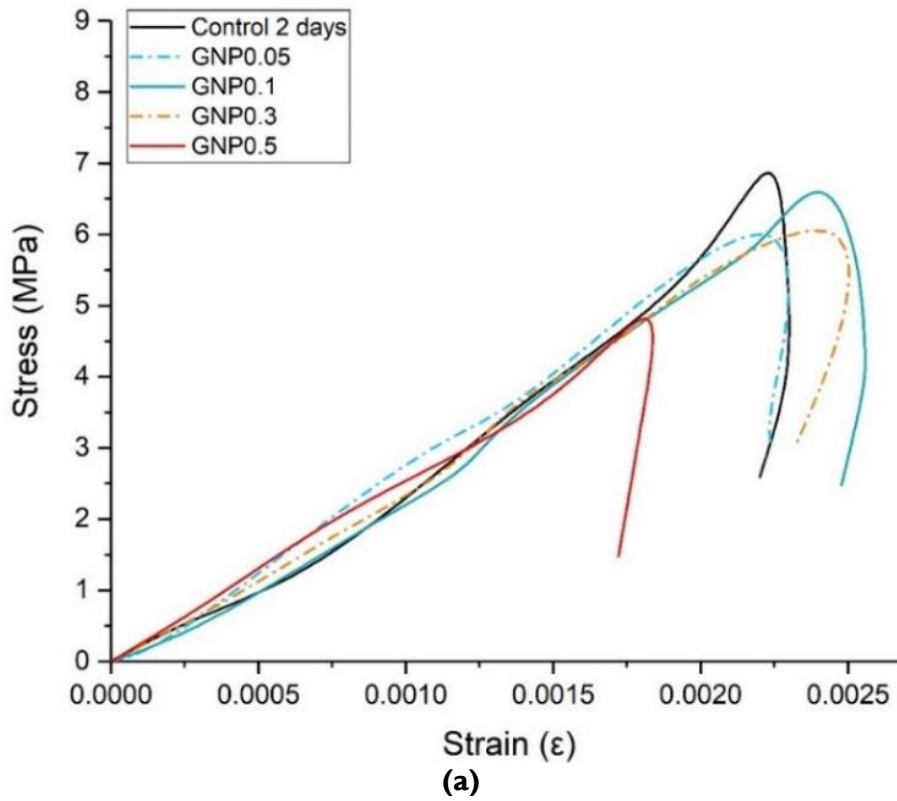


Figure 5-21: Stress-strain curves of CEMI mortars with varying GNP contents at (a) 2 days and (b) 28 days

Table 5.5: Flexural stiffness of CEMI mortars with varying GNP contents calculated from the stress-strain curves

GNP (wt%)	Flexural stiffness (GPa) – 2 days	% change	Flexural stiffness (GPa) – 28 days	% change
0	3.3395	0%	3.318	0%
0.05	2.9491	-12%	3.888	17%
0.1	2.8737	-14%	3.632	9%
0.3	2.6859	-20%	2.716	-18%
0.5	2.4022	-28%	2.583	-22%

In comparison to the *i-lab* results presented in Section 4.5.3, the difference in strength here is greater for 0.3wt% GNP. This could be due to many factors; including different surfactant and sonication treatment, difference in fine aggregate and differences in cement which could affect porosity and compatibility with the admixture and GNP. Nonetheless, in all cases, a reduction in the mechanical properties was observed with GNP addition. Small GNP contents (GNP0.05% and GNP0.1%) had an insignificant effect on flexural strength and a very small impact on compressive strength. These results also agree with the tests with GNPs in cement pastes presented in Figure 5-10, where GNPs reduced the compressive strength of CEMI paste by ~25%. As discussed in Section 5.1.4, the strength reduction can be explained due to the weak bonding of GNPs with cement hydration products. GNPs act as fillers and create planes of weakness between the compact hydration microstructure and their flakes, which result in a reduction in the compressive strength of the mortar.

5.2.5. Effect on permeability

The effect of GNPs on the permeability of cement mortars was investigated as an indicator for durability. GNPs could act as barriers to gases and refine the porosity and hence reducing the permeability to water, gases, and chlorides. Water sorptivity tests, gas permeability and rapid chloride penetration tests were carried out at 2 and 28 days.

5.2.5.1. Water sorptivity

Water sorptivity by capillary action was measured for duplicate specimens at 2 and 28 days. The water sorptivity of cementitious composites can be characterised by two distinct phases. The initial phase, which is a linear regression of the first 6 hours that the specimen is exposed to water, indicates how quickly the water fills the large pores. The secondary rate

of absorption, which is measured from 6 hours to 9 days of exposure, shows how quickly the water fills the air voids and smaller pores in the sample. Figure 5-22 illustrates the overall and initial rates of absorption for all samples at 2 and 28 days. The initial rate of absorption (Figure 5-22 (b, d, e)) was found to reduce as the hydration progressed in all cases. This was expected since the porosity and the number of large pores reduce with curing time. Therefore, at 28 days, it was more difficult for the water to penetrate the specimens through capillary absorption compared to 2 days. The initial rate of absorption can only be calculated accurately if the correlation coefficient from the linear regression analysis from 1 minute to 6 hours satisfies $R^2 > 0.98$ (ASTM C1585-13, 2013). At both test ages, all samples had a $R^2 > 0.99$ for the initial rate of absorption so it could be accurately determined. At 2 days, the addition of 0.05% GNPs had an insignificant effect on the initial absorption rate. However, the 0.1wt% and 0.3wt% GNP additions led to a ~12% and 9% reduction in the initial rate of absorption, meaning that the presence of larger pores was reduced. Further GNP addition at 0.5wt%, compromised the performance slightly and the beneficial effects of refined microstructure and reduced porosity were not observed. At 28 days, a reduction in the initial rate of water sorptivity was observed when the GNP dosage was low, i.e. at GNP0.05% and GNP0.1% (Figure 5-22 (d-e)) and the sorptivity coefficient reduced by ~12%. However, at higher GNP concentrations, the sorptivity coefficient increased again slightly, which could mean that larger pores were re-introduced in the sample. Therefore, at moderate GNP dosages, GNPs could act as nano-fillers and fill the larger pores, leading to a reduction in porosity and pore refinement. As the GNP dosage increased, the mixing and compaction of samples became difficult due to a large reduction in the fluidity, which could consequently lead to slightly increased porosity. Therefore, higher GNP concentrations might compromise the pore structure refinement that was observed for moderate GNP dosages and the mixing methodology would need to be adjusted.

The secondary rate of absorption could not be accurately determined as the R^2 was < 0.98 . However, the total water sorptivity was calculated for all samples after they were exposed to water for 9 days. From Table 5.6, in all cases the total absorption was less at 28 days compared at 2 days. A beneficial effect was observed with moderate additions of GNPs, with the trend reversing with GNPs were added at 0.3% and 0.5%. Overall, these results agree with earlier findings around hydration, microstructure, and mechanical properties, where higher additions of GNPs compromised the performance of the mortars.

Other studies also showed that the water penetration depth reduced with GNPs. Du and Pang (2015) and Du *et al.* (2016) showed that GNP dosages <1wt% had an insignificant effect on water permeability whilst a 1.5wt% GNP dosage reduced the penetration depth by 80%. Other studies showed that other GRMs can reduce the water absorption of cement composites, albeit their effect is not easily comparable due to the differences between GRMs, mix methods and testing conditions.

Table 5.6: Total water absorption (mm) for mortars at 2 and 28 days

	Total absorption (mm) - 2 days of hydration	Total absorption (mm) - 28 days of hydration
Control (0% GNP)	6.02	5.04
GNP0.05%	6.16	4.41
GNP0.1%	5.40	4.89
GNP0.3%	6.54	5.04
GNP0.5%	6.68	5.36

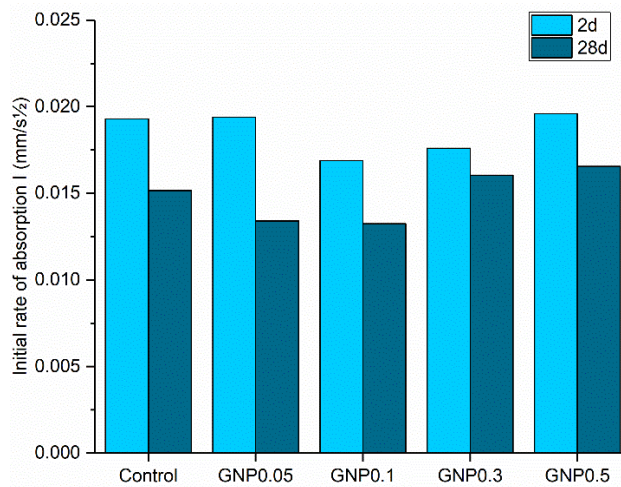
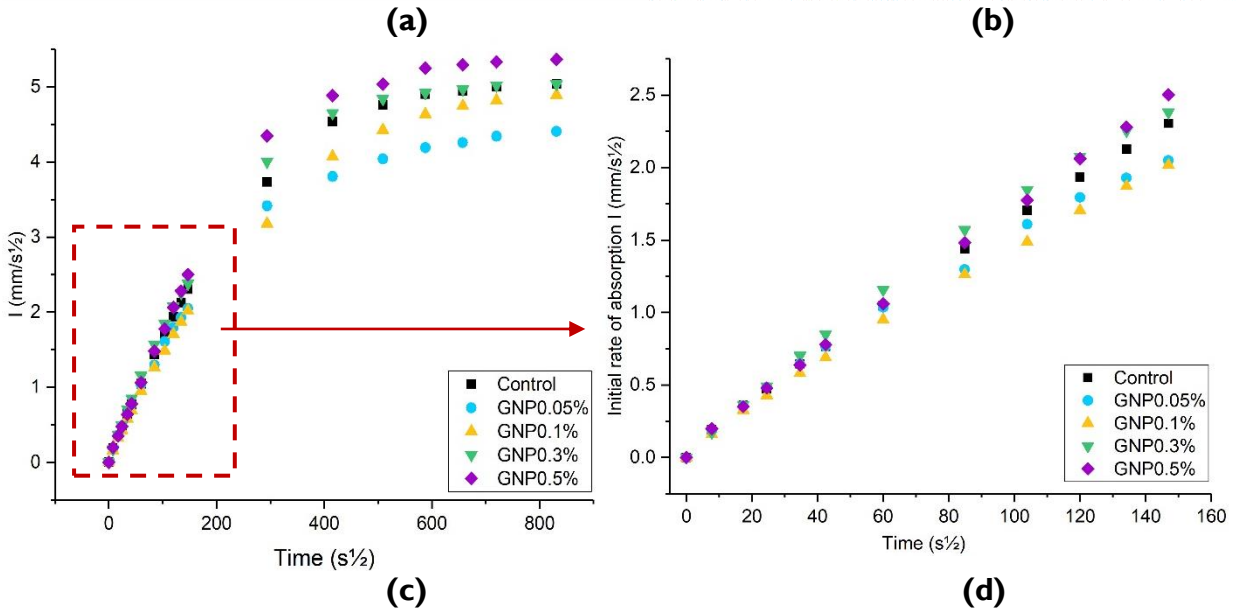
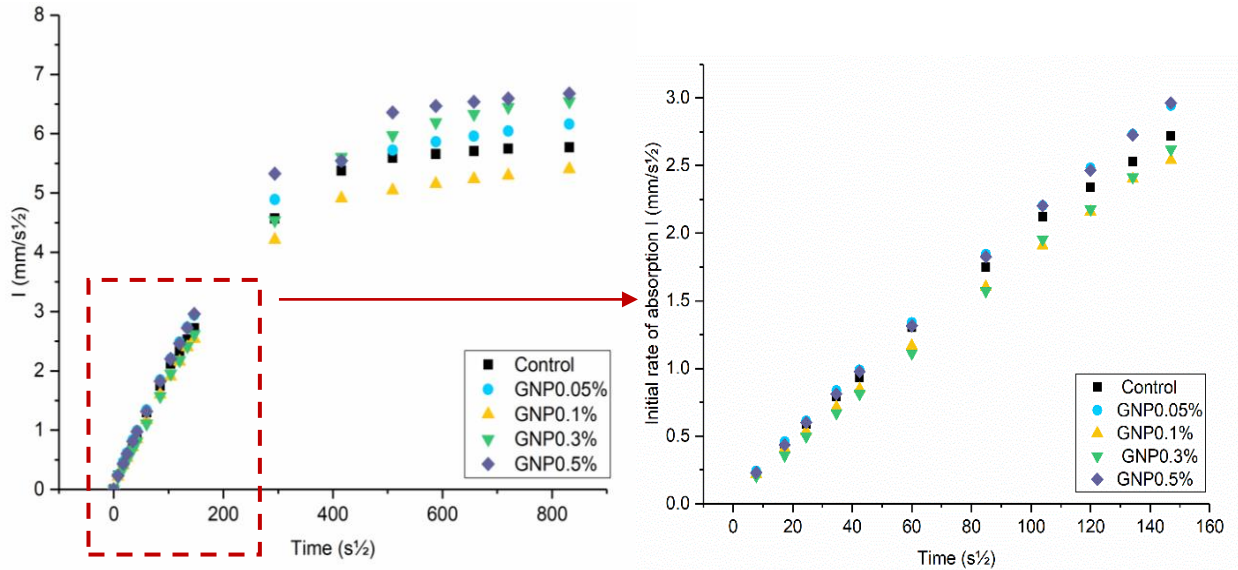


Figure 5-22: Water sorptivity of CEMI mortars with varying GNP contents at (a-b) 2 and (c-d) 28 days and (e) initial rate of absorption for all samples

5.2.5.2. Gas permeability

Gas permeability is important when the material is to be exposed in aggressive gases such as in roads, and is a non-evasive test, which is advantageous compared to other permeability measurement techniques. Gas permeability (Section 3.3.3.2), was performed on duplicate disc mortar specimens (10 mm thick, 50 mm diameter) at 2 days and triplicates at 28 days and the results are presented in Figure 5-23. At 2 days, the control had a significantly higher gas permeability coefficient compared to the GNP samples. The maximum reduction was seen for 0.1%GNP which halved the permeability. When the GNP content increased further, this reduction was slightly reversed, although the GNP specimens were still ~ 40% less permeable compared to the control. The continuous reduction with increasing GNP dosage showed that GNPs acted as a physical barrier to gases and that they might also have reduced the overall porosity of the sample. Two mechanisms were present; firstly, increasing the GNP dosage helped in forming a physical barrier to aggressive gases, whilst secondly, as the GNP dosage increased, compaction became more difficult which could induce more pores in the mix. In all cases (except for 0.1% GNP), the 28-day samples were less permeable than the 2-day samples. This was expected due to the ongoing hydration that reduced the porosity of the mix. However, at 28 days, the addition of GNPs did not result in any significant reduction in gas permeability and the difference in coefficients was statistically insignificant.

The fact that the gas permeability reduction with GNPs was only observed at 2 days and not at 28 days is a limitation for practical applications. At 2 days, the porosity was still very high due to a low degree of hydration and hence the physical barrier that GNPs formed was effective. Instead, at 28 days, the physical barrier from GNPs was masked because cement hydration had progressed, and GNPs were integrated within the cement hydration products so they could not act as a physical barrier to the gases. Graphene sheets have been found to be impermeable to standard gases (Bunch *et al.*, 2008). However, there is very limited literature on the gas permeability of cementitious composites with GRMs. Gao, Jing, Zhou, *et al.* (2019) followed the same testing methodology to understand the effects of GO and MWCNTs on the cement pastes of different w/c ratios. The authors found that in all cases, the gas permeability coefficient reduced with GRM addition and as an example, for w/c = 0.45, the gas permeability coefficient reduced from $6.54 \times 10^{-17} \text{ m}^2$ for the control to $5.62 \times 10^{-17} \text{ m}^2$ when GO and MWCNTs were added. Their specimens were tested at 28 days and

their control was more porous than the one on this study due to the lack of aggregates and the different concentration of superplasticisers. However, there are no studies to date that investigate the effect of GNPs on the gas permeability of the cement composites and further research is needed in this area.

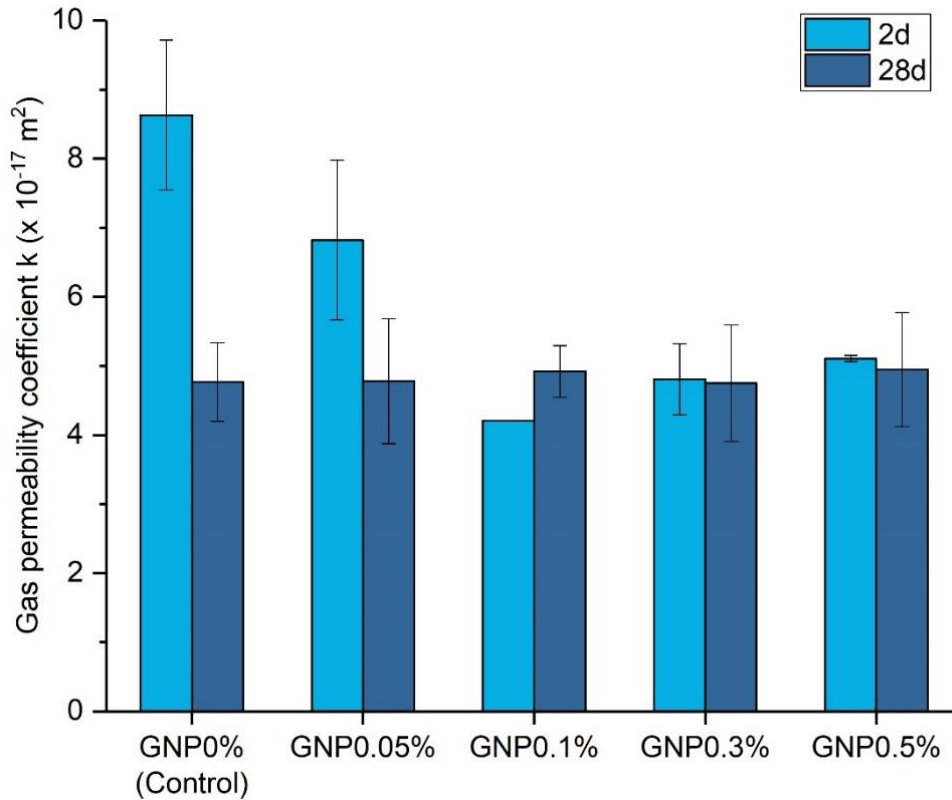


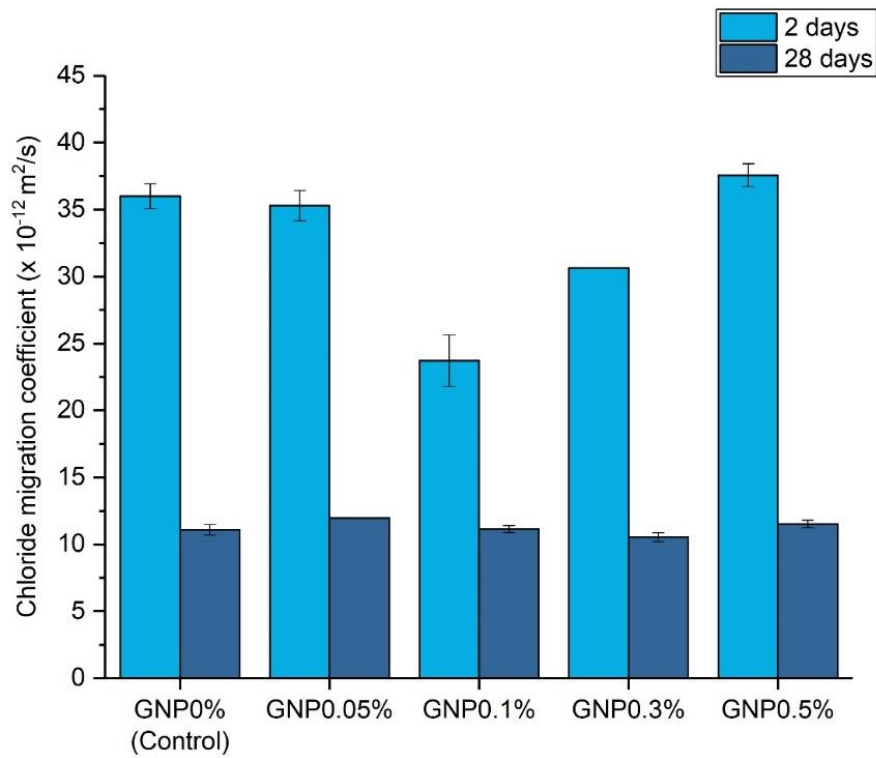
Figure 5-23: Gas permeability coefficient of CEMI mortars with varying GNP contents

5.2.5.3. Rapid chloride penetration testing (RCPT)

RCPT was undertaken to understand the effect of GNPs on the chloride resistance capability of cement mortars at 2 and 28 days, with duplicate samples tested (Section 3.3.3.3). The non-steady state migration coefficient was calculated, and the results are shown in Figure 5-24. For all samples, the chloride migration coefficient was much smaller at 28 days compared to 2 days, irrespective of GNP addition. Starting from the early age performance, GNP0.05% had an insignificant effect, however, as the GNP dosage increased to GNP0.1% and GNP0.3%, the coefficient reduced by ~31% and ~11% respectively. This trend was then reversed for the higher GNP content of 0.5wt%. These findings are similar to the results from the gas permeability tests, where moderate additions of GNPs were beneficial for refining the overall porosity and acting as physical barriers, which was then

reversed for higher concentrations as mixing and compaction became challenging. On the contrary, at 28 days, the addition of GNPs did not have any effect on the chloride migration coefficient and all the results were within margin of error. This confirms that moderate additions of GNPs can lead to a significant improvement of barrier properties during the early age of the composite. If the specimen is exposed to aggressive conditions during its early life, then GNPs will form a physical barrier to prevent damage. This is particularly beneficial in the case of airport runways and motorways that could be exposed to aggressive gases and chlorides in the first days after casting (from the airplane/vehicle engines). As the hydration progresses the effect of GNPs becomes insignificant as the GNPs are integrated in the hydration products and cannot act as a physical barrier.

These findings are in general agreement with the literature that was presented in Section 2.4.4. A 0.1wt% GNP addition has been found to reduce the chloride migration coefficient at 28 days by 34% from $10.8 \times 10^{-12} \text{ m}^2/\text{s}$ to $7.10 \times 10^{-12} \text{ m}^2/\text{s}$, however, such reduction was only observed at 2 days here. Other studies have also shown a reducing trend in the chloride penetration depth with GNP addition however, different dosages, GNP properties and mix methods mean that the results are not directly comparable. GNPs have shown promising barrier properties at an early curing age when the mix is still very porous, and their impact should be investigated further.



(a)



(b)

Figure 5-24: RCPT results of CEM I mortars with varying GNP dosages (a) non-steady state chloride migration coefficient (b) photos of split specimens sprayed with silver nitrate

5.3. Effect of natural graphite on CEMI paste

Three different natural graphites were tested to understand their effect in enhancing the electrical conductivity of CEMI paste, which could then be used as a cement-graphite coating layer. As presented in Chapter 3, these products were: coarse, medium and fine graphite. A cement paste with $w/c = 0.45$ was used with no chemical admixture, using the dispersion protocol described in Section 3.2.2. Cement paste was investigated rather than mortars as graphite is a soft material and it was expected that it would negatively affect the performance of composites. Therefore, it would not be viable to use graphite in bulk applications such as mortars and concrete. Instead, a cement-based coating that incorporates graphite or GNPs is more practical for sensing applications and for improving the durability of the cover layer of concrete. The effect of graphite on the rheological properties, hydration and mechanical performance is discussed in this section.

5.3.1. Rheological performance with graphite

The effect of the graphites on the viscosity of CEMI paste was measured with a rheometer in triplicates for each concentration. The graphite dosage ranged from 0% to the percolation threshold of each respective product (percolation threshold results are in Chapter 6). The percolation thresholds varied from 20% - 40% of graphite by weight of cement depending on the product. When graphite dosages exceeded the percolation threshold, mixing became difficult as graphite formed large agglomerates with the cement. It was not possible to run a mini-slump test for workability, as the samples comprised of cement paste that had much higher fluidity than mortars and the measurements would not be accurate. The rheology results were fitted with the Bingham model and are illustrated in Figure 5-25. In all cases, graphite addition resulted in an increase in the viscosity of cement paste. Starting from the coarse graphite, the viscosity increased progressively by 76% to 171% compared to the control when graphite was added at concentrations of 10% - 40% by weight. Moving to the medium graphite, viscosity also increased dramatically, and it was not possible to mix after the 20wt% concentration (percolation threshold for this graphite). In this case, the viscosity increased by 126% and 148% for the 10wt% and 20wt% concentrations, which is much higher than the coarse graphite at the same dosages. This can be explained as the fine graphite for the same weight dosage, would have more particles that caused inter-particle friction with cement and therefore the viscosity increased dramatically. Furthermore, the

smaller size graphite is expected to have a higher surface area which would require more water to wet its surface. Finally, the fine graphite also increased the viscosity significantly. At 10wt% concentration, the increase was similar to the medium fineness graphite but at 20wt% dosage, the viscosity was almost three times higher compared to the control. Furthermore, it can be observed that the error bar was large, and this was due to difficulties in mixing this high concentration of the fine graphite.

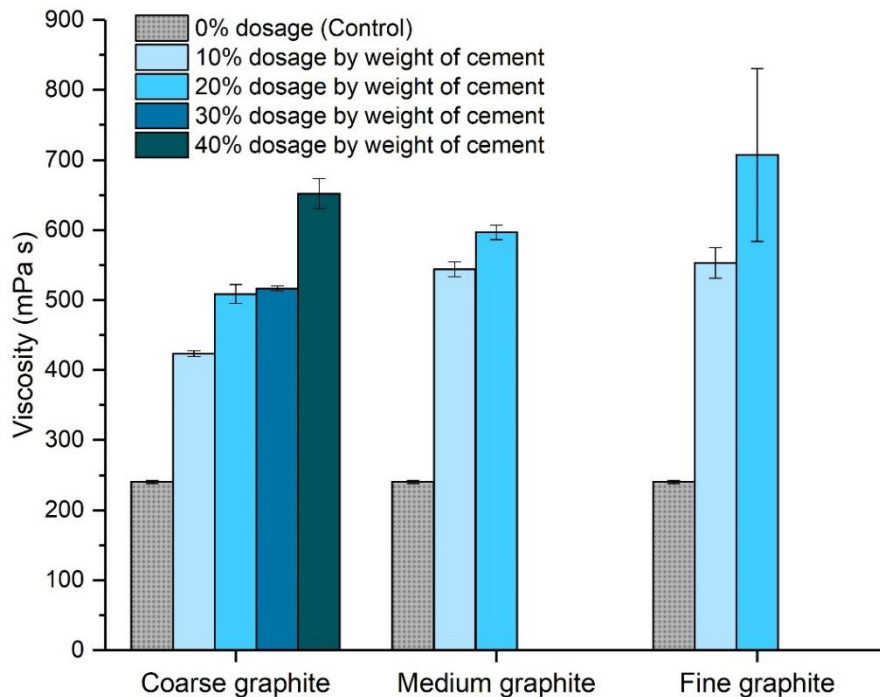


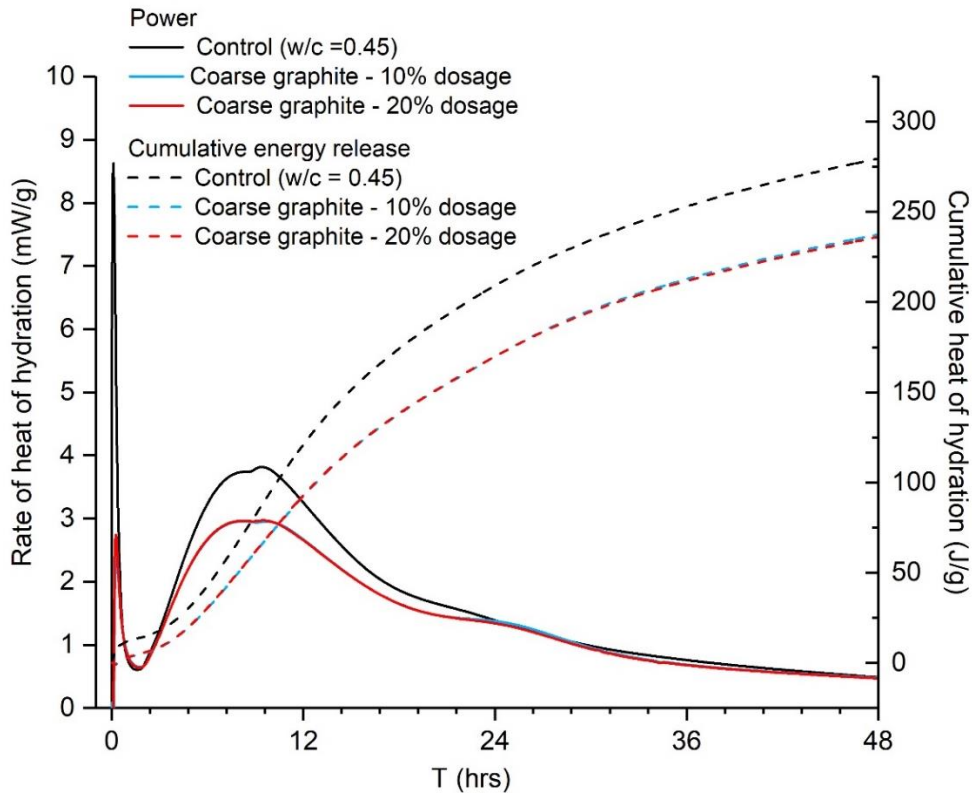
Figure 5-25: Effect of natural graphite type and concentration on the viscosity of fresh cement paste

Graphite reduced the fluidity of cement paste significantly, due to the interparticle friction with cement particles and its low hydrophilicity (Kozbial *et al.*, 2016). The finer the graphite, the more pronounced the reduction in workability as the aspect ratio increased and more particles were needed for each dosage. These findings agree with the literature. El-Dieb *et al.* (2018) found that replacing the fine aggregates with 7wt% graphite powder, resulted in a 33% reduction in the slump of fresh concrete due to the high specific surface area of the graphite. The graphite was in the range of a few microns, therefore, it is assumed that it was finer than the graphite used in this study. Wang *et al.* (2019) found that even a 4wt% graphite addition resulted in a 50% reduction in CEMI paste fluidity due to the graphite being non-polar and not very hydrophilic (contact angle of 59.8° with water whilst with

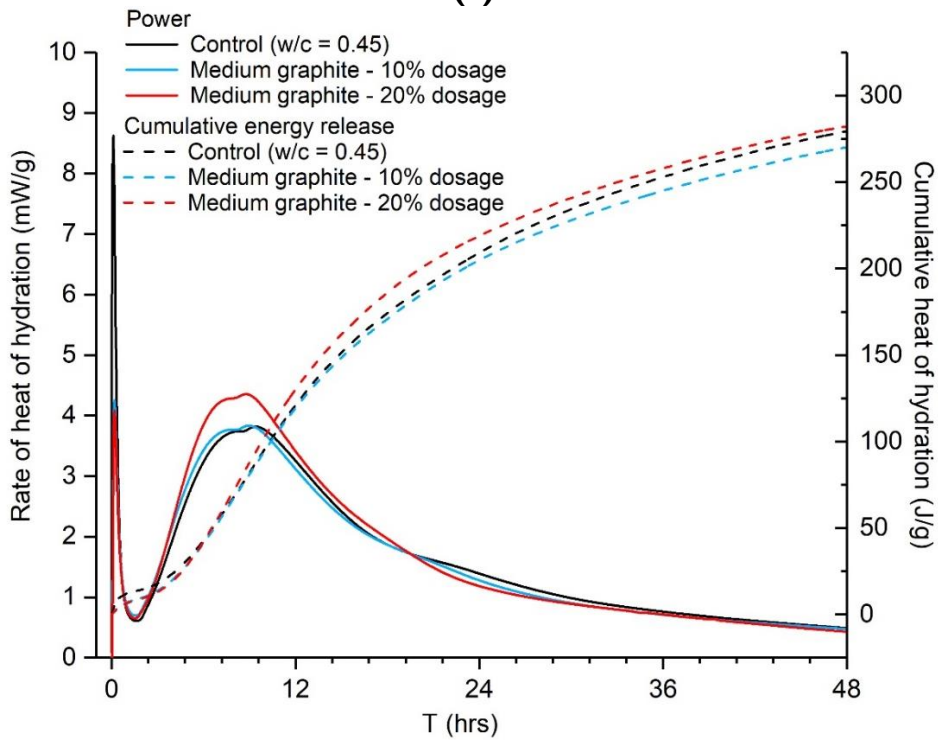
cement was only 39.9°). The authors used an 8 μm graphite (the fine one here is 44 μm) hence, their reduction in fluidity was even more pronounced and at much lower concentrations. Further studies, such as Wu *et al.* (2015), Climent *et al.* (2016), Frattini *et al.* (2017), had to adjust the w/c or introduce surfactants to ensure that a target fluidity was maintained in the presence of graphite.

5.3.2. Effect on hydration

The effect of graphite on the hydration of CEMI paste was investigated by isothermal calorimetry testing. For comparative reasons, all graphites were tested at 10wt% and 20wt% concentration and the higher dosages for the coarse graphite were not tested. The control refers to CEMI paste with w/c = 0.45, and it is the same in all graphs in Figure 5-26. In all cases, the same peaks were observed meaning that cement hydration was not affected by graphite addition. This agrees with Yuan *et al.* (2012) who found that graphite did not participate directly in the cement hydration. It can be observed, however, that the three graphites had a somewhat different effect on the hydration of Portland cement paste. The coarse graphite clearly depressed and widened the main hydration peak (Figure 5-26(a)). The cumulative heat release was also lower with this graphite and hence, a lower strength is expected. However, for the two finer graphites, the effect on hydration becomes less pronounced. For the medium graphite at 10% concentration, the impact on the hydration peak was insignificant (Figure 5-26(b)). When the dosage increased to 20wt%, the peak power increases slightly from 3.82 mW/g for the control to 4.35 mW/g whilst, the total cumulative heat of hydration remains unaltered. Finally, for the fine graphite, the effect on hydration is even less pronounced, and the curves only change slightly, whilst again, the total cumulative heat of hydration remains almost the same.



(a)



(b)

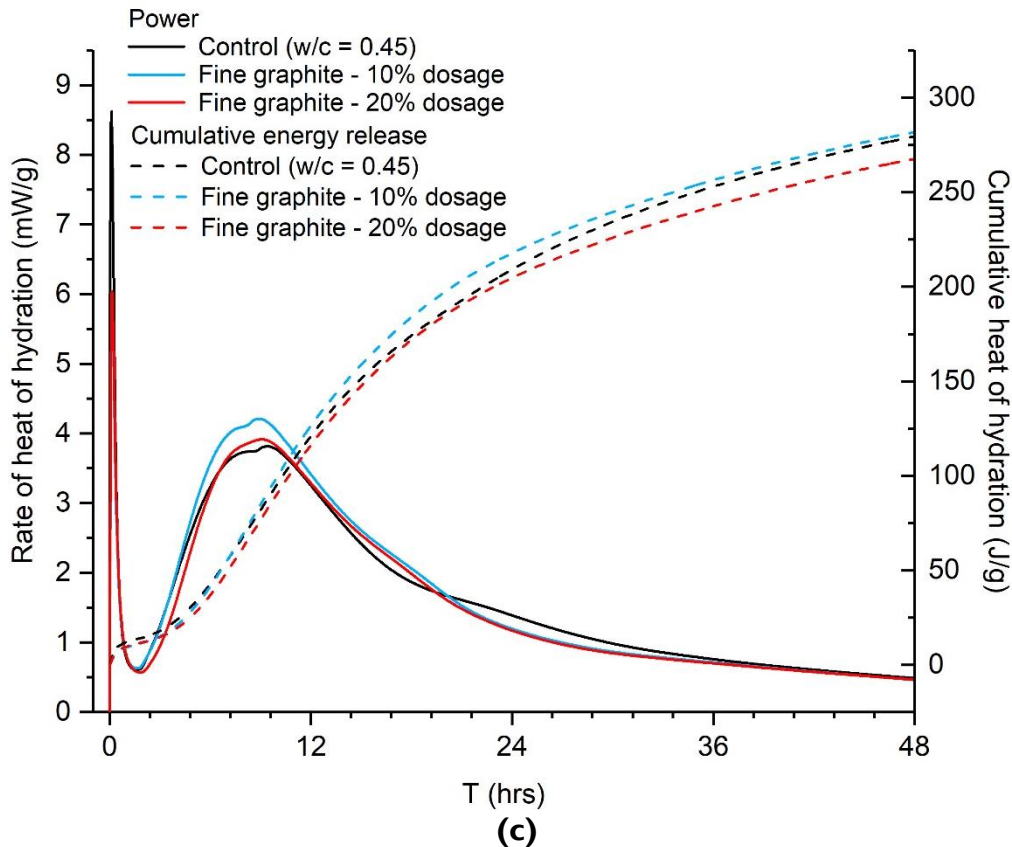


Figure 5-26: Effect of graphite size and concentration on the hydration of CEM I paste measured by isothermal calorimetry (a) coarse (b) medium and (c) fine graphite

The above results can be explained by one physical and one chemical/thermal mechanism. The w/c was fixed and therefore the addition of graphite resulted in an increase of the water/solids ratio. The effect of water on the hydration of Portland cement has been widely reported with higher water contents resulting in accelerated cement hydration and increased cumulative heat (Neville, 2011; Scrivener *et al.*, 2015). In the coarse graphite, the large graphite particles could have acted as physical blockers for the water to reach the cement grains and therefore, resulted in a depression of the main hydration peak at ~10 hours. As the graphite size reduced, a filler effect started being present (Frattini *et al.*, 2017; Hamad, 2019) and graphite particles helped in improving the packing density without physically blocking the water from reaching the individual cement grains. Graphite particles are also slightly hydrophobic (Kozbial *et al.*, 2016) and would push the water towards the cement grains therefore promoting hydration. Moreover, graphite is a thermally conductive material (Tiedje and Guo, 2014) which would conduct the exothermic heat produced during cement hydration (Yuan *et al.*, 2012). It should be noted, that this experiment could also be

affected by baseline drift (Jing *et al.*, 2017) and therefore, the changes in the hydration curves of Figure 5-26(b-c), could be considered insignificant. Therefore, the graphites were not found to affect hydration, however, the very coarse graphite could block the water from reaching the cement grains and result in a strength reduction.

The results of the initial set as calculated by isothermal calorimetry are summarised in Table 5.7 and it can be observed that the effect on the initial setting time was very limited. All samples underwent their initial set at $\sim 3 \pm 0.5$ hours. Given the limited accuracy of this method for calculating setting time, it could be argued that the graphite additions did not impact the setting process. This would need to be confirmed in future studies by further hydration testing and Vicat apparatus testing for setting time of cement.

Table 5.7: Initial setting times and peak power for CEMI pastes containing the three natural graphites

	Peak power (mW/g)	Initial set (hr)
Control (w/c =0.45)	3.817	3.05
Coarse graphite – 10wt%	2.957	2.7
Coarse graphite – 20wt%	2.971	2.73
Medium graphite – 10wt%	3.833	2.8
Medium graphite – 20wt%	4.353	3.1
Fine graphite – 10wt%	4.212	3.27
Fine graphite – 20wt%	3.916	3.58

5.3.3. Effect on microstructure

SEM analyses were carried out at 5 months at the respective percolation threshold of the three graphites. Figure 5-27 shows that the individual graphite flakes could be identified in all cases. A proximity between the flakes is observed, which was expected as graphite concentrations are very high, but no obvious agglomerates are seen. Therefore, dispersion of graphite particles can be assumed to be adequate with dry mixing. Observing the interaction between the graphite flakes and cement, an interfacial transition zone similar to that of aggregates can be seen for the coarse graphite (Figure 5-27(a)). The graphite addition did not affect the microstructure of CEMI paste.

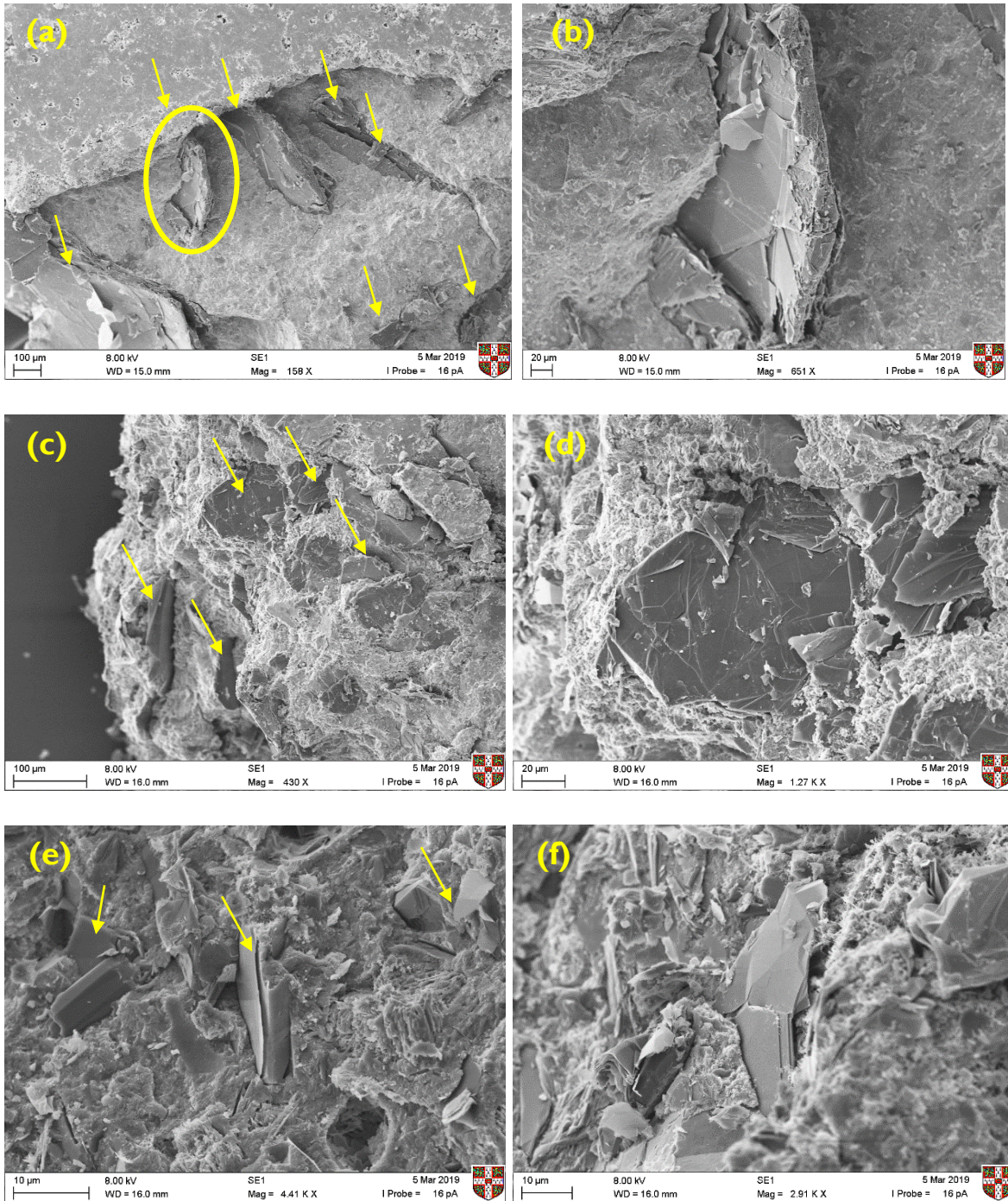


Figure 5-27: Microstructural characterisation of the three graphites – cement paste after ~5 months by SEM (a) coarse (b) medium and (c) fine graphite

5.3.4. Effect on mechanical properties

The effect of the three graphites on the mechanical properties of CEM I paste was investigated. The compressive strength was measured at 2, 7 and 28 days, and the hardness was tested by micro-indentation. Figure 5-28 shows the effect of the three graphites when used at 10wt% and 20wt% concentrations on the compressive strength. At all test ages, when graphite was added, the compressive strength reduced, irrespective of the graphite size. Moreover, in all cases, the higher the graphite dosage, the lower the compressive strength. The summary of the % reduction in strength comparing to the control is presented in Table 5.8. The compressive strength had an inverse relationship with graphite size; the coarse graphite produced the lowest strength, whilst the fine graphite had the least reduction compared to the control.

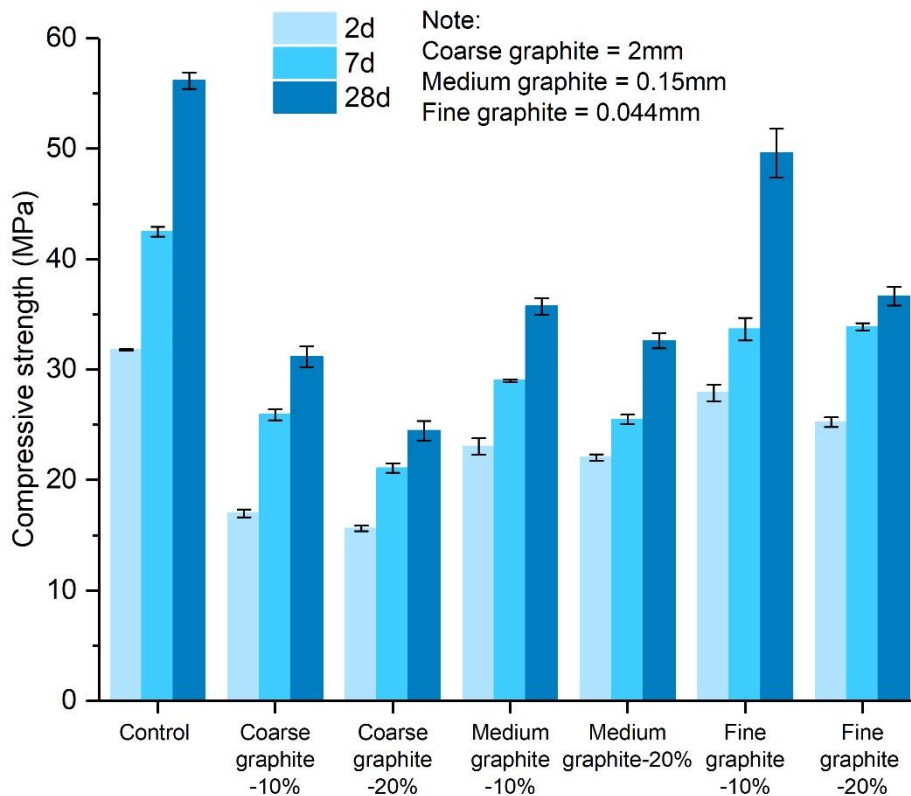


Figure 5-28: Compressive strength of cement paste with the three different graphites at 2, 7 and 28 days

Table 5.8: Reduction in compressive strength (%) with the different graphites over time compared to the control

Graphite used and dosage %	2d	7d	28d
Coarse graphite – 10%	-47%	-39%	-45%
Coarse graphite – 20%	-51%	-50%	-56%
Medium graphite – 10%	-28%	-32%	-36%
Medium graphite – 20%	-31%	-40%	-42%
Fine graphite – 10%	-12%	-21%	-12%
Fine graphite – 20%	-21%	-20%	-35%

Micro-indentation testing was undertaken, with 15 measurements, on the graphite samples at 56 days and all samples were tested with 20wt% graphite concentration. The compressive strength results would suggest that the hardness would reduce with graphite addition and the effects would be more pronounced for the coarse graphite. Indeed, as shown in Figure 5-29 (left), the coarser the graphite, the lower the hardness. The fine graphite maintained the same hardness as the control mix, whilst the coarse graphite reduced the hardness by 28%. This is due to the graphite softness, which naturally reduces the hardness of the paste, and also because of packing density, where the finer graphite reduced the porosity more and resulted in a more compact mix which improved the overall hardness of the sample. The hardness results also provide a further indication of sufficient dispersion of graphite. The error bars are small for all samples and in the same range as that of the control. This further supports the SEM and μ CT scan testing (Chapter 4) that showed that graphite was uniformly dispersed in the cement paste.

Young's modulus values in Figure 5-29 (right), show a reduction for the coarse graphite by 15% but increased for the two finer graphites compared to the control (14% improvement for fine graphite). The modulus of elasticity increases with an increase in compressive strength (Neville 2011) and this is part of the reason why the coarser the graphite the lower the Young's modulus. The increase in stiffness with the fine graphite can be explained by changes in porosity. Due to better packing density, the cement paste with the fine graphite has a reduced porosity and therefore it becomes stiffer compared to the control and the coarser two.

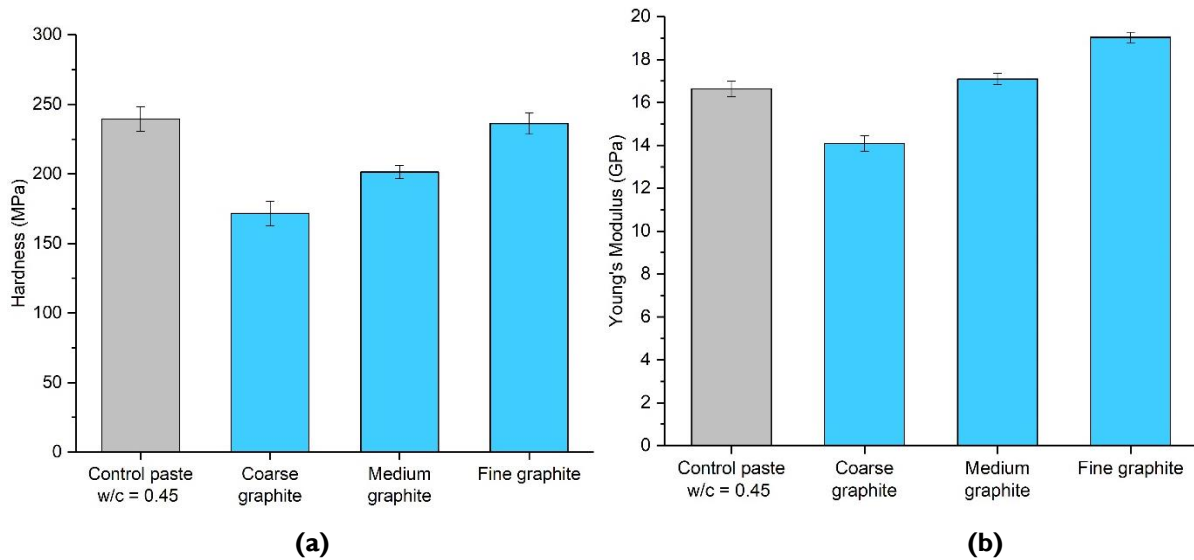


Figure 5-29: Microindentation results of the effect of 20wt% graphite addition on the of cement paste at 56 days in terms of (a) hardness (b) and Young's modulus

5.4. Summary

This chapter investigated the effect of GNPs on the properties of cement pastes and mortars, followed by the effect of three natural graphites on cement paste. The intention was to investigate the use of GNPs for both cement paste coatings and bulk applications whilst natural graphite would only be used as a cement-based coating. For the effect of GNPs in cement pastes, two different cements were tested; CEMI 52,5N and CEMII/A-LL 32,5R and with a single dosage of GNPs of 0.3wt%. GNPs were found to have a negligible effect on the cement hydration and no new hydration phases were found. SEM observation showed that GNPs were not well linked with the cement hydration products and they could form planes of weakness. Small reductions in flexural strength were found but the reduction was more pronounced in the compressive strength. Hardness of the composites increased slightly with GNP addition whilst no significant effect was observed for the Young's modulus. Micro-indentation confirmed that the dispersion protocol developed was sufficient to disperse GNPs homogeneously. The effect of GNPs on the fresh, mechanical and permeability performance of CEMI mortars was investigated at 2 and 28 days. The fluidity reduced in all cases with increasing GNP concentration from 0.05% to 0.5%, whilst the early age hydration was delayed with GNPs as confirmed by TGA and XRD testing. SEM showed that GNPs could form some agglomerates at higher dosages and, they were not intimately integrated with cement hydration products which could create planes of weakness and

could limit bulk applications. Indeed, the compressive and flexural strength of the mortars reduced with GNP addition. On the contrary, GNPs were beneficial for permeability at 2 days as measured by water sorptivity, gas permeability and RCPT. However, no beneficial effect was observed at 28 days. Their beneficial barrier properties could be explored in coatings that could also possess other functionalities such as enhanced electrical and thermal conductivity. This should be considered in the future development of this novel composite material. For the three natural graphites, coarse, medium and fine, added in cement paste, the fluidity reduced significantly, whilst a minimal effect on hydration was observed. The coarse graphite affected the hydration to an extent and resulted in the greatest reduction in strength and hardness. All graphites reduced the compressive strength of the paste and therefore, their negative effect on the fresh and mechanical properties of cement composites must be accounted for before these composites are used as coatings for sensing applications. The electrical conductivity will be investigated in more detail in Chapter 6.

Chapter 6. ELECTRICAL CONDUCTIVITY OF CEMENT COMPOSITES WITH GRMs

The aim of this chapter is to investigate the electrical conductivity of cement composites with graphene-related materials (GRMs), to solve the infrastructure monitoring challenge that was discussed in Chapter 2. The motivation here is to remove the need for visual surveys and external sensors, by developing a cementitious material that could not only have an enhanced structural capability but could also be used as a sensor to monitor its own condition and possess a self-sensing mechanism. The structural performance of the GRM-composite material was investigated in detail in Chapter 5, whereas this chapter focuses on the electrical conductivity of the cement composites with the GRMs that have been already tested in this thesis. This chapter is split in three sections. Firstly, the different intrinsic properties of the cementitious material that influence the electrical conductivity are investigated, including the effect of w/c, curing regime and the method of measuring the electrical conductivity. The second section then focuses on the use of GRMs - namely the three products of coarse, medium and fine graphite and also GNPs – and assesses the percolation threshold required for conductivity. The third section explores the potential use of GNPs for self-sensing in cement-based coatings, rather than in the bulk.

6.1. Effect of intrinsic material properties on the electrical conductivity

Several parameters can affect the electrical conductivity of cement composites, including w/c, moisture conditions, presence and type of aggregates and admixtures, temperature, clinker composition and overall mix design as well as the measurement technique (Chung, 2002b; Neville, 2011). Some of these parameters were investigated in the literature over the years with w/c having a pronounced impact on the electrical conductivity (Davey *et al.*, 2019). It was found that moist concrete behaves like an electrolyte with a conductivity in the range of semi-conductors, whilst oven-dried concrete acts as an insulator (Monfore, 1968). As discussed in Section 2.4.5, there are different types of electrical conduction, including ionic, electronic, and tunnelling; and the presence of water directly affects the ionic

conduction. To develop an appropriate measurement technique and to have a baseline for future measurements, some of the parameters were investigated here. Specifically, the effect of the w/c, curing regime and measurement technique for plain cement pastes were tested. CEMI 52,5N was chosen for all the experiments in this chapter and no aggregate was used as the intention was to develop electrically conductive cement-based coatings rather than use the electrically conductive composite for structural applications.

6.1.1. Effect of w/c and curing regime

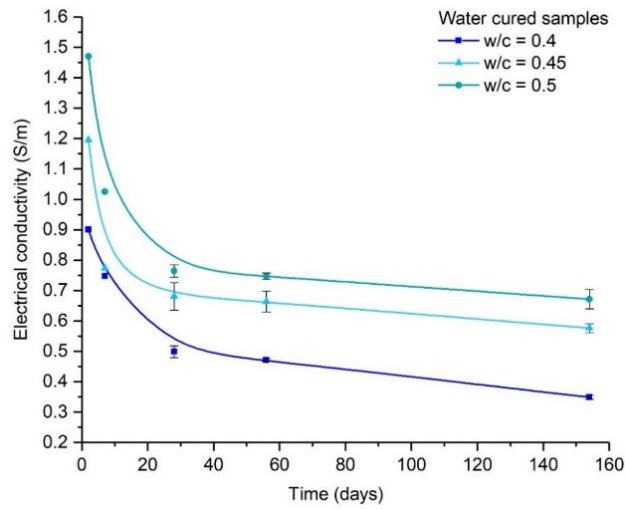
The effects of the w/c and the curing regime on the electrical conductivity of plain cement pastes were investigated. Three w/c ratios, 0.4, 0.45 and 0.5, were used and tests were carried out at 2, 7, 28, 56 days and 154 days. The curing regime was varied and included either water curing, by immersing the samples in water until the test age, or air curing, where the samples were left exposed in ambient temperature ($23^{\circ}\text{C}\pm 2^{\circ}\text{C}$) and 50% relative humidity. A third curing regime involved water curing the samples and then exposing them to air for 24 hours before the test to reduce the effect of moisture. Water curing allows for better hydration of cement composites whilst air curing is more representative of site exposure conditions where the specimens would be used in real-life applications. A four-probe method with embedded electrodes was followed (Section 3.4.4.1) with DC of 10V supplied in the outer probes for 60 minutes to get a stable reading (as DC leads to polarisation initially but the reading stabilises after some time) and the measurement from the last 5 minutes was used to calculate the resistivity. As described in Section 3.3.4.1, the electrical resistance was measured as the ratio between voltage and current and based on this value, the resistivity was calculated that was then converted in conductivity (the inverse of resistivity). This test set-up was maintained to avoid differences in the results (Büteführ *et al.*, 2006). It is important to establish these baseline measurements with the specific cement, environmental conditions, and test set-up available in the laboratory as these parameters can affect the electrical conductivity measurements.

Figure 6-1 shows the electrical conductivity of the prisms at the different time intervals for the three different w/c ratios and three different curing regimes. The error bars show the variability between the measurements for the triplicate samples (from 28-day testing onwards). In all cases the variability in measurements between the different specimens was very small. From Figure 6-1, in all cases, the electrical conductivity reduced over time, irrespective of the w/c ratio or curing regime. The reduction in conductivity was more

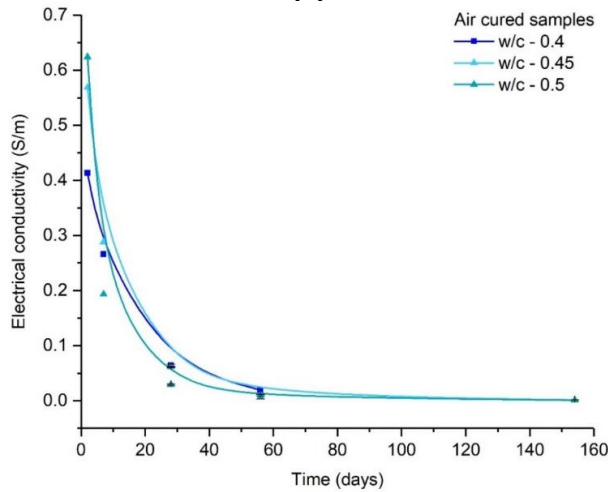
pronounced in the first 28 days, after which, the rate of reduction slowed down. This can be attributed to the ongoing hydration of the pastes, where over time, more water is consumed by hydration and therefore less water is available for electrolytic conduction through the paste. As a result, the electrical conductivity of the cement paste reduces, i.e. the resistivity increases. These findings agree with Monfore (1968), who showed an increase in resistivity with curing age (from 7 to 90 days, resistivity increased by 52% for $w/c = 0.4$) and a reduction in resistivity with increasing w/c ratio (resistivity reduced by 67% at 28 days when w/c increased from 0.4 to 0.6). In all cases, the water cured samples (Figure 6-1(a)), had almost double the conductivity of the air cured samples (Figure 6-1(b)) which was due to the removal of the evaporable water with air curing that resulted in a loss of ionic conduction. Demircilioğlu *et al.* (2019) also found that as the moisture content of the sample reduced from 5.2% to 0% (by heating the samples at 90°C for a period ranging from 10 minutes to 92.5 hours), the electrolyte behaviour was lost, and the electrical resistance more than doubled from 2000 Ohm to circa 5000 Ohm.

By observing the water cured samples in Figure 6-1(a), it can be seen that the higher the w/c , the higher the electrical conductivity of the sample. This was expected as the samples with higher w/c have more water available and since water acts as an electrolyte, it allows for electrical current to pass through the sample (Neville, 2011; Davey *et al.*, 2019). The air cured samples only showed variations in conductivity at the very early curing ages (2 and 7 days), whilst the results were similar as curing progressed. This is because in the first few days of hydration, the differences in the water content were more pronounced but as hydration progressed and the samples were exposed to air, some of the water evaporated whilst some was used for the hydration. Hence, for the air cured samples, the long-term differences in electrical conductivity did not depend on the w/c ratio. Finally, in Figure 6-1(c), the hybrid curing regime was used and the results around the w/c ratio were more mixed, with $w/c = 0.5$ having the highest conductivity. However, the curves for $w/c = 0.4$ and $w/c = 0.45$ were very close and therefore, it was not possible to deduce the effect of w/c on the electrical conductivity. This curing method is the least reliable as the environment is less controlled compared to the other two where the samples are either fully water cured, or air cured. Nonetheless, in construction applications, this situation could be encountered; with structures being cured under moisture in the first days and then

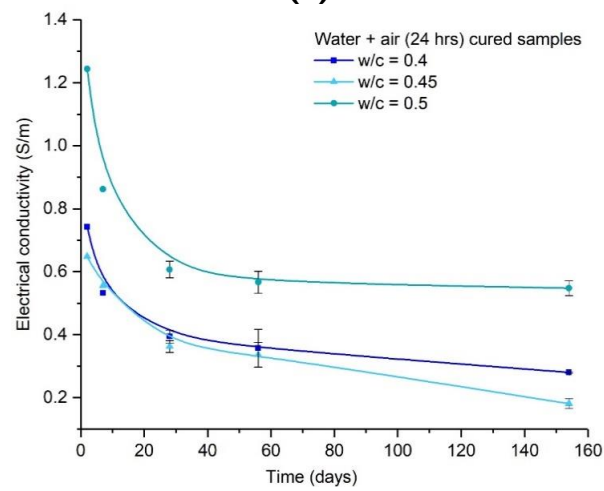
exposed to air. On the contrary, the fully water cured samples are not representative of real-life applications unless they are water submerged structures.



(a)



(b)



(c)

Figure 6-1: Effect of w/c ratio and curing on the electrical conductivity of cement pastes (a) water curing (b) air curing and (c) water and air curing for 24 hours prior to testing

The above results showed that both the curing regime and the w/c affect the electrical conductivity measurements. Air curing almost halved the electrical conductivity compared to water curing due to water evaporation. The w/c ratio played a significant role in water cured samples; with higher w/c resulting in higher electrical conductivity. Nonetheless, over time all samples had an electrical conductivity which was almost zero (even the water cured samples) and therefore, cement paste is expected to act as an insulator in the long-term. This means that it would not be possible to use plain cement pastes, irrespective of their water content and moisture state, to monitor changes in the electrical conductivity and assess damage. Hence, a conductive filler is needed to ensure that the samples possess sufficient electrical conductivity for a sensing mechanism to be developed and this will be investigated in more detail in Section 6.2.

6.1.2. Relationship between embedded electrodes and surface conductivity

The conductivity measurement technique and the test set-ups can lead to considerable differences in the measurements of the results (Büteführ *et al.*, 2006). A four-probe direct current (DC) technique with embedded electrodes was selected for the tests carried out in Section 6.1.1, because it provides reliable readings and avoids the contact resistance (Chung, 2012). However, due to the embedded electrodes and the application of DC current, this method would not be suitable for field applications and is limited to lab-based investigations. Instead, the suitability of a surface resistivity meter, based on a 4-probe principle, was assessed. The handheld device was supplied by Proceq, called Resipod (Section 3.3.4.2) According to the supplier, the correlation between surface resistivity and embedded electrodes was not known (Proceq, 2018) and hence, needed to be established. The three w/c ratios of 0.4, 0.45 and 0.5 were investigated again. Although the combination of water and air curing is the most likely scenario in real applications, only purely water curing and purely air curing were tested as they provide a more controlled way of assessing and comparing the differences of the testing methods. The measurements were carried out at 2, 7, 28 and 56 days and the correlation curves are illustrated in Figure 6-2. Irrespective of the curing method, the surface resistivity technique provided a much lower conductivity measurement, ~2 orders of magnitude less, compared to the embedded electrodes technique. The main reason for this is the contact resistance between the external probes and the sample, that result in much higher resistivity measurements and therefore lower

conductivity (Han *et al.*, 2014). To reduce the contact resistance challenge, the probes were immersed in water before measurement as per advice from the device supplier (Proceq, 2017), however, still the resistivity values were higher compared to the embedded electrodes technique, indicating that contact resistance was not completely eliminated. The correlation between the two techniques was very high with the correlation coefficient R^2 being higher than 0.9 in most cases. Only the w/c = 0.4 water cured samples had a lower correlation coefficient which was due to a higher than expected measurement in surface conductivity at 7 days, associated with experimental error. Nonetheless, the remaining of the samples had very high correlation coefficients irrespective of the curing regime or w/c, meaning that the surface resistivity technique can provide comparative results for field measurements but the measured conductivity will be much lower than the true value. Both methods are proven to be reliable and the results show good repeatability between, indicating that the mixing and curing methods provide samples of good quality and demonstrate consistency.

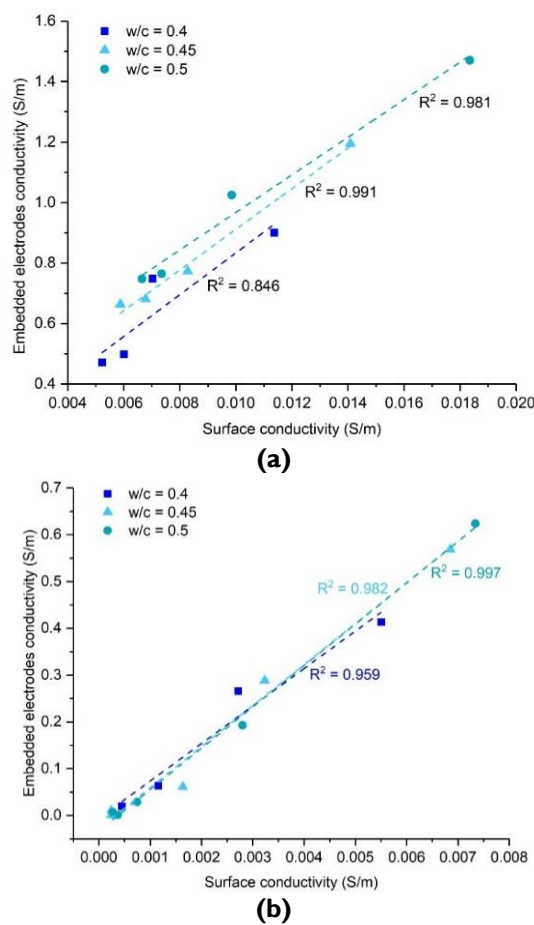


Figure 6-2: Correlation curves between embedded electrodes and surface resistivity measurements for (a) water cured samples and (b) air cured samples

In summary, the surface conductivity technique might not be suitable for identifying small conductivity changes due to the high contact resistance between the probes and the sample and therefore it would not be recommended for self-sensing applications. The correlation with the embedded electrodes technique is very high, however, in all cases, the surface measurement underestimated the electrical conductivity by approximately two orders of magnitude. Hence, for field applications, surface conductivity measurements could provide comparable results, but this technique is not suitable for investigating the intrinsic behaviour of new composite materials. Hence, the embedded electrode technique was utilised in the following sections. Furthermore, due to the pronounced effect of the curing regime and w/c ratio in the early hydration ages, the curing technique and w/c were kept consistent.

6.2. Effect of GRMs on the electrical conductivity of cement paste

As discussed in Section 6.1, cement paste allowed for some electrically conductive behaviour in the early hydration ages, however, as curing progressed, the cement paste became an insulator and the electrical conductivity approached zero. Therefore, to impart additional functionalities in the cement paste, a conductive filler is necessary. This section investigates the effect of GRMs on the electrical conductivity of cement pastes. The aim is to identify the percolation threshold for conducting electricity, i.e. the minimum filler dosage required to achieve stable electric current conduction (Han *et al.*, 2015).

6.2.1. Effect of natural graphite using 4 probe and direct current tests

Firstly, the effect of three natural graphites was investigated including coarse graphite (2mm), medium graphite (0.15 mm) and fine graphite (0.044mm). These three graphites were previously tested in Section 5.3 for their effect on the rheology, hydration, microstructure, and mechanical performance (compressive strength, hardness, and Young's modulus) of CEMI 52.5N pastes. Graphite has been used as a conductive filler in the literature (Section 2.4.5.1), however, the effect of graphite on conductivity could depend on a number of parameters such as the shape, size, origin and manufacturing process (Rew *et al.*, 2017). The effect of the three different graphites on the electrical conductivity behaviour

was investigated here, to understand how their changing size will affect the electrical measurements.

The w/c was kept constant at 0.45 in all cases and the samples were water cured. No admixture was used and the graphite was dry mixed with cements for two minutes to ensure its homogenous dispersion and then the water was added and mixing continued as per BS EN 196-1 (2016). Tests were carried out at 2, 7 and 28 days and the results in terms of electrical conductivity vs graphite content as % of the cement, for the three different graphites, are illustrated in Figure 6-3. From the figure, a clear percolation threshold, where the conductivity changed rapidly, could be observed for all three graphites and at all test ages. Before the sudden increase in electrical conductivity, the conductivities of all samples were less than 2 S/m irrespective of the test age or the graphite size. Furthermore, conductivity clearly reduced as curing progressed. The 2-day samples (solid lines) had higher conductivities than those tested at 7 or 28 days (dashed lines).

Looking at the effect of graphite size, the coarse graphite (blue lines) had a percolation threshold between 30wt% and 40wt% dosages. At 28 days of hydration the conductivity at 40wt% concentration of the coarse graphite was over nine times higher than the control cement paste with no graphite. The percolation threshold was not affected by curing age. However, an interesting finding with the coarse graphite is that the conductivity was compromised at low graphite concentration and was reduced by ~ 30% at 28 days with 30wt% concentration. This phenomenon can be explained by changes in porosity and water content in the mix. Even though the w/c remained constant, as graphite was added in the mix, the effective water/solids ratio was reduced. This resulted in less water available for electrolytic conduction and at the same time, the graphite concentration was not sufficient to create electronic conduction paths through the specimen. As a result, the conductivity of the sample was compromised due to a reduction in the effective water in the mix. By observing the medium graphite (green lines), clearly the percolation threshold was moved to a lower concentration, between 20% and 30% graphite addition. This percolation threshold was observed at all curing ages and conductivity reduced with curing age. At 30wt% concentration, the electrical conductivity was ~17 times higher compared to the control. Therefore, the medium graphite resulted in much higher conductivity at a lower concentration compared to the coarse graphite. Finally, for the fine graphite (red lines), the percolation threshold could again be found between 20% and 30%.

the fine graphite had a conductivity twenty-eight times higher than the control and a 37% higher conductivity compared to the medium graphite at the same dosage.

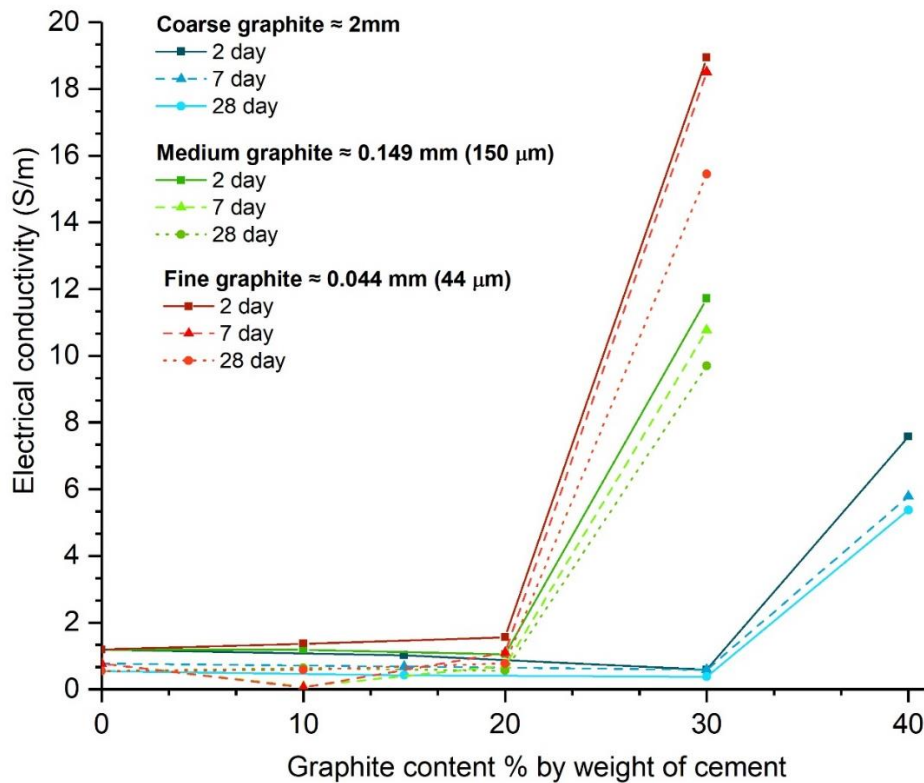


Figure 6-3: Effect of graphite size and dosage on the electrical conductivity of CEMI pastes ($w/c = 0.45$)

The main finding from the above results is that the finer the graphite, the lower the dosage that is needed to establish a percolation threshold and the higher the conductivity at that dosage compared to a coarser graphite. These results agree with the literature and can be explained by packing density principles. As discussed by Nagata et al. (1999), the formation of conduction paths related to the particle size and aspect ratio of the conducting graphite filler. The finer graphite particles tend to stabilise in dense configurations resulting in more interparticle contacts compared to coarser materials, creating inevitably more paths for current to pass through (Sbia et al., 2015). Bhattacharya et al. (2008) used graphite powder in cement pastes with a particle size of 10-20 μm , which is much smaller than the fine graphite used in this thesis (of 44 μm), and found that the percolation threshold was at $\sim 10\text{wt.}\%$ graphite, as compared to 20wt.% here, and agreed with the trend observed with size. Fan et al. (2011) found a percolation threshold of $\sim 20\text{wt.}\%$ when a graphite of 74 μm

size was used (which is roughly twice the size of the fine graphite and half the size of the medium graphite used here). This agrees well with the findings of the work reported here showing that this graphite size range gives the same percolation threshold value. Frattini *et al.* (2017) used a very fine graphite with a d_{50} of $4.5\mu\text{m}$ at concentrations from 5wt% to 80wt%. The authors found that the electrical conductivity did not increase linearly with graphite concentration, while a percolation threshold was found between 40wt% and 50wt% graphite. This percolation threshold is much higher compared to this study, where for the fine graphite it was at $\sim 20\text{wt}\%$, however, the difference could be due to the different mix methods and curing ($w/c = 0.5$, CEMIII/A-LL 42.5R and the specimens were oven-dried for 48 hours at 110°C after 28 days of water curing). Pichór and Frac (2019) showed that adding 2–3 wt% of expanded graphite (a modified graphite structure with a “worm-like shape” that consists of spaced layers and has a higher electrical conductivity compared to natural graphite) to cement composites was sufficient to form conductive networks (in comparison to the addition of 30–40 wt% of graphite powder). Recently, Fulham-lebrasseur *et al.* (2020) found that 10% of graphite powder with size $<20\mu\text{m}$, in combination with other conductive fillers (steel fibers and carbon fibers) was efficient in improving the electrical conductivity of the cement composites. Therefore, the percolation threshold of electrical conductivity depends on several factors and the critical volume fraction needed could reduce by using finer graphite or other types, such as expanded graphite.

At very high concentrations, the graphite-cement pastes were very weak and fragile. As an example, Figure 6-4 shows the prisms with the medium and fine graphite products at 30wt% concentration each and it can be seen clearly that the paste was very fragmented and the mix was not consistent. As presented in Table 5.7, as the graphite concentration increased, the compressive strength reduced dramatically, in some cases reaching even a 50% reduction in strength. These findings agree with Frattini *et al.* (2017) who also found that at high graphite dosages (70%-80% bwoc), the graphite-cement pastes had no consistency and could easily disintegrate due to insufficient volume of cement and therefore, it would be difficult to use them as electrically conductive pastes. Fulham-lebrasseur *et al.* (2020) also found that 10wt% graphite powder reduced the compressive and tensile strengths of the composites due to the amount of absorbed water and hence, the water content should be adjusted to ensure sufficient mixing and compaction. Therefore, this is a limitation of applying the graphite-cement paste as a conductive layer. In this case, $40\times 40\times 160\text{ mm}$ prisms

were tested to obtain reliable readings from the 4-probe technique and therefore it was more difficult to sufficiently compact the mixes. Nonetheless, to ensure sufficient cohesiveness and compaction, the depth and application technique of the coating should be controlled.

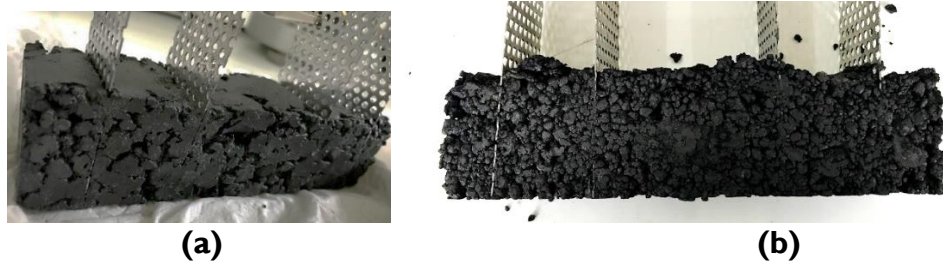
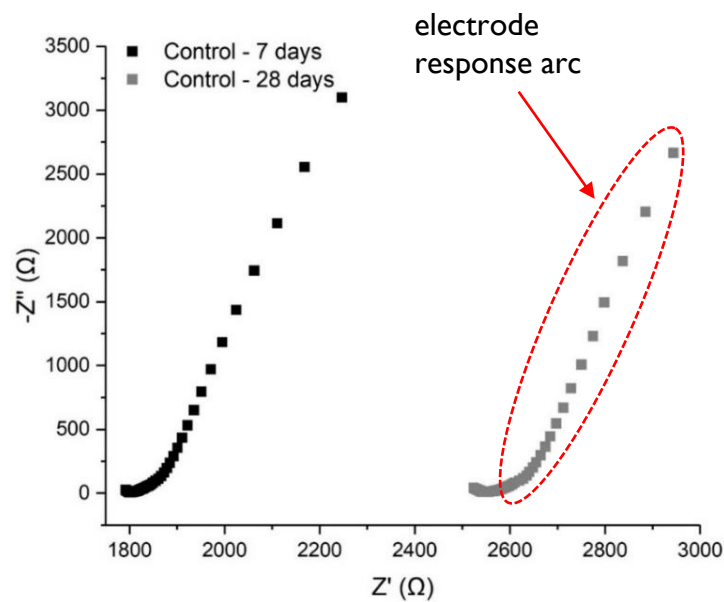


Figure 6-4: Photos from graphite-cement paste prisms at 30wt% concentrations (a) medium graphite (b) fine graphite

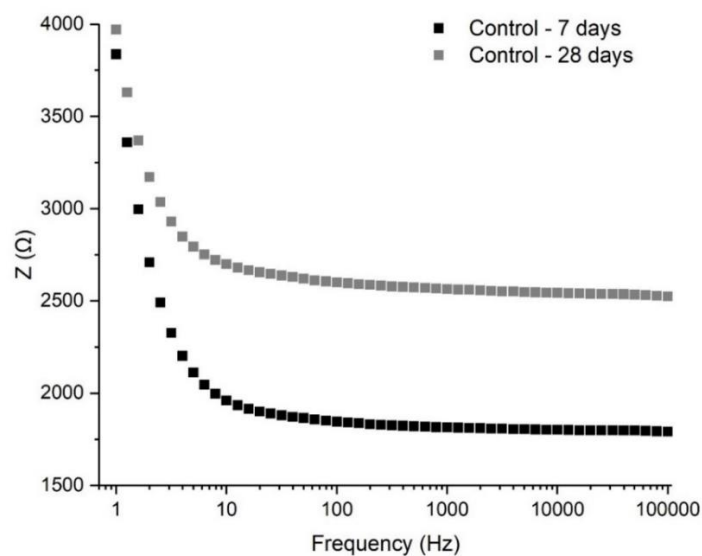
6.2.2. Effect of natural graphite using electrical impedance spectroscopy

To better understand the electrical behaviour of cement pastes with natural graphite, electrical impedance spectroscopy (EIS) testing was carried out. Alternating current (AC) impedance spectroscopy can be used to characterise the electrical parameters of the materials and to investigate the frequency-dependent electrical response of the materials as well as the material-electrode interface (Li and Li, 2019). By applying an AC current with a set amplitude over a range of frequencies, the response of the specimen could be measured in terms of magnitude and phase angle. A 2-probe set up with embedded electrodes was followed with AC instead of DC which eliminated the risk of polarisation (Section 3.3.4.3). The size of the specimens were reduced by half (20x20x80 mm) and two dosages were selected for each graphite type, one at 10wt% and one at the start of the percolation threshold (either 20wt% or 40wt% for the coarse graphite). Triplicate tests were run at 7 and 28 days. The results of the EIS testing are shown in the form of Nyquist plots, with the real part of the impedance shown in the x-axis ($Z'(\Omega)$), and the imaginary part in the y-axis ($-Z''(\Omega)$) and the average of three samples is represented with each Nyquist plot. The Nyquist plot contains semicircles or arcs, and their diameters correspond to the resistances of the different components in the composite microstructure (Wansom *et al.*, 2006). As illustrated in Figure 6-5(a) the control sample was tested first (cement paste w/c = 0.45) and it was found that the real part of the impedance (x-axis) had a very short range irrespective of the test age. Only a very depressed arc was formed for the main material, whilst the

incomplete right arc (marked with a red circle), corresponded to the response of the electrodes that were used for the measurements (Wansom *et al.*, 2006). Therefore, the cement paste material was not responsive to the AC current, which is because the paste has a very low conductivity to electricity. From Figure 6-5 (b) it is observed that irrespective of frequency, the electrical resistance of the sample increased from 7 to 28 days which was expected as hydration progressed. The electrical resistance appears to be frequency dependant at low frequencies (<100Hz) and therefore, higher frequencies are suggested to get stable and reliable readings.



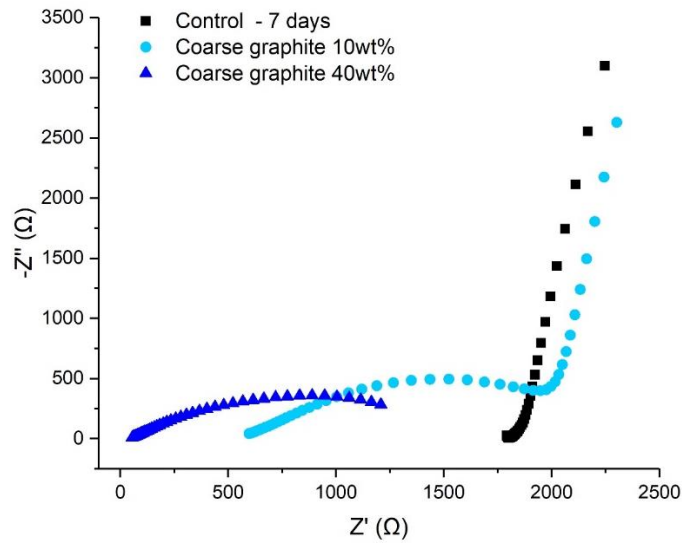
(a)



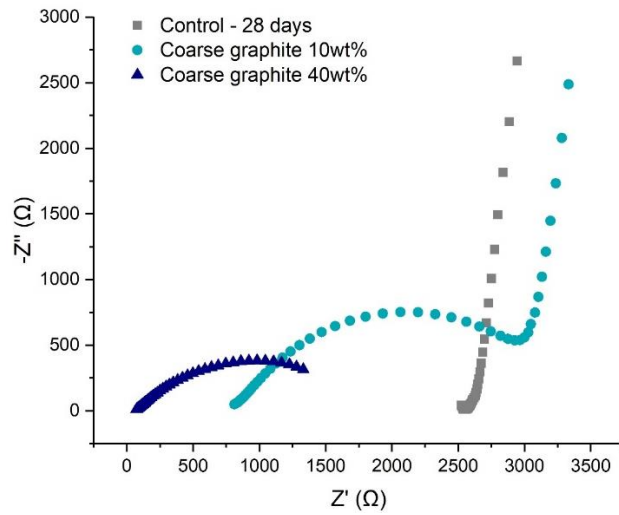
(b)

Figure 6-5: Control cement paste ($w/c = 0.45$) (a) Nyquist plot (b) frequency vs resistance plot

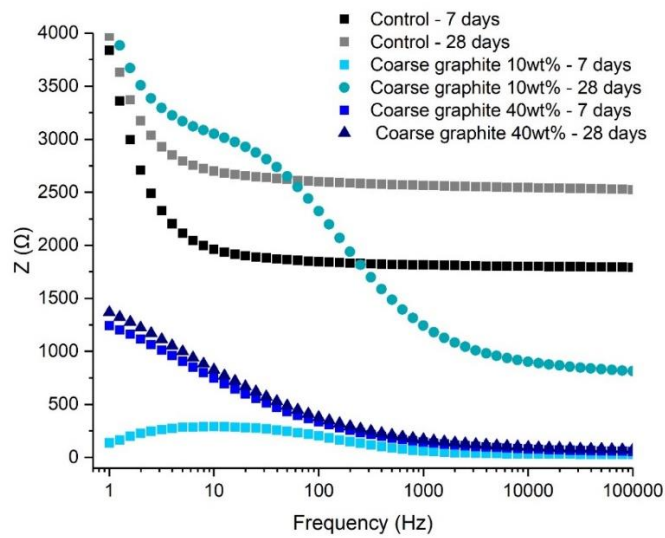
The samples with the coarse graphite (2mm), were investigated and the conductive filler was added at 10wt% and 40wt% dosage, with the former being below and the latter above the percolation threshold. The Nyquist plots for 7 and 28 days are shown in Figure 6-6(a-b), whilst the resistance vs frequency plot is illustrated in Figure 6-6(c), with the control measurements included in all graphs for comparison. As the hydration progressed from 7 to 28 days, the Nyquist plots shifted to the right, at higher true resistance values on the x-axis. This was expected as the hydration progressed, and resistance increased. The incomplete electrode arc was very clear for the 10wt% graphite, meaning that the resistance measurement comprised of both the inherent electrical conductivity of the material and that of the electrode. Furthermore, the resistance of the 10wt% coarse graphite increased over time, irrespective of frequency, and this is clearly shown in Figure 6-6(c). However, when the graphite concentration reached 40wt% and exceeded the percolation threshold, the Nyquist plot was obviously different. The electrode arc was not present, and the measured response corresponded only to the bulk response of the material, meaning that a fully conductive path was formed through the cement composites. The arc of the 40wt% graphite remained almost unchanged from 7 to 28 days and no increase in resistance over time was observed. There was only a slight change in resistance for low frequencies (<10Hz) and in this range the measurements were not stable, as discussed earlier. Hence, for the control sample and the 10wt% coarse graphite, the electrical conduction depended on the water content available and therefore the resistivity increased over time as the hydration progressed. This is because at early age (7 days) there is much more water available in the mix due to un-hydrated cement and below the percolation threshold there is a combination of electrolytic and electronic conduction. Therefore, at these low dosages, the resistivity is also dependent on the water content. When the percolation threshold is exceeded, the electrolytic conduction mechanism becomes irrelevant and current travels primarily due to electronic conduction via the conductive network that is formed with the graphite particles. In this case, the continuous cement hydration which reduces the free water, has an insignificant effect on the electrical resistivity. Overall, the frequency-dependent response stabilises at ~10Hz for the control samples, ~100Hz for the samples above percolation but only ~1000Hz for the samples below percolation due to the presence of water.



(a)



(b)



(c)

Figure 6-6: Cement paste with coarse graphite (a) 7-day Nyquist plot (b) 28-day Nyquist plot (c) frequency dependant resistance

The cement pastes with the medium graphite (0.150mm), at 10wt% and 20wt% were then examined and the results are presented in Figure 6-7. The Nyquist plots at 7 and 28 days showed similar arcs, with the electrode effect present in all cases and shown by the incomplete rightmost arc. In all cases, the resistance increased as the hydration progressed, due to the consumption of free water for cement hydration which meant that less water was available for electrolytic conduction. The fact that the arcs showed both the electrode effect and the bulk material response, meant that the conductive network was not fully formed at 20wt% and that the percolation threshold was slightly higher for this medium graphite (but less than 30wt% which was shown as having exceeded the percolation threshold in Figure 6.3). From Figure 6-7(c), it was found that at all frequencies, the total resistance reduced with increasing graphite content. The electrical response was frequency-dependant until circa 10000 Hz frequency and it only stabilised at very high frequencies. However, at 20wt% dosage, the total resistance was low at high frequencies, meaning that the sample was very conductive to electricity. Nonetheless, the electrode effect was still observed with the medium graphite, and to achieve conductivity percolation, a dosage between 20wt% and 30wt% would be needed.

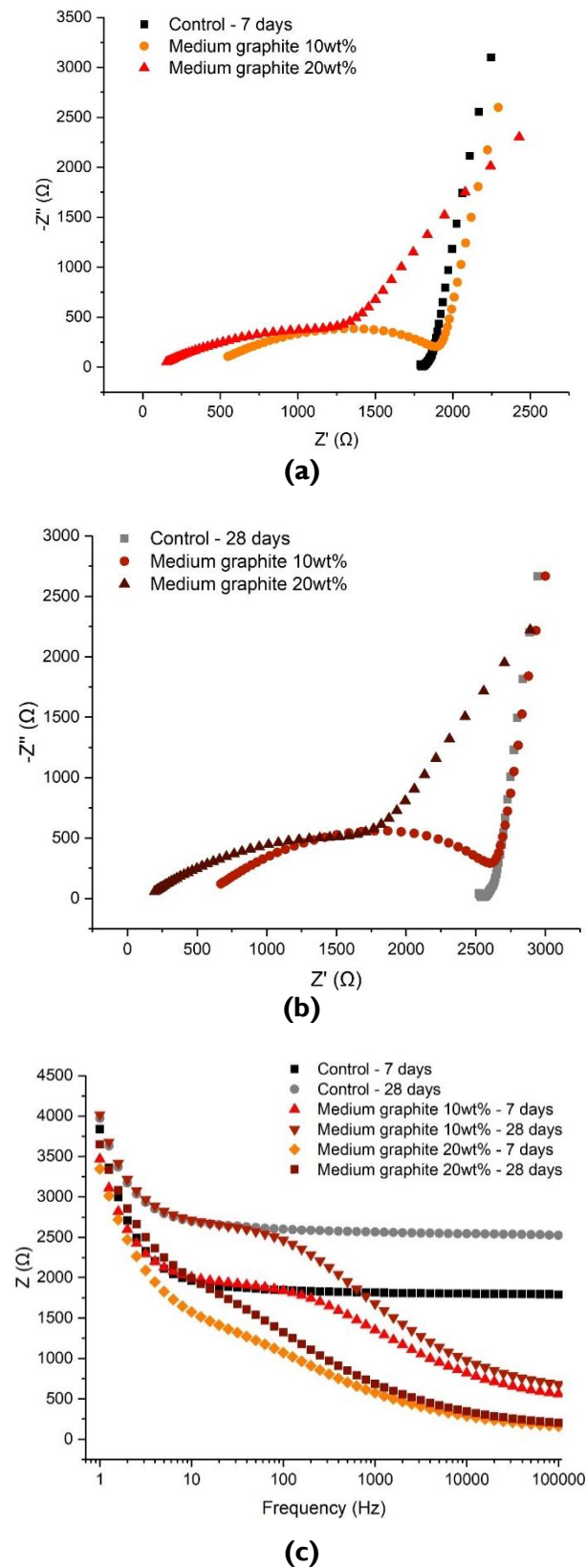


Figure 6-7: Cement paste with medium graphite (a) 7-day Nyquist plot (b) 28-day Nyquist plot (c) frequency dependant resistance

The results for the fine graphite (44 μm) at 10wt% and 20wt% are shown in Figure 6-8, and it can be seen that the Nyquist plots between the two graphite concentrations were different. The 10wt% graphite was characterised by two arcs, a full semi-circle representing the bulk material response and an incomplete arc on the right side which showed the electrode response to the electric current. For the 10wt% fine graphite, the resistance increased with age due to cement hydration, therefore, the electrical conduction was due to both the presence of water (electrolytic) and conductive filler (electronic). Instead, at 20wt%, only a semi-circle arc was found at the Nyquist plots, which remained almost unchanged with age. This meant that the percolation threshold was reached, and that the electrolytic conduction was irrelevant, with electronic conduction via the conductive fine graphite particles being the dominant mechanism. As found for the coarse and medium graphite, the electrical response of the material was frequency dependant, especially below the percolation threshold. The response stabilised at $\sim 1000\text{Hz}$ for 20wt% fine graphite but only after $\sim 10000\text{Hz}$ for the lower graphite concentration. This is due to the combination of electrolytic and electronic conduction mechanisms present in the sample as well as the bulk/electrode interface. Comparing to the medium graphite, the percolation threshold was reached at 20wt% concentration, which was not the case for the medium graphite where a higher graphite dosage was needed. This agrees with earlier findings from the DC resistivity measurements, where the percolation threshold for electrical conductivity was found to depend on the graphite size and dosage. For the coarse graphite, the 40wt% concentration showed the semi-circle arc with no electrode interface whilst this was reduced to 20wt% concentration for the fine graphite. For the medium graphite, the electrode interface was still present at 20wt%, and the conductivity was due to a combination of electrolytic and electronic mechanism. Therefore, the percolation threshold would be at a slightly higher dosage.

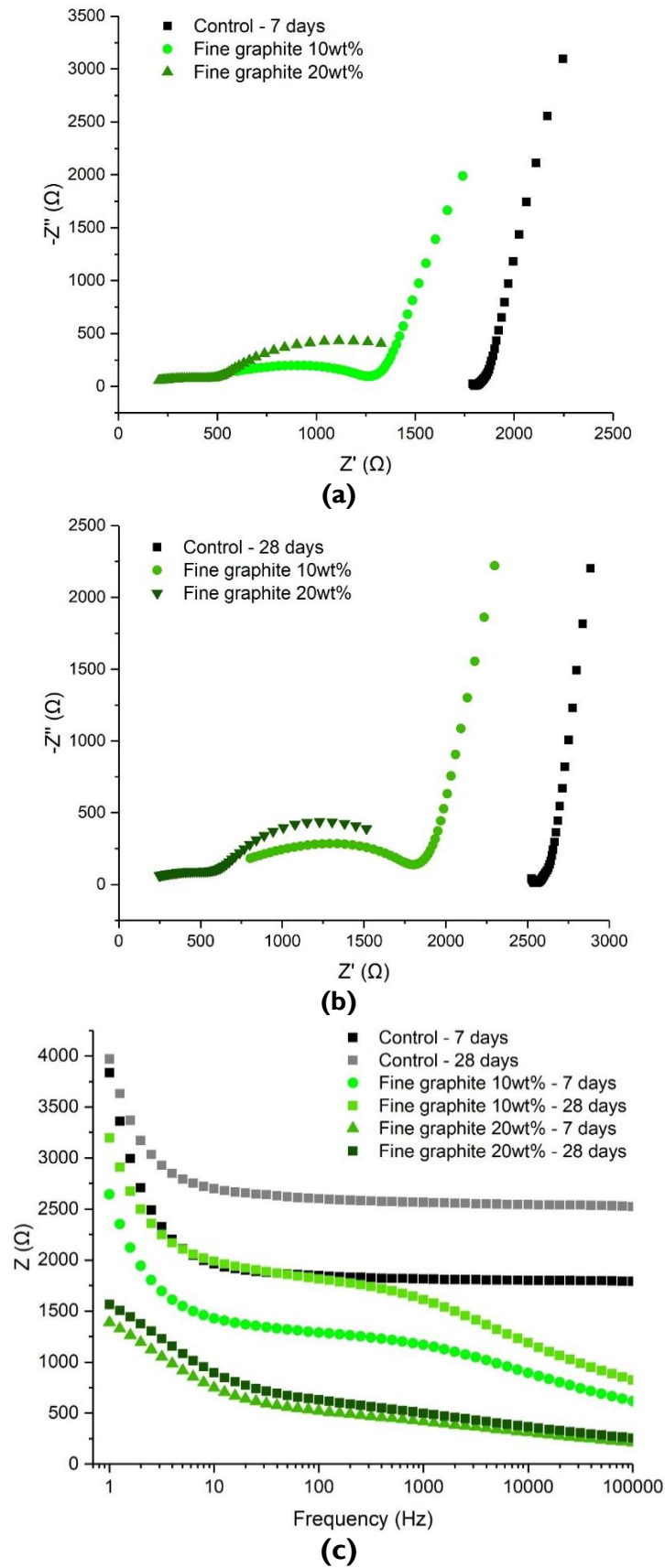


Figure 6-8: Cement paste with fine graphite (a) 7-day Nyquist plot (b) 28-day Nyquist plot (c) frequency dependant resistance

In summary, EIS allowed for a more thorough investigation of the electrical response of the graphite-cement composite samples. All graphite samples showed a lower electrical resistivity than the controls, meaning that they are more conductive to electricity. The resistivity reduced in all cases when the dosage increased from 10wt% graphite to the percolation threshold. At low dosages, electric current travelled through both the free water and conductive particles whilst electronic conduction became the dominant mechanism once the percolation threshold was reached. The measurements were frequency dependant and at low frequencies the measured resistance was higher due to electrode polarisation, whilst at high frequencies, the electrical conduction of the graphite filler along with the electrolytic conduction became the most important mechanism. This agrees with Goracci and Dolado (2020) and Belli *et al.* (2020) who found that both the electrolytic and the electronic conduction mechanisms with conductive fillers play a role and lead to a frequency dependant electrical response of the material.

6.2.3. Effect of GNPs on the electrical conductivity

GNPs were beneficial for gas and water permeability and for reducing the chloride migration when used at 0.05wt% - 0.5wt% dosages (Section 5.2.5). To investigate whether these dosages are also effective for electrical conductivity, samples with 0.05wt% and 0.5wt% GNPs were prepared here, along with a higher concentration at 1wt% GNP. Four-probe DC measurements were taken at 2, 7 and 28 days on water cured samples, whilst measurements were carried out both with embedded electrodes and with the surface resistivity meter. The w/c was kept constant at 0.45 and the dispersion protocol developed in Section 4.4 was followed. As illustrated Figure 6-9, the correlation between surface and embedded conductivity measurements was almost perfect (R^2 close to 1) in all cases. This high correlation was attributed to the fact that the samples were water cured and that the environment was very controlled. Also, this is an indication that GNPs were well dispersed between the samples used for surface and embedded electrode measurements. In all cases, the conductivity reduced as the curing progressed from 2 to 28 days, which was expected due to the ongoing hydration of the cement. However, the addition of GNPs did not result in any improvement in conductivity as all the points in each test age were almost identical. Only at 2 days some conductivity improvement was observed with 0.05wt% and 0.5wt% GNPs, with the latter enhancing the electrical conductivity by ~13% compared to the control mix. This could be due to the porous structure of the mix that allowed a

combination of electrolytic conduction through the water and electronic conduction through the GNP particles. As the hydration progressed, the cement hydrated around the GNP particles and broke any conductive paths that might have formed. The electrical conductivity with 1wt% GNP was less than the control at 2 days which is attributed to poor mixing when this high dosage was utilised. Therefore, even the 1wt% GNP concentration was not sufficient to create conductive paths and it also resulted in poor mixing, hence the dispersion protocol would need to be adjusted to ensure that higher GNP concentrations could be dispersed.

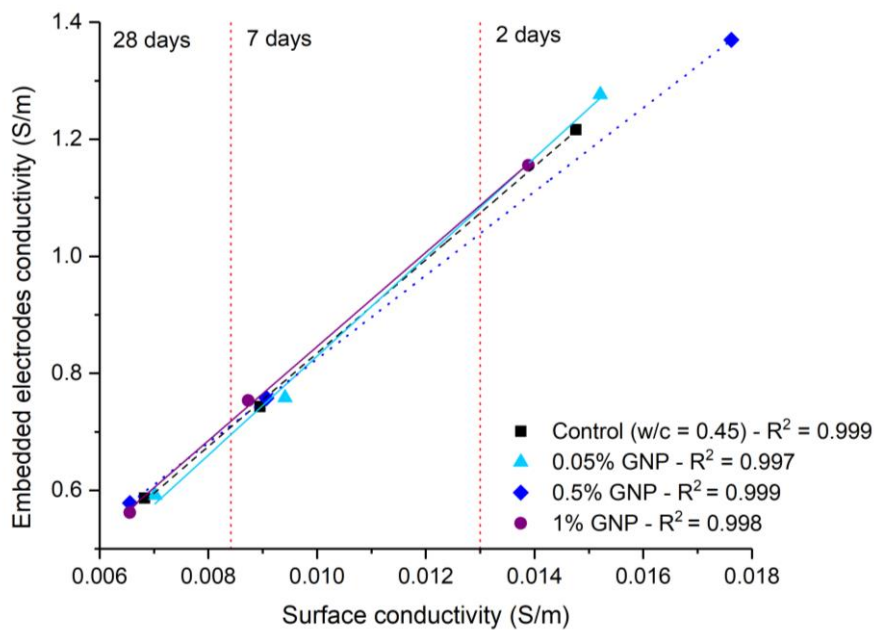


Figure 6-9: Correlation curves between embedded electrodes and surface resistivity measurements for GNP samples with different GNP concentrations

The content of GNPs was increased further, and the w/c was adjusted to accommodate these higher GNP concentrations, whilst the superplasticiser concentration and mixing methodology remained the same. GNPs at 2wt% and 3wt% were tested and to ensure sufficient mixing, the w/c increased to 0.9. Unfortunately, it was not possible to mix a control paste and insert electrodes at this high w/c ratio and superplasticiser content as the specimens could not be cast. The GNP addition made the fresh pastes more viscous and it was easier to cast them and insert the electrodes. According to Figure 6-10, the 2wt% GNP was still not sufficient to improve the electrical conductivity of the cement paste. The correlation between surface conductivity and embedded electrode measurements was also

poor with a low R^2 value. The 2wt% GNP specimens had a higher R^2 coefficient compared to the 3wt% GNP specimens due to better mixing that led to more repeatable specimens. When the GNP content was increased to 3wt%, the electrical conductivity was increased to ~ 3.0 S/m depending on the test age, however the mixing became more challenging compared to 2wt% GNPs. In both cases, the conductivity reduced with test age, with the rightmost points showing the conductivity at 2 days, the middle points representing the 7 days and the left side points representing the 28-day measurements. As discussed in Section 6.1.2, the surface conductivity measurements were two orders of magnitude less compared to the embedded electrodes, due to the contact resistance between the Recipod and the specimen.

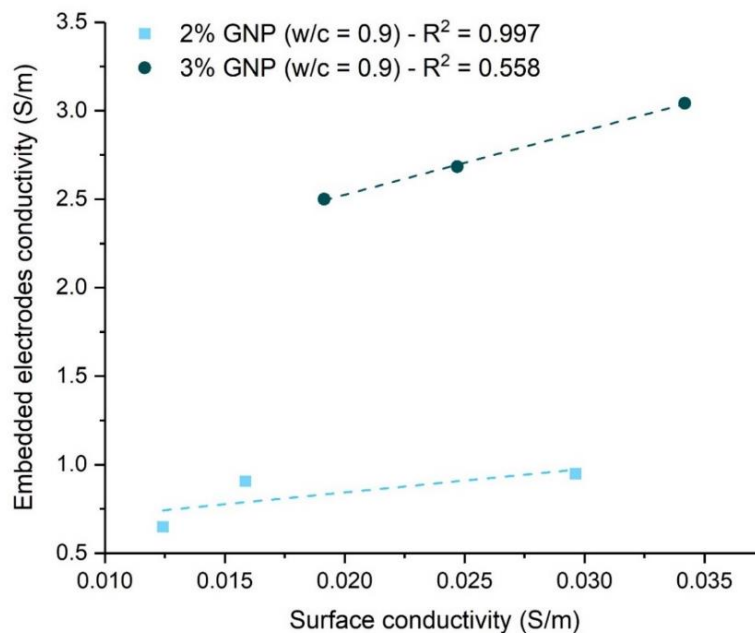


Figure 6-10: Correlation curves between embedded electrodes and surface resistivity measurements for GNP samples with different GNP concentrations

Nonetheless, when comparing the GNPs with Figure 6-3, it is clear that even 3wt% GNPs only reduced the electrical conductivity slightly and therefore even higher concentrations would be needed to create an uninterrupted electrical path. This re-introduces the dispersion challenge, as it is not possible to disperse this high concentration of GNPs without altering both the w/c and the superplasticiser content. Furthermore, if w/c and superplasticiser are increased and the GNP content is also enhanced, it is likely that the fresh, mechanical and durability properties of the cement composite will be compromised.

In summary, modest GNP additions up to 0.5wt% can be well dispersed and can enhance certain properties of the cement composites and this was investigated in detail in Chapter 5. However, these concentrations would not be sufficient to improve the electrical conductivity of cement composites to create a self-sensing mechanism. Higher GNP concentrations would result in a compromise of the other properties and therefore it would not be advisable to disperse the material in the bulk as then the GNP-cement composite would lose its structural functionality. Instead, a new approach would be to create a coating layer with the conductive filler. In this way, the base material will maintain its structural functions, whilst the coating layer would have the additional functionalities, such as an enhanced electrical conductivity. Some preliminary investigation in this area has been undertaken as part of this work and is presented in the following section.

6.3. GNP-cement pastes as electrically conductive coatings

A new strategy to improve the electrical conductivity of a coating layer is investigated in this section with the aim that electrical conductivity will allow for monitoring of damage and loading. This will counteract the dispersion problem to an extent but also allow for reduced volumes of conductive filler to be used, which will improve both the sustainability and cost performance. Firstly, the application of a water-based GNP coating directly onto the cement paste specimens is investigated, followed by the application of a cement-GNP coating. This initial investigation in the use of coatings will pave the way for further research in this area.

6.3.1. Water-based GNP coating layer

Initially, the application of the GNPs product, G2Nan paste, as a coating layer on a cement paste substrate was tested. The GNP coating comprised of water and the G2Nan paste, with an active GNP concentration of 2.5% by weight of the solution. The water-based GNP coating was applied directly onto the fresh cement paste and then the specimen was exposed to ambient temperature for curing. The reason that fresh cement paste was investigated as a substrate was to imitate site applications where concrete would be cast in layers and a final coating layer would be applied before the underlying layers have hardened or fully cured. Two techniques for applying the GNPs-coating were followed; spreading and drop coating (by applying with a pipette). As illustrated in Figure 6-11(b), the drop coating technique was difficult to implement and did not achieve a uniform coating layer, with the

droplets penetrating the substrate. In future, a pipette with a bigger opening or a more fluid solution should be used for drop coating applications. However, this might still not be a suitable technique for applying the coating in fresh cement composites. Instead, spreading appeared to be a better technique when applying the water-based GNP coating to fresh cement paste (Figure 6-11(a)). The coating could be spread more uniformly on the surface, without penetrating the substrate. After 24 hours of being exposed to ambient temperature, the discs were demoulded. The samples where the coating was spread are shown in Figure 6-11(c), and it can be seen that the water had evaporated from the coating and the GNPs were adhered to the underlying cement paste in a fairly uniform manner. However, the stability of this coating to abrasion was not tested. The specimens here were prepared by hand, however, if industrial scale equipment was used along with an experienced operator, this could be a potential technique for site applications and should be investigated further.

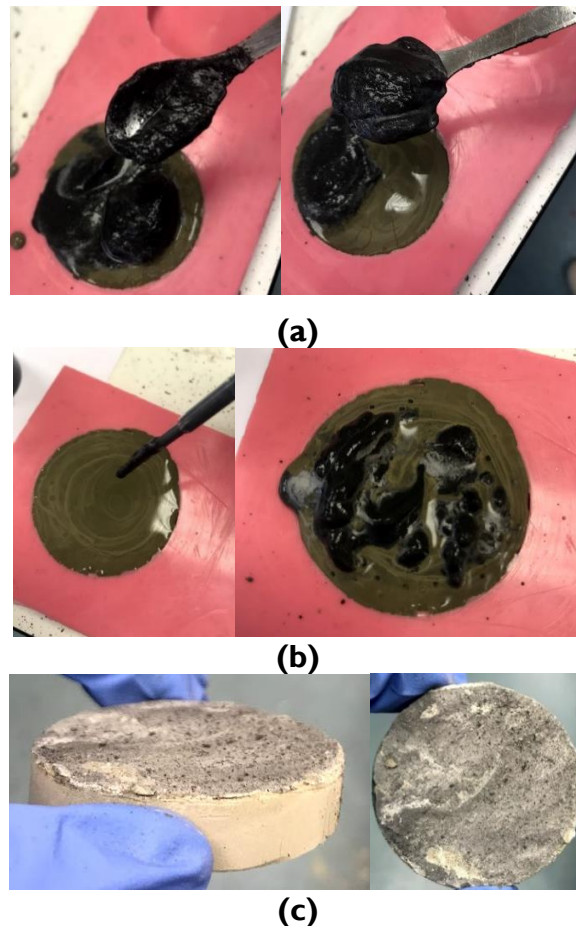


Figure 6-11: Applying a water based GNP coating directly onto fresh cement paste after 15 minutes of casting (a) spreading (b) drop coating (c) specimens after 24 hours

The spreading and drop coating techniques were also tested for a substrate that comprised of a 2-month old cement paste specimen. The substrate had $w/c = 0.45$, was cured in water for 28 days and then in ambient conditions for the remaining time. This test aimed to investigate the applicability of a water-based GNP coating on older concrete structures rather than new-build applications. From Figure 6-12(a), it was very difficult to control the uniformity with spreading. The water-based GNP coating formed a very thick layer on top of the substrate however, it was not uniform. With drop coating (Figure 6-12(b)), the coating layer was thinner and more uniform, which can also be observed in the photos by the lighter colour of the coating. However, this technique still proved to be challenging and the outlet of the pastette along with the viscosity of the coating can significantly affect the success of this technique. The samples were then left to dry for 24 hours in ambient conditions. Indeed at 24 hours, the water had evaporated from the coating layer, however, the coating could be removed by hand (Figure 6-12(c)), hence, there was no adhesion between the coating layer and the cementitious substrate. Instead, better adhesion was observed when the water-based GNP coating was applied to the fresh cement paste, as shown in Figure 6-11(c). The adhesion between the coating and the substrate could also depend on the age of the substrate, its pore structure, and the application technique as well as the nature of the coating. For example, if the substrate was very porous (eg. with a high w/c ratio or early curing age), the adhesion between the coating and substrate could be better. However, these parameters were not investigated in this work in detail and should be further tested in future work for GNP-coatings. As an example, an investigation by Marcu (2020) found that graphene inks had a “coffee-ring” effect when applied on a cement paste substrate, with a technique that aimed to imitate inkjet-printing. This effect resulted in higher graphene concentrations at the edges compared to the middle of the specimen and the author also found that alcohol-based graphene inks showed good dry time compared to water-based inks, at the expense of reduced uniformity.

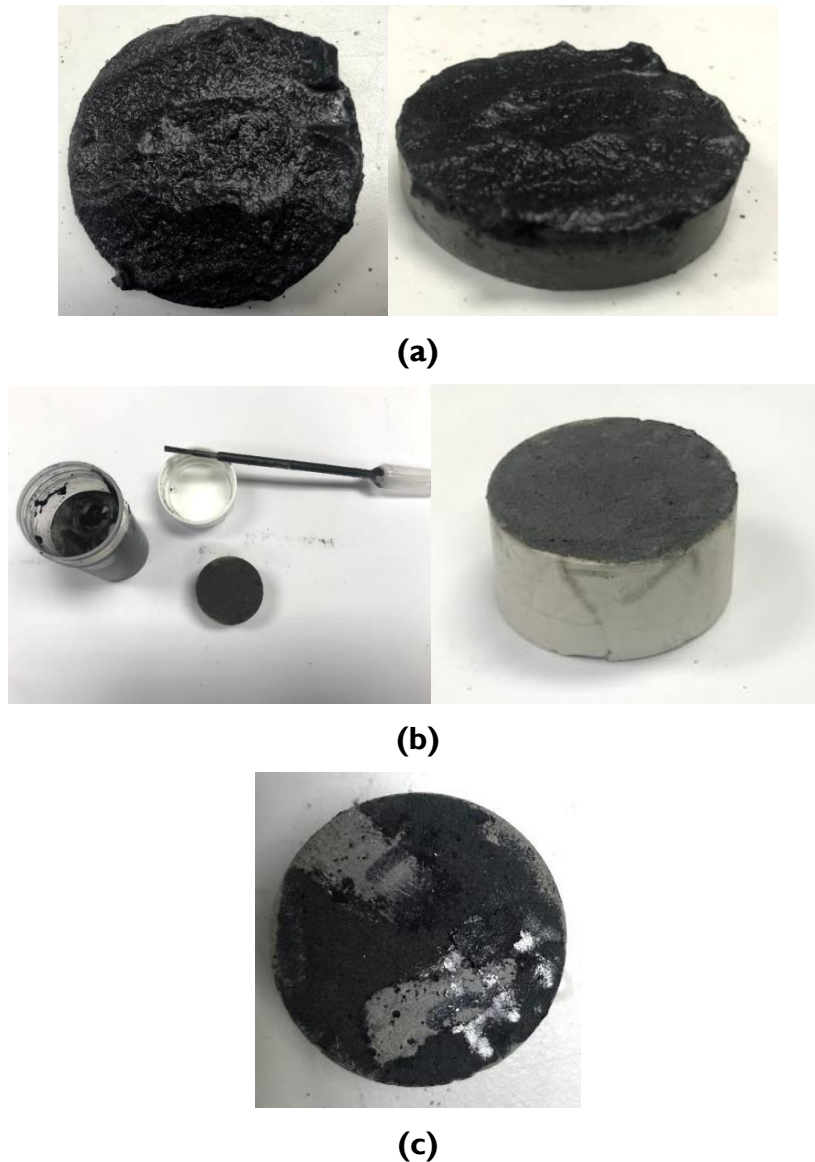


Figure 6-12: Water based GNP coating directly onto 2-month old cement paste substrate (a) spreading (b) drop coating (c) specimens after 24 hours

6.3.2. Cement-based GNP coating layer

The application of water-based GNP coatings was not very effective (Section 6.3.1) in terms of adhesion to the substrate and could depend on the application technique as well as the substrate properties. Here, the application of a cement-based coating containing GNPs was tested. In earlier chapters, GNPs were successfully dispersed in cement composites and the application of a cement-based coating on a cementitious substrate would ensure better bonding between the layers and the specimen would be a composite system rather than just two unconnected layers. The cement-based GNP coating was applied directly onto the fresh

cement paste that formed the substrate, to imitate construction applications. The cementitious substrate ($w/c = 0.45$) was cast first and remained the same in all mixes and fifteen minutes later, the cement-based GNP coating was applied. The final specimen size was 20x20x80 mm (Figure 6-13). The GNP content ranged from 2wt% to 3.5wt%, with two w/c at 0.7 and 0.9 and two polycarboxylate superplasticiser contents (MasterGlenium) at 0.99wt% and 1.76wt%. Varying the water and superplasticiser contents ensured that the mix was of sufficient fluidity to apply with the spreading technique. The specimens were then demoulded after 24 hours and the bonding between the layers was observed.

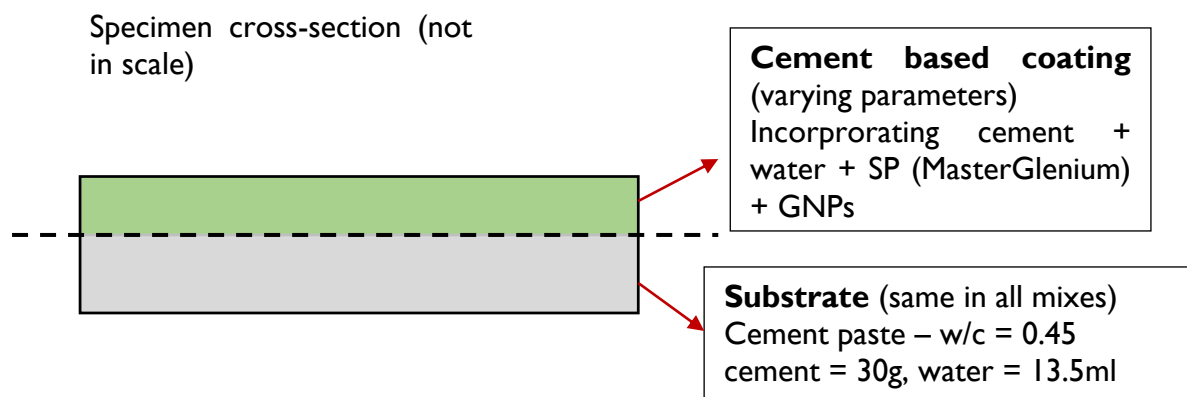


Figure 6-13: Schematic of the cement-based GNP coating application

Starting with the $w/c = 0.7$ mixes, the bonding between the substrate and the coating layer appeared to be good, as illustrated in Figure 6-14. However, the thickness of the coating was not sufficiently controlled, and it was difficult to ensure a uniform spread. In some areas the coating layer is very thin and in others, it is too thick. This could be due to the application technique and does not appear to be related to the GNP content or the superplasticiser dosage that was used. However, the poor control of the thickness could result in electrical conductivity measurements that are not representative of the whole specimen as the coating layer is thicker in some areas. The coatings with $w/c = 0.9$ were also tested to achieve higher fluidity. However, it was difficult to get a good bond and the samples were very weak. Therefore, with the higher w/c ratio, it was difficult to achieve sufficient coating strength and bond with the substrate. Again, uniform coating thickness was difficult and was not achieved. Hence, even if the cement-based GNP composite is applied as a coating layer instead of being dispersed in the bulk, new challenges are created around

uniformity and thickness of the coating layer, as well as ensuring sufficient bonding with the substrate so that the system possesses a composite behaviour.

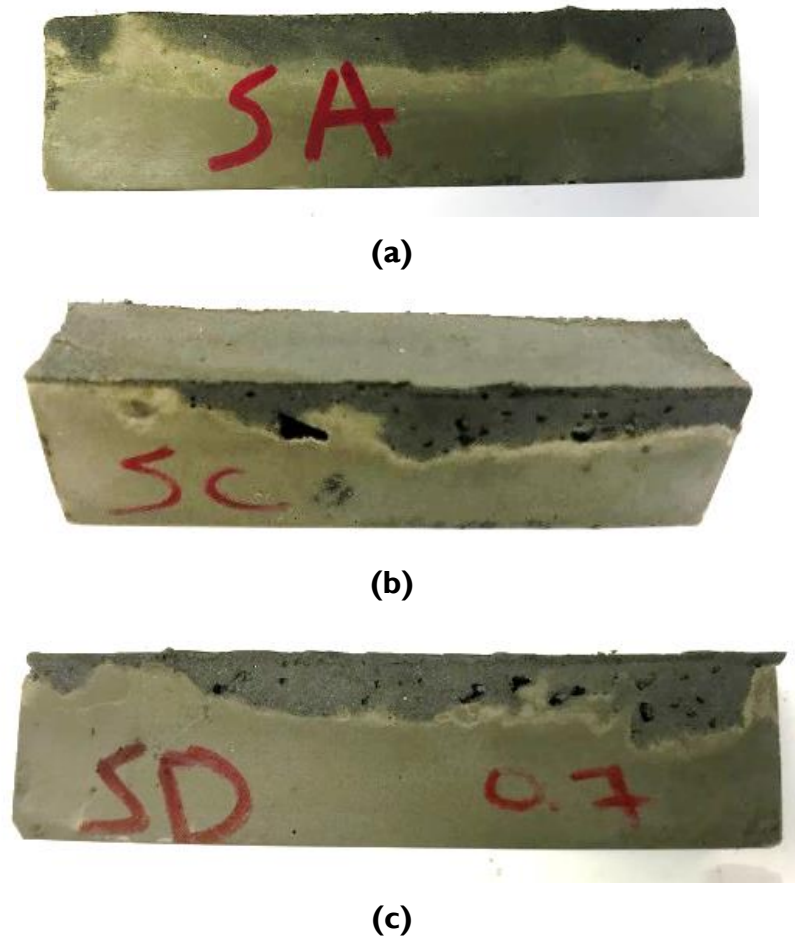


Figure 6-14: Application of cement-based GNP coating with varying GNP and superplasticiser contents on a substrate comprising fresh cement paste with $w/c = 0.7$ (a) 2wt% GNP + 0.99% MasterGlenium (b) 3wt% GNP + 1.66% MasterGlenium (d) 3.5wt% GNP + 1.66 MasterGlenium. Samples were 20 x 20 x 80 mm

The electrical conductivity of the coating layers was measured, however, the embedded electrodes technique was not possible as the electrodes would penetrate both the coating and the substrate layers. Smaller electrodes could be used, however, a uniform coating would be a pre-requisite, which was not the case here. Instead, a digital multimeter was used and the surface resistivity of the coating was used with a 2-probe technique (Figure 6-15). Only the samples with $w/c = 0.7$ were tested as the $w/c = 0.9$ were found to be very weak and therefore they would not be able to be used further. The control sample with no coating had a resistivity of 4249 kOhms. When GNPs were added at 2wt%, the resistivity of the sample was measured to be 2509.4 kOhms, whilst when the GNP content of the coating

layer was increased to 3.5wt% the resistivity reduced to 6.78 kOhms. However, even though the increasing GNP content reduced the resistivity significantly, both values show an insulating behaviour to electric current. This could be due to the measurement technique (contact resistance between surface electrodes and samples) as well as intrinsic coating properties. Nonetheless, this technique to measure the electrical conductivity was not very effective and should be refined to ensure that the true electrical behaviour of the sample can be monitored.

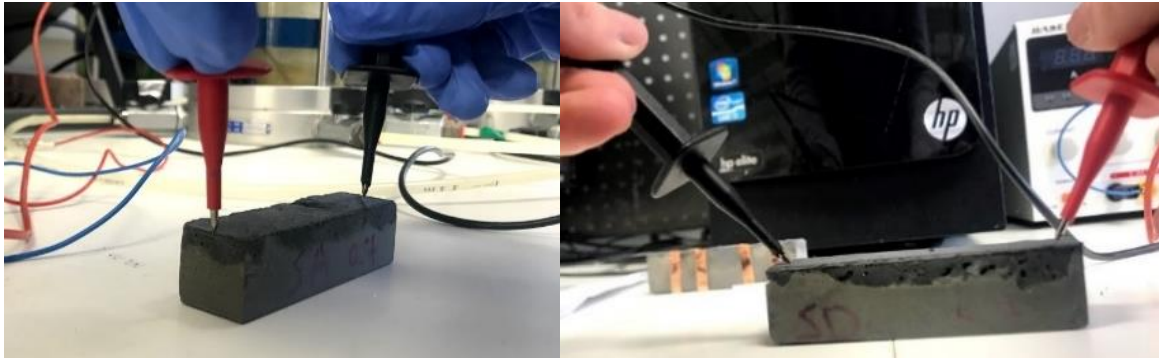


Figure 6-15: Surface resistivity measurement of the coating layer

6.4. Summary

This chapter investigated the electrical behaviour of cementitious pastes and the effect of conductive fillers. Initially, the intrinsic material properties that affect the electrical conductivity measurements were explored, including the w/c and the curing regime. Higher water contents in the mix resulted in higher electrical conductivity due to the electrolytic conduction and this was also true when the specimens were water cured compared to air curing. The electrical conductivity reduced with curing age and in the plain cement pastes, the conduction mechanism depended greatly on the presence of water. Two measurement techniques were tested, including the 4-probe embedded electrodes technique and the 4-probe surface resistivity technique. The results had a very good correlation, however, in all cases the surface resistivity measurements provided lower conductivity values due to contact resistance between the electrode and the specimen.

Following the above, the effect of conductive fillers was examined, and three different graphites of varying sizes were tested. The coarse graphite had a percolation threshold at ~30wt% - 40wt% concentration. This percolation threshold reduced to between 20wt% and

30wt% when a medium and a fine graphite were used. The percolation thresholds did not depend on the curing age. The electrical behaviour of the samples was tested further with EIS and it was found that a combination of an electrolytic and electronic conduction mechanism was present when the conductive filler was added below the percolation threshold. Instead, when the percolation threshold was reached and an uninterrupted conductive path was formed, the electronic conduction became the dominant mechanism, and the conductivity did not depend on the presence of water. GNPs were investigated as conductive fillers and this chapter built upon the findings from the earlier research. It was found that the GNP dosages that were suitable for permeability improvement, were not sufficient to improve the electrical conductivity. Higher GNP dosages were needed for an electrical conduction path to be formed, however, at these higher dosages the mixing and dispersion of GNPs became challenging. The mixing protocol was adjusted by increasing the water and superplasticiser contents; however, this was not investigated in detail.

To counteract the mixing problem, it was proposed to use a conductive coating layer rather than disperse the GNPs in bulk. Initially, a water-based GNP coating applied on both fresh cement pastes and on two-month-old samples using two techniques; spreading and drop coating. Spreading was more suitable compared to drop coating, however, the water-based coating was not effectively adhered to the substrate. A cement-based GNP coating was tested, which provided better adhesion with the substrate, but it was difficult to control the thickness and uniformity of the coating layer. This investigation in coatings was preliminary and has created a clear need for further research in this area. Firstly, the effect of the substrate on the adhesion needs to be investigated as the porosity, surface texture and water content of the substrate can significantly affect the interaction and bonding with the coating layer. The conductivity and application of the coating itself must be further explored, in terms of optimising the dispersion protocol for achieving higher GNP concentrations and using a suitable application technique. Measuring the electrical conductivity of thin coatings and ensuring that their behaviour is representative of the whole specimen is also necessary. This research paves the way for further exploration in smart coatings and structural “skins” with advanced functionalities, such as a self-sensing mechanism.

Chapter 7. INDUSTRY SURVEY AND LIFECYCLE ASSESSMENT ON THE USE OF GRMs IN CEMENT COMPOSITES

In addition to the experimental work, an industry survey was carried out in Nov-Dec 2018, to understand the industrial perceptions on the use of graphene in cement composites. Furthermore, a Lifecycle Assessment (LCA) was performed to investigate the impact of GNP production and its incorporation in concrete. This chapter firstly presents the industry survey methodology and findings, followed by the LCA methodology and results.

7.1. Industry survey

The motivation for the industry survey was to gain a better understanding of the problems associated with concrete repairs and of the industry perceptions of structural-health monitoring (SHM). Moreover, the survey aimed to identify the key opportunities and barriers for using GRMs in cementitious composites. The findings were published in the International Conference on Smart Infrastructure and Construction (ICSIC) in Cambridge in 2019 (Papanikolaou, Al-Tabbaa, *et al.*, 2019). A ‘light-touch’ review was carried out prior to the survey and ethical approval was granted by the University.

7.1.1. Industry survey design

The design of the survey was based on a similar approach followed by Orr *et al.*, (2019) for an industry survey on material efficiency, run in early 2018. The survey here comprised of given lists, 5-point Likert scales and free text questions and all questions were optional. The given lists, involved a set of predetermined answers to the question where the respondents could select one or two choices; the 5-point Likert scales were weighting scales from 1-5 where the respondents had to provide a weighting on the question that was asked; and free text questions were answer boxes that did not limit the text that the participants could provide as a response. In total, fifteen questions were asked, that could be grouped in four main sections (Table 7.1). The types of questions have been annotated as A, B and C, where type A is a given list question, type B is 5-point Likert scale question and type C is a free text question. Section 1 focused on the performance issues encountered with concrete structures and associated repairs; Section 2 focused on the industry’s views on structural health monitoring and the use of sensors; Section 3 focused on the use of GRMs in

construction and finally Section 4 gathered information about the respondents' background. The industry survey, in the form of a questionnaire (Table 7.1), was provided online using the survey tool "SurveyMonkey". The questionnaire was chosen because it could reach many participants and therefore the results would be more reliable and representative of the industry. Furthermore, questionnaires are free from bias of the interviewers as the respondents answer on their own and also they have adequate time to consider their answers (Kothari, 1990).

A questionnaire, as a survey method, has certain limitations. These include difficulty of interpreting free text questions; lack of knowledge that leads to uninformed opinions and an inherent inflexibility in amending the questions once the questionnaire has been sent out (Kothari, 1990). To overcome the first limitation, only two free text questions were used. However, closed questions should also be used with caution as the given lists could be influenced by the bias of the interviewer (Oppenheim, 2001). The potential limited knowledge of the respondents was a main limitation of this survey, especially for the questions in Section 3, because research in GRMs is limited and their effect on concrete structures has not been investigated thoroughly. Nonetheless, it is expected that the industry respondents that had some years of experience and exposure to new materials would be able to identify the perceived opportunities and barriers for graphene-cement composites. For this reason, Questions 13 and 14 were introduced to understand the professional qualifications and years of experience of the respondents.

Prior to distribution, five volunteers, with prior or current industry experience, reviewed the survey to ensure that the questions were clear and presented in a logical sequence (Gillham, 2000). Furthermore, they checked that there were no leading or assumptive questions and that the closed questions covered a wide range of possible answers so that the questionnaire was free from interviewer bias (Arksey and Knight, 1999). The survey link was distributed via email (starting from 21/11/2018) to approximately 500 professionals working in the construction and materials sectors in the UK and abroad, who were chosen based on the author's contacts. However, it was not possible to determine how many times the survey link had been forwarded to other professionals. Although the survey was anonymised, the respondents were asked to identify their organisation's area of operation, years of experience and personal qualifications to ensure that the results were representative of the wider industry. A four-week response period was allowed, and the

response rate was monitored daily. No email reminders were sent as the response rate was adequate.

Table 7.1: The industry survey questions

	Questions	Type
Section 1	1. What are the most common performance issues that you have encountered with concrete structures?	A
	2. For two cases within the last three years where concrete issues arose, how would you rate the degree of concrete failure?	B
	3. What are the most common effects of poor concrete performance that you have encountered?	A
	4. Typically, when concrete requires remedial work, how long does it take before the concrete is fully repaired?	A
Section 2	5. Is your company involved with the inspection and monitoring of concrete structures (such as sensor installation, carrying out and commissioning inspections etc.)?	A
	6. Do you have a positive/negative outlook towards external sensors on concrete structure?	B
	7. What are the most common challenges you have encountered with sensors?	A, C
Section 3	8. Are you familiar with graphene materials and their potential applications in construction?	A
	9. The following are material properties that could be improved to an extent if graphene is added in concrete. Please choose the top 2 areas where you would like to see improvement.	A
	10. What do you see as the main barriers to using a graphene-reinforced cement composite in construction?	A
	11. How long do you estimate that it will take for such a novel material to be commercialised and used on a construction project?	C
Section 4	12. What best describes your organisation?	A
	13. What is your job title, professional qualifications? (This question will be used for credibility weighting in the research).	C
	14. How many years of professional experience do you have? (This question will be used for credibility weighting in the research).	A
	15. Which is the primary country where you operate?	C
Type A: Given list, Type B: 5-point Likert, Type C; Free text		

7.1.2. Industry survey results

There were 78 responses to the survey, which is a 15% response rate assuming the email link was only viewed by the initial recipients. Question 11 was completed in 57 responses only and the remaining of the questions had at least 76 responses. Therefore, all 78 questionnaires were included in the analysis of the results. Data on the respondents' background is presented first for context, but these were the last questions to be asked on

the survey (Section 4). As illustrated in Figure 7-1, over half of the respondents came from a contracting organisation, whilst 22% came from consulting. Contractors and subcontractors are mainly involved with the construction of infrastructure whilst consultants primarily work in design of structures. However, it is not exclusive that someone from a contracting background does not work in design and vice versa. Infrastructure clients and materials manufacturers (including chemical and cement companies) accounted for 10% each whilst 7% represented academia, trade bodies or technology vendors. Since half of the respondents were from contracting organisations, the results could be biased towards construction-phase issues and perspectives. Over half of the respondents had more than 15 years of professional experience and 30 respondents (39%) had 5-15 years of experience so they are expected to hold mid-senior positions. Some of the respondents were Technical Directors and Chief Engineers in their organisations, with 8% being at Fellow level, whilst 28% held a PhD and/or were professionally qualified. From the 78 respondents, 61 operated in the UK whilst the remaining operated in countries including mainland Europe (Germany, France, Italy), Australia, New Zealand and Hong Kong.

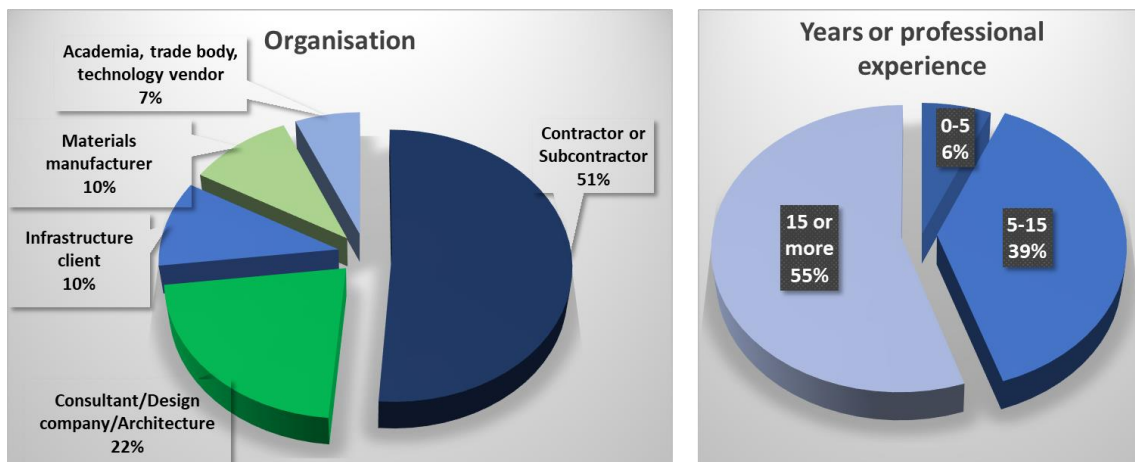


Figure 7-1: Survey respondents' organisation background and years of experience

7.1.2.1. Performance issues with concrete infrastructure

Cracking due to poor workmanship was found to be the most common performance issue (48.7%), followed by cracking due to poor specification and material performance (38.5%) as shown in Figure 7-2. Poor workmanship is a construction-phase issue, however since half of the questionnaire respondents came from a contracting organisation, it might not have represented the views of the wider industry. Water ingress and reinforcement corrosion

were also found to be important issues with ~30% of the responses each. This is an indication that barrier properties of concrete that would prevent or delay reinforcement should be considered when developing new materials. “Other” included issues with design; insufficient performance in tension without reinforcement; chemical attack; chloride/carbonation attack and inadequate training of those placing the concrete or supervising the works. These results agree with a survey run in 2018 by Gardner *et al.*, where cracking (including due to poor workmanship) was found, by 90% of the respondents, to be the most common issue (Figure 2-2). Water ingress was also experienced by 73% of the respondents, which is a much higher percentage compared to this survey.

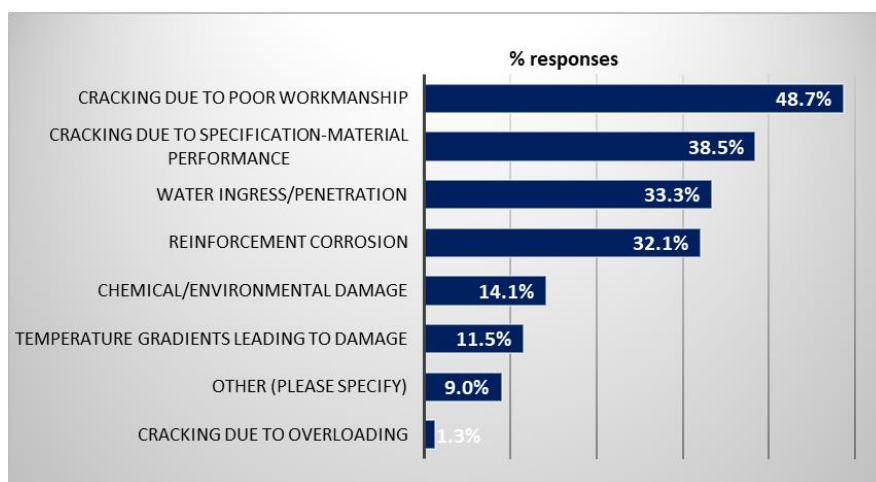


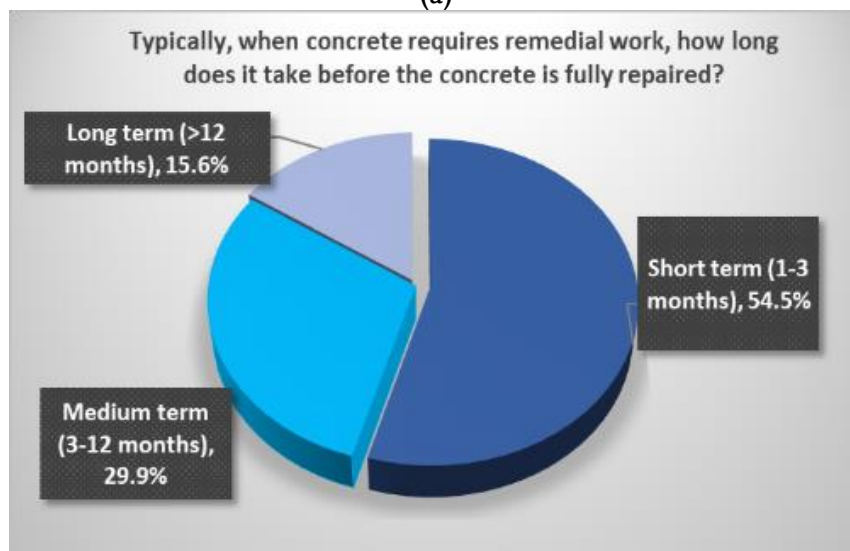
Figure 7-2: Performance issues encountered with concrete structures (up to two choices allowed)

The survey participants were asked to rate the concrete failures they had encountered in the last three years from mild (=1) to strong (=5). The average number on this 5-point Likert scale question was found to be 2.01 (76 responses) which showed that despite the occurrence of concrete failures, they were usually mild/moderate. Figure 7-3 shows that immediate repair of the structure was the most common outcome of poor concrete performance (66.7%), followed by enhanced structural monitoring (41%). These findings agreed with the survey by Gardner *et al.* (2018), where the need for repairs and regular structural monitoring were found to be the most common consequences. The potential damage to the company brand (i.e. the company being associated with poor quality work) and change in the planned maintenance regime were also outcomes of poor concrete performance. For “Other”, the responses related to programme delays and resequencing of

works. Inconvenience to public due to loss of service of the structure was found to be an important consequence by Gardner *et al.* (2018), however, this was not mentioned by any of the respondents here. Finally, when concrete requires remedial work, over half of the respondents (54.5%) said that repairs take place within 3 months, 29.9% said that it takes place within 3-12 months, whilst 15.6% said that it takes longer than a year for the repair to take place (Figure 7-3).



(a)



(b)

Figure 7-3: Outcomes of poor concrete performance (a) and repair timescales (b) obtained from the survey

Some of the questions from Section I were similar to those asked by Gardner *et al.* (2018). The aim of Gardner's survey was to understand the problems encountered with concrete construction and the potential benefits of self-healing concrete, however, that survey focused on semi-structured and structured interviews with a small number of participants.

These participants were pre-selected for in-depth and structured interviews. Instead, the survey presented here, aimed to reach a wider number of professionals within the construction industry and get their views on the use of GRMs in cement composites. The survey link was sent to over 500 professionals, with varied backgrounds in terms of years of experience and type of organisation where they work. Therefore, the questions around concrete damage had to be repeated in this survey to get the views of the respondents to the questionnaire, before moving on to the inspection of structures and the use of GRMs.

7.1.2.2. Inspection and monitoring of concrete structures

The questionnaire then focused on the use of sensors for SHM as it was recognised (*Question 3*) that enhanced monitoring of the structure was a common outcome when concrete was damaged. Just over half of the respondents said that their company was involved with inspection and monitoring of concrete structures (such as sensor installation, carrying out and commissioning inspections etc.), whilst the rest said either “No” or “I don’t know”. However, based on the experience and qualifications of the survey sample, all respondents were expected to have had some understanding of how SHM worked. When asked whether they have a very negative (=1) or very positive view (=5) of external sensors for concrete structures, the average was 3.5, showing an inclination towards a positive view. However, due to the large number of respondents that were not actively involved in SHM, it was not clear whether this finding was reliable and representative of the wider industry. The cost of installation, data interpretation, lifetime and durability of the sensors were frequent concerns when using sensors for structural sensing, as shown in Figure 7-4. 14% of the respondents have not encountered any challenges with sensors, whilst in “Other”, respondents quoted the lack of client support for lifecycle management as a key challenge when using external sensors.

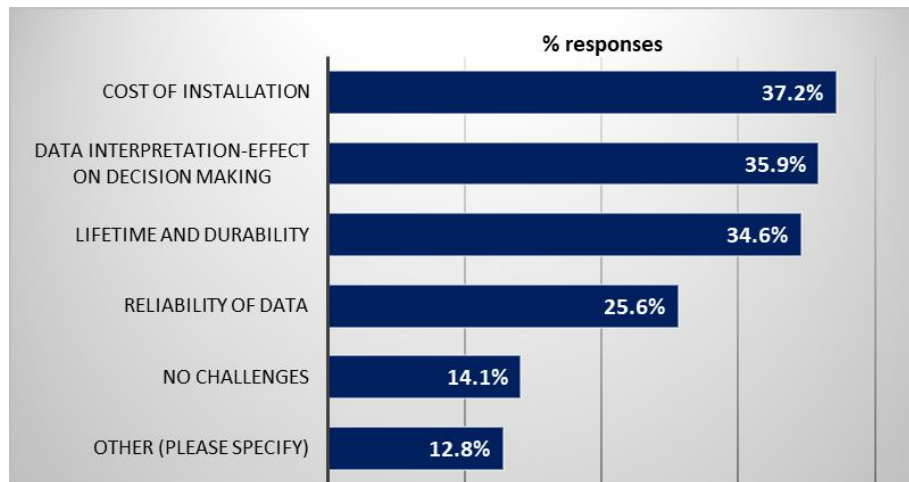


Figure 7-4: Common challenges associated with sensors for structural health monitoring identified from the survey results.

7.1.2.3. GRM-cement composites

The last section of the survey focused on the use of GRMs in concrete structures. When asked about their familiarity with GRMs, 37% of the respondents responded positively and 63% negatively. This is a slight improvement compared to a similar survey run in 2017, where only 32% of the respondents (34 in total) were familiar with GRMs (Papanikolaou *et al.*, 2018). This finding was expected as research in this area is still very novel. The participants were also asked to identify the main opportunities and key barriers for GRMs in concrete structures (Figure 7-5). Improvements in tensile and flexural strengths were chosen by 41% of the respondents as the main opportunity, closely followed by the potential for generating a self-sensing mechanism (39.7%). Gardner *et al.* (2018) also found that a material which detects changes in the environment was of interest to half of the respondents; however, self-sensing was not the focus of their survey. Durability performance, including a reduction in porosity, an improvement in chloride attack resistance and a reduction in the water penetration, were considered secondary opportunities for GRMs. This could be because half of the respondents came from a contracting organisation and would not often deal with the long-term effects of poor concrete performance. Improvement in compressive strength was found to be the least interesting point for engineering professionals. “Other” refers to the overall reduction in concrete sections due to advanced performance that would improve the sustainability, as well as to an improvement in fresh properties and the thermal conductivity.

From Figure 7-5(b), the potential upfront cost of the material was found to be the biggest barrier (61.5% of the participants). It was cited by a participant that “As I understand it, the cost of graphene is prohibitively expensive and the lack of availability for use on a commercial scale will inhibit growth.” This is followed by lack of industry standards and guidance (50%) and technical understanding (35.9%). Participants focused on the dispersion, flowability and long-term performance challenges with some quotes as follows: “ensuring a consistent spread of the material throughout each batch of concrete”, “Still need 75mm slump for pumping. Needs a good flow to get around the rebar and fill the shutter properly” and “Confidence in long term behaviour”. 1 of the 78 respondents mentioned health, safety and environmental effects as a potential barrier for GRMs by saying “Small particulates are particularly (very) harmful. Civil construction does not show suitable levels of control to permit materials as dangerous as these for general use. Use may only be acceptable if proper control can be implemented and through life cost, including disposal can be assured”.

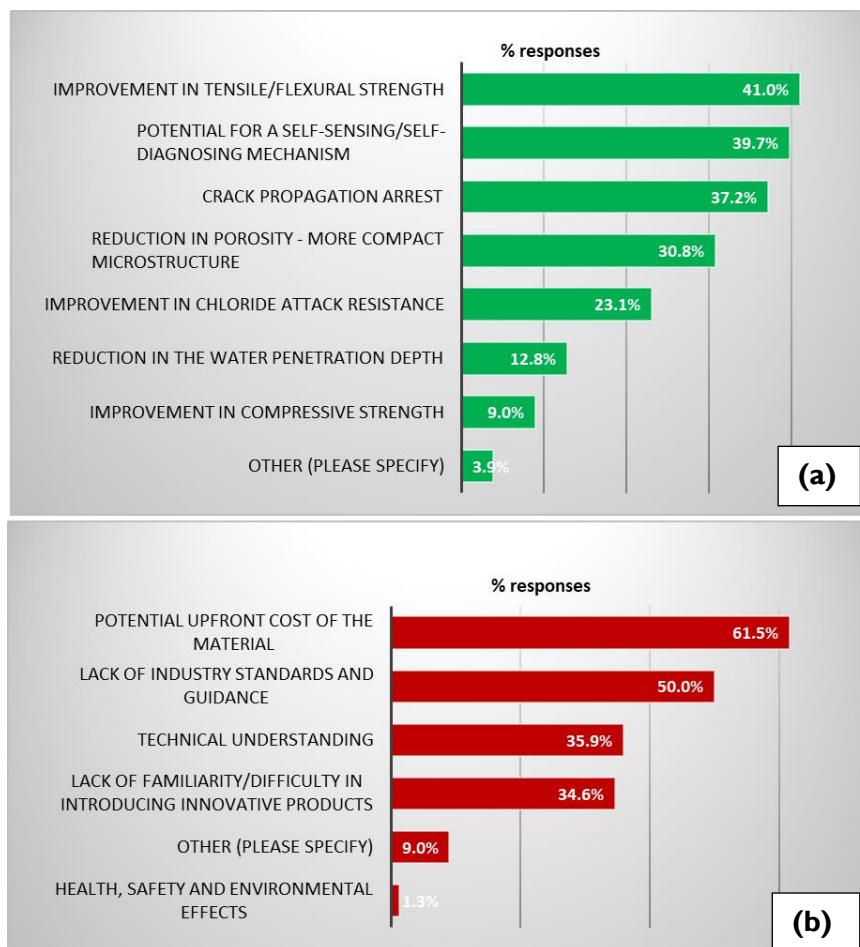


Figure 7-5: Survey responses on the (a) opportunities and (b) barriers for GRM-cement composites.

In summary, the industry survey showed that some issues with concrete structures still exist and a repair/maintenance regime is needed. SHM is often used, however, the use of external sensors is also associated with some challenges. The survey also indicated that using GRMs-cement composites for self-sensing and for durability improvement, was a promising research direction. Finally, the cost of the material along with a lack of industry standards, were found to be key limitations for using GRMs. Overall, this survey provided a useful insight and direction for the research, particularly due to its timing in relation to the experimental programme since it was carried out at the end of the first year of the PhD. This allowed for better planning of the experimental work to include the different areas that were raised by the participants, including durability performance as well as the use of GRMs for self-sensing applications. It is hoped that this survey will guide future research in GRM-cement composites.

7.2. Lifecycle Assessment (LCA)

Concrete production results in several environmental impacts such as carbon emissions and use of virgin resources (Section 2.1.1). Here, a GNP-cement composite material was investigated experimentally and was found to enhance some durability aspects whilst it also showed the potential for introducing an electrically conductive path in cementitious systems. However, the literature on the environmental impact of GNP production was scarce and there was no research to date on their impact when added in concrete. Therefore, it was deemed necessary to investigate the environmental performance of this new composite, to complement the technical findings of this research, by carrying out a Lifecycle Assessment (LCA) study. This section presents the first LCA of the use of GNPs in concrete and the findings were published in the journal of Cleaner Production (Papanikolaou, Arena, *et al.*, 2019).

7.2.1. LCA goal and scope definition

The goal of the LCA was to evaluate the environmental impacts associated with the production of the graphene nanoplatelets (GNPs), “G2NanPaste” supplied by Nanesa, that were experimentally tested in this thesis and their subsequent incorporation in a standard concrete mix. This study was intended for an audience in the infrastructure sector who are interested in using advanced materials in their projects to solve durability and monitoring

challenges. The boundaries of this study were from “**cradle-to-gate**”, which included the processing of raw materials for GNP production and the subsequent processing of the GNPs in concrete to be used in the UK. The use and final disposal of the product were not considered due to many unknowns that would exist without a focused application (e.g. a specific bridge or building where this concrete would be used). The system boundaries are illustrated in Figure 7-6.

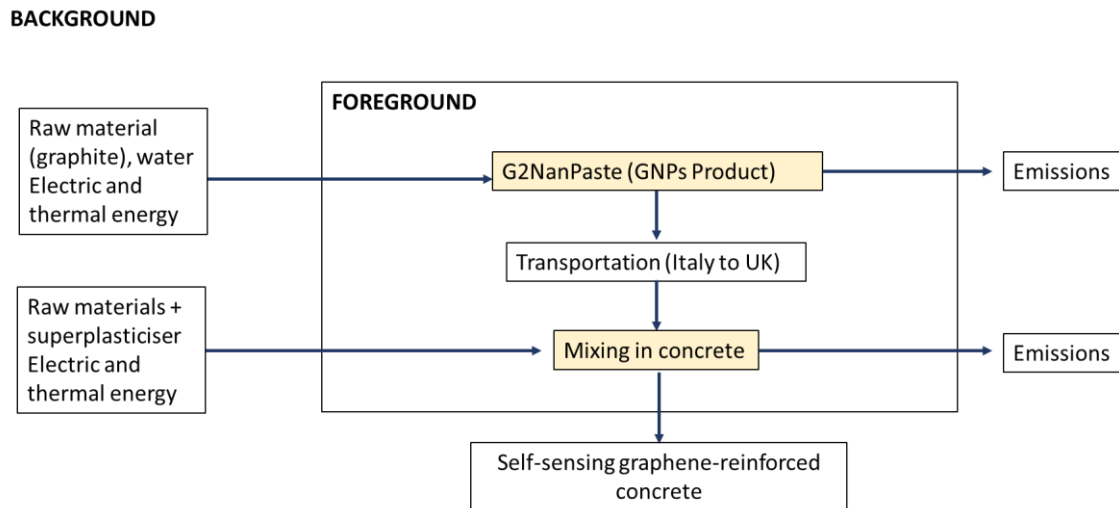


Figure 7-6: System boundaries for the GNP-concrete system under analysis

The *Foreground* system included the production of GNPs and their subsequent mixing in concrete. To narrow down the scope of the study, a single product of GNPs, produced by Liquid Phase Exfoliation (LPE), was considered. The chosen GNP product was G2NanPaste, which was also experimentally tested in this thesis. The product was produced in Italy and it was then assumed to be mixed in concrete in the UK. However, the transportation (Italy to UK), was not considered in this study because the production in Italy was considered as a worst case scenario in terms of environmental impact (Italian energy mix is more damaging than UK) and there are now alternative suppliers in the UK that produce the same product. The *Background* system included the raw materials and energy used to produce GNPs and concrete and finally the emissions. The comparative evaluation of different GRM production methods (such as chemical vapour deposition, mechanical exfoliation etc.) was outside the scope of this LCA study and would not provide a meaningful comparison as each production method is suitable for different GRM applications (Section 2.5). Following the selection of

the GNPs, it was assumed that they would be introduced in a standard concrete mix in the UK. The UK was selected because the experimental work in this thesis was carried out in a UK academic institution and therefore the LCA findings would be more representative of the experimental work.

The functional unit for this LCA study was 1m^3 of concrete. This functional unit is commonly used in the construction industry to calculate the composition of the concrete mix, estimate costs and to quantify the environmental impact, making this study easily comparable to others. Other functional units (such as the total volume of concrete required for a specific application) were not suitable due to the many unknowns that still exist on the effect of GNPs in the resultant properties of concrete.

The LCA was carried out using the software SimaPro (2015) with the Ecoinvent 3.0 database. The life cycle environmental impacts were assessed using the Impact 2002+ methodology (Jolliet et al., 2003). This methodology provides impact (mid-point) and damage (end-point) categories and gives an overall and complete analysis on the whole life cycle (Section 2.5 and Figure 2-36). These two types of results (Figure 2-36), allow different audiences to understand the results as one is more general (damage category) and the other one is more scientific for a technical audience. In this study, the results were mainly reported in terms of mid-point categories and those selected for this study were: *carcinogens* and *non-carcinogens*, *respiratory inorganics*, *aquatic and terrestrial ecotoxicity*, *global warming*, *non-renewable energy* and *mineral extraction*. A normalisation process was then carried out to identify the highest impact categories for the system (ISO-14040, 2006).

7.2.2. LCA inventory

The data for the LCA was obtained from commercial companies (Nanesa, who provided the GNPs and Costain Group) as well as from scientific literature. The remaining data were obtained from the life cycle inventory databank Ecoinvent 3.0. The lifecycle inventory of the materials, emissions and energy consumption for GNP production was based on the data supplied by Nanesa (2018). Concrete was not experimentally investigated in this thesis; however, a concrete mix design was chosen for the LCA analysis (rather than mortar or paste) since it would be more representative of bulk applications and more relevant to industry. Since no concrete was experimentally tested, the mix design that was used for the LCA was provided by Costain as it was used in one of the projects at the time when the

LCA study was undertaken and it is representative of a standard mix. Table 7.2 lists the primary and secondary data that were considered in this study and the exact composition of the concrete mix is found in Table 7.3 and is termed “Base case”.

Table 7.2: Inventory data source classification

Primary data	Source
Concrete mix design	Information supplied by Costain
Production of G2NanPaste	GNP manufacturer (Nanesa)
Graphene solution mixing - duration and energy requirements	Experimental work for duration. Nanesa for electric energy consumption
Superplasticiser composition	Information from the chemical companies
Secondary data	Source
Italian energy mix for GNP production	Ecoinvent 3.0
UK energy mix for concrete mix requirements	Ecoinvent 3.0
GNP dosage	Based on the literature review findings
Raw materials such as graphite and water	Ecoinvent 3.0

In this study, the following assumptions were made:

- GNPs were produced by LPE in Italy, Europe.
- A 100% production yield of GNPs through LPE.
- G2NanPaste (GNPs) included only water and GNPs; no chemical agent was considered as this was not disclosed by the manufacturer.
- The concrete mix was prepared in the UK, but no particular location was considered. The input energy is representative of the whole UK energy mix.
- Input energy was representative of the energy mix of the two countries, Italy and UK. Initiatives to reduce energy consumption or use clean energy sources in the production of either GNPs or concrete were not considered.
- The chosen dosage of G2NanPaste in concrete was representative of what was used in the literature and within the range that was experimentally investigated in this thesis.
- The avoided impacts related to the use of ground granulated blast furnace slag (GGBS) were assumed to replace the average mix of virgin and recycled material actually used in the market rather than just virgin materials (Gala *et al.*, 2015; Arena *et al.*, 2017).

Starting with the GNP production, the simplified process is shown in Figure 7-7, which included two main phases; the graphite expansion phase followed by the exfoliation phase. The production of 1kg of G2NanPaste required graphite and water as raw materials and electrical and thermal energy. Following GNP production, to produce 1m³ of GNP-concrete (the functional unit of this study) at least 2wt% of G2NanPaste was required (0.1wt% active GNPs). Table 7.3 includes the material quantities for the base case, the GNP-concrete and for the sensitivity analysis. The sensitivity analysis assumed that the quantity of the CEMI reduced by 5% whilst the GNP quantity remained the same as in the rest of the study (3kg/m³). The concrete mix process involved two steps; firstly, an aqueous suspension with water, a polycarboxylate superplasticiser and GNPs was prepared, which was followed by the addition and mixing of the remaining raw materials - CEMI, GGBS, limestone (coarse aggregate) and sand (fine aggregate). In preparing the GNPs-aqueous suspension, two mixing methods were considered. The first, involved sonication of the suspension for 2 hours, whilst the second involved high-speed shear mixing at 4500 and 7000 rpm for a total of 10 minutes. The electric energy consumption of the sonicator was taken as 4 kW (Nanesa, 2018) and that of the highspeed shear mixer was taken as 1.1 kW (Nanesa, 2018). Upon preparation of the aqueous suspension, a power consumption of 1.9 kW was assumed for the electricity consumption at the ready-mix concrete batching plant.

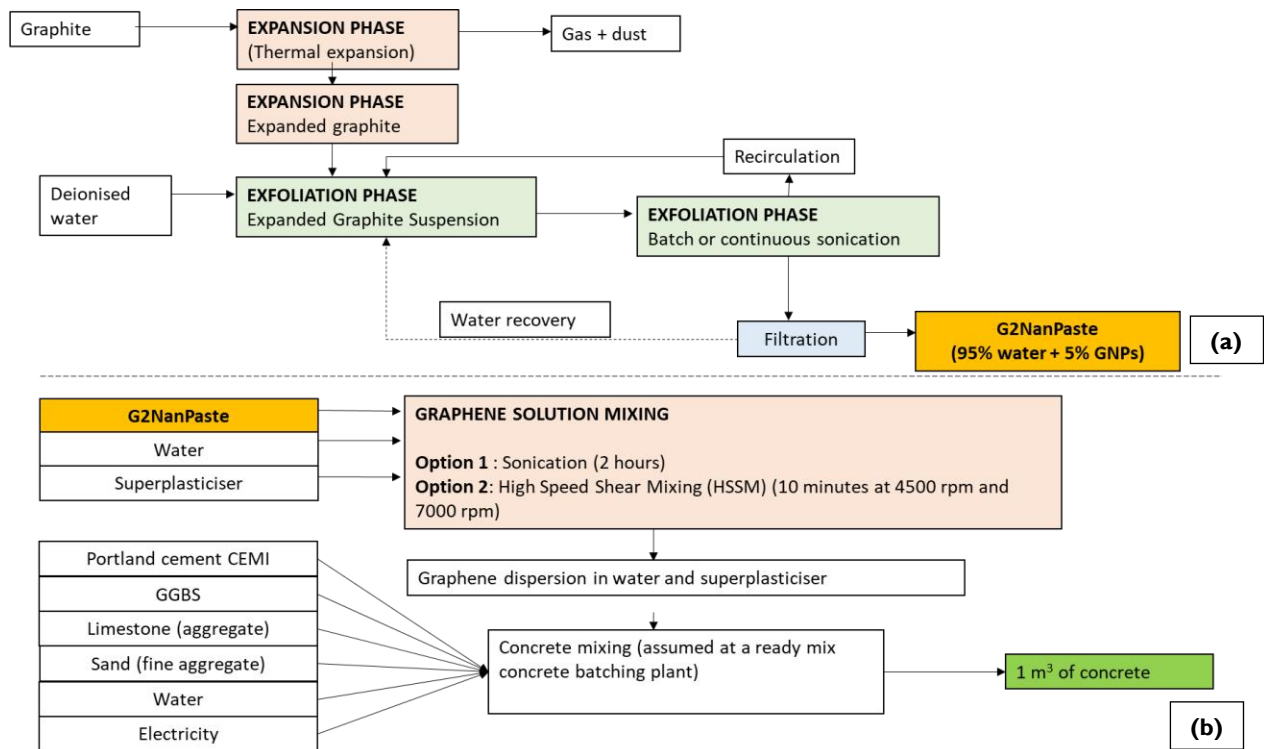


Figure 7-7: Methodology for producing (a) the G2NanPaste (GNPs) and (b) the GNP-concrete.

Table 7.3: Material quantities used in this study for the different concrete mixes.

Material	Base case	GNP-concrete	Sensitivity analysis
Portland cement: CEM I kg/m ³	150	150	142.5
GGBS: kg/m ³	310	310	310
Limestone (Aggregates): kg/m ³	900	900	900
Sand: kg/m ³	805	805	805
Water: kg/m ³	185	182.15 ¹	182.15
Superplasticiser: kg/m ³	-	1.35	1.35
G2NAN Paste (95% water): kg/m ³	-	3	3
Total density: kg/m ³	2350	2351.5	2344

Note¹: Water in GNP-concrete is reduced to account for the water available in the G2NanPaste. The total water content in the mix remains the same and is equal to 185 kg/m³

7.2.3. GNPs production

The GNP production was analysed and the values for each impact category prior to normalisation are shown in Table 7.4 and the normalised results are presented in Figure 7-8. Starting from Table 7.4, the different impact categories along with their respective units are presented. The unit of measuring the impact of carcinogens and non-carcinogens is kg

C_2H_3Cl eq., which is the kilograms of vinyl chloride equivalent units. Respiratory inorganics are measured in kg $PM_{2.5}$ eq., which is kilograms of atmospheric particulate matter with a diameter less than 2.5 μm . Aquatic ecotoxicity is measured in kilograms of triethylene glycol (TEG) in water whilst terrestrial ecotoxicity is measured in kilograms of TEG in soil. The impact of global warming is measured in kg CO_2 eq., which is kilograms of carbon dioxide equivalent and the non-renewable energy and mineral extraction are measured in megajoule (MJ). These units in the impact categories will remain the same throughout the analysis.

Looking at these values in more detail and focusing on the effect of G2NanPaste on global warming, 1 kg of G2NanPaste corresponded to 0.17 $kgCO_{2eq}$, whilst the production of 1 kg of CEM I corresponded to 0.86 $kgCO_{2eq}$ for the particular cement that was used for this mix design. However, a 100% yield was assumed for the GNP manufacturing process, which might not be representative of the true conditions. Nonetheless, the yield of the ultrasonication for GNP production was found to vary between 95% and 99% by Arvidsson *et al.* (2014), so it is close to 100%. This means that the environmental impact of the GNP production is much less than that of CEM I and if it added in cementitious mixes, it is not likely to cause additional environmental burdens given the extremely small dosages. Furthermore, if it was to be used as a CEM I replacement, or if it reduces the overall volumes of cementitious material required, then this could reduce the overall environmental burden. This will be investigated in a later section as part of the sensitivity analysis. There have been very limited studies on the environmental impact of GRMs production, hence, it is difficult to directly compare the results. A study by Long *et al.* (2018) found that graphene oxide (GO) accounted for 0.38 $kgCO_{2eq}$, however, they acquired the embodied impact of GO directly from the eBalance database rather than collecting primary data. Cossutta *et al.* (2017) investigated by LCA, the impact of different graphene production methods and found that the global warming impact ranged from 0.33 to 0.62 $kgCO_{2eq}$, depending on the electrolyte and the different input voltages when graphene was fabricated via electrochemical exfoliation. However, their study focused on laboratory scale production of single layer graphene, which was associated with several inefficiencies and a significantly lower yield of production (25%-33%). Instead, the impact values presented here in Table 7.4 are more accurate for this specific GNP as they were calculated based on primary data obtained by the supplier.

Table 7.4: Mid-point impact categories of 1 kg of G2NanPaste production.

Impact category	Unit	Impact
Carcinogens	kg C ₂ H ₃ Cl eq	0.001083
Non-carcinogens	kg C ₂ H ₃ Cl eq	0.000918
Respiratory inorganics	kg PM _{2.5} eq	0.000125
Aquatic ecotoxicity	kg TEG water	8.755249
Terrestrial ecotoxicity	kg TEG soil	2.425684
Global warming	kg CO ₂ eq	0.17296
Non-renewable energy	MJ primary	2.969442
Mineral extraction	MJ surplus	0.001146

Figure 7-8 shows the normalised results of producing 1kg of G2NanPaste in terms of the different mid-point impact categories that were also shown in Table 7.4. In this figure and in the following figures, the criteria for normalisation are per person equivalent units, where one-person equivalent represents the annual average impact, globally per capita, in the specific category. From Figure 7-8 it is apparent that the greatest GNP production impact comes from the electricity consumption during the exfoliation and expansion phases, followed by thermal energy (heat) and the use of graphite as a raw material. The consumption of water appears to be negligible in the whole GNP manufacturing process. Looking at the electricity consumption during expansion and exfoliation of graphite in more detail, the non-renewable energy consumption is shown to be the most significant localised impact followed by global warming potential and respiratory inorganics. The impacts of producing GNPs on the carcinogens, non-carcinogens, aquatic and terrestrial ecotoxicity and mineral extraction is secondary.

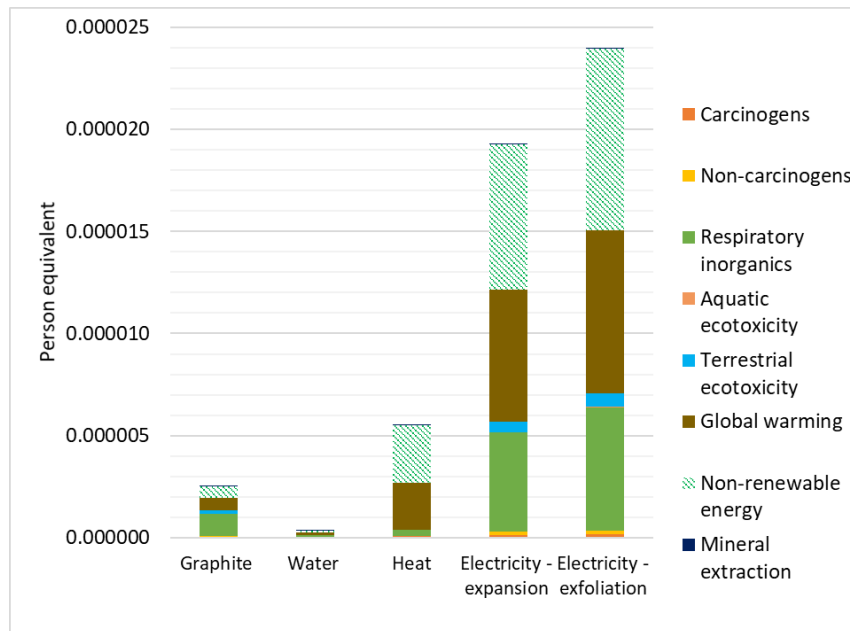


Figure 7-8: Normalised results in terms of impact (mid-point) categories of 1 kg of G2NanPaste production

The impacts of GNP production could be reduced by optimising the manufacturing process. For example, since non-renewable energy consumption was the greatest localised impact, GNP manufacturers should seek to use renewable energy (such as solar and wind) for generating the required electricity for GNP production. It should be noted that the impact from electricity will vary greatly based on the country where the GNPs are manufactured. In this study, the whole energy mix of the country was used as an input and Italy has only 24% of its electricity coming from wind, solar and biomass (considered some of the renewables) whilst the UK has 28% (Jones *et al.*, 2018). Therefore, the impact from electricity consumption is sensitive to the country where the GNPs are manufactured and to any local clean energy measures that are adopted by the manufacturer. Graphite (as a raw material) can be mined or synthesised, with the latter being much purer (>99.9%). However, the GNP production is not very sensitive to graphite purity and therefore due to lower costs, mined graphite has been assumed as a raw material in this case, in agreement with a similar study (Arvidsson *et al.*, 2014). In this analysis, raw graphite information was directly acquired from Ecoinvent 3.0 database and represented the average global emissions associated with graphite mining and transport. Reducing the impact from the use of graphite as a raw material can be achieved by making the mining process more efficient and by reducing the transport requirements from graphite mining to GNP manufacture.

7.2.4. GNPs incorporation in concrete

This section presents the LCA findings of incorporating GNPs in a standard concrete mix. Initially, the base case is presented that does not include any GNPs. Then, two GNP dispersion methods are compared.

7.2.4.1. Base case

A standard concrete mix was used to establish the baseline for this study and was then compared with the GNP-concrete mix. This concrete mix design was provided by Costain and it was used for some of the concrete elements on the Tideway project in London, UK. The mix comprised of CEM I, tap water, sand, crushed limestone, GGBS and electricity required for mixing (Table 7.3). No chemical additives such as superplasticisers, accelerators and retarders were considered in the base case, as their use would depend on the site-specific requirements and concrete performance, which is outside the scope of this LCA.

The impact values prior to normalisation are shown in Table 7.5 and Figure 7-9 illustrates the normalised results for producing 1m³ of the base case concrete. From Figure 7-9, it is evident that CEM I had the greatest impact, followed by aggregates (sand and limestone as fine and coarse aggregate respectively). The use of water had a negligible effect and the same applied to the electricity. This is because modern concrete batching plants have improved their energy efficiency and the energy intensity has reduced from 132.1 kWh/tonne in 2008 to 122.7 kWh/tonne in 2015 (The Concrete Centre, 2016a). In addition, in the UK, approximately 28% of the total electricity demand was covered by renewable energy sources whilst around 20% of the electricity comes from nuclear energy (World Nuclear Association, 2018). GGBS is considered a by-product of the blast furnaces used in the iron industries (Cementitious Slag Makers Association, 2018) and as discussed in Section 7.2.2, it was considered as avoided impact since it is used as partial replacement of virgin raw materials (CEM I). The impact of iron production is outside the boundaries of GGBS impact and it is assumed that GGBS is only used as a by-product rather than being produced specifically for use in concrete. The benefits of using GGBS are twofold; firstly, the environmental impact of disregarding GGBS as waste from the manufacturing process of iron is avoided, and secondly, the need for consuming raw materials in concrete is reduced by partly replacing CEM I with GGBS.

Global warming was the largest mid-point impact category and the production of 1m³ of concrete corresponded to 19.42 kgCO_{2eq}. This is significantly less than what has been quoted in the literature for a standardised mix in 2008 that resulted in 73.8 kgCO_{2eq} per tonne of concrete (The Concrete Centre, 2016a). The difference can be attributed to the efficiencies in concrete production in the past decade that reduced the consumption of electricity and virgin resources, as well as on the high contents of GGBS that substitute CEMI in this mix. The impact of global warming was followed by the consumption of non-renewable energy and respiratory inorganics, which shows that the effect on public health should also be considered.

Table 7.5: Mid-point impact categories of 1m³ of the base case concrete production.

Impact category	Unit	Impact
Carcinogens	kg C2H3Cl eq	0.4861
Non-carcinogens	kg C2H3Cl eq	0.6555
Respiratory inorganics	kg PM2.5 eq	0.0478
Aquatic ecotoxicity	kg TEG water	7912.6726
Terrestrial ecotoxicity	kg TEG soil	2310.6124
Global warming	kg CO ₂ eq	19.4209
Non-renewable energy	MJ primary	265.6770
Mineral extraction	MJ surplus	5.7572

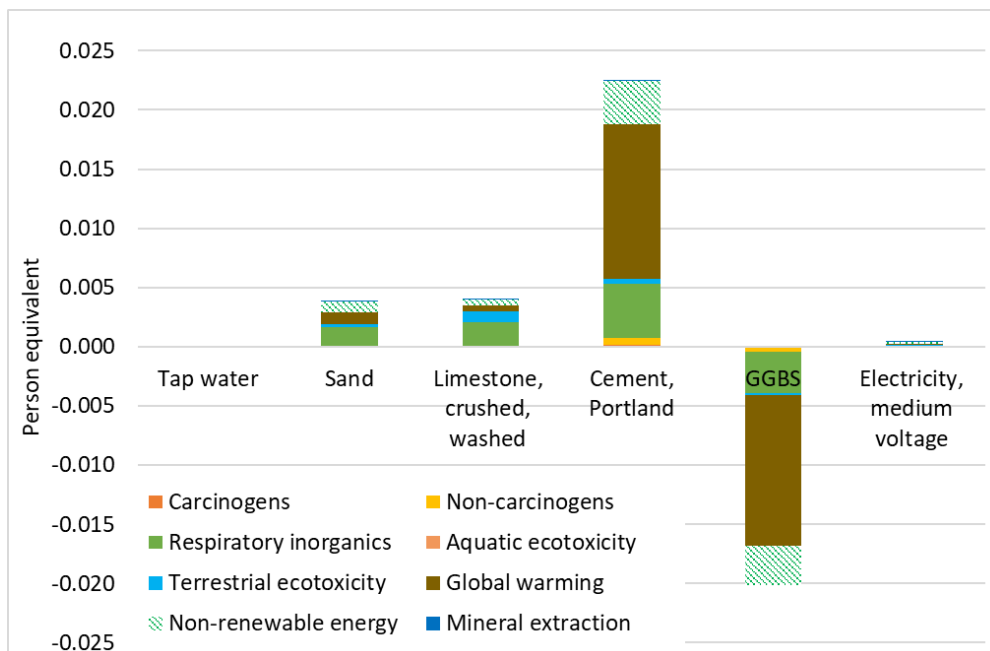


Figure 7-9: Normalised results in terms of impact (mid-point) categories of 1m³ of the base case concrete.

7.2.4.2. GNP dispersion methods in concrete

Homogeneous dispersion of GNPs in the cement matrix was a key challenge and the combined use of a mechanical mixing method along with a polycarboxylate superplasticiser was found to result in homogeneous mixing of GNPs (Chapter 4). Two mechanical mixing methods were analysed and compared in this LCA - one was the sonication of the suspension for 2 hours and the other was high-speed shear mixing for 10 minutes. Then, the GNP suspension was added in the base concrete mix and the whole system was analysed again by LCA. In these two cases, a polycarboxylate superplasticiser was also considered to aid the GNP mixing. The results are tabulated in Table 7.6 and in normalised form in Figure 7-10. In both cases, as observed for the base case scenario, CEMI had the greatest contribution followed by limestone and sand, whilst GGBS had an avoided impact. Overall, the plasticiser had a greater effect compared to G2NanPaste, with its effect on global warming being 3.22 times that of the G2NanPaste whilst this increased to 6.13 times for respiratory inorganics. These results agree with Long *et al.* (2018) who found that the greenhouse gas emission of GO were less than that of the polycarboxylate superplasticiser (GO had 0.38 kgCO_{2eq} compared to 0.91 kg CO_{2eq} for the superplasticiser). The addition of G2NanPaste was more damaging when sonication was used compared to high-speed shear mixing which was reflected in the higher electricity impact. This was expected due to the longer duration of sonication required and because sonicators have a greater power requirement compared to the high-speed shear mixer. GNPs can be considered as an admixture for concrete, whose effect remains insignificant compared to that of CEMI.

Table 7.6: Mid-point impact categories of 1m³ of GNP-concrete production with two different dispersion methods.

Impact category	Unit	Impact with sonication	Impact with high-speed shear mix (HSSM)
Carcinogens	kg C2H3Cl eq	0.599807	0.575793
Non-carcinogens	kg C2H3Cl eq	0.814938	0.714875
Respiratory inorganics	kg PM2.5 eq	0.055255	0.051492
Aquatic ecotoxicity	kg TEG water	8456.594	8136.901
Terrestrial ecotoxicity	kg TEG soil	2458.72	2374.508
Global warming	kg CO ₂ eq	27.3963	21.74442
Non-renewable energy	MJ primary	422.6675	342.3018
Mineral extraction	MJ surplus	5.856365	5.842924

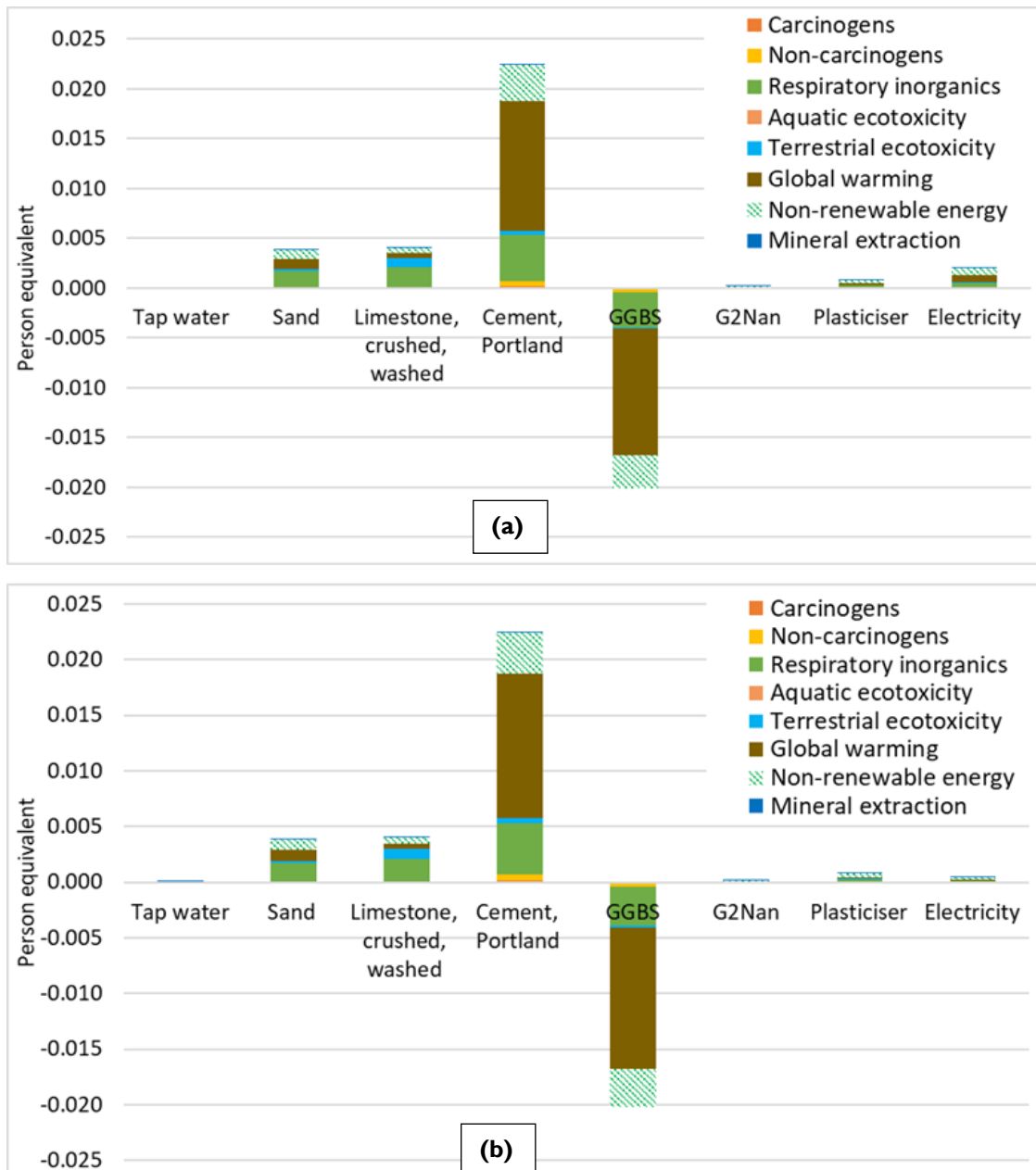


Figure 7-10: Normalized results in terms of impact (mid-point) categories of life cycle impact assessment of producing 1m³ of concrete with sonicated (a) and high-speed shear mixed G2NanPaste (b)

A comparison between all scenarios, including the base case with no GNPs (normal concrete), the concrete with sonicated GNPs and the concrete with GNPs that were high-speed shear mixed (HSSM), is presented Figure 7-11 and the global warming coefficient is shown at the inset. All alternative scenarios had a greater impact compared to the base case concrete mix, because G2NanPaste was considered as an addition rather than replacement.

The impact was more pronounced when sonication was used for dispersing G2NanPaste. It is important to note, that concrete production had a significant impact on human health (respiratory inorganics) in addition to global warming.

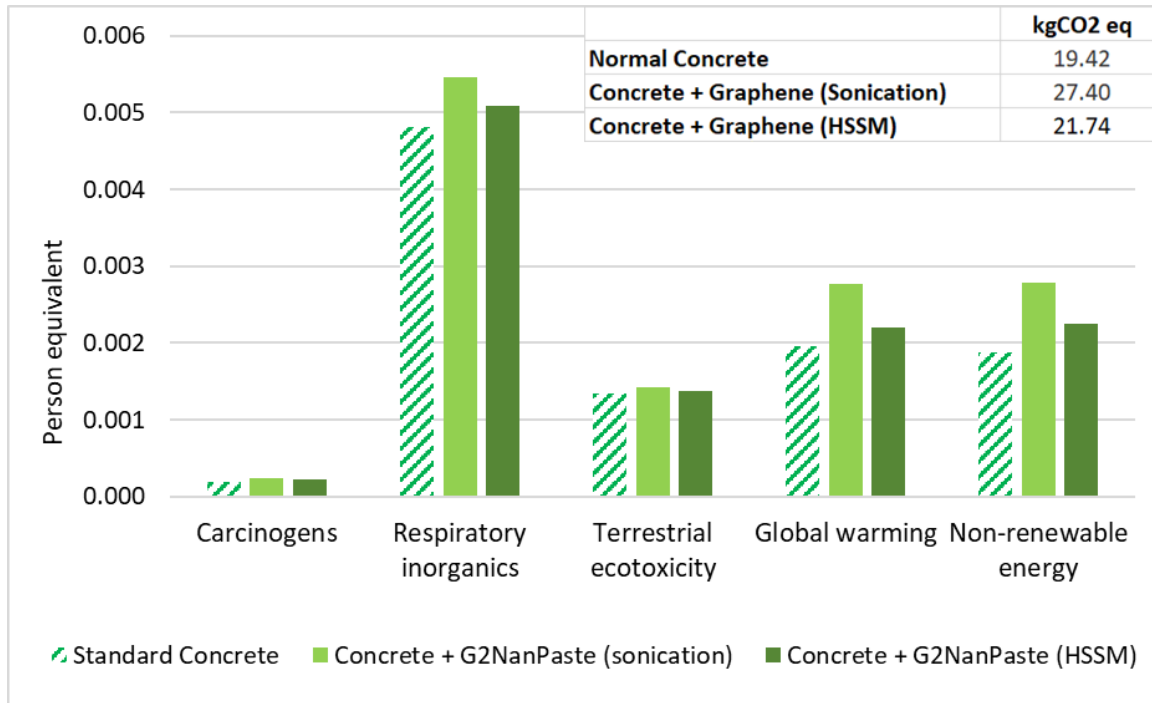


Figure 7-11: Comparison between all scenarios in terms of the greatest mid-point impact categories

7.2.5. Sensitivity analysis

This LCA showed that G2NanPaste had a very small impact compared to other concrete components such as CEM I and aggregates. Therefore, a change in the dosage of G2NanPaste would not significantly affect the overall impact of the concrete mix and hence it was not investigated further. However, the use of GNPs could allow for an enhancement in certain aspects of concrete performance (such as durability) which could in turn lead to a reduction of the cement content required and ultimately to a reduction of the overall volume of concrete that would be needed to get the same performance. The aim of this sensitivity analysis was to reduce the initial cement dosage by 5%, assuming that the performance is maintained through the addition of GNPs. It should be noted that a cement reduction when using GNPs was not tested experimentally in this thesis and therefore it is an assumption that GNPs could have this effect, while the results from Chapter 5 do not support this as a valid assumption. Nonetheless, it is useful to understand how the environmental impact

would change if cement content could be reduced. The results for the mid-point impact categories are shown in Table 7.7. To produce 1 m^3 of this new concrete mix that used 5% less CEM I, the effect on global warming was $15.29\text{ kgCO}_{2\text{eq}}$ which was significantly less than the base case ($19.42\text{ kgCO}_{2\text{eq}}$). Therefore, reducing cement by only 5% could result in a 21% reduction in the global warming potential. This highlights the significance of reducing the cement content whilst maintaining the same service. From Figure 7-12, it is shown that the effect of G2NanPaste was minimal. CEM I remained the biggest contributor, with the effect being more pronounced for climate change followed by human health. In another study, it was shown that for the equivalent mechanical strength, recycled fine aggregates (RFA) mortar with graphene oxide (GO) could reduce greenhouse gas emissions by 6.7% compared to natural aggregates (NA) mortar, whilst the GO was responsible for $0.38\text{ kgCO}_{2\text{eq}}$ out of the $421.3\text{ kgCO}_{2\text{eq}}$ for the whole mix (Long *et al.*, 2018). However, the reduction in greenhouse gas emissions was due to the combined effect of RFA and GO that were used to achieve the same strength performance. Figure 7-13 illustrates the sensitivity analysis findings in terms of damage categories. The biggest impact of producing this type of concrete was on climate change due to the greenhouse gas emissions and energy consumption. However, clearly the impact on human health was also significant and this was due to the release of carcinogens, non-carcinogens, and respiratory inorganics. Therefore, future studies and the optimisation of concrete mixes should not be purely focused on the environmental effects of concrete, but also on the impacts on human health.

Table 7.7: Mid-point impact categories of 1 m^3 of GNP-concrete with 5% less CEM I.

Impact category	Unit	Impact
Carcinogens	kg C2H3Cl eq	0.55551031
Non-carcinogens	kg C2H3Cl eq	0.6441251
Respiratory inorganics	kg PM2.5 eq	0.049159
Aquatic ecotoxicity	kg TEG water	8013.236
Terrestrial ecotoxicity	kg TEG soil	2340.7609
Global warming	kg CO ₂ eq	15.293221
Non-renewable energy	MJ primary	314.44374
Mineral extraction	MJ surplus	5.7961721

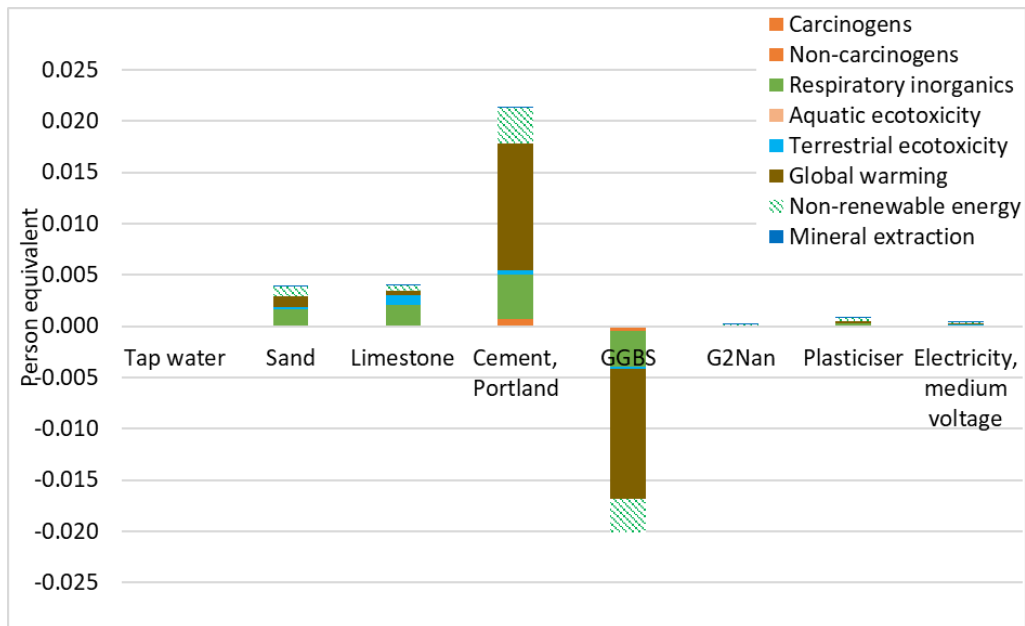


Figure 7-12: Normalised results of the overall impact of producing 1m³ GNP-concrete with 5% less CEMI, expressed in mid-point categories.

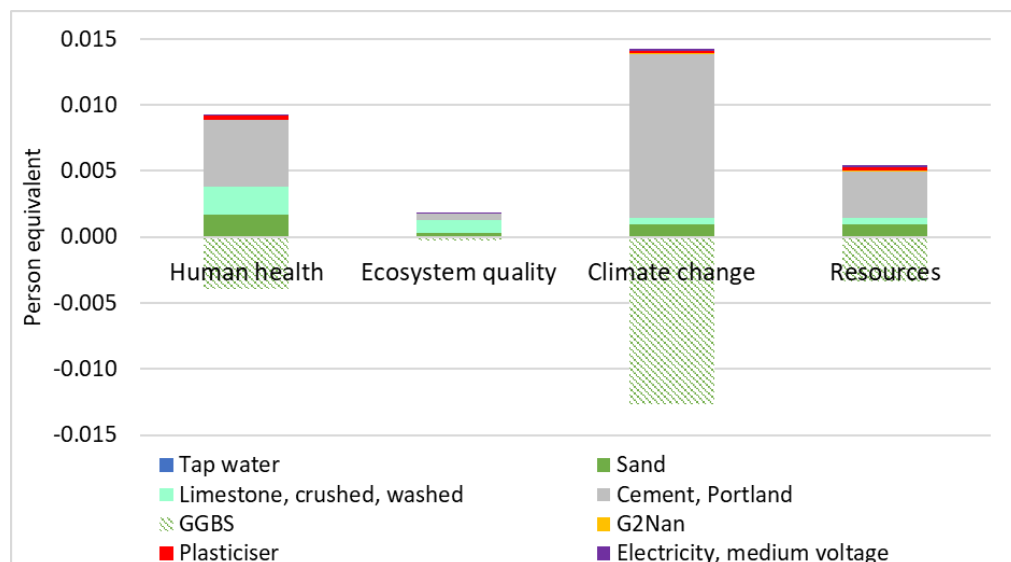


Figure 7-13: Normalised results of the overall impact of reducing 5% of Portland cement content on human health, ecosystem quality, climate change and resources (damage categories).

In summary, this LCA study provided for the first time, an analysis of the impact of multi-layer GNP production in a European country and their consequent addition in concrete. The LCA used primary and secondary data that represented the materials that were used for the experimental work in this thesis. It was found that producing 1 kg of G2NanPaste with Liquid Phase Exfoliation resulted in 0.17 kgCO_{2eq}, while the electricity that was

produced for its fabrication had the greatest impact. To incorporate the GNPs in concrete, high-speed shear mixing was more sustainable compared to sonication, whilst the impact of GNPs in the mix was lesser than that of the polycarboxylate superplasticiser, which is a commonly used admixture. CEMI resulted in the greatest impact and therefore, the focus should be on reducing the cement content whilst maintaining the same structural performance.

7.3. Summary

The first section of this chapter presented the findings of an industry survey, in the form of a questionnaire, that was carried out in the UK. The survey aimed to understand the main problems encountered with the repair of concrete structures, the use of sensors and to also identify the key opportunities and blockers for using GRMs in cement composites. There were 78 responses, and it was found that tensile/flexural strength improvements and the self-sensing functionalities would be the greatest opportunities for GRMs in concrete. The high cost of the material was cited as the main barrier followed by the lack of industry standards. This survey provided a useful insight in the industry perceptions of this new material and will help in targeting future research towards the high-impact areas for industrial applications.

In the second section, the environmental impact of producing G2NanPaste was investigated by means of a Life Cycle Assessment. The production of 1 kg of G2NanPaste with Liquid Phase Exfoliation resulted in 0.17 kgCO_{2eq} which was less than the production of CEMI, which corresponded to 0.86 kgCO_{2eq}. The impact of using GNPs in a standard concrete mix was also analysed and it was found that CEMI was 248 times more damaging than G2NanPaste in terms of global warming and 124 times more damaging in terms of respiratory inorganics (human health) for the specific concrete mix that was investigated. CEMI was the concrete ingredient that resulted in the greatest impact in all cases. The sensitivity analysis showed that if the addition of GNPs resulted in a 5% reduction of the CEMI content, the effect of the concrete mix on global warming could reduce by 21%. Therefore, if GNPs are proven to maintain or enhance the concrete performance, they could be a promising additive from an environmental perspective.

Chapter 8. CONCLUSIONS AND FUTURE OUTLOOK

This thesis investigated the use of graphene-related materials (GRMs) in cementitious composites with an overarching aim to create advanced, multifunctional composites. This chapter summarises the key findings and the conclusions drawn from this research. Then, based on the findings from this work, recommendations for further research are presented.

8.1. Conclusions

8.1.1. Overview

A general introduction of the key challenges associated with concrete infrastructure was presented in *Chapter 1*. Cementitious structures suffer from poor durability performance which results in frequent repair and maintenance activities; have a great environmental impact due to the emission of carbon dioxide and the consumption of natural resources; and need to be frequently inspected and monitored to ensure that they maintain their structural and serviceability performance. The motivation for this research was to take advantage of new and emerging nanomaterials that could solve the challenges associated with cement composite structures.

8.1.2. Literature review

In *Chapter 2*, the main challenges with concrete infrastructure were studied in more detail. It was found that each tonne of concrete has ~100-300 kg of embodied CO₂, hence, the environmental impact of concrete structures needs to be managed. At the same time, concrete structures suffer from poor durability and in the UK, £10 bn was spent on repair and maintenance from 2011 to 2015, which was equivalent to 35-45% of the total infrastructure budget (HM Treasury, 2010). This poor durability has resulted in an increased need for structural inspections; however, these inspections happen primarily by visual observations. Structural health monitoring (SHM) that involves the integration of sensors, data transmission and processing has been used in recent years to solve the monitoring challenge, however, sensors themselves suffer from high costs, low sensitivity, incompatibility with structural materials and poor durability (Spencer, 2009; Ou and Han, 2009). Hence, there is a clear need to re-think the way concrete structures are built, inspected, and maintained, to ensure that these challenges are mitigated. Biomimetic

materials that can self-diagnose their condition, self-immunise against threats and self-heal if they are damaged could help in extending the service life of the structures and in turn, reducing the demand for inspections and repairs (Al-Tabbaa *et al.*, 2018). One such material is self-sensing concrete, which can monitor its condition and identify damage, whilst maintaining or improving the mechanical and durability performance (Han *et al.*, 2015). The principle of self-sensing concrete is that when functional fillers are homogeneously dispersed in a cementitious binder and allow the passage of electric current; as the material is deformed or stressed, the conductive network will change and consequently affect the electrical resistivity.

Over the past decade, there has been increasing academic research and many breakthroughs with a material termed as “Graphene” (Geim, 2009), which was isolated in 2004 after graphite exfoliation. 2D graphene is one atom thick it is considered the base material for carbon materials of all other dimensionalities, hence, there is a family of graphene-related materials (GRMs). As reviewed in Section 2.3.2, there are many different GRM fabrication techniques which result in varying fundamental properties (e.g. number of graphene layers, average lateral size and carbon-to oxygen (C/O) atomic ratio) and they also affect the cost and scalability. To achieve sufficient electrical conductivity, GRMs without oxygen groups had to be tested, and it was found that GNPs would be the most appropriate GRM to be investigated in detail. The most suitable GNP fabrication technique for bulk applications in cementitious composites was found to be Liquid Phase Exfoliation (LPE), which is one of the most scalable techniques, with controlled costs and reasonable GNP quality.

However, if progress is to be made in the successful use of GNPs in cementitious composites then the literature was clear: the problem of homogeneous dispersion of GNPs in the cement matrix was a challenge that must be addressed. The different dispersion techniques were discussed in Section 2.4.1, and a combination of a mechanical treatment, such as sonication, along with a surfactant were effective in homogeneously dispersing the GNPs. Studies also showed that pre-dispersion of GNPs in water and a surfactant was better compared to dry mixing with cement. When GNPs were added in cement composites, they reduced the fluidity significantly, with mini slump reducing by up to 40% when 0.4wt% GNPs were added in the mix. No new hydration products were found with GNP addition, however, there were discrepancies as to whether GNPs accelerate or reduce the rate of cement hydration (Section 2.4.2.2). Likewise, some studies found

improvements in microstructure whilst others observed agglomerates and low interfacial bonding between the GNPs and the cement hydration products. Therefore, the effect on the early age performance, including the hydration and microstructure of cement composites, needs to be investigated in greater detail.

Mechanical properties of the GNP-cement composites were also examined in several studies, and some showed improvements in the compressive and flexural strengths, while some found reductions. Overall, there was no clear agreement on the effect of GNPs, with many studies showing less than 5% change compared to the control which could be statistically insignificant, based on the number of tested samples. This, along with the fact that many authors did not report standard deviations or sufficient detail around the mixing parameters, gives low confidence on the effect of GNPs on the mechanical performance of cement composites. In particular, controlling the w/c and the temperature of the suspension during sonication could play a critical role in ensuring that the water does not evaporate and that the w/c between the control mix and the GNP samples was the same. Some changes in the mechanical properties could be attributed to changes in the water content in the mix rather than due to the GNP addition. In terms of durability, there were very few studies that investigated the effects of GNPs; however, positive effects were reported. GNPs reduced the total pore area, median and average pore diameter (Section 2.4.5), which is beneficial for reducing permeability. Indeed, studies showed that the chloride penetration depth and the chloride migration coefficient reduced with GNPs (Liu *et al.*, 2016; Du *et al.*, 2016; Wang *et al.*, 2018). Similarly, water permeability was also reduced (Du and Pang, 2015). There was no study that tested the effect of GNPs on the gas permeability. Since only a few studies investigated the effects of GNPs on the permeability performance of cement composites, there were clear gaps in the literature.

The effect of GRMs on the electrical conductivity of cement composites was also examined to understand the formation of electrically conductive paths that could lead to self-sensing. In terms of functional fillers, both the use of natural graphite and that of GNPs was investigated. The main finding from the literature was that different filler quantities were needed to achieve stable and uninterrupted conductivity paths (percolation threshold). The percolation threshold was dependant on the intrinsic GRM properties, the cement composite properties (such as w/c, mixing technique, cement type, presence of aggregates, curing regime etc.) and on the measurement technique that was followed.

The environmental effect of GRMs and their use in concrete was also considered but literature was scarce. Arvidsson (2017) provided a summary of the environmental impact of different GNP production methods however, most of the studies had focused on laboratory scale GNP production rather than industrial fabrication of GNPs. Furthermore, there was no study on the environmental effects of using GNPs in cementitious systems. Hence, a Lifecycle Analysis (LCA) was proposed to understand the environmental impact of this novel composite material. Overall, there were some clear gaps in the literature around the use of GNPs in cement composites, which this thesis aimed to cover, by selecting a suitable GNP material for large scale production and by experimentally investigating the research gaps.

8.1.3. Materials and experimental procedures

The materials and experimental procedures that were followed in this study were presented in *Chapter 3*. A range of materials, including different cements and GRMs, were used in this study. The techniques to prepare the samples, both in terms of the GNP-suspensions and the cementitious composites, were explained in this chapter. A detailed description of the experimental procedures to assess the microstructure, dispersion, mechanical, durability and electrical conductivity properties was also provided.

8.1.4. GRM dispersion studies

The GNP dispersion challenge that was highlighted in the literature was experimentally investigated in *Chapter 4*. Initially, the GRMs, including the GNPs and three products of natural graphite, were further characterised. Based on the key findings from the literature review, the dispersion of GNPs in water was tested first and it was found that GNPs dispersion in water with a mechanical treatment was not sufficient, hence a combination of a mechanical and chemical treatment was needed. The effect of chemical admixtures on the dispersion of GNPs was investigated, and four plasticisers/superplasticisers including a lignosulphonate, a naphthalene-based and two polycarboxylates, were selected based on the literature and because they are widely used in commercial concrete mixes. Initially, the dispersion of GNPs in water and the superplasticisers was tested and zeta-potential testing showed that the lignosulphonate and naphthalene-based products did not have a strong repulsion mechanism, on contrary to what was expected. Instead, the polycarboxylate products, that worked by a combination of electrostatic repulsion and steric hindrance mechanisms showed a higher zeta-potential which was an indication of better dispersion. UV-Vis spectroscopy then tested the effect of the polycarboxylate superplasticiser (PCE)

concentration as well as the impact of increasing GNP dosage on the dispersion efficiency. An optimum polycarboxylate plasticiser concentration was found, after which further plasticiser contents did not aid the dispersion. A PCE/GNP ratio of approximately 9:1, significantly improved the GNP dispersion and kept it in suspension for over 1 hour. Next, the dispersion of GNPs in cement was tested with the same chemical dispersion products, however, a range of GNP concentrations was tested. Rheology testing showed that the polycarboxylate products indeed could disperse higher GNP concentrations and they also maintained a good rheological behaviour for the samples.

In addition, *Chapter 4* presented the results from the dispersion investigation that was carried out as part of a secondment in the HeidelbergCement Italcementi research facility, 'i-lab'. The parameters and techniques that were investigated included the use of a high-speed shear mixer; hydrophobic mixing; different GRMs; two alternative cements (P2 (hydrophobic-treated) and P3 (hydrophilic-treated)); silica fume and a functionalised graphene product. High-speed shear mixing was employed in the literature by some authors but practical limitations around the contamination of the equipment and the loss of GRM product that remains stuck on the equipment meant that this technique was not suitable. Hydrophobic mixing also proved to be ineffective and high dosages of GRM could not be dispersed in a hydrophobic medium. Testing the different GRMs in CEMI mortars did not show any promising results as the curing progressed and no pronounced improvements in the mechanical performance were observed. It was also found that the hydrophobically-treated cement was more effective in dispersing the GRMs compared to the hydrophilic one and GRMs improved the flexural strength but slightly compromised the compressive strength. The use of silica fume did not yield the expected dispersion improvements that were reported in the literature, whilst the functionalised graphene product led to some performance improvement however, no information on its composition was disclosed. In summary, different techniques for dispersing GNPs were investigated and a successful protocol was developed following a mechanical treatment along with the use of a polycarboxylate superplasticiser.

8.1.5. Effect of GRMs on the performance of cement composites

Chapter 5 focused on the effect of GRMs on the early age, mechanical and durability performance of cement composites. Initially, the effect of a single dosage of 0.3wt% GNPs on cement pastes with two cements, CEMI 52,5N and CEMII/A-LL 32,5R, was investigated.

The effect on hydration was negligible with no new hydration phases, whilst microstructural characterisation revealed that the GNPs were not well integrated with the cement hydration products. Small reductions in flexural strength were noticed with more pronounced decreases in compressive strength, which could be due to planes of weakness formed between the GNPs and the cement hydration products. The hardness of the specimens increased with GNP addition whilst the effect on Young's modulus was negligible. Since the cement type made no difference on the performance of pastes with GNPs, CEMI mortars were investigated next. The GNP concentration ranged from 0.05wt% to 0.5wt%, with the fluidity of the mortars reducing with increasing GNP dosage. GNPs delayed the hydration of the mortars at 2 days; however, no effect was observed at 28 days. GNPs formed planes of weakness, whilst some agglomerates were seen for the high concentrations, indicating that the dispersion protocol developed in *Chapter 4* would not be suitable for high GNP contents. The flexural and compressive strengths reduced with GNPs due to both a delay in hydration and a poor microstructural interaction. Instead, a beneficial effect with GNPs was found for water, gas, and chloride permeability at 2 days whilst no obvious effect was seen at 28 days. *Chapter 5* also investigated three natural graphites of varying sizes with the intention that they would be used to enhance the electrical conductivity of cement pastes. The fluidity reduced significantly with increasing graphite concentration and smaller particle size, whilst the graphites had a minimal effect on hydration. Graphite addition led to a reduction in compressive strength and hardness, with increasing dosage and particle size having more pronounced effects.

8.1.6. Electrical conductivity studies of GRM-cement composites

Building up on these findings, *Chapter 6* aimed to investigate the effect of the GRMs on the electrical conductivity of cement pastes. *Chapter 6* firstly investigated the effect of the intrinsic cement composite material properties on the electrical conductivity. Higher water contents and water curing of specimens resulted in enhanced conductivity measurements due to electrolytic conduction through the ions. Electrical conductivity reduced with curing age as the cement hydration progressed. Two 4-probe measurement techniques with embedded and surface electrodes were tested, and a good correlation was found between the two methods. The percolation threshold for electrical conductivity depended on both the graphite size and concentration whilst it did not depend on curing age. For the coarse graphite, the percolation threshold was at 30wt% - 40wt%, whilst for the medium and fine

graphite it was at 20wt% - 30wt%. Hence, the finer the graphite, the lower the dosage needed to form an uninterrupted electrical conduction path. Below the percolation threshold, a combination of electrolytic and electronic conduction was present, while above that threshold, the electrical conductivity depended only on the presence of the conductive filler with the effect of water being minimal. Furthermore, *Chapter 6* examined the effect of GNPs and it was found that the dosages that were used in *Chapter 5* for permeability improvement, were not sufficient to create electrically conductive paths. When higher GNP dosages were tested, mixing became very challenging again and the dispersion protocol had to be adjusted by increasing the water and superplasticiser contents. These mixes could not be used for structural applications and to reduce the mixing challenge, the use of GNP-cement coatings was investigated. A water-based GNP coating was tested first using spreading and drop coating techniques. This coating was not effectively adhered to the substrate whilst drop coating was not a useful technique. A cement-based GNP coating was developed which provided better adhesion with the cementitious substrate, however, the thickness and the uniformity of the coating became a challenge. Therefore, coatings could be promising as they reduce the required GRM volume and the dispersion challenge to an extent, however, further research in coatings is needed.

8.1.7. Industry survey and LCA

Chapter 7 was then divided in two parts. Firstly, the findings from an industry survey that was run in the UK were presented. It was found that cracking due to poor workmanship or due to poor specification and materials performance were the most common challenges associated with concrete structures. The poor structural performance resulted in immediate repair and an enhanced monitoring regime, reinforcing the key findings from the literature. A tensile/flexural strength improvement and a self-sensing functionality would be the greatest opportunities for GRMs in concrete according to the survey respondents, whilst the high material cost and the lack of industry standards were cited as the primary blockers. The cost barrier was mitigated in this research by selecting a suitable GNP product that was already manufactured at scale by LPE. Choosing this GNP product ensured that other than the technical performance, the material would also be viable to use at the required scales needed for civil engineering applications.

Finally, the second part of *Chapter 7* aimed to investigate the environmental impact of using GNPs in concrete by carrying out a *cradle-to-gate* Lifecycle Assessment (LCA) study. Since

literature was scarce, this study was essential for ensuring the sustainable development of novel construction materials. Initially, the GNP production was assessed, and it was found that the greatest impact came from the consumption of electricity during the exfoliation and expansion of graphite and this was followed by the use of heat and the use of graphite as a raw material. The fabrication of 1kg of GNPs, equated to 0.17 kgCO_{2eq}. When GNPs were then added in a standard concrete mix design, it was found that CEM I remained the most impactful ingredient and was 248 times more damaging than GNPs in terms of global warming. GNPs had a lesser impact compared to other admixtures used in the mix (a polycarboxylate superplasticiser) and therefore their impact is in the range of commonly used admixtures.

8.2. Future outlook

The work that was carried out and presented in this thesis was the first investigation in self-sensing cementitious materials in civil engineering at Cambridge and it illustrated the ability of traditional and novel GRMs to be used for functional applications as well as to enhance certain structural aspects. However, it also revealed additional future work that is needed to advance our understanding around the role of GRMs in cementitious systems. The future work that is proposed here focuses on two main areas that could be improved based on the findings of this research: dispersion of GRMs in bulk applications and use of GRMs in coatings.

The dispersion of GRMs in bulk applications was the focus of Chapters 4 and 5, where one product of GNPs was selected along with three products of natural graphite. The chosen GNPs product was suitable for large-scale applications from a cost and quality perspective; however, it compromised some structural functions of the material while it improved the early-age permeability performance. Since enhancement of mechanical performance was not an objective of this study, the review of other GRMs was not within the research scope. However, if GRMs are to be used in bulk applications for structural functions, a parametric study of different GRMs with varying fundamental properties (e.g. presence of oxygen groups, number of layers etc.) needs to be undertaken. Consequently, the dispersion protocol should be adjusted to ensure the compatibility and dispersion within cementitious systems. For example, a small set of experiments in this study showed promising results

with a functionalised GNP product and even though no details were provided, functionalised GRMs could be investigated as a way of enhancing structural properties. Such a parametric study of GRMs and their dispersion will allow for a more in-depth understanding of their effect in cementitious composites and for an optimisation of the system.

Instead, for enhancing the electrical conductivity and creating a self-sensing mechanism, the GRMs could be used as a coating rather than dispersed in the bulk. A preliminary investigation in GNP coatings was carried out in this thesis and revealed several areas that need to be investigated further. The intrinsic properties of the substrate, such as its porosity and surface texture, will directly affect the adhesion and performance of the coating and therefore need to be systematically tested. Two types of coatings were tested here, a water-based and a cement-based GNP coating, however, other coating types should be investigated including alcohol-based coatings and polymeric systems. Their compatibility with the underlying cementitious substrate as well as the required GNP dosage needed to form a percolation threshold within each coating system needs to be explored. It is critical that the coating and substrate act as one composite system and that the electrical conductivity measurements are representative of the behaviour of the whole system. Furthermore, a technique that will allow accurate measurements of the electrical conductivity of thin coatings and can translate the measurements into insights around damage and loading also needs to be developed. For example, if the coating is damaged at different loading conditions compared to the concrete structure, then the sensing mechanism would not be realistic and would only allow for sensing of the coating layer. Hence, a GNP coating which is compatible, and representative of its respective substrate needs to be developed.

Bibliography

- Adresi, M., Hassani, A., Javadian, S., and Tulliani, J.-M., 2016. Determining the Surfactant Consistent with Concrete in order to Achieve the Maximum Possible Dispersion of Multiwalled Carbon Nanotubes in Keeping the Plain Concrete Properties. *Journal of Nanotechnology*, 2016, 1–9.
- Al-Tabbaa, A., Lark, B., Paine, K., Jefferson, T., Litina, C., Gardner, D., and Embley, T., 2018. Biomimetic cementitious construction materials for next-generation infrastructure. *Proceedings of the Institution of Civil Engineers - Smart Infrastructure and Construction*, 171 (2), 67–76.
- Al-Tabbaa, A., Litina, C., Giannaros, P., Kanellopoulos, A., and Souza, L., 2019. First UK field application and performance of microcapsule-based self-healing concrete. *Construction and Building Materials*, 208 (2019), 669–685.
- Allwood, J. and Cullen, J., 2012. *Sustainable materials with both eyes open*. Cambridge: UIT Cambridge Ltd.
- Alshamsi, A.M. and Imran, H.D.A., 2002. Development of a permeability apparatus for concrete and mortar. *Cement and Concrete Research*, 32 (6), 923–929.
- Amieva, E.J., López-Barroso, J., Martínez-Hernández, A.L., and Velasco-Santos, C., 2016. Graphene-Based Materials Functionalization with Natural Polymeric Biomolecules. *intechopen*.
- Andrade, C., Garce, P., Baeza, F.J., Galao, O., and Zornoza, E., 2015. Electronic and Electrolytic Conduction of Cement Pastes with Additions of Carbonaceous Materials. In: C. Andrade et al. (eds.), ed. *Durability of Reinforced Concrete from Composition to Protection*. Springer International Publishing.
- Arabzadeh, A., Ali, M., Kazemiyan, A., Nahvi, A., Sassani, A., and Ceylan, H., 2019. Electrically conductive asphalt concrete: An alternative for automating the winter maintenance operations of transportation infrastructure. *Composites Part B*, 173 (April), 106985.
- Arena, N., 2016. Life Cycle Engineering of a system to deliver self-chilled beverages.
- Arena, N., Sinclair, P., Lee, J., and Clift, R., 2017. Life cycle engineering of production, use and recovery of self-chilling beverage cans. *Journal of Cleaner Production*, 142, 1562–1570.
- Arksey, H. and Knight, P., 1999. *Interviewing for Social Scientists*. I Oliver's Yard, 55 City Road, London England EC1Y 1SP United Kingdom: SAGE Publications, Ltd.
- Arup, 2020. How do you use technology to better manage a major new road bridge? [online]. Available from: <https://www.arup.com/projects/queensferry-crossing-digital> [Accessed 15 Mar 2020].
- Arvidsson, R., 2017. Review of environmental life cycle assessment studies of graphene production. *Advanced Materials Letters*, 8 (3), 187–195.
- Arvidsson, R., Kushnir, D., Sanden, B.A., and Molander, S., 2014. Prospective life cycle

- assessment of graphene production by ultrasonication and chemical reduction. *Environmental Science and Technology*, 48 (8), 4529–4536.
- ASTM C1585-13, 2013. Standard Test Method for Measurement of Rate of Absorption of Water by Hydraulic Cement Concretes. *ASTM International*.
- ASTM C1679-08, 2008. Standard Practice for Measuring Hydration Kinetics of Hydraulic Cementitious Mixtures Using Isothermal Calorimetry.
- ASTM E384 – 16, 2016. Standard Test Method for Microindentation Hardness of Materials.
- ASTM Standard C33, 2018. Standard Specification for Concrete Aggregates. *ASTM International*, 8.
- Azhari, F. and Banthia, N., 2012. Cement-based sensors with carbon fibers and carbon nanotubes for piezoresistive sensing. *Cement and Concrete Composites*, 34 (7), 866–873.
- Bai, S., Jiang, L., Jiang, Y., Jin, M., Jiang, S., and Tao, D., 2018. Research on electrical conductivity of graphene / cement composites.
- Bai, S., Jiang, L., Xu, N., Jin, M., and Jiang, S., 2018. Enhancement of mechanical and electrical properties of graphene/cement composite due to improved dispersion of graphene by addition of silica fume. *Construction and Building Materials*, 164, 433–441.
- BASF, 2017. Superplasticiser - internal communication.
- Bastos, G., Patiño-Barbeito, F., Patiño-Cambeiro, F., and Armesto, J., 2016. Nano-inclusions applied in cement-matrix composites: A review. *Materials*, 9 (12), 1–30.
- Bautista-Gutierrez, K.P., Herrera-May, A.L., Santamaría-López, J.M., Honorato-Moreno, A., and Zamora-Castro, S.A., 2019. Recent Progress in Nanomaterials for Modern Concrete Infrastructure: Advantages and Challenges. *Materials*, 12, 3548.
- Belli, A., Mobili, A., Bellezze, T., and Tittarelli, F., 2020. Commercial and recycled carbon/steel fibers for fiber-reinforced cement mortars with high electrical conductivity. *Cement and Concrete Composites*, 109 (September 2019), in press.
- Bennetts, J., Vardanega, P.J., Taylor, C.A., Denton, S.R., and Brinckerhoff, W.S.P.P., 2016. Bridge data – what do we collect and how do we use it?, 531–536.
- Bhattacharya, S., Sachdev, V.K., Chatterjee, R., and Tandon, R.P., 2008. Decisive properties of graphite-filled cement composites for device application. *Applied Physics A: Materials Science and Processing*, 92 (2), 417–420.
- Braga, A.M., Silvestre, J.D., and de Brito, J., 2017. Compared environmental and economic impact from cradle to gate of concrete with natural and recycled coarse aggregates. *Journal of Cleaner Production*, 162 (2017), 529–543.
- BS EN 1015-3, 1999. Methods of Test for Mortar for Masonry. Part 3: Determination of consistence of fresh mortar (by flow table).
- BS EN 196-1, 2016. Methods of testing cement. Determination of strength.
- BS EN 197-1:2011, 2011. Cement. Composition, specifications and conformity criteria for common cements.

- BS EN 480-8, 2012. Test methods. Determination of the conventional dry material content.
- Bunch, J.S., Verbridge, S.S., Alden, J.S., Van Der Zande, A.M., Parpia, J.M., Craighead, H.G., and McEuen, P.L., 2008. Impermeable atomic membranes from graphene sheets. *Nano Letters*, 8 (8), 2458–2462.
- Businesswire, 2017. Global Concrete Repair Mortars Market 2017-2021: Market Segmentation and Forecast by Technavio [online]. Available from: <https://www.businesswire.com/news/home/20170707005459/en/Global-Concrete-Repair-Mortars-Market-2017-2021-Market> [Accessed 11 Mar 2020].
- Büteführ, M., Fischer, C., Gehlen, C., Wenzel, K., and Nürnberger, U., 2006. On-site investigations on concrete resistivity a parameter of durability calculation of reinforced concrete structures. *Materials and Corrosion*, 57 (12), 932–939.
- Calmetrix, 2016. *Application videos - Application 1 - Effect of Changes in Mix Parameters on Performance*
- Caputo, F., 2015. *Measuring zeta potential*. Zeta potential determination of nanoparticles in aqueous dispersions by PALS.
- Cembureau, 2017. Cement 101 - Key facts & figures.
- Cementitious Slag Makers Association, 2018. What is GGBS?
- Chen, P.W. and Chung, D.D.L., 1996. Concrete as a new strain stress sensor. *Composites Part B-Engineering*, 27 (1), 11–23.
- Chen, X., Wu, S., and Zhou, J., 2013. Influence of porosity on compressive and tensile strength of cement mortar. *Construction and Building Materials*, 40 (March), 869–874.
- Chia, L. and Huang, Y., 2017. Dispersion effectiveness of carbon nanotubes in smart cementitious materials. *Advances in Cement Research*, 29 (6), 1–12.
- Chiarello, M. and Zinno, R., 2005. Electrical conductivity of self-monitoring CFRC. *Cement and Concrete Composites*, 27 (4), 463–469.
- Choi, K., Min, Y.K., Chung, W., Lee, S.E., and Kang, S.W., 2020. Effects of dispersants and defoamers on the enhanced electrical performance by carbon nanotube networks embedded in cement-matrix composites. *Composite Structures*, 243 (March), 112193.
- Chougan, M., Hamidreza Ghaffar, S., Jahanzat, M., Albar, A., Mujaddedi, N., and Swash, R., 2020. The influence of nano-additives in strengthening mechanical performance of 3D printed multi-binder geopolymer composites. *Construction and Building Materials*, 250, 118928.
- Chougan, M., Marotta, E., Lamastra, F.R., Vivio, F., Montesperelli, G., Ianniruberto, U., and Bianco, A., 2019. A systematic study on EN-998-2 premixed mortars modified with graphene-based materials. *Construction and Building Materials*, 227, 116701.
- Chuah, S., Li, W., Chen, S.J., Sanjayan, J.G., and Duan, W.H., 2018. Investigation on dispersion of graphene oxide in cement composite using different surfactant treatments. *Construction and Building Materials*, 161, 519–527.
- Chuah, S., Pan, Z., Sanjayan, J.G., Wang, C.M., and Duan, W.H., 2014. Nano reinforced

- cement and concrete composites and new perspective from graphene oxide. *Construction and Building Materials*, 73, 113–124.
- Chung, D., 2002a. Piezoresistive Cement-Based Materials for Strain Sensing. *Journal of Intelligent Material Systems and Structures*, 13 (9), 599–609.
- Chung, D., 2002b. Electrical conduction behavior of cement-matrix composites. *Journal of Materials Engineering and Performance*, 11 (2), 194–204.
- Chung, D., 2012. Carbon materials for structural self-sensing, electromagnetic shielding and thermal interfacing. *Carbon*, 50 (9), 3342–3353.
- Climent, M.-Á., Carmona, J., and Garcés, P., 2016. Graphite–Cement Paste: A New Coating of Reinforced Concrete Structural Elements for the Application of Electrochemical Anti-Corrosion Treatments. *Coatings*, 6 (3), 32.
- Cossutta, M., McKechnie, J., and Pickering, S.J., 2017. A comparative LCA of different graphene production routes. *Green Chemistry*, 19 (24), 5874–5884.
- Costain, 2020. Internal communication. Approximate cost of ready mix concrete.
- Davey, S., Paine, K., and Soleimani, M., 2019. A multi-variable study of factors affecting the complex resistivity of conductive mortar. *Magazine of Concrete Research*, (2007), 1–33.
- Davies, R., Teall, O., Pilegis, M., Kanellopoulos, A., Sharma, T., and Davies, R., 2018. Large Scale Application of Self-Healing Concrete: Design, Construction, and Testing, 5 (September), 1–12.
- Demircilioğlu, E., Teomete, E., Schlangen, E., and Baeza, F.J., 2019. Temperature and moisture effects on electrical resistance and strain sensitivity of smart concrete. *Construction and Building Materials*, 224, 420–427.
- Devi, S.C. and Ahmad, R., 2019. Effect of graphene oxide on mechanical and durability performance of concrete. *Journal of Building Engineering*, 6 (November 2018), 201–214.
- Dimov, D., Amit, I., Gorrie, O., Barnes, M.D., Townsend, N.J., Neves, A.I.S., Withers, F., Russo, S., and Craciun, M.F., 2018. Ultrahigh Performance Nanoengineered Graphene-Concrete Composites for Multifunctional Applications. *Advanced Functional Materials*, 28 (23), 1705183.
- Do, V.N. and Pham, T.H., 2010. Graphene and its one-dimensional patterns: From basic properties towards applications. *Advances in Natural Sciences: Nanoscience and Nanotechnology*, 1 (3).
- Dreyer, D.R., Park, S., Bielawski, C.W., and Ruoff, R.S., 2010. The chemistry of graphene oxide. *Chemical Society Reviews*, 39 (1), 228–240.
- Du, H., Gao, H.J., and Pang, S.D., 2016. Improvement in concrete resistance against water and chloride ingress by adding graphene nanoplatelet. *Cement and Concrete Research*, 83, 114–123.
- Du, H. and Pang, S.D., 2015. Enhancement of barrier properties of cement mortar with graphene nanoplatelet. *Cement and Concrete Research*, 76, 10–19.
- Du, H. and Pang, S.D., 2018. Dispersion and stability of graphene nanoplatelet in water and

- its influence on cement composites. *Construction and Building Materials*, 167, 403–413.
- Du, M., Jing, H., Gao, Y., Su, H., and Fang, H., 2020. Carbon nanomaterials enhanced cement-based composites: advances and challenges. *Nanotechnology Reviews*, 9 (1), 115–135.
- Du, S., Wu, J., AlShareedah, O., and Shi, X., 2019. Nanotechnology in Cement-Based Materials: A Review of Durability, Modeling, and Advanced Characterization. *Nanomaterials*, 9 (9), 1213.
- El-Dieb, A.S., El-Ghareeb, M.A., Abdel-Rahman, M.A.H., and Nasr, E.S.A., 2018. Multifunctional electrically conductive concrete using different fillers. *Journal of Building Engineering*, 15 (September 2017), 61–69.
- Fan, X., Fang, D., Sun, M., and Li, Z., 2011. Piezoresistivity of carbon fiber graphite cement-based composites with CCCW. *Journal Wuhan University of Technology, Materials Science Edition*, 26 (2), 339–343.
- Ferrari, A.C., Bonaccorso, F., Fal'ko, V., Novoselov, K.S., Roche, S., Bøggild, P., Borini, S., Koppens, F.H.L., Palermo, V., Pugno, N., Garrido, J.A., Sordan, R., Bianco, A., Ballerini, L., Prato, M., Lidorikis, E., Kivioja, J., Marinelli, C., Ryhänen, T., Morpurgo, A., Coleman, J.N., Nicolosi, V., Colombo, L., Fert, A., Garcia-Hernandez, M., Bachtold, A., Schneider, G.F., Guinea, F., Dekker, C., Barbone, M., Sun, Z., Galiotis, C., Grigorenko, A.N., Konstantatos, G., Kis, A., Katsnelson, M., Vandersypen, L., Loiseau, A., Morandi, V., Neumaier, D., Treossi, E., Pellegrini, V., Polini, M., Tredicucci, A., Williams, G.M., Hee Hong, B., Ahn, J.H., Min Kim, J., Zirath, H., Van Wees, B.J., Van Der Zant, H., Occhipinti, L., Di Matteo, A., Kinloch, I.A., Seyller, T., Quesnel, E., Feng, X., Teo, K., Rupesinghe, N., Hakonen, P., Neil, S.R.T., Tannock, Q., Löfwander, T., and Kinaret, J., 2015. Science and technology roadmap for graphene, related two-dimensional crystals, and hybrid systems. *Nanoscale*, 7 (11), 4598–4810.
- Fishedick, M., Roy, J., Abdel-Aziz, A., Acquaye, A., Alwood, J.M., Ceron, J., Geng, Y., Kheshgi, H., Lanza, A., Perczyk, D., Price, L., Santalla, E., Sheinbaum, C., and Tanaka, K., 2014. *Climate Change 2014: Mitigation of Climate Change. Contribution of Working Group III to the Fifth Assessment Report of the Intergovernmental Panel on Climate Change. A Judgment of the Old Régime*. Cambridge, United Kingdom: Cambridge University Press.
- Frattini, D., Accardo, G., Ferone, C., and Ciof, R., 2017. Fabrication and characterization of graphite-cement composites for microbial fuel cells applications, 88, 188–199.
- Fu, X. and Chung, D.D.L., 1997. Effect of curing age on the self-monitoring behavior of carbon fiber reinforced mortar. *Cement and Concrete Research*, 27, 1313–1318.
- Fulham-lebrasseur, R., Sorelli, L., and Conciatori, D., 2020. Development of electrically conductive concrete and mortars with hybrid conductive inclusions. *Construction and Building Materials*, 237, 117470.
- Gala, A.B., Raugei, M., and Fullana-i-Palmer, P., 2015. Introducing a new method for calculating the environmental credits of end-of-life material recovery in attributional LCA. *International Journal of Life Cycle Assessment*, 20 (5), 645–654.
- Gao, Y., Jing, H., and Zhou, Z., 2019. Fractal analysis of pore structures in graphene oxide-carbon nanotube based cementitious pastes under different ultrasonication.

- Nanotechnology Reviews*, 8 (1), 107–115.
- Gao, Y., Jing, H., Zhou, Z., Chen, W., Du, M., and Du, Y., 2019. Reinforced impermeability of cementitious composites using graphene oxide-carbon nanotube hybrid under different water-to-cement ratios. *Construction and Building Materials*, 222, 610–621.
- Gao, Y., Jing, H.W., Chen, S.J., Du, M.R., Chen, W.Q., and Duan, W.H., 2018. Influence of ultrasonication on the dispersion and enhancing effect of graphene oxide–carbon nanotube hybrid nanoreinforcement in cementitious composite. *Composites Part B: Engineering*, 164 (November 2018), 45–53.
- Gardner, D., Lark, R., Jefferson, T., and Davies, R., 2018. A survey on problems encountered in current concrete construction and the potential benefits of self-healing cementitious materials. *Case Studies in Construction Materials*, 8 (October 2017), 238–247.
- Geim, A.K., 2009. Graphene : Status and Prospects, 324 (June), 1530–1535.
- Geim, A.K. and Novoselov, K.S., 2007. The rise of graphene. *Nature Materials*, 6 (3), 183–191.
- Ghattas, R., Gregory, J., Noori, M., Miller, T.R., Olivetti, E., and Greene, S., 2016. Life Cycle Assessment for Residential Buildings: A Literature Review and Gap Analysis (Revised), 2016 (October), 1–23.
- Gholampour, A., Valizadeh Kiamahalleh, M., Tran, D.N.H., Ozbakkaloglu, T., and Losic, D., 2017. From Graphene Oxide to Reduced Graphene Oxide: Impact on Physiochemical and Mechanical Properties of Graphene–Cement Composites. *ACS Applied Materials & Interfaces*, acsami.7b16736.
- Gillham, B., 2000. *Developing a Questionnaire*.
- Goracci, G. and Dolado, J., 2020. Elucidation of Conduction Mechanism in Graphene Nanoplatelets (GNPs)/Cement Composite Using Dielectric Spectroscopy. *Materials*, 13 (2), 275.
- Graphenea, 2017. Graphene & Graphite - How Do They Compare? [online]. Available from: <https://www.graphenea.com/pages/graphene-graphite#.Wc5PnmhSzD5>.
- Graybeal, B.A., Phares, B.M., Rolander, D.D., Moore, M., and Washer, 2002. Visual Inspection of Highway Bridges. *Journal of Nondestructive Evaluation*, 21, 67–83.
- Guo, L., Wu, J., and Wang, H., 2020. Mechanical and perceptual characterization of ultra-high-performance cement-based composites with silane-treated graphene nanoplatelets. *Construction and Building Materials*, 240, 117926.
- Haddad, A.S. and Chung, D., 2017. Decreasing the electric permittivity of cement by graphite particle incorporation, 122, 702–709.
- Hamad, H., 2019. Modification and performance of activated carbon for CO₂ sequestration in pervious concrete. PhD thesis. University of Cambridge
- Han, B., Ding, S., and Yu, X., 2015. Intrinsic self-sensing concrete and structures: A review. *Measurement: Journal of the International Measurement Confederation*, 59, 110–128.
- Han, B., Yu, X., and Ou, J., 2014. *Self-sensing concrete in smart structures*. Oxford: Elsevier Inc.

- Han, B., Zheng, Q., Sun, S., Dong, S., Zhang, L., Yu, X., and Ou, J., 2017. Enhancing mechanisms of multi-layer graphenes to cementitious composites. *Composites Part A: Applied Science and Manufacturing*, 101, 143–150.
- HM Treasury, 2010. *Infrastructure Cost Review: Main Report*.
- Ho, V.D., Ng, C.T., Coghlan, C.J., Goodwin, A., Mc Guckin, C., Ozbakkaloglu, T., and Losic, D., 2020. Electrochemically produced graphene with ultra large particles enhances mechanical properties of Portland cement mortar. *Construction and Building Materials*, 234, 117403.
- Honorio, T., Carasek, H., and Cascudo, O., 2020. Electrical properties of cement-based materials: Multiscale modeling and quantification of the variability. *Construction and Building Materials*, 245, 118461.
- Horgan, R., 2019. Construction error to blame for Polcevera viaduct collapse, Italian professor claims. *New Civil Engineer*, Nov.
- Horszczaruk, E., Sikora, P., and Lukowski, P., 2016. Application of Nanomaterials in Production of Self-Sensing Concretes: Contemporary Developments and Prospects. *Archives of Civil Engineering*, 62 (3), 61–74.
- Hou, D., 2014. Generalised and Hybrid Sustainability Assessments in Contaminated Site Remediation and Associated Sustainable Behaviour.
- Iijima, S., 1991. Helical microtubules of graphitic carbon, 354 (November), 56–58.
- IMARC Group, 2019. *Cement Market: Global Industry Trends, Share, Size, Growth, Opportunity and Forecast 2019-2024*.
- IPA, 2016. *National Infrastructure Delivery Plan 2016-2021*. HM Infrastructure and Projects Authority.
- IPCC, 2013. *Climate Change 2013: The Physical Science Basis. Contribution of Working Group I to the Fifth Assessment Report of the Intergovernmental Panel on Climate Change*. Cambridge, United Kingdom: Cambridge University Press.
- ISO-14040, 2006. *Environmental Management- Life Cycle Assessment- Principles and Framework*. Geneva, Switzerland.
- ISO-14044, 2006. *Environmental management - Life cycle assessment - Requirements and guidelines*. Geneva, Switzerland.
- ISO-18401:2017, 2017. *Nanotechnologies — Plain language explanation of selected terms from the ISO/IEC 80004 series*.
- Italcementi, 2010. *TX active - The Photocatalytic Active Principle*. Bergamo.
- Jiang, Y., Ling, T.C., Shi, C., and Pan, S.Y., 2018. Characteristics of steel slags and their use in cement and concrete—A review. *Resources, Conservation and Recycling*, 136 (December 2017), 187–197.
- Jiao, D., Shi, C., Yuan, Q., An, X., Liu, Y., and Li, H., 2017. Effect of constituents on rheological properties of fresh concrete-A review. *Cement and Concrete Composites*, 83, 146–159.

- Jing, G., Ye, Z., Lu, X., and Hou, P., 2017. Effect of graphene nanoplatelets on hydration behaviour of Portland cement by thermal analysis. *Advances in Cement Research*, 29 (2), 63–70.
- Jolliet, O., Margni, M., Charles, R., Humbert, S., Payet, J., Rebitzer, G., and Rosenbaum, R., 2003. Impact 2002+: A new life cycle impact assessment methodology. *The International Journal of Life Cycle Assessment*, 8 (324).
- Jones, D., Sakhel, A., Buck, M., and Graichen, P., 2018. *The European Power Sector in 2017*. Agora Energiewende and Sandbag.
- Jones, W., Gibb, A., Goodier, C., Bust, P., Song, M., and Jin, J., 2016. Nanomaterials in construction – what is being used, and where? *Proceedings of the Institution of Civil Engineers - Construction Materials*, 1–14.
- Kauling, A.P., Seefeldt, A.T., Pisoni, D.P., Pradeep, R.C., Bentini, R., Oliveira, R.V.B., Novoselov, K.S., and Castro Neto, A.H., 2018. The Worldwide Graphene Flake Production. *Advanced Materials*, 1803784, 1–6.
- Kirgiz, M.S., 2020. Nanosize particle packing for nanoconcretes and cement based materials: Mathematical models, theory and technology. In: *Smart Nanoconcretes and Cement-Based Materials: Properties, Modelling and Applications*. Elsevier, 42–64.
- Konsta-Gdoutos, M.S., Metaxa, Z.S., and Shah, S.P., 2010. Highly dispersed carbon nanotube reinforced cement based materials. *Cement and Concrete Research*, 40 (7), 1052–1059.
- Korayem, A.H., Ghoddousi, P., Javid, A.A.S., Oraie, M.A., and Ashegh, H., 2020. Graphene oxide for surface treatment of concrete: A novel method to protect concrete. *Construction and Building Materials*, 243, 118229.
- Korayem, A.H., Tourani, N., Zakertabrizi, M., Sabziparvar, A.M., and Duan, W.H., 2017. A review of dispersion of nanoparticles in cementitious matrices: Nanoparticle geometry perspective. *Construction and Building Materials*, 153, 346–357.
- Kothari, C.R., 1990. *Research Methodology: Methods and Techniques*. Second Rev. New Delhi: New Age International (P) Ltd., Publishers.
- Kovtun, A., Treossi, E., Mirotta, N., Scidà, A., Liscio, A., Christian, M., Valorosi, F., Boschi, A., Young, R.J., Galiotis, C., Kinloch, I.A., Morandi, V., and Palermo, V., 2019. Benchmarking of graphene-based materials: Real commercial products versus ideal graphene. *2D Materials*, 6 (2).
- Kozbial, A., Zhou, F., Li, Z., Liu, H., and Li, L., 2016. Are Graphitic Surfaces Hydrophobic? *Accounts of Chemical Research*, 49 (12), 2765–2773.
- Krishnamoorthy, K., Veerapandian, M., Yun, K., and Kim, S.J., 2013. The chemical and structural analysis of graphene oxide with different degrees of oxidation. *Carbon*, 53, 38–49.
- Krystek, M. and Górski, M., 2018. Nanomaterials in Structural Engineering. *New Uses of Micro and Nanomaterials*.
- Le, J.L., Du, H., and Pang, S.D., 2014. Use of 2-D Graphene Nanoplatelets (GNP) in cement composites for structural health evaluation. *Composites Part B: Engineering*, 67, 555–563.

- Lea, F., 1970. *The chemistry of cement and concrete*. 3rd Editio. London: Edward Arnold.
- Lee, H., Jeong, S., Park, S., and Chung, W., 2019. Enhanced mechanical and heating performance of multi-walled carbon nanotube-cement composites fabricated using different mixing methods. *Composite Structures*, 225 (March), 111072.
- Leenaerts, O., Partoens, B., and Peeters, F.M., 2009. Water on graphene: Hydrophobicity and dipole moment using density functional theory. *Physical Review B - Condensed Matter and Materials Physics*, 79 (23), 1–5.
- Li, G., Yuan, J.B., Zhang, Y.H., Zhang, N., and Liew, K.M., 2018. Microstructure and mechanical performance of graphene reinforced cementitious composites. *Composites Part A: Applied Science and Manufacturing*, 114 (August), 188–195.
- Li, G. and Zhang, L.W., 2019. Microstructure and phase transformation of graphene-cement composites under high temperature. *Composites Part B: Engineering*, 166 (August 2018), 86–94.
- Li, X., Korayem, A.H., Li, C., Liu, Y., He, H., Sanjayan, J.G., and Duan, W.H., 2016. Incorporation of graphene oxide and silica fume into cement paste: A study of dispersion and compressive strength. *Construction and Building Materials*, 123, 327–335.
- Li, X. and Li, M., 2019. Multifunctional self-sensing and ductile cementitious materials. *Cement and Concrete Research*, 123 (November 2018).
- Liebscher, M., Dinh, T.T., Schröfl, C., and Mechtcherine, V., 2020. Dispersion of different carbon-based nanofillers in aqueous suspension by polycarboxylate comb-type copolymers and their influence on the early age properties of cementitious matrices. *Construction and Building Materials*, 241, 118039.
- Liu, C., Huang, X., Wu, Y., Deng, X., Liu, J., and Zheng, Z., 2020. Review on the research progress of cement-based and geopolymer materials modified by graphene and graphene oxide. *Nanotechnology Reviews*, 9(1), 155-169.
- Liu, J., Fu, J., Ni, T., and Yang, Y., 2019. Fracture toughness improvement of multi-wall carbon nanotubes / graphene sheets reinforced cement paste. *Construction and Building Materials*, 200, 530–538.
- Liu, J., Fu, J., Yang, Y., and Gu, C., 2019. Study on dispersion, mechanical and microstructure properties of cement paste incorporating graphene sheets. *Construction and Building Materials*, 199, 1–11.
- Liu, K., Cheng, X., Li, J., Gao, X., Cao, Y., Guo, X., Zhuang, J., and Zhang, C., 2019. Effects of microstructure and pore water on electrical conductivity of cement slurry during early hydration. *Composites Part B: Engineering*, 177 (January), 107435.
- Liu, Q., Xu, Q., Yu, Q., Gao, R., and Tong, T., 2016. Experimental investigation on mechanical and piezoresistive properties of cementitious materials containing graphene and graphene oxide nanoplatelets. *Construction and Building Materials*, 127, 565–576.
- Liu, Y., Wang, M., and Wang, W., 2018. Electric induced curing of graphene/cement-based composites for structural strength formation in deep-freeze low temperature. *Materials and Design*, 160, 783–793.

- Loamrat, K., Sappakittipakorn, M., Sukontasukkul, P., and Banthia, N., 2014. Effect of Carbon Fiber and Graphite Powder on Resistivity of Cement-based Sensor under Compression. *KMUTNB International Journal of Applied Science and Technology*, 7 (1), 29–35.
- Long, W., Li, H.-D., Fang, C.-L., and Xing, F., 2018. Uniformly Dispersed and Re-Agglomerated Graphene Oxide-Based Cement Pastes: A Comparison of Rheological Properties, Mechanical Properties and Microstructure. *Nanomaterials*, 8 (1), 31.
- Long, W.J., Zheng, D., Duan, H. bo, Han, N., and Xing, F., 2018. Performance enhancement and environmental impact of cement composites containing graphene oxide with recycled fine aggregates. *Journal of Cleaner Production*, 194, 193–202.
- Lu, Z., Chen, B., Leung, C.Y., Li, Z., and Sun, G., 2019. Aggregation size effect of graphene oxide on its reinforcing efficiency to cement-based materials. *Cement and Concrete Composites*, 100 (October 2018), 85–91.
- Lu, Z., Hanif, A., Ning, C., Shao, H., Yin, R., and Li, Z., 2017. Steric stabilization of graphene oxide in alkaline cementitious solutions: Mechanical enhancement of cement composite. *Materials and Design*, 127 (April), 154–161.
- Lu, Z., Hou, D., Hanif, A., Hao, W., Sun, G., and Li, Z., 2018. Comparative evaluation on the dispersion and stability of graphene oxide in water and cement pore solution by incorporating silica fume. *Cement and Concrete Composites*, 94 (July), 33–42.
- MacLeod, A.J.N., Fehervari, A., Gates, W.P., Garcez, E.O., Aldridge, L.P., and Collins, F., 2020. Enhancing fresh properties and strength of concrete with a pre-dispersed carbon nanotube liquid admixture. *Construction and Building Materials*, 247, 118524.
- Marcu, A.M., 2020. Self-sensing graphene coatings for smart infrastructure. University of Cambridge.
- MarketLine, 2020. *Global Civil Engineering*.
- Meehan, D.G., Shoukai Wang, and Chung, D.D.L., 2010. Electrical-resistance-based sensing of impact damage in carbon fiber reinforced cement-based materials. *Journal of Intelligent Material Systems and Structures*, 21 (1), 83–105.
- Mehmood, A., Mubarak, N.M., Khalid, M., Walvekar, R., Abdullah, E.C., Siddiqui, M.T., Ahmed Baloch, H., Nizamuddin, S., and Mazari, S., 2020. Graphene based nanomaterials for Strain Sensor Application A-review. *Journal of Environmental Chemical Engineering*, 8 (3), 103743.
- Meng, W. and Khayat, K.H., 2016. Mechanical properties of ultra-high-performance concrete enhanced with graphite nanoplatelets and carbon nanofibers. *Composites Part B: Engineering*, 107, 113–122.
- Metaxa, Z., 2015. Polycarboxylate Based Superplasticizers as Dispersant Agents for Exfoliated Graphene Nanoplatelets Reinforcing Cement Based Materials. *Journal of Engineering Science and Technology Review*, 7 (1), 19–24.
- Minghua, D., 2001. Concrete Pouring of Three Gorges Project Sets World Record. *People's Daily Online*, 4 Jan.

- Monajjemi, M., 2017. Liquid-phase exfoliation (LPE) of graphite towards graphene: An ab initio study. *Journal of Molecular Liquids*, 230, 461–472.
- Monfore, G., 1968. The electrical resistivity of concrete. *Journal of The PCA Research and Development laboratories*, 10 (2), 35–48.
- Muthoosamy, K. and Manickam, S., 2017. State of the art and recent advances in the ultrasound-assisted synthesis, exfoliation and functionalization of graphene derivatives. *Ultrasonics Sonochemistry*, 39 (February), 478–493.
- Nagata, K., Iwabuki, H., and Nigo, H., 1999. Effect of particle size of graphites on electrical conductivity of graphite/polymer composite. *Composite Interfaces*, 6 (5), 483–495.
- Nanasa, 2018. Resource consumption - Private communication.
- Neville, A., 2011. *Properties of concrete*. 5th ed. Pearson Education Limited.
- NobelPrize.org, 2020. The Nobel Prize in Physics 2010 [online]. *Nobel Media AB 2020*. Available from: <https://www.nobelprize.org/prizes/physics/2010/summary/> [Accessed 11 Jan 2020].
- Novoselov, K.S., Fal, V.I., Colombo, L., Gellert, P.R., Schwab, M.G., Kim, K., Ko, V.I.F., Colombo, L., Gellert, P.R., Schwab, M.G., and Kim, K., 2012. A roadmap for graphene. *Nature*, 490 (7419), 192–200.
- NRMCA, 2012. Concrete CO₂ Fact Sheet. *National Ready Mixed Concrete Association*.
- NT BUILD492, 1999. *NT BUILD 492. Concrete, mortar and cement-based repair materials: Chloride migration coefficient from Non-steady-state migration experiments*. Finland.
- Oppenheim, A., 2001. *Questionnaire Design, Interviewing and Attitude Measurement*. Continuum.
- Orr, J., Drewniok, M.P., Walker, I., Ibell, T., Copping, A., and Emmitt, S., 2019. Minimising energy in construction: Practitioners' views on material efficiency. *Resources, Conservation and Recycling*, 140 (June 2018), 125–136.
- Ortiz, O., Castells, F., and Sonnemann, G., 2009. Sustainability in the construction industry: A review of recent developments based on LCA. *Construction and Building Materials*, 23 (1), 28–39.
- Ou, J. and Han, B., 2009. Piezoresistive cement-based strain sensors and self-sensing concrete components. *Journal of Intelligent Material Systems and Structures*, 20 (3), 329–336.
- Ozbulut, O.E., Jiang, Z., and Harris, D.K., 2018. Exploring scalable fabrication of self-sensing cementitious composites with graphene nanoplatelets. *Smart Materials and Structures*, 27 (11).
- Papanikolaou, I., 2017. Graphene/cement composites for sprayed concrete linings in underground construction. MRes thesis. University of Cambridge.
- Papanikolaou, I., Al-Tabbaa, A., and Goisis, M., 2019. An industry survey on the use of graphene-reinforced concrete for self-sensing applications. In: M. DeJong, J. Schooling, and G. Viggiani, eds. *International Conference on Smart Infrastructure and Construction*

- 2019 (ICSIC). Cambridge: ICE Publishing, 613–622.
- Papanikolaou, I., Arena, N., and Al-Tabbaa, A., 2019. Graphene nanoplatelet reinforced concrete for self-sensing structures – A lifecycle assessment perspective. *Journal of Cleaner Production*, 240.
- Papanikolaou, I., Davies, A., Jin, F., Litina, C., and Al-Tabbaa, A., 2018. Graphene oxide/cement composites for sprayed concrete tunnel linings. In: *ITA - AITES WORLD TUNNEL CONGRESS 2018*. 103–108.
- Papo, A., 1988. Rheological models for cement pastes. *Materials and Structures*, 21 (1), 41–46.
- Paul, S.C., van Rooyen, A.S., van Zijl, G.P.A.G., and Petrik, L.F., 2018. Properties of cement-based composites using nanoparticles: A comprehensive review. *Construction and Building Materials*, 189, 1019–1034.
- PCA, 2002. *IS536 - Types and Causes of Concrete Deterioration*. Portland Cement Association.
- Pei, S. and Cheng, H.M., 2012. The reduction of graphene oxide. *Carbon*, 50 (9), 3210–3228.
- Peinado, F., Roig, A., Vicente, F., Vilaplana, J., and Lopez, J., 1994. Electrochemical Characterization of Cement Graphite and Cement Aluminum Materials. *Journal of Materials Science Letters*, 13 (8), 609–612.
- Phiri, J., Gane, P., and Maloney, T.C., 2017. General overview of graphene: Production, properties and application in polymer composites. *Materials Science and Engineering: B*, 215, 9–28.
- Pichór, W. and Fraç, M., 2019. Multifunctional cement composites with expanded graphite for temperature monitoring of buildings. *Advances in Cement Research*, 1–8.
- Poco Graphite Inc., 2015. *Properties and Characteristics of Graphite*. Decatur, Texas.
- Prabavathy, S., Jeyasubramanian, K., Prasanth, S., Hikku, G.S., and Robert, R.B.J., 2019. Enhancement in behavioral properties of cement mortar cubes admixed with reduced graphene oxide. *Journal of Building Engineering*, 28 (November 2019), 101082.
- Proceq, 2017. Resipod - Operating manual.
- Proceq, 2018. Proceq internal communication (8 Nov 2018).
- Raccichini, R., Varzi, A., Passerini, S., and Scrosati, B., 2015. The role of graphene for electrochemical energy storage. *Nature Materials*, 14 (3), 271–279.
- Rashid, A. and Yusoff, S., 2015. A review of life cycle assessment method for building industry. *Renewable and Sustainable Energy Reviews*, 45, 244–248.
- Rehman, S.K.U., Ibrahim, Z., Jameel, M., Memon, S.A., Javed, M.F., Aslam, M., Mehmood, K., and Nazar, S., 2018. Assessment of Rheological and Piezoresistive Properties of Graphene based Cement Composites. *International Journal of Concrete Structures and Materials*, 12 (1).
- Rew, Y., Baranikumar, A., Tamashauskyy, A. V., El-Tawil, S., and Park, P., 2017. Electrical and mechanical properties of asphaltic composites containing carbon based fillers. *Construction and Building Materials*, 135, 394–404.

- de Rooij, M., Van Tittelboom, K., De Belie, N., and Schlangen, E., 2013. *Self-Healing Phenomena in Cement-Based Materials. State-of-the-Art Report of RILEM Technical Committee 221-SHC: Self-Healing Phenomena in Cement-Based Materials*. Springer International Publishing.
- Royal Society of Chemistry, 2009. *Ultraviolet - Visible Spectroscopy (UV)*.
- Royal Society of Chemistry, 2013. *Should we worry about nanomaterials?*
- Sabziparvar, A.M., Hosseini, E., Chiniforush, V., and Korayem, A.H., 2019. Barriers to achieving highly dispersed graphene oxide in cementitious composites: An experimental and computational study. *Construction and Building Materials*, 199, 269–278.
- Sachdev, V.K., Sharma, S.K., Bhattacharya, S., Patel, K., Mehra, N.C., Gupta, V., and Tandon, R.P., 2015. Electromagnetic shielding performance of graphite in cement matrix for applied application. *Advanced Materials Letters*, 6 (11), 965–972.
- Sbia, L.A., Peyvandi, A., Soroushian, P., Balachandra, A.M., and Sobolev, K., 2015. Evaluation of modified-graphite nanomaterials in concrete nanocomposite based on packing density principles. *Construction and Building Materials*, 76 (1), 413–422.
- Schlangen, E. and Joseph, C., 2008. Self-Healing Processes in Concrete. In: *Self-healing Materials: Fundamentals, Design Strategies, and Applications*. 306.
- Scrivener, K.L., Juilland, P., and Monteiro, P.J.M., 2015. Advances in understanding hydration of Portland cement. *Cement and Concrete Research*, 78, 38–56.
- Seabrook, P.T., Balck, L.F., Bawa, K.S., Bortz, S.A., Chynoweth, G.L., Crom, T.R., Dikeou, J.T., Drudy, W.A., Fredericks, J.C., Glassgold, I.L., Henager, C.H., Heneghan, J., Kaden, R.A., Lanclos, J., and Litvin, A., 2001. *ACI 544.1-96. State-of-the-Art Report on Fiber Reinforced Concrete*. Concrete International.
- Shabafrooz, V., Bandla, S., and Hanan, J.C., 2018. Graphene dispersion in a surfactant-free, polar solvent. *Journal of Materials Science*, 53 (1), 559–572.
- Shamsaei, E., de Souza, F.B., Yao, X., Benhelal, E., Akbari, A., and Duan, W., 2018. Graphene-based nanosheets for stronger and more durable concrete: A review. *Construction and Building Materials*, 183, 642–660.
- Shang, Y., Zhang, D., Yang, C., Liu, Y., and Liu, Y., 2015. Effect of graphene oxide on the rheological properties of cement pastes. *Construction and Building Materials*, 96, 20–28.
- Siddique, R., 2011. Utilization of silica fume in concrete: Review of hardened properties. *Resources, Conservation and Recycling*, 55, 923–932.
- Sika Services, 2009. *Sika® ViscoCrete® Technology*. Zürich.
- Simapro, 2015. LCA, 8.3. Release date: 2015-05-29. Available at: <http://www.simapro.co.uk>.
- Sobolkina, A., Mechtcherine, V., Khavrus, V., Maier, D., Mende, M., Ritschel, M., and Leonhardt, A., 2012. Dispersion of carbon nanotubes and its influence on the mechanical properties of the cement matrix. *Cement and Concrete Composites*, 34 (10), 1104–1113.
- Spencer, B.F., 2009. *Structural Health Monitoring of Civil Infrastructure: from Research to*

Engineering Practice. Cambridge.

- Srinivasan, S., Barbhuiya, S.A., Charan, D., and Pandey, S.P., 2010. Characterising cement-superplasticiser interaction using zeta potential measurements. *Construction and Building Materials*, 24 (12), 2517–2521.
- Stewart, M.G., Wang, X., and Nguyen, M.N., 2011. Climate change impact and risks of concrete infrastructure deterioration. *Engineering Structures*, 33 (4), 1326–1337.
- Sun, S., Ding, S., Han, B., Dong, S., Yu, X., Zhou, D., and Ou, J., 2017. Multi-layer graphene-engineered cementitious composites with multifunctionality/intelligence. *Composites Part B: Engineering*, 129, 221–232.
- Taheri, S., 2019. A review on five key sensors for monitoring of concrete structures. *Construction and Building Materials*, 204, 492–509.
- Tang, K., 2019. Corrosion of steel fibre reinforced concrete (SFRC) subjected to simulated stray direct (DC) interference. *Materials Today Communications*, 20 (June), 100564.
- Tao, J., Wang, X., Wang, Z., and Zeng, Q., 2019. Graphene nanoplatelets as an effective additive to tune the microstructures and piezoresistive properties of cement-based composites. *Construction and Building Materials*, 209, 665–678.
- Tarmac, 2015. Ultiglow [online]. Available from: <https://www.tarmac.com/solutions/aggregates-asphalt/ultiglow/> [Accessed 9 Jan 2020].
- Taylor, H.F.W., 1997. *Cement chemistry*. 2nd ed. London, UK: Thomas Telford Services Ltd.
- Texter, J., 2014. Graphene dispersions. *Current Opinion in Colloid and Interface Science*, 19 (2), 163–174.
- The Concrete Centre, 2016a. 9th Concrete Industry Sustainability Performance Report. 2015 Performance data, 16.
- The Concrete Centre, 2016b. *Whole-Life Carbon and Buildings*.
- Tian, X. and Hu, H., 2012. Test and Study on Electrical Property of Conductive Concrete. *Procedia Earth and Planetary Science*, 5 (2011), 83–87.
- Tian, Z., Li, Y., Zheng, J., and Wang, S., 2019. A state-of-the-art on self-sensing concrete: Materials, fabrication and properties. *Composites Part B: Engineering*, 177 (September), 107437.
- Tiedje, E. and Guo, P., 2014. Thermal Conductivity of Bentonite Grout Containing Graphite or Chopped Carbon Fibers. *Journal of Materials in Civil Engineering*, 26 (7), 06014013.
- Tilly, G. and Jacobs, J., 2007. *Concrete Repairs: Performance in Service and Current Practice*. BREpress.
- Van Tittelboom, K. and De Belie, N., 2013. Self-Healing in Cementitious Materials—A Review. *Materials*, 6 (6), 2182–2217.
- Tong, T., Fan, Z., Liu, Q., Wang, S., Tan, S., and Yu, Q., 2016. Investigation of the effects of graphene and graphene oxide nanoplatelets on the micro- and macro-properties of cementitious materials. *Construction and Building Materials*, 106, 102–114.

- Turk, J., Cotič, Z., Mladenovič, A., and Šajna, A., 2015. Environmental evaluation of green concretes versus conventional concrete by means of LCA. *Waste Management*, 45 (305), 194–205.
- Wallevik, O.H., Feys, D., Wallevik, J.E., and Khayat, K.H., 2015. Avoiding inaccurate interpretations of rheological measurements for cement-based materials. *Cement and Concrete Research*, 78, 100–109.
- Wang and Aslani, F., 2019. A review on material design , performance , and practical application of electrically conductive cementitious composites. *Construction and Building Materials*, 229, 116892.
- Wang, B. and Deng, S., 2019. Effect and mechanism of graphene nanoplatelets on hydration reaction, mechanical properties and microstructure of cement composites. *Construction and Building Materials*, 228, 116720.
- Wang, B., Jiang, R., and Wu, Z., 2016. Investigation of the Mechanical Properties and Microstructure of Graphene Nanoplatelet-Cement Composite. *Nanomaterials*, 6 (11), 200.
- Wang, B., Jiang, R., and Zhao, R., 2018. Dispersion of Graphene in Aqueous Solution. *Russian Journal of Physical Chemistry*, 92 (8), 1558–1562.
- Wang, B. and Pang, B., 2019. Mechanical property and toughening mechanism of water reducing agents modified graphene nanoplatelets reinforced cement composites. *Construction and Building Materials*, 226, 699–711.
- Wang, B. and Zhao, R., 2017. Effect of graphene nano-sheets on the chloride penetration and microstructure of the cement based composite. *Construction and Building Materials*, 161, 715–722.
- Wang, B., Zhao, R., and Zhang, T., 2018. Pore structure and durability of cement-based composites doped with graphene nanoplatelets. *Materials Express*, 8 (2), 149–156.
- Wang, D., Wang, Q., and Huang, Z., 2019. Investigation on the poor fluidity of electrically conductive cement-graphite paste: Experiment and simulation. *Materials and Design*, 169, 107679.
- Wang, J., Tao, J., Li, L., Zhou, C., and Zeng, Q., 2020. Thinner fillers, coarser pores? A comparative study of the pore structure alterations of cement composites by graphene oxides and graphene nanoplatelets. *Composites Part A: Applied Science and Manufacturing*, 130 (December 2019).
- Wang, X., Dong, S., Ashour, A., Zhang, W., and Han, B., 2020. Effect and mechanisms of nanomaterials on interface between aggregates and cement mortars. *Construction and Building Materials*, 240, 117942.
- Wansom, S., Kidner, N.J., Woo, L.Y., and Mason, T.O., 2006. AC-impedance response of multi-walled carbon nanotube/cement composites. *Cement and Concrete Composites*, 28 (6), 509–519.
- Webb, G., Vardanega, P., and Middleton, C., 2015. Categories of SHM Deployments: Technologies and Capabilities. *Journal of Bridge Engineering*, 20 (11), 04014118.

- Wei, Y. and Sun, Z., 2015. Liquid-phase exfoliation of graphite for mass production of pristine few-layer graphene. *Current Opinion in Colloid and Interface Science*, 20 (5–6), 311–321.
- Wen, S. and Chung, D., 2006a. Spatially resolved self-sensing of strain and damage in carbon fiber cement. *Journal of Materials Science*, 41 (15), 4823–4831.
- Wen, S. and Chung, D., 2006b. The role of electronic and ionic conduction in the electrical conductivity of carbon fiber reinforced cement. *Carbon*, 44 (11), 2130–2138.
- Whiteley, D., Goethert, K., Goodwin, F., Golter, H.P., Kennedy, J., Komar, T.W., Meyer, J., Petree, M., Smith, B., Trepanier, S., Whitmore, D., and Winkler, P., 2015. *Sustainability for Repairing and Maintaining Concrete and Masonry Buildings*.
- World Nuclear Association, 2018. Nuclear Power in the United Kingdom [online]. Available from: <http://www.world-nuclear.org/information-library/country-profiles/countries-t-z/united-kingdom.aspx> [Accessed 15 Nov 2018].
- Worrell, E., Bernstein, L., Roy, J., Price, L., and Harnisch, J., 2009. Industrial energy efficiency and climate change mitigation. *Energy Efficiency*, 2 (2), 109–123.
- Wu, J., Liu, J., and Yang, F., 2015. Three-phase composite conductive concrete for pavement deicing. *Construction and Building Materials*, 75, 129–135.
- Xu, Y., 2012. Health Monitoring of Large Civil Structures. In: *The Second Future Infrastructure Forum (FIF2)*. Cambridge, 17–18.
- Xu, Y., Zeng, J., Chen, W., Jin, R., Li, B., and Pan, Z., 2018. A holistic review of cement composites reinforced with graphene oxide. *Construction and Building Materials*, 171, 291–302.
- Yuan, H.-W., Lu, C.-H., Xu, Z.-Z., Ni, Y.-R., and Lan, X.-H., 2012. Mechanical and thermal properties of cement composite graphite for solar thermal storage materials. *Solar Energy*, 86 (11), 3227–3233.
- Zhang, B. and Chen, T., 2019. Study of Ultrasonic Dispersion of Graphene Nanoplatelets. *Materials*, 12 (11), 1757.
- Zhang, Q., Le Roy, R., Vandamme, M., and Zuber, B., 2014. Long-term creep properties of cementitious materials: Comparing microindentation testing with macroscopic uniaxial compressive testing. *Cement and Concrete Research*, 58, 89–98.
- Zhao, L., Guo, X., Liu, Y., Ge, C., Chen, Z., Guo, L., Shu, X., and Liu, J., 2018. Investigation of dispersion behavior of GO modified by different water reducing agents in cement pore solution. *Carbon*, 127, 255–269.
- Zhao, L., Guo, X., Song, L., Song, Y., Dai, G., and Liu, J., 2020. An intensive review on the role of graphene oxide in cement-based materials. *Construction and Building Materials*, 241, 117939.
- Zhu, S., Qin, X., Zou, Z., Zhang, R., and Jiang, Y., 2019. Preparation and evaluation of surfactant-stabilized graphene sheets and piezoresistivity of GPs/cement composite. *Carbon Letters*, (0123456789).
- Zhu, W. and Bartos, P.J.M., 2000. Application of depth-sensing microindentation testing to

study of interfacial transition zone in reinforced concrete. *Cement and Concrete Research*, 30 (8), 1299–1304.

Zhu, Y., Murali, S., Cai, W., Li, X., Suk, J.W., Potts, J.R., and Ruoff, R.S., 2010. Graphene and graphene oxide: Synthesis, properties, and applications. *Advanced Materials*, 22 (35), 3906–3924.